International Conference

Advanced Laser Technologies

ALT'16

The 24th Annual International Conference on Advanced Laser Technologies ALT'16

Galway, Ireland
September 12–16, 2016

BOOK of ABSTRACTS

Contents

Organizers and Sponsors

General Physics Institute
of Russian Academy of Sciences
Russia

National University of Ireland
Galway, Ireland

Lomonosov Moscow State University
Russia

Fáilte **Ireland**
National Tourism Development Authority
Ireland

Science Foundation
Ireland

National Research Nuclear University
MEPhI, Russia

Center of Laser Technology
and Material Science, Russia

Conference Chairman

Ivan SHCHERBAKOV, Russia

Program Committee Co-Chairs

Vitaly KONOV, Russia
Gerard O'CONNOR (Ireland)

International Program Committee

Liam BARRY (Ireland)
Ekaterina BORISOVA (Bulgaria)
Hugh BYRNE (Ireland)
J.-L. COUTAZ (France)
Aladar CZITROVSKY (Hungary)
Boris DENKER (Russia)
Dan DUMITRAS (Romania)
Costas FOTAKIS (Greece)
Thomas GRAF (Germany)
Sergey GARNOV (Russia)
Leonid GOLOVAN (Russia)
Patrick HAYDEN (Ireland)
Fatih HUSEYINOGLU (Turkey)
Lan JIANG (China)
Izabela NAYDENOVA (Ireland)
Pavel KASHKAROV (Russia)
Tia KEYES (Ireland)
Yuri KULCHIN (Russia)
Pascal LANDAIS (Ireland)
Yong Feng LU (USA)
Vladimir MAKAROV (Russia)
John MCINERNEY (Ireland)
Ion MIHAILESCU (Romania)
Kyung Hyun PARK (Korea)
Ivan PELIVANOV (USA)
Valentin PETROV (Germany)
Alexei POPOV (Finland)
Alexander PRIEZZHEV (Russia)
Valerio ROMANO (Switzerland)
Philippe DELAPORTE (France)
Marc SENTIS (France)
Alexander SHKURINOV (Russia)
Nikolai A. SOBOLEV (Portugal)
Vadim VEIKO (Russia)
Alexey ZHELTIKOV (Russia)
Ioanna ZERGIOTI (Greece)

Organizing Committee Co-Chairs

Vladimir PUSTOVOY (Russia)
Martin LEAHY (Ireland)

International Organizing Committee

Sergey ALEXANDROV (Ireland)
Roshan DSOUZA (Ireland)
James MCGRATH (Ireland)
Cerine LAL (Ireland)
Natalia KHAKAMOVA (Russia)
Kai NEUHAUS (Ireland)
Tatiana VOLYAK (Russia)

Plenary Talks

Plenary session - 1

The semiconductor laser in optical communications- future challenges for energy efficient networks

John F. Donegan

Photonics Group, School of Physics, (CRANN/AMBER) Nanoscience and Advanced Materials Research Institute and Centre for Future Networks (CONNECT) Trinity College Dublin, Dublin 2, Ireland.

jdonegan@tcd.ie

Invented in 1964, the semiconductor laser has become the most important device operating in optical communications systems. The laser emission is modulated to encode data such as e-mail and webpages to be transported over the fiber based systems. May different semiconductor laser devices have been developed, but of these, the distributed feedback laser (DFB) has now become the industry standard. Our research group has taken another course, developing a laser platform based on high-order surface gratings which allow for re-growth free fabrication. We can also use a foundry model for the fabrication, in which the designs produced in our group are fabricated in a commercial foundry dedicated to production of laser devices. To date, we have shown that the ability to develop novel devices such as the Vernier laser with tuning over the C-band [1] and in recent times, we have also developed a laser array which was developed with a simple change in the pitch of the high-order grating used to make the laser operate in a single mode [2].

In the next period of its development, the power consumed by the devices will become a controlling issue in their further deployment. Projections show that the electricity supply for fixed fiber based networks could exceed 10% of global supply by 2020, which is simply unsustainable. Athermal operation of the laser in which the operating wavelength is unchanged for variation in temperature of about 50^{o}C are under investigation. Working with Nokia Bell Labs, we have some excellent early results showing how such athermal performance can be used in our high-order grating devices. The next big challenge for optical communications will be to incorporate the internet of things (IoT) into the optical networks. This will in turn require devices of the highest possible power efficiency.

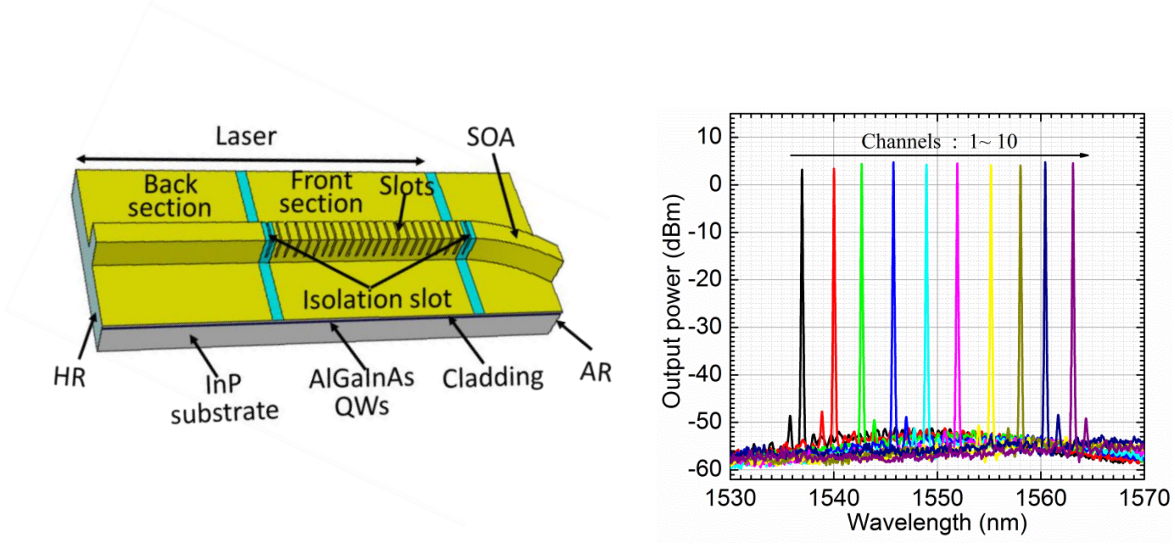

Figure 1, Schematic of the high-order surface grating, Output power versus wavelength for a 10 channel laser array based on high-order grating, showing tenability across the C band.

[1] M. Nawrocka, Q. Lu, W-H Guo, A. Abdullaev, F. Bello, J. O'Callaghan, T.Cathcart and J. F. Donegan, Widely tunable six-section semiconductor laser based on etched slots, Optics Express, 22, 18949-18957, (2014).

[2] A. Abdullaev, Q. Lu, W-H Guo, M. Wallace, M. Nawrocka, F. Bello, A. Benson, J. O'Callaghan and J. F. Donegan, Improved Performance of tunable single-mode laser array based on high-order slotted surface grating, Optics Express, 23, 12072-12078, (2015)

Fiber technological lasers: current status and prospects

N. Evtihiev

Plenary session - 3

What Will It Take for Photoacoustic Imaging to be Used Routinely in the Clinic?

Matthew O'Donnell
odonnel@uw.edu

Department of Bioengineering, University of Washington, Seattle, WA 98195, USA

Keywords: *ultrasound imaging, photoacoustic imaging, molecular imaging, molecular therapies*

With recent developments in molecular-scale bioconjugated contrast agents and integrated system design, photoacoustics (PA) is rapidly bringing molecular sensitivity to ultrasound (US) imaging for many biomedical applications. The same agents can potentially be used for molecularly-targeted therapies as well, opening the possibility for molecular theranostics using integrated photoacoustics/ultrasonics (PAUS). In this presentation, we will explore a class of nanoemulsion-based contrast agents that can potentially be used for photoacoustic imaging, ultrasonic imaging, and molecularly-targeted therapies combining light/ultrasound excitation. In particular, excitation techniques have been developed exploiting the non-linear characteristics of the nanoemulsions to provide both high sensitivity and specificity for molecular imaging and therapy. Finally, a system capable of integrated PAUS imaging at real-time frame rates will be presented that can monitor molecular theranostic procedures enabled by these nanoemulsions.

Plasmonics and Metasurfaces: Generation and Manipulation of Optical Wavefronts

Byoungho Lee

School of Electrical and Computer Engineering, Seoul National University, Gwanak-Gu Gwanakro 1, Seoul 08826, South Korea

byoungho@snu.ac.kr

Nanophotonics, which controls light by using nanostructure, has attracted tremendous attention for recent years. By tailoring light-matter interaction in the scale of light wavelength, nanophotonics provides strong controllability on light. Stronger light-matter interaction can be exploited for various applications including compact nanoscale optical devices, sensors with high sensitivity, and nonlinear optics. Particularly, plamonics and metamaterials are the major topics which have led the boom of nanophotonics research. Plasmonics has emerged as a route to subwavelength optics by using surface plasmon polaritons (SPPs) which are bound electromagnetic waves on metal surfaces. Due to the SPP's capability to confine light in deep subwavelength space, several plasmonic applications such as integrated photonic circuits, surface plasmon resonance-based sensors, surface enhanced Raman spectroscopy, and high harmonic generation using plasmonic antennas have been investigated [1]. Meanwhile, the metamaterials which exhibit exotic electromagnetic responses such as negative refractive index materials or epsilon-near-zero materials have been extensively studied [2, 3]. It was found that wide range of material responses can be obtained by designing subwavelength nanoantennas. More recently, planar metamaterials, which are named as metasurfaces, have been found to enable holographic wavefront reconstruction by using metasurfaces of thickness only several tenth of light wavelength [4].

For design of nanophotonic devices, it is necessary to understand and balance the couplings of free space lights with nanoantennas. For instance, plasmonic devices including plasmonic lenses and plasmonic beaming devices are designed by synthesizing plasmonic or optical wavefronts by using nanoslits or gratings which behave as nanoantennas [5]. In addition, if nanoantennas are designed for multiple input lights with different polarizations, incidence angles or wavelengths, it is possible to control the function of nanophotonic devices by modulating input light. Indeed, there have been various types of plasmonic devices and metasurfaces which can be controlled by external input light including polarization-multiplexed meta-holograms and coherent perfect absorbers [6, 7].

In this presentation, schemes for plasmonic field and optical far field synthesis and their manipulation will be presented. Firstly, physical mechanisms of nanoscale scatterers including nanoslits, rods and cavity-aperture will be explained. Then, nanoslit arrays for plasmonic focal spots, plasmonic vortices, directive optical beams and compact Airy beams will be shown as examples of near- and far-field synthesis techniques [5]. Lastly, polarization-controlled unidirectional SPP launching structures, plasmonic focusing structures, plasmonic color filtering pixels and wavelength-controlled Airy beam generating metasurfaces will be presented [8-10].

[1] J. A. Schuller, E. S. Barnard, W. Cai, Y. C. Jun, J. S. White, and M. L. Brongersma, "Plasmonics for extreme light concentration and manipulation," Nat. Mater., vol. 9, pp.193-204 (2010).
[2] V. M. Shalaev, "Optical negative-index metamaterials," Nat. Photon., vol. 1, pp.41-48 (2007).
[3] R. Maas, J. Parsons, N. Engheta, and A. Polman, "Experimental realization of an epsilon-near-zero metamaterial at visible wavelengths," Nat. Photon., vol. 7, pp. 907-912, (2013).
[4] A. V. Kildishev, A. Boltasseva, and V. M. Shalaev, "Planar photonics with metasurfaces," Science, vol. 339, 1232009 (2013).
[5] B. Lee, S. Kim, H. Kim, and Y. Lim, "The use of plasmonis in light beaming and focusing," Prog. Quant. Electron., vol. 34, pp. 47-87 (2010).
[6] D. Wen, F. Yue, G. Li, G. Zheng, K. Chan, S. Chen, M. Chen, K. F. Li, P. W. H. Wong, K. W. Cheah, E. Y. B. Pun, S. Zhang, and X. Chen, "Helicity multiplexed broadband metasurface holograms," Nat. Commun., vol. 6, 8241 (2015).
[7] S.-Y. Lee, I.-M. Lee, J. Park, S. Oh, W. Lee, K.-Y. Kim, and B. Lee, "Role of magnetic induction currents in nanoslit excitation of surface plasmon polaritons," Phys. Rev. Lett., vol. 108, 213907 (2012).
[8] S.-Y. Lee, W. Lee, Y. Lee, J.-Y. Won, J. Kim, I.-M. Lee, and B. Lee, "Phase-controlled directional switching of surface plasmon polaritons via beam interference," Laser Photon. Rev., vol. 7, pp. 273-279 (2013).
[9] S.-Y. Lee, H. Yun, Y. Lee, and B. Lee, "Switchable surface plasmon dichroic splitter modulated by optical polarization," Laser Photon. Rev., vol. 8, pp. 777-784 (2014).
[10] H. Yun, S.-Y. Lee, K. Hong, J. Yeom, and B. Lee, "Plasmonic cavity-apertures as dynamic pixels for the simultaneous control of colour and intensity," Nat. Commun., vol. 6, 7133 (2015).

Biophotonics

BP-1-1 (Invited)

Emerging Methods of Optical Coherence Elastography

K.V. Larin

University of Houston, Houston, TX 77204, USA

klarin@uh.edu

In this talk I overview recent progress made in the field of Optical Coherence Elastography in quantities assessment of ocular and cardiac tissues. We have developed novel combined focused ultrasound/air-puff and phase-sensitive optical coherence elastography (OCE) system to assess biomechanical properties of tissues *in situ* and *in vivo* in 3D. Low-amplitude elastic deformations in mice and rabbit ocular tissues and mice hearts (both *ex vivo* and in vivo) were measured by the OCE system consisting of a spectral-domain optical coherence tomography (OCT) combined with focused ultrasound (lens excitation) and air-puff (cornea and heart muscle excitation) systems used to produce a transient force on the tissue surface. The amplitude, temporal profile, and the speed of the deformations were used to reconstruct tissue biomechanical properties using novel analytical models. Gold standard uniaxial compressional tests were used to validate the OCE data. These results of these studies demonstrate that the OCE system can be used for noninvasive analysis and quantification of tissue biomechanical properties in 2D and 3D in normal and pathological tissues and as a function of tissue aging or therapy (e.g. CLX procedures). At the end, I'll introduce our recent advances in ultra-high speed imaging and assessment of the elastic waves using several configurations such as MHz laser swept source or optimizing scanning/imaging methods (such line-field OCE).

BP-1-2 (Invited)

Dynamic in vivo Imaging of Reproductive Events in Mouse Models with OCT

Irina V. Larina

Molecular Physiology & Biophysics, Baylor College of Medicine, Houston, TX 77030 USA

The understanding of the reproductive events and the molecular mechanisms regulating fertility and infertility in humans relies heavily on the analysis of the corresponding phenotypes in mouse models. While molecular genetic approaches provide significant insight into the molecular regulation of these processes, the lack of live imaging methods that allow for detailed visualization of the mouse reproductive organs limits our investigations of dynamic events taking place during ovulation, fertilization, and pre-implantation stages of embryonic development. For its normal function, the mammalian oviduct relies heavily on the motility of cilia that line the lumen. The role of cilia is well recognized, but due to their small size (~5–10 μm in length and ~300 nm in diameter), live visualization of oviduct cilia and their activity in the lumen of the oviduct through tissue layers represents a major challenge not yet overcome. For the first time, we developed an in vivo three-dimensional imaging approach for visualizing the mouse reproductive events with micro-scale spatial resolution using optical coherence tomography (OCT). Animal surgical procedures similar to the ones used for production of transgenic mice are utilized to expose the reproductive organs for imaging in anesthetized females. OCT imaging relies on the natural tissue optical contrast and does not require the application of any contrast agents or vital reporters, which makes our approach easily applicable to analysis of mutant phenotypes. We also developed functional imaging method based on spectral analysis of the OCT speckle variations produced by the beat of cilia in the oviduct for *in vivo* micro-scale mapping of cilia and cilia beat frequency (CBF) in the mouse oviduct. We will present *in vivo* structural imaging of the mouse oviduct capturing the oocyte and the preimplantation embryo and then show the result of depth-resolved high-resolution CBF mapping in the oviduct of live mice. We validated our approach with widely-used microscopic imaging methods and demonstrated the ability of this approach to differentiate CBF in different locations of the oviduct at different post-conception stages. Furthermore, structural analysis of mutant phenotypes has been initiated and has provided additional insight into developmental defects not previously revealed using standard approaches. Our data suggest that the described structural and functional OCT imaging approach is a useful tool for a variety of live investigations of mammalian reproduction and infertility.

BP-1-3 (Invited)

Quantitative Techniques in Optical Coherence Tomography: Simulations, Processing, Quantification

M.Yu. Kirillin[1], N.M. Shakhova[1], E.A. Sergeeva[1], P.D. Agrba[1,2],M.A. Pasukhin[1,2], E.S. Plankina[2], M.A. Shakhova[1,3], A.E. Meller[1,3], E.V. Gubarkova[3], E.B. Kiseleva[3], N.D. Gladkova[3], V.V. Dudenkova[2,3], and I.A. Vitkin[3,4]

1 - Institute of Applied Physics RAS, Nizhny Novgorod, Russia
2 - N.I. Lobachevsky State University of Nizhny Novgorod, Nizhny Novgorod, Russia
3 - Nizhny Novgorod Medical Academy, Nizhny Novgorod, Russia
4 - University of Toronto, Toronto, Canada

Main author email address: mkirillin@yandex.ru

Optical coherence tomography is a rapidly developing imaging modality based on principles of low-coherence interferometry. OCT allows to image internal structure of biotissues at depths up to 2 mm with micron-scale spatial resolution. Due to its non-invasive nature and high spatial resolution, OCT is actively introduced into clinical practice. It is already in common use in ophthalmology and is on the verge of wide clinical penetration for intravascular imaging; however, many clinical OCT applications are limited by multiple light scattering, in particular, in skin and mucous membranes. This complicates interpretation of diagnostic OCT images, especially by clinicians who may not be familiar with physical principles of OCT image formation. A convenient solution is image quantification, to provide an objective evaluation and to avoid subjective interpretation.

In this report we review our different approaches to quantification and classification of diagnostic OCT images in a variety of clinical sites. The images were obtained both by traditional and cross-polarization (CP) OCT modalities. The latter is sensitive to tissue depolarizing properties and birefringence, in part caused by collagen, thus providing additional diagnostic information. Illustrative examples include gynecology, otorhinolaryngology, urology, and cardiology.

Algorithms for numerical image processing and quantification can be derived from model experiments and simulation studies. A Monte Carlo model of 2D OCT images of different media for simulating OCT image texture was developed and validated with controlled phantom experiments. Both simulations and phantom results demonstrated that OCT image histograms characterizing speckle statistics are sensitive to optical properties of media for image quantification.

Texture analysis was applied to automated classification of diagnostic OCT images of fallopian tubes obtained in course of standard laparoscopy procedure. The use of image histogram statistics and OCT signal variation achieved diagnostic accuracy of 98%, compared to 63% for traditional laparoscopy. Application of neural network for image classification yielded an accuracy >93% in detecting tissue pathology.

In otorhinolaryngology, histogram analysis also demonstrated the ability to differentiate between normal tissue, vasomotor rhinitis, allergic rhinitis and subatrophy in diagnostic OCT images of nasal mucosa.

Some applications require evaluation of collagen state within biotissue (e.g., bladder cancer detection, atherosclerotic plaque risk assessment, skin ageing studies). Calculation of integral depolarization factor and birefringence from CP OCT images indicated high potential of OCT image quantification for these tasks, specifically detection of bladder cancer at scar, identification of vulnerable atherosclerotic plaques, and evaluation of the efficacy of anti-ageing photodynamic therapy (where traditional diagnostic techniques suffer from low accuracy). Atherosclerosis investigation included complementary numerical analysis of nonlinear laser scanning microscopy images, confirming CP OCT study results.

The study was supported by RFBR grant No. 15-32-20250, RSF grant No.14-15-00538, and the Ministry of Education and Science of the Russian Federation (grant 14.B25.31.0015).

BP-1-4 (Invited)

Modelling of speckle pattern formation in Optical Coherence Tomography with the Monte Carlo method

I. Meglinski[1,*] and A. Doronin[2]

[1]- Opto-Electronics and Measurement Techniques Laboratory, University of Oulu, Oulu 90014, Finland
[2]- Department of Computer Science, Yale University, P.O. Box 208285, New Haven, CT 06520-8285, USA
** Email: igor.meglinski@oulu.fi*

Optical Coherence Tomography (OCT) is used extensively in various medical applications, starting originally from ophthalmology and achieving vast expansion to other biomedical and clinical applications. Nowadays, there are many different technical embodiments of OCT systems that utilizing diverse optical engineering solutions and fundamental properties of light, such as coherence, polarization, interference, diffraction, and other. In spite of the variety of the developed experimental systems the images obtained by OCT very often include characteristic repetitive patterns, known as speckles. Speckles are the product of interference of light multiply scattered within the medium, and typically, in biomedical applications considered as an unwanted noise. Thus, the correct interpretation of OCT images, as well as the quantitative assessment of optical properties of scattering medium, require an ultimate understanding of OCT speckle patterns formation. Due to a complex structure of biological tissues exposing high scattering of light and its reflection/refraction on the surface and at the boundaries of the internal layers and inclusions the known analytical approaches are strictly limited to be applied for this purpose. The Monte Carlo (MC) method – a stochastic computational numerical technique is extensively used for modeling of light propagation in scattering media, and considered as a 'gold standard' for imitation of photons migration in biological tissues. MC modelling has also been introduced in the studies of OCT signal formation, although the coherent properties of probing light were not included in these simple computational models. Based on the extended Huygens-Fresnel principle [1] the spatial coherence properties of the sample field have been introduced in MC [2]. A plane wavelet formalism with phase recording for modelling OCT signals and speckles has been suggested in [3]. For the same purpose a modelling of OCT signal as a sum of stationary random phasors and treating it as a statistical signal has been reported in [4]. Polarization and temporal coherence of incident light has been introduced to MC OCT model in [5], and successfully used for modeling of 2D time-domain OCT (tdOCT) images of human skin [6]. The simulation of OCT speckles by convolving the point-spread function of the OCT system with the numerically synthesized random sample field has been suggested recently in [7]. In spite of quite intense development and implementation of MC modeling in OCT studies none of the previous models took into account interference of scattering waves that plays a critical role in the formation of swept-source OCT (ssOCT) signal [8]. In current report we discuss the swept-source OCT approach in terms of speckle pattern formation and introduce a new MC based model for simulation of OCT signals and images.

[1] H.T. Yura, "Signal-to-noise ratio of heterodyne lidar signal systems in the presence of atmospheric turbulence," Opt. Acta 26, 627 – 644 (1979).
[2] L. Thrane, H.T. Yura, and P.E. Andersen, "Analysis of optical coherence tomography systems based on the extended Huygens-Fresnel principle," J. Opt. Soc. Am. A 17, 484 – 490 (2000).
[3] Q. Lu, X. Gan, M. Gu, and Q. Luo, "Monte Carlo modeling of optical tomography imaging through turbid media," Appl. Opt. 43, 1628 – 1636 (2004).
[4] B. Karamata, K. Hassler, M. Laubscher, and T. Lasser, "Speckle statistics in optical coherence tomography," J. Opt. Soc. Am. A 22, 593 - 596 (2005).
[5] D.Y. Churmakov, V.L. Kuzmin, and I. Meglinski, "Application of the vector Monte Carlo method in Polarization Optical Coherence Tomography," Quantum Electron. 36, 1009 – 1015 (2006).
[6] I. Meglinski, M. Kirillin, V. Kuzmin, and R. Myllyla, "Simulation of polarization-sensitive optical coherence tomography images by a Monte Carlo method," Opt. Lett. 33, 1581 – 1583 (2008).
[7] X. Liu, J.C. Ramella-Roman, Y. Huang, Y. Guo, and J.U. Kang, "Robust spectral-domain optical coherence tomography speckle model and its cross-correlation coefficient analysis," J. Opt. Soc. Am. A 30, 51 - 59 (2013).
[8] C. Dainty, "Laser Speckle and Related Phenomena," (Springer Verlag, 1984).

BP-1-5 (Invited)

Tissue optical clearing for Enhancing performance of optical imaging: from in vitro to in vivo

Dan Zhu[1, 2]

1-Britton Chance Center for Biomedical Photonics, Wuhan National Laboratory for Optoelectronics

2-Key Laboratory of Biomedical Photonics of Ministry of Education, Department of Biomedical Engineering, Huazhong University of Science and Technology, Wuhan 430074, China

dawnzh@mail.hust.edu.cn

The optical technology has provided significant tool for molecular imaging and medical diagnosis with high sensitivity and resolution. However, the high scattering of turbid biological tissues limits the penetration of visible and near-infrared light in tissue, which affects its applicability in preclinical and clinical medicine, and other life science. The tissue optical clearing technique based on immersion of tissues into optical clearing agents (OCAs) with high refractive indices, hyperosmolarity and biocompatibility allows one to effectively control optical properties of tissues, leads to essential reduction of scattering, therefore, enhances the depth to which light penetrates in tissue, and currently attracts great attentions. This technique, combined with various optical techniques has shown a great potential for improving the capabilities of optical imaging, diagnosis and therapeutic treatments.

In this presentation, I will show some progress in tissue optical clearing for enhancing optical imaging performance. Combination of in vitro tissue optical clearing methods and various microscopies could obtain microstructure of tissue blocks without section. Moreover, in vivo skin and skull optical clearing methods access to vascular and cell function, such as blood flow, blood oxygen, vascular structure and cell movement by using laser speckle imaging, hyperspectral imaging, photoacoustic imaging and fluorescence imaging, respectively.

BP-2-1 (Invited)

Advances in tissue optics, laser medical imaging and treatment during optical clearing

Valery V. Tuchin

Research-Education Institute of Optics and Biophotonics,
Saratov National Research State University, Saratov 410012, Russia
Institute of Precision Mechanics and Control of Russian Academy of Sciences,
Saratov 410028, Russia
Interdisciplinary Laboratory on Biophotonics,
National Research Tomsk State University, Tomsk 634050, Russia

Advances of tissue optics and optical clearing (OC) for enhanced imaging of living tissues aiming laser medical imaging and treatment will be discussed. The OC technology is based on controllable and reversible modification of tissue optical properties by their impregnation by exogenous or endogenous optical clearing agents (OCAs) [1-4]. Impact of different OCAs on tissue dehydration, free and bound water migration in tissues and kinetics of tissue optical properties will be analyzed. The specific features of OC of different healthy and pathological tissues and blood flows investigated using OCT, different microscopies and spectroscopies, such as spectrophotometry, polarimetry, photoacoustic, linear and nonlinear fluorescence, and SHG, and speckle dynamic imaging will be discussed. Enhancement of probing depth and image contrast in *in vitro*, *ex vivo*, and *in vivo* studies of a variety of human and animal tissues, including skin, fat, muscle, digestive tract tissue, cartilage, bone, blood vessels, and blood will be demonstrated. The technologies of effective OCA delivery, including hidden free diffusion, local heating, hemoglobin injection, enforced tissue permeability (laser perforation), OCA encapsulation, and using blood and lymph vessel networking, will be also discussed. Examples of applications OC technology in clinical studies will be presented.

[1] D. Zhu, K. V. Larin, Q. Luo, and V. V. Tuchin, "Recent progress in tissue optical clearing," *Laser Photonics Rev*. **7**(5), 732–757 (2013).
[2] V.V. Tuchin, "*In vivo* optical flow cytometry and cell imaging," *Rivista Del Nuovo Cimento*, **37**(7), 375–416 (2014).
[3] E. A. Genina, A. N. Bashkatov, Yu. P. Sinichkin, I. Yu. Yanina, V.V. Tuchin, "Optical clearing of biological tissues: prospects of application in medical diagnostics and phototherapy [Review]," *J. Biomed. Photonics & Eng*. **1**(1), 22–58, 2015.
[4] V. V. Tuchin, "Polarized light interaction with tissues [Tutorial]," *J. Biomed. Opt*. **21**(7), 071114-1-37 (2016)

BP-2-2 (Invited)

Multimodal optical imaging of the injured brain

F. Bari, Á. Menyhárt, D. Zölei-Szénási, T. Puskás, E. Farkas

Department of Medical Physics, Faculty of Medicine, University of Szeged, Hungary
Main author email address:bari.ferenc@med.u-szeged.hu

Research Background: Ischemia-related spreading depolarizations (SDs) are part of the pathophysiology of cerebrovascular diseases and predict worse outcome. SDs may exacerbate ischemic injury via related atypical hemodynamic responses, but their consequences on tissue pH changes are not yet understood. The regulation of pH changes of neurons is crucial in both physiological and ischemic conditions, because acid loading makes them susceptible for injury. Therefore we set out to compare intracellular pH changes associated with SDs propagating across the intact and the ischemic cortex of rats, visualized by live optical brain imaging.
Aims: We set out to compare intracellular pH changes associated with SDs propagating across the intact and the ischemic cortex of rats, visualized by live optical brain imaging.
Methods: A closed cranial window was mounted over the right parietal bone of isoflurane anesthetized adult male Sprague-Dawley rats (n=13). The cranial window incorporated a glass capillary through which 1 µl 1M KCl was applied topically for SD elicitation. Neutral red (NR), a pH sensitive fluorescent dye was injected i.p. (35mM, 2 x 1 ml,) 30 min before the start of image acquisition. Following a baseline period of 50 min, transient global forebrain ischemia was created by 60 min of bilateral common carotid artery occlusion (2VO). SDs were elicited at 15 min intervals prior ischemia induction and during ischemia. Two separate CCD cameras, synchronized to suitable illumination, were used for the dual imaging of changes in cerebral blood flow (CBF, laser speckle contrast imaging) and intracellular pH (NR fluorescence intensity) (Fig. 1). The pH signal was validated with the use of traditional pH-sensitive electrodes in a separate set of rats.

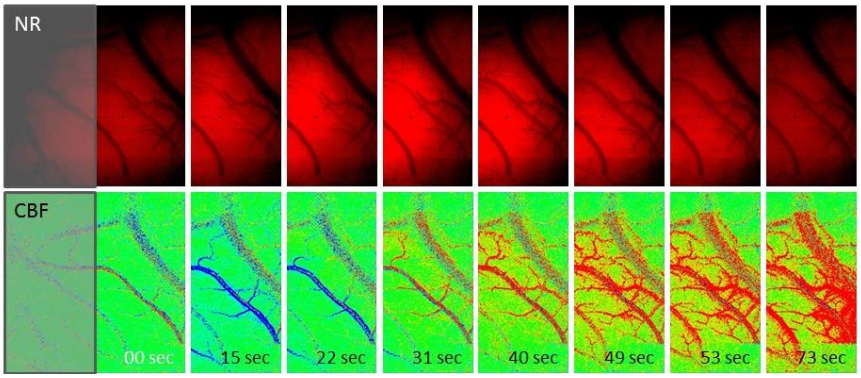

Figure 1. Sequential images of changes in pH (NR fluorescence) and cerebral blood flow (CBF) in the rat cerebral cortex.

Result: In both young and old groups, ischemia caused an acidic shift of 0.2 pH units, while reperfusion induced an alkalotic shift of 0.1 pH unit with respect to baseline. In the young group, ischemia significantly deepened the SD-related acidosis (6.65±0.12 vs. 6.91±0.09 unit, ischemia vs. baseline), and elongated its duration (3.55±1.08 vs. 1.47±0.27 min, ischemia vs. baseline). The SD-related pH variation during reperfusion was similar to baseline. In the old group, the SD-related acidosis was milder, especially during ischemia, indicated by a smaller peak (6.81±0.11 vs. 6.65±0.12 units, old vs. young.), and shorter duration (2.39±0.36 vs. 3.55±1.08 min, old vs. young).
Conclusions: Marked tissue acidosis correlates with the extent of brain injury, and has been traditionally considered as a damaging component of cerebral ischemia. On the other hand, mild acidosis appears to be neuroprotective by delaying SDs and limiting ischemic injury. We propose that the SD-associated, prominent, transient acidosis superimposed on ischemic acidosis worsens tissue survival, thereby rendering SDs malignant in cerebral ischemia. In contrast, the less pronounced pH changes with SDs in the non-ischemic cortex are suggested not to be harmful.

BP-2-3

In vivo deep-brain imaging with reconnectable neurointerfaces

I.V.Fedotov[1,2], M.S.Pochechuev[3], O.I.Ivashkina[2], M.A.Roshina[2], A.B.Fedotov[1,3], K.V.Anokhin[3], A.M.Zheltikov[1,2,3,4]

1 - Physics Department, International Laser Center, M.V. Lomonosov Moscow State University, Moscow 119992, Russia
2 - Kurchatov Institute National Reseacrch Center, pl.akad.Kurchatova 1, Moscow 123182, Russia
3 - Russian Quantum Center, ul. Novaya 100, Skolkovo, Moscow Region, 143025 Russia
4 - Department of Physics and Astronomy, Texas A&M University, College Station TX 77843, US

a.b.fedotov@phys.msu.ru, zheltikov@physics.msu.ru

Modern optics provides unique opportunities for the investigation of brain and higher nervous activity. The combination of advanced laser technologies and neurosciences is opening a new multi-disciplinary direction of natural sciences — neurophotonics. Neurophotonics is providing the development of a wide spectrum of tools for functional brain diagnostics, stimulation of individual neurons and neural networks, as well as molecular engineering of brain cells aimed at a diagnosis and therapy of neurodegenerative and psychic diseases. Optical fibers suggest unique approaches helping to confront the most challenging problems in brain research, including the analysis of cellular and molecular mechanisms behind memory and cognition. Optical fibers of new generation offer new solutions for the development of fundamentally new, unique tools for neurophotonics and laser neuroengineering — fiber-optic neuroendoscopes and neurointerfaces [1-3]. Neurointerfaces open new horizons for the investigation of the most complex brain functions, enabling a long-term multiplex detection of fluorescent protein markers, as well as photostimulation of neuronal activity in deep brain areas in living, freely behaving animals with an unprecedented spatial resolution and minimal invasiveness [4-6]. This emerging technology opens new horizons for understanding learning and long-term memory through experiments with living, freely behaving mammals.

In the present work, we demonstrate optical reconnectable neurointerface based on bundles of microscaled fibers integrated with scanning fast galvanometric mirrors. We used reconnectable neurointerface and different lines of transgenic mice for low invasive i*n vivo* experiments, that demonstrated multiplex visualization of marker proteins in the brain of freely moving animals with cellular space resolution at long temporal scale. This work was supported by the Program ‘Research and Development in Priority Areas of Development of the Russian Scientific and Technological Complex for 2014–2020’ (Contract 14.607.21.0092 of November 21, 2014; unique identifier of applied research: RFMEFI60714X00.

[1] E.S. Boyden, F. Zhang, E. Bamberg, G. Nagel, and K. Deisseroth, "Millisecond-timescale, genetically targeted optical control of neural activity." Nature Neuroscience, vol. **8**, pp.1263–1268 (2005).
[2] K. Deisseroth, “Optogenetics.” Nature Methods, vol.**8**, pp. 26–29 (2011).
[3] D.R. Sparta, A.M. Stamatakis, J.L. Phillips, N. Hovelsø, R. van Zessen, and G.D. Stuber, “Construction of implantable optical fibers for long-term optogenetic manipulation of neural circuits.” Nature Protocols, vol. **7**, pp.12 – 23 (2012).
[4] L.V. Doronina-Amitonova, I. V. Fedotov, O. I. Ivashkina, M. A. Zots, A. B. Fedotov, K. V. Anokhin, and A. M. Zheltikov, "Implantable fiber-optic interface for parallel multisite long-term optical dynamic brain interrogation in freely moving mice." Scientific Reports. vol. 3, n.3265 (2013).
[5] L.V. Doronina-Amitonova, I.V. Fedotov, O.I. Ivashkina, M.A. Zots, A.B. Fedotov, K.V. Anokhin, and A.M. Zheltikov. “Enhancing the locality of optical interrogation with photonic-crystal fibers.“ Applied Physics Letters. vol.101, pp. 021114 (2012).
[6] L.V.Doronina-Amitonova, I.V.Fedotov, A.B.Fedotov, K.V.Anokhin, A.M.Zheltikov. “Neurophotonics: optical methods to study and control the brain.” Physics-Uspehi. vol. 58, pp. 345–364 (2015).

BP-2-4 (Invited)

Microvascular Blood Flow Autoregulation Quantified with Near-Infrared Spectroscopy

A. Ruesch[1], M. Smith[2], G. Wollstein[2], I. Sigal[2], S. Nelson[2], J.M. Kainerstorfer[1]

1- Department of Biomedical Engineering, Carnegie Mellon University, 5000 Forbes Avenue, Pittsburgh, PA 15213
2- Department of Ophthalmology, University of Pittsburgh, Eye and Ear Institute, 3 Lothrop Street, Pittsburgh, PA 15213
jkainers@andrew.cmu.edu

Cerebral autoregulation (CA) is the mechanism that maintains cerebral blood supply, hence cerebral blood flow (CBF), approximately constant despite changes in mean arterial blood pressure (MAP) or, more precisely, despite changes in cerebral perfusion pressure (CPP) (defined as the difference between MAP and intracranial pressure (ICP)) [1-3]. Maintaining an adequate blood perfusion is of paramount importance for brain health and the mechanism of CA is known to be impaired in a variety of diseases, such as stroke and traumatic brain injury.

Typically, CA can be quantified based on continuous measurements of systemic mean arterial blood pressure (MAP) and global cerebral blood flow (CBF), where the time delay between low frequency changes in MAP and CBF is indicative of CA. Recently, we have demonstrated that near-infrared spectroscopy (NIRS) has the potential to be used to quantify CA [4]. Since NIRS is sensitive to microvascular changes in oxy- [$\Delta HbO(t)$], deoxy- [$\Delta Hb(t)$], and total- [$\Delta HbT(t)$] hemoglobin concentration, which are related to CBF changes, we used a modeling approach to disentangle contributions from CBF and cerebral blood volume (CBV) changes. With this, combined with continuous MAP recordings, we performed measurements on healthy volunteers during hyperventilation, which is known to enhance CA. Based on a high pass filter analysis between ΔHbT and changes in CBF (related to ΔHbO), we demonstrated enhanced CA with hyperventilation as quantified with NIRS measurements. CA is known to be an important indicator of cerebral health, but the limits of CPP where CA is valid are typically not known, but thought to be valid within 50 to 150mmHg.

Typically MAP changes are induced in order to induce changes in CPP and to quantify CA. However, changes in ICP, leading to MAP changes, are characteristic in traumatic brain injury. How changes in ICP, leading MAP changes, influence CA is not well understood. To address this question, we performed measurements on non-human primates (n=4). A frequency domain NIRS system (ISS Inc.) was used to measure cerebral hemodynamic changes, while recording MAP and ICP. Changes in ICP have been induced via cannulating the brain and responses in hemodynamic and systemic signals have been recorded. Figure 1 shows an example of such changes, where the measured $\Delta HbT(t)$ signals are highly correlated to changes in $CPP(t)$. We will present results from this NIRS based approach for quantifying CA as well as the analytical model used for analysis. Furthermore, we will demonstrate the potential ability of NIRS to monitor ICP changes without the need of invasive ICP monitors.

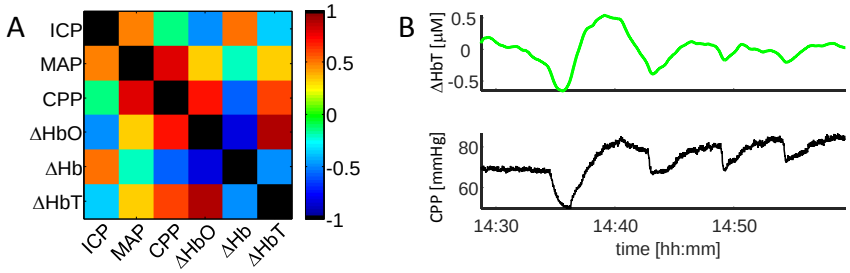

Figure 1. (A) Correlation map of NIRS measured hemodynamic signals and ICP, CPP, and MAP. ICP was modulated around a baseline value of ICP_0=8mmHg. (B) Time traces of measured $\Delta HbT(t)$ and $CPP(t)$. A high correlation is seen between them.

[1] Lassen NA. Cerebral blood flow and oxygen consumption in man. Physiol Rev, 39(2)**:** 183-238, (1959)
[2] Paulson OB, Strandgaard S, Edvinsson L. Cerebral autoregulation. Cerebrovasc Brain Metab Rev, 2(2)**:** 161-192 (1990)
[3] Panerai RB. Assessment of cerebral pressure autoregulation in humans--a review of measurement methods. Physiol Meas, 19(3)**:** 305-338, (1998)
[4] Kainerstorfer JM, Sassaroli A, Tgavalekos KT, Fantini S. Cerebral autoregulation in the microvasculature measured with near-infrared spectroscopy, J Cereb Blood Flow Metab, 35(6), 959-66, (2015)

BP-2-5 (Invited)

Multi-laser illumination designs for skin chromophore mapping

J.Spigulis

Biophotonics Laboratory, Institute of Atomic Physics and Spectroscopy, University of Latvia

Raina Blvd.19, Riga, LV-1586, Latvia

janis.spigulis@lu.lv

Use of lasers for spectrally specific illumination is a challenging but still undeveloped area of laser technologies. There are several interesting applications of laser illumination, one of them – monochromatic spectral imaging. We have shown that three monochromatic spectral images can be extracted from a single RGB image data set at simultaneous three-wavelength illumination [1,2]. It allows mapping the spatial distribution of three different chromophores of the object – e.g. painting, unknown material or living tissue - by a single snapshot. As concerned to a living tissue, the shorter is acquisition time of the spectral image data set, the lower is probability of image motion artefacts to be corrected afterwards. On the other hand, the narrower are the selected spectral bands, the higher is performance and reliability of spectral imaging and the subsequent parametric mapping. Consequently, single-snapshot monochromatic spectral imaging at fixed wavelengths appears a promising technology for less expensive, faster and more reliable parametric mapping of *in-vivo* skin features. Viability of this concept recently has been confirmed experimentally by means of a table-top RGB camera setup that provided simultaneous illumination of skin by the 473nm, 532 nm and 659 nm laser lines; physiologically reasonable distribution maps of melanin, oxy-hemoglobin and deoxy-hemoglobin in pigmented and vascular skin lesions have been obtained [3]. We have also demonstrated how the RGB single-snapshot approach for skin chromophore mapping can be implemented in a mobile system comprising a smartphone with appropriate software and attached three-wavelength illuminator [4].

Three optical designs of laser 3-wavelength skin illumination systems will be discussed in this presentation: (i) multi-fiber ring direct illuminator, (ii) diffusive ring illuminator with six radial input laser beams, (iii) illuminator based on vibrating mirror with a diffusive coating. Advantages and drawbacks of each design option (e.g. uniformity of illumination, formation of laser speckles) will be analysed, as well as their application prospects in clinical dermatology, cosmetology, oncology, post-surgery recovery monitoring and forensics.

This study was supported by the Latvian national research program SOPHIS under the grant agreement #10-4/VPP-4/11.

[1] J.Spigulis and L.Elste,"Single snapshot RGB multispectral imaging at fixed wavelengths: proof of concept", *Proc.SPIE*, 8937, 89370L (2014).
[2] WO 2013135311 (A1), 2012.
[3] J.Spigulis andI.Oshina, "Snapshot RGB mapping of skin melanin and hemoglobin", *J.Biomed.Opt*., 20(5), 050503 (2015).
[4] J.Spigulis, I.Oshina and Z.Rupenheits, "Smartphone single-snapshot mapping of skin chromophores", *Biomedical Optics 2016***,** OSA Technical Digest (online), JTu3A.46, doi:10.1364/CANCER.2016.JTu3A.46 (2016).

BP-3-1 (Invited)

WREAKING HAVOC WITH POLARIZED LIGHT – MUELLER MATRIX POLARIMETRY IN BIOLOGICAL TISSUES

Alex Vitkin, Adam Gribble, and Arash Zarrine-Afsar

University of Toronto / Princess Margaret Cancer Centre

vitkin@uhnres.utoronto.ca

Polarized light is a sensitive tool for measuring various important biophysical tissue properties, for example its state of organization / heterogeneity revealed by depolarization, and anisotropy/alignment revealed by birefringence. Mueller matrix methodology is one embodiment of polarimetry that offers particularly rich tissue characterization information. Biomedical applications of this approach include measurements of connective tissue remodeling during breast cancer development and spread, and rapid wide-field guidance for molecularly-sensitive mass spectrometry for tumour margin assessment. In this talk, we discuss the enabling technology for Mueller matrix polarimetric imaging and illustrate its use with selected preclinical examples.

BP-3-2 (Invited)

Seeing Invisible Cells in 3D without Labelling - New Horizons in In-Vitro Fertilization and Cancer Monitoring

Natan T. Shaked

Department of Biomedical Engineering, Faculty of Engineering, Tel Aviv University, Tel Aviv 69978, Israel

nshaked@tau.ac.il
www.eng.tau.ac.il/~omni

One of the major challenges in the field of optical imaging of live cells is to achieve label-free but still fully quantitative measurements, which afford high-resolution morphological mapping at the single cell level. In particular, developing efficient, non-subjective, quantitative optical imaging technologies for single-cell imaging with clinical value is a challenging task. Live biological cells are three-dimensional (3D) dynamic microscopic objects that constantly adjust their sizes, shapes and other biophysical features. Visualizing cellular phenomena requires microscopic techniques that can achieve high data acquisition rates, while retaining both resolution and contrast to observe fine cellular features. However, cells *in vitro* are mostly-transparent 3D objects with absorbance and reflection characteristics that are very similar to their surroundings, and thus conventional intensity-based light microscopy approaches lack the required sensitivity. Conventional phase contrast imaging methods, such as Zernike's phase contrast and differential interference contrast, are not quantitative, and present significant imaging artefacts. Exogenous labelling agents such as fluorescent dyes can be used to improve contrast. However, fluorescent agents tend to photo-bleach, reducing the available imaging time. Other concerns include cytotoxicity and the possibility that the exogenous agents will influence cellular behavior. Still, the widely used methods for detection and diagnosis of medical conditions in the cellular level cancer are based on indirect and subjective histological and cytological examination of tissues or samples from bodily fluids. Alternatively, if the sample has to stay alive, such as in sperm selection for *in-vitro* fertilization, the cells cannot be well visualized. In this lecture, I will review our latest advances in developing new imaging modalities to achieve affordable label-free but still fully quantitative measurements, which offer high-resolution morphological and mechanical mapping of dynamic cells. Optical interferometry is able to provide a platform to imaging live cells quantitatively without the risk of effects caused by using external contrast agents. This is done by capturing the sample quantitative thickness and refractive index map via recording its interferogram. By overcoming critical technological barriers, we suggest novel hybrid optical interferometric approaches that provide a powerful nano-sensing tool for label-free quantitative measurement of live cells. I will review two specific applications with a great clinical value: cancer monitoring and sperm selection in *in-vitro* fertilization. First, we developed rapid interferometric tomographic approach for fully capturing the cell 3D refractive-index distribution [1], as a potential tool to characterize cancer cell nucleus changes during cancer progression. In this tool, interferometry is combined with micro-manipulation of single cells to enable cell rotation, providing label-free 3D imaging of non-adherent cells. Furthermore, we have lately presented a portable interferometric module, using which it is possible to significantly enhance the selection of sperm cells for injection into the female egg during *in-vitro* fertilization. Using this module, we have shown that label-free interferometry can characterize sperm cells as good as label-based imaging [2]. The parameters provided are expected to pave the way to new clinical diagnosis and monitoring tools in the single-cell level.

[1] M. Habaza, B. Gilboa, Y. Roichman, and N. T. Shaked, Tomographic phase microscopy with 180° rotation of live cells in suspension by holographic optical tweezers, Optics Letters, vol. 40, pp. 1881-1884 (2015).
[2] M. Haifler, P. Girshovitz, G. Band, G. Dardikman, I. Madjar, and N. T. Shaked, Interferometric phase microscopy for label-free morphological evaluation of sperm cells, Fertility and Sterility, vol. 104, pp. 43-47 (2015).

BP-3-3 (Invited)

Simultaneous Raman scattering and quantitative phase imaging as label-free probes of immune cells

N. Pavillon, A.J. Hobro, N. Smith

Biophotonics Laboratory, IFReC, Osaka University, 3-1, Suita, Osaka, Japan

nsmith@ap.eng.osaka-u.ac.jp

Multimodal imaging techniques are useful for imaging living cells, particularly since the cell samples impose limits on the amount of laser power or physical conditions that can be used for measurements. After optimizing one imaging mode, say for signal-to-noise, or resolution, it makes sense to diversify and attempt to retrieve different types of information from the cell. In our institute, we are interested in the fundamental nature of immune cells, and how they react to during and after their exposure to pathogen-associated triggers. Using Raman spectroscopic imaging, we enable a label-free map of the molecular distribution of the cell. This allows us to distinguish different cell types, or determine chemically distinct locations of interest in a given cell. It can be measured in a time-resolved manner, so that the spatiotemporal evolution of the chemical response to stress or pathogens can be mapped. However, due to the inherently low probability of Raman scattering, the emitted signal is generally low, and can only be increased by either increasing the excitation power or by changing the type of Raman scattering. Increases in power are usually already limited by sample damage considerations, while plasmonic, or coherent excitation changes the nature of the detected spectra. For this reason, we evaluate other modes that can be applied simultaneously with the spectral measurements [1]. Using digital holographic microscopy with an excitation wavelength longer than the Raman spectral region of interest, we can measure quantitative phase from the sample at approximately video rates [2]. This gives a rapid view of sample morphology, which is already a sufficient motivation, but furthermore it also allows us to measure a more complete set of information. This is because the molecular contributions to the phase image data are not exactly the same as the molecules that contribute most strongly to Raman imaging [3]. The use of both sets of information also allows high-throughput analysis [4]. These types of measurements are highly useful for analysis of pathogen associated triggers of immune response as well as to investigate the response of active cells to stimulation by recognizable pathogens such as bacteria or malarial byproducts [5, 6].

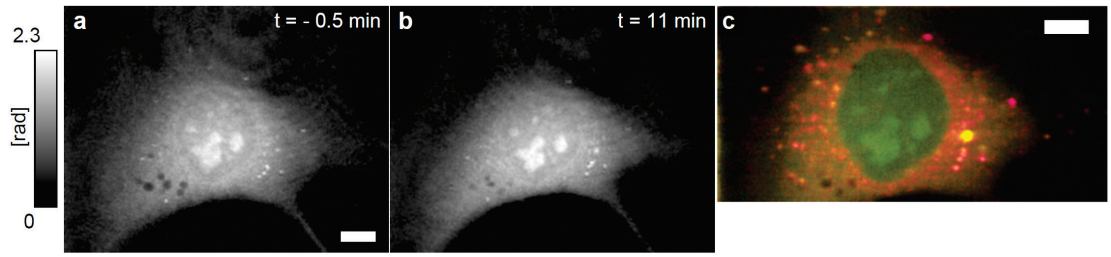

Fig. 1. Simultaneous digital holographic (quantitative phase) and Raman scattering image of a live mouse embryonic fibroblast cell. From Pavillon et al, see Reference [2] for details. Scale bars are 10μm. The Raman image contains a red channel corresponding to lipids with a Raman shift of 2865cm-1, and for contrast the green channel corresponding to C-H stretching lipid and protein molecules with a Raman shift of 2973cm-1.

[1] N. Pavillon, K. Fujita and N. I. Smith, "Multimodal Label-free Microscopy", J. Innov. Opt. Health Sci. 7(5), pp. 1330009-1-22, 2014.
[2] N Pavillon, NI Smith, Implementation of simultaneous quantitative phase with Raman imaging, EPJ Techniques and Instrumentation 2 (1), 1-11, 2015
[3] N. Pavillon, A. Hobro, and N. Smith, "Cell Optical Density and Molecular Composition Revealed by Simultaneous Multimodal Label-Free Imaging," Biophys. J., 105, 1123-1132, 2013.
[4] N. Pavillon and N. I. Smith, "Maximizing throughput in label-free microspectroscopy with hybrid Raman imaging", J. Biomed. Opt. 20(1), pp. 016007-1-016007-10, 2015.
[5] A. J. Hobro, A. Konishi, C. Coban and N. I. Smith, "Raman spectroscopic analysis of malaria disease progression via blood and plasma samples", Analyst 138(14), pp. 3927-3933, 2013
[6] A. J. Hobro, N. Pavillon, K. Fujita, M. Ozkan, C. Coban and N. I. Smith, "Label-free Raman imaging of the macrophage response to the malaria pigment hemozoin", Analyst 140, pp. 2350-2359, 2015.

BP-3-4 (Invited)

Thermogenetic activation of individual cells and neurons by infrared and microwave radiation

A.B.Fedotov[1,2], Yu.G.Ermakova[3], I.V.Fedotov[1,2], A.A.Lanin[1,2], V.V.Belousov[3], A.M.Zheltikov[1,2,4]

1 - Physics Department, International Laser Center, M.V. Lomonosov Moscow State University, Moscow 119992, Russia
2 - Russian Quantum Center, ul. Novaya 100, Skolkovo, Moscow Region, 143025 Russia
3 - M.M. Shemyakin and Yu.A. Ovchinnikov Institute of Bioorganic Chemistry, Russian Academy of Sciences, Moscow 117997, Russia
4 - Department of Physics and Astronomy, Texas A&M University, College Station TX 77843, US

a.b.fedotov@phys.msu.ru, zheltikov@physics.msu.ru

Modern technologies enabling precision control over the electrical activity of specific cells or neurons in a living organism offer unique opportunities for the functional analysis of complex biological systems. Thermogenetics is a promising innovative neurostimulation technique, which enables a robust activation of cells and neurons using thermosensitive transient receptor potential (TRP) cation channels [1, 2]. The TRP channels are three orders of magnitude more conductive than conventionally associated with optogenetic channelrhodopsin (ChR) channels and can be activated by heat induced with infrared light [3]. However, a broader application of this approach is hindered by a limited variety of suitable ion channels, as well as by low spatial and temporal resolution.

In the present study, we demonstrate addressed thermogenetic activation of individual cells and neurons using infrared radiation and microwave field. We use TRPA1 channels from snakes as a thermogenetic stimulator of Human Embryonic Kidney 293 (HEK-293) cells, mouse neurons, as well for induction of zebrafish larvae behavioral response. To investigate addressed heating of the transfected cells and neurons by infrared radiation, we used tunable radiation at wavelengths from 1.1 to 1.5 μm that the infrared radiation could be focused to a spot with the diameter about 30 μm, that guaranteed heating of single cell. The neuronal response to the activation by IR laser radiation is fully characterized by means of Ca^{2+} imaging technique. A unique fiber-optic probe that integrates a nitrogen–vacancy diamond quantum sensor with optical and microwave waveguide delivery enables thermometry with a single-cell resolution, allowing neurons to be activated by exceptionally mild heating, thus preventing toxic effects of excessive heat [4]. From the other hand, in specific regimes, this fiber probe can operate as the local source of the heat and microwave radiation enabling changing of the temperature and addressed activation of transfected cells and neurons.

With this arsenal, we carried out a systematic, in-depth characterization of the performance of TRPA1 channels in HEK-293 cells and neurons, including accurate measurements of the pertinent Ca^{2+} dynamics and electrophysiological analysis of the response. Our study demonstrates that the snake TRPA1 channels are ideally suited as a tool for addressed thermogenetics of individual cells, neurons in living animals. The work was supported by Russian Foundation for Basic Research (projects 14-29-07263, 14-29-07182, 16-32-80141). Research into thermogenetic stimulation of TRPA1 expressing cells has been supported by the Russian Scientific Foundation (project No. 14-14-00747).

[1] J.G.Bernstein, P.A.Garrity, E.S.Boyden. Optogenetics and thermogenetics: technologies for controlling the activity of targeted cells within intact neural circuits. Current Opinion in Neurobiology, vol. 22, pp. 61-71 (2012).
[2] E.O.Gracheva, N. T. Ingolia, Y. M. Kelly, et al., Molecular basis of infrared detection by snakes. Nature. vol. 464, pp. 1006-1001 (2010).
[3] D.E.Bath, J.R.Stowers, D.Hormann, A.Straw. FlyMAD: rapid thermogenetic control of neuronal activity in freely walking Drosophila. Nature methods vol. 11, pp. 756-762 (2014).
[4] I.V. Fedotov, N.A.Safronov, Yu.G.Ermakova, et.al., Fiber-optic control and thermometry of single-cell thermosensation logic. Scientific reports. vol. 5, n.15737 (2015).

BP-3-5 (Invited)

Raman Spectroscopic signature of life states in biological systems

Yu-Chung Lin, Chang-You Song, Chia-Liang Cheng*

Department of Physics, National Dong Hwa University, Hualien 97401, Taiwan

**Email: clcheng@mail.ndhu.edu.tw*

A systematic methodology to evaluate the feasibility of using the non-invasive Raman spectroscopy nature in accessing the life states of biological objects is developed. Previously, an *in vivo* Raman spectroscopic study of Amoeba (Acanthamoeba polyphaga) was presented. The changes of the spectra during the Amoeba cystactivation and excystation stages were analyzed. The spectra show the changes of the relative intensities of bands for protein, lipid and carotenoid components during cyst activation. The presence of carotenoids in the Amoeba is observed *via* characteristic Raman bands. These signals in the Raman spectra are intense in cysts but decrease in intensity with cyst activation and exhibit a correlation with the life cycle of Amoeba. This work indicates the feasibility of using Raman spectroscopy for the detection of single Amoeba microorganisms *in vivo* and for the analysis of the Amoeba life activity. It also shows the intensity level of carotenoid component and its Raman signals are directly linked to the life states of the microorganism.

To further test and implement this model, we examined several biological systems on the evolution of carotenoid Raman signals regarding its life states; bio-systems including Triops shrimps, zebrafish, mung bean and Aeolosoma were investigated. These are of very different biological objects ranging from small animal, plant, and microorganism. We found the unique characteristics of carotenoid relate to different stages of life in these specimens. Therefore, not only does carotenoid play important role in the life forms' activities, but it also serves as a unique signal to the development of the life forms we examined. The information obtained may have implications for the estimation of epidemiological situations, and a unique biological marker for the diagnostics of life stages in these biological objects.

BP-4-1 (Invited)

Laser Microscope Imaging

Colin J. R. Sheppard
Department of Nanophysics, Istituto Italiano di Tecnologia, Genova 16163, Italy

Image scanning microscopy (ISM) is a fast-developing topic in biological imaging, giving simultaneous improvements in both resolution and signal level compared with confocal microscopy, whilst retaining the confocal optical sectioning property [1-3]. It can be considered as a variant of confocal microscopy, with the pinhole replaced by a detector array. The fundamental principle is based on the concept of pixel reassignment, where an individual detector pixel gives an image of a different point of the sample than that directly illuminated. ISM can also be performed with multiple beam illumination, as in the spinning disk microscope, in which case it can be considered as a form of structured illumination microscopy.

Focal modulation microscopy (FMM) is a development of confocal microscopy that improves penetration into scattering media such as tissue [4]. Interestingly, it can also result in an improved spatial resolution [5]. It can be considered as a scanning form of structured illumination microscope, where the illuminating fringe pattern is contained within an envelope determined by the focal spot.

Both ISM and FMM also result in an image sampling rate that is four times the illumination sampling rate, thus increasing the effective imaging speed.

[1] C. J. R. Sheppard, "Super-resolution in confocal imaging," Optik **80**, 53-54 (1988).
[2] C. B. Müller and J. Enderlein, "Image scanning microscopy," Phys. Rev. Letts. **104**, 198101 (2010).
[3] C. J. R. Sheppard, S. B. Mehta, and R. Heintzmann, "Superresolution by image scanning microscopy using pixel reassignment," Opt. Letters **38**, 2889-2892 (2013).
[4] N. G. Chen, C. H. Wong, and C. J. R. Sheppard, "Focal modulation microscopy," Optics Express **16**, 18764-18769 (2008).
[5] W. Gong, K. Si, N. G. Chen, and C. J. R. Sheppard, "Improved spatial resolution in fluorescence focal modulation microscopy," Opt. Lett. **34**, 3508-3510 (2009).

BP-4-2 (Invited)

Shaped Light for Light Sheet Imaging

K. Dholakia

SUPA, School of Physics & Astronomy, University of St Andrews, North Haugh, St Andrews, Fife, KY16 9SS, UK

Main author email address: kd1@st-andrews.ac.uk

Optically based methods for imaging have gained major visibility in the last decade. However in many photonics fields there is a recognition that using the direct form a laser output – the Gaussian beam – is restrictive for a number of applications in biophotonics including manipulation, imaging and beyond [1]. I will describe the use of shaped light fields namely propagation invariant ('non-diffracting') light fields and complex beam shaping. Propagation invariant light fields, as the name suggests retain their transverse intensity profile upon propagation. Bessel light fields and Airy light fields are prime examples of such beams. This talk will describe use of shaped beams and new uses of materials science for enhanced optical manipulation of particles.

In terms of imaging, single plane illumination (light sheet) microscopy (SPIM) offers a myriad of unique advantages. Orthogonal detection allows rapid imaging of large, three-dimensional, samples of living tissue. Illumination with a thin sheet of light ensures high contrast by minimizing the fluorescent background. Moreover, by restricting the sample exposure to a single plane, photo-bleaching and damage are minimized. This is crucial when imaging photo-sensitive samples over a larger period of time. Recent enhancements to the original technique attempt to overcome the inherent trade off between axial resolution and field-of-view of conventional light sheet microscopy. Until recently, this was only achieved by compromising on one or more of its key advantages: high contrast, time-resolution, or minimal sample exposure. I will discuss the use of propagation invariant light fields for the enhancement within this imaging modality [2-4] and discuss the latest advances, for depth penetration and development of compact geometries.

References

[1] K Dholakia & T. Čižmár, "Shaping the future of manipulation. Nature Photonics 5, 335 (2011)

[2] T.A. Planchon et al. "Rapid three-dimensional isotropic imaging of living cells using Bessel beam plane illumination" Nature Methods 8, 417 (2011)

[3] T. Vettenburg et al. "Light sheet microscopy using an Airy beam", Nature Methods 11, 541 (2014)

[4] Zhengyi Yang, Martynas Prokopas, Jonathan Nylk, Clara Coll-Llado, Frank J. Gunn-Moore, David E.K.Ferrier, Tom Vettenburg and Kishan Dholakia: "A compact Airy beam light sheet microscope with a tilted cylindrical lens", Biomedical Optics Express, 10, (5), 3435 (2014)

BP-4-3 (Invited)

Axial tomography in Live Cell Laser Microscopy

Herbert Schneckenburger[1], Sarah Bruns[1], Thomas Bruns[1], Verena Richter[1], Petra Weber[1], Christoph Cremer[2]

[1]Aalen University, Institute of Applied Research, Beethovenstr. 1, 73430 Aalen, Germany
[2]Institute of Pharmacy and Molecular Biology, University of Heidelberg, 69120 Heidelberg, Germany

corresponding author: herbert.schneckenburger@htw-aalen.de

Single cell microscopy in a 3-dimensional environment is reported. Cells are grown in an agarose culture gel, located within micro-capillaries and observed from different sides using an innovative device for sample rotation [1]. Thus, z-stacks can be recorded (by confocal laser scanning microscopy, structured illumination or light sheet microscopy) in different directions and used for illustration in 3 dimensions. This gives additional information, since cells or organelles which appear superimposed in one direction, may be well resolved in another one. In addition, an increased optical resolution in lateral direction compared to axial direction can be utilized upon rotation, which represents an important step towards super-resolution microscopy of living cells.

In Figure 1 3D projections of an image stack of single cells are depicted for eight different observation angles (lower part) and compared with images which were recorded under 0° and calculated for the other angles (upper part), thus revealing a pronounced increase of image quality. The method was further tested and validated with single cells expressing a mitochondrially associated green fluorescent protein or cells accumulating fluorescent quantum dots. In addition, uptake of the cytostatic drug doxorubicin in HeLa cells was examined. This drug was rapidly accumulated in the cell nucleus (2-6 h after incubation) and re-localized in the cytoplasm after longer incubation times (24 h).

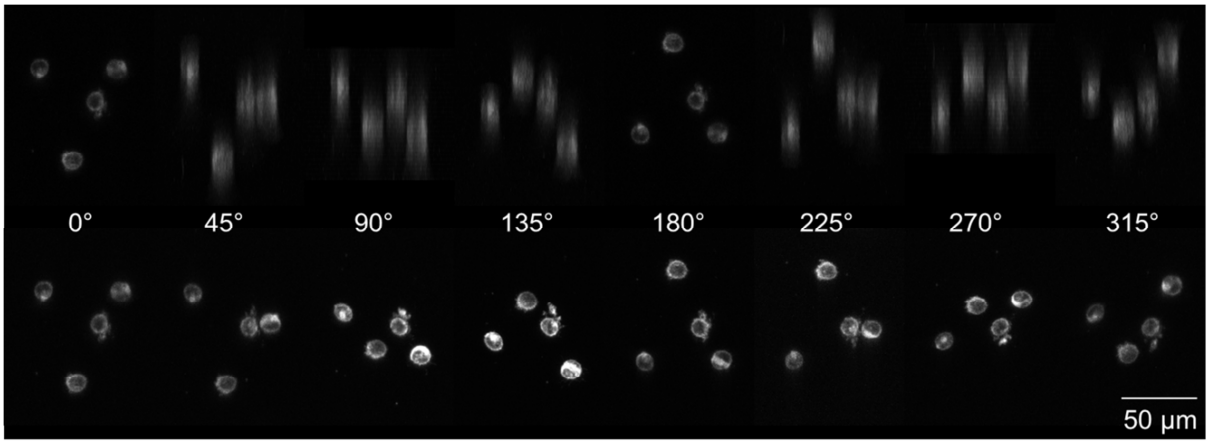

Figure 1. CHO-pAcGFP1-Mem single cells with membrane associated green fluorescent protein in agarose matrix upon observation under one angle and calculation for the other angles (top) or observation under 8 angles in 45° steps (bottom). Each image corresponds to a z projection of 31-36 individual images with $\Delta z = 3.13$ µm (excitation wavelength: $\lambda_{ex} = 488$ nm; detection: $\lambda_d \geq 505$ nm; 20x/0.5 objective lens).

Reference

T. Bruns, S. Schickinger, H. Schneckenburger: Sample holder for axial rotation of specimens in 3D Microscopy, J. Microsc. 260(1) (2015) 30-36.

Label free visualization of sub-micron structure with nano-sensitivity

Sergey A. Alexandrov[1], James McGrath[1], Hrebesh Subhash[2], Francesca Boccafoschi[3], Cinzia Giannini[4] and Martin Leahy[1]

1-Tissue Optics & Microcirculation Imaging Group, School of Physics, National University of Ireland, Galway, Ireland

2-Colgate-Palmolive Global Technology Center, 909 River Road, Piscataway, NJ 08855 USA

3-Department of Health Sciences, University of Piemonte Orientale "A. Avogadro", 28100 Novara, Italy

4-Institute of Crystallography, National Research Council, via Amendola 122/O, Bari 70126 Italy

Main author email address: sergey.alexandrov@nuigalway.ie

Information about nanoscale structure is very important for understanding of fundamental properties of biological objects and early diagnosis of different pathologies. Nowadays nanoscopy is a rapidly developing area, but almost all currently known methods rely upon the contrast created by fluorescent labels attached to the object or molecule of interest. This causes limitations due to the impact of the label on the molecule and its environment as well as its applicability in vivo, particularly in humans.
A new label-free approach to probe three-dimensional structures at the nanoscale, based on spectral encoding of spatial frequency (SESF), has been developed. Super-resolution imaging, based on spectral encoding of the lateral spatial frequency, has been demonstrated [1]. Ability to reconstruct the axial (along depth) spatial frequency profiles for each point of the image with nano-sensitivity to structural changes was also shown [2], and adaptation of the SESF approach for depth resolved imaging was published [3,4]. Recently the SESF approach has been applied to break the diffraction limit and dramatically improve resolution in lateral direction [5]. Resolution of about 3 times better than the diffraction limit of the imaging system has been demonstrated experimentally.
Here we present an extension of the srSESF approach to be able to compare structure of different objects with nano-sensitivity to structural changes. We show that it is possible to resolve fine features, with separation in the lateral direction significantly less than the diffraction resolution limit, via detecting a difference between the axial (in depth direction) spatial frequency profile of the numerically synthesized structure and axial spatial frequency profile at points in the object we want to resolve. We demonstrate that this contrast mechanism is very sensitive to structural alterations and nanoscale changes in space and/or in time can be detected and visualized. Both results of numerical simulation and preliminary experimental results, including biological objects, will be presented.

[1] S. Alexandrov, S. Uttam, R. Bista, & Y. Liu, Spectral contrast imaging microscopy, Opt. Lett. vol.36, pp. 3323-3325 (2011).
[2] S. Alexandrov, S. Uttam, Bista, K. Staton, & Y. Liu, Spectral encoding of spatial frequency approach for characterization of nanoscale structures, Applied physics letters, vol.101, 033702 (2012).
[3] S. Uttam, S. Alexandrov, K. Bista, & Y. Liu, Tomographic imaging via spectral encoding of spatial frequency, Optics Express, vol.21, pp. 7488-7504 (2013).
[4] S. Alexandrov, H. Subhash, A. Zam, & M. Leahy, Nano-sensitive optical coherence tomography, Nanoscale, vol.6, pp. 3545-3549 (2014).
[5] S. Alexandrov, J. McGrath, H. Subhash, F. Boccafoschi, C. Giannini and M. Leahy, Novel approach for label free super-resolution imaging in far field, Sci. Rep., vol.5, 13274; doi: 10.1038/srep13274, (2015).

BP-4-5 (Invited)

Towards multimodal 3D digital histology

Francesco Saverio Pavone
LENS, Via N. Carrara 1, 50019 Sesto Fiorentino, Florence

One of the key aspects of the tissue pathology comprehension is related to the correlations between morphology and functionality, which is one of the major issues in oncology, for example, in the comprehensions of the mechanisms of tumor development. Also, the extension of digital histopathology images from 2D to 3D will help in the tridimensional comprehension of the pathology development.
Nowadays, there are several imaging techniques offering a complementary approach to visualize large area volumes. Each of those offers a different strategy and furnish complementary information.
We will show how light sheet microscopy will be useful in a correlative approach with other microscopies to move from sub micron details to whole organ imaging both on functional and morphological point of view, connecting the nano world to the macro one. Also, some techniques of sample preparation will be shown.

BP-4-6

Collagen organization assessment by polarization resolved second harmonic generation

R. Hristu, S.G. Stanciu, D.E. Tranca, G.A. Stanciu
Center for Microscopy-Microanalysis and Information Processing, University Politehnica of Bucharest,313 Splaiul Independentei, 060042, Bucharest, Romania

hristu_radu@yahoo.com

Imaging collagen in histopathological samples by polarization-resolved second harmonic (PSHG) generation microscopy enables a label-free and quantitative insight into collagen organization [1]. Going beyond simple intensity-based imaging by adding the incident laser polarization component and by applying different quantitative metrics such as the anisotropy factor, second harmonic signal provides information about arrangement and structure of collagen, information which would not be available from intensity measurements alone. With established approaches limited to calculating the anisotropy factor for only a single incident laser polarization, there are currently no general guidelines on how to select the best incident polarization. Here, we describe a broadly applicable methodology for choosing the best incident laser polarization for cancer assessment. This is achieved by combining polarization-resolved second harmonic generation and the collagen orientation index computed by Fast Fourier Transform (FFT) analysis of the images.

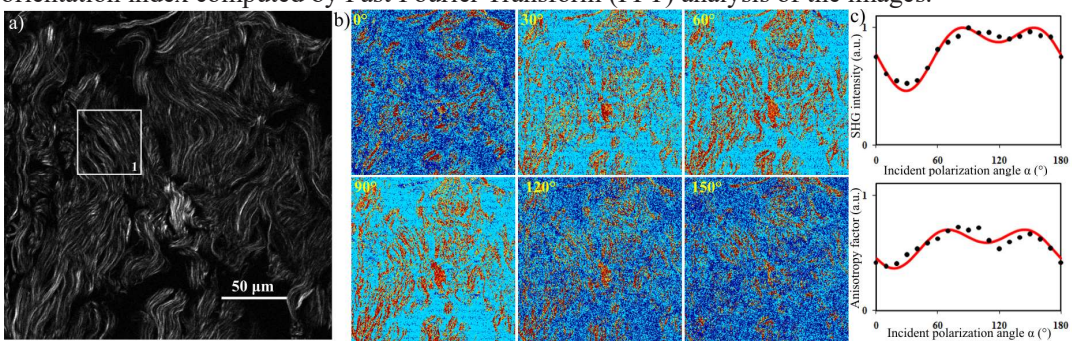

Fig. 1. SHG and anisotropy factor images for human skin samples prepared for the histopathological examination. (a) SHG image obtained as the sum of all the images acquired with tunable linear incident polarization; (b) Anisotropy maps for six different incident polarizations, displayed as a color-coded map, where the β values are represented from blue to red; (c) Laser polarization dependence of the average value of the SHG intensity and of the anisotropy factor for ROI1 in a).

We show that the anisotropy factor has a laser polarization dependence similar to the second harmonic intensity. For random distributions of collagen across the investigated areas the dependence is less evident, while for aligned collagen fibers, the anisotropy factor strongly depends on the incident laser polarization. Corroborating this information with the collagen orientation index computed from the FFT spectra of the PSHG images we propose a framework for choosing the optimal incident laser polarization for a better differentiation between dysplastic and cancer areas.

The proposed methodology is not only limited to skin samples but can also be implemented across various tissues. Our study advances the application of second harmonic generation microscopy towards quantitative, label-free imaging of collagen in tissue samples.

[1] X. Chen, O. Nadiarynkh, S. Plotnikov and P.J. Campagnola, Second harmonic generation microscopy for quantitative analysis of collagen fibrillar structure, Nature protocols, vol. 7, pp. 654-669(2012).

BP-4-7 (Invited)

Investigating changes in oxygen delivery with age with two-photon phosphorescence lifetime microscopy.

M. Moeini[1,2], A. Kakkar[3], F. Lesage[1,2]

1- Biomedical Engineering Institute, École Polytechnique de Montréal, Montréal, QC, Canada
2- Montreal Heart Institute, Montréal, QC, Canada
3- Department of Chemistry, McGill University, Montréal, QC, Canada

Main author email address: frederic.lesage@polymtl.ca

With increasing age, cognitive function declines even in healthy aging [1-4].Among important mechanisms, cerebrovascular function has been the subject of intense investigations due to the crucial role that brain vasculature has in oxygen supply to the neuronal units [5]. Thus, gradual changes in brain microvasculature and cerebral capillary blood flow occurring with aging may significantly contribute to cognition decline due to their role in brain tissue oxygenation. This work aimed to investigate vascular changes with age and concomitant changes in brain tissue pO_2. We measured capillary RBC dynamics in sensory-motor cortex of young, middle-aged and old mice under isoflurane anesthesia using two-photon fluorescence microscopy. It was observed that RBC velocity, RBC flux and hematocrit tend to increase until middle-age, but decline with further aging. In a separate cohort, we measured changes of brain tissue pO_2 using the O_2-sensitive phosphorescent probe PtP-C343 and two-photon phosphorescent lifetime microscopy under similar conditions. Our results show decreased tissue pO_2 near large vessels with age (Figure 1), which is accentuated after middle-age. On the other hand, tissue pO_2 in the capillary bed remains unchanged until middle-age, followed by a significant decrease afterwards. These findings suggest possible regulation of capillary blood flow until middle-age to maintain the capillary bed tissue pO_2 despite a decrease in arteriolar oxygen content.

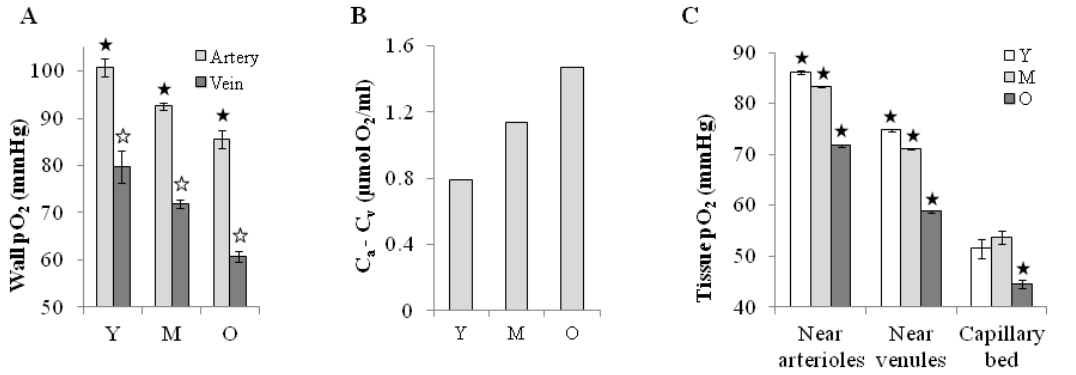

Figure 1. (A) Vascular wall pO_2 (mean±SEM) for the age groups. Star symbols indicate $p<0.003$ for age comparisons (black asterisk: arteriolar wall pO_2, white asterisk: venular wall pO_2). (B) Arteriovenous difference in total oxygen content for the age groups obtained by Eq. (2). (C) Average tissue pO_2 (mean±SEM) for the age groups near arterioles, near venules and in the capillary bed. Star symbols indicate $p<0.0003$ for age comparisons in each category.

[1] Bertsch, K., Hagemann, D., Hermes, M., Walter, C., Khan, R., Naumann, E., Resting cerebral blood flow, attention, and aging. Brain Res. 1267, 77–88, (2009)
[2] Cepeda, N.J., Kramer, A.F., Gonzalez de Sather, J.C., Changes in executive control across the life span: examination of task-switching performance. Dev. Psychol. 37, 715–30, (2001)
[3] Eustache, F., Rioux, P., Desgranges, B., Marchal, G., Petit-Taboué, M.-C., Dary, M., Lechevalier, B., Baron, J.-C., Healthy aging, memory subsystems and regional cerebral oxygen consumption. Neuropsychologia 33, 867–887.
[4] Hasher, L., Zacks, R.T., 1988. Working Memory, Comprehension, and Aging: A Review and a New View, in: Gordon H. Bower (Ed.), Psychology of Learning and Motivation. Academic Press, pp. 193–225, (1995)
[5] Kalaria, R.N., Cerebral vessels in ageing and Alzheimer's disease. Pharmacol. Ther. 72, 193–214, (1996).

BP-5-1 (Invited)

Non-linear transient absorption for sub-diffraction imaging

N. Liu[1], S. Daly[1], A. A. Mani[2], S. A. M. Tofail[1], A. Peremans[2], C. Silien[1]

1- Department of Physics, Bernal Institute, University of Limerick, Ireland

2- LaserSpec SPRL, Malonne, Belgium

christophe.silien@ul.ie

The development of optical microscopy in the 17th century allowed for a series of breakthroughs in life sciences including the discovery of cells and microbial life. After centuries of refinement, light imaging still remains a key instrument for the analysis of materials, and plays a major role in biological science as well as in the medical diagnosis. Near-field observations have allowed for unprecedented spatial resolution at surfaces with the resolution not limited by diffraction. Yet, far-field measurements remain preferable in most fields of application due to their flexibility to reliably map deep inside a specimen while remaining at practical distance from it. Remarkably, a series of methods are being developed to image samples in the far-field with super-resolution, which is beyond the optical bandwidth defined by the numerical aperture of the optics used for imaging. The Nobel Prize in Chemistry was awarded in 2014 for a series a breakthroughs leading to today's routine ability to image labelled fluorescent specimens at nano-resolution. At present, several groups across the world including ours are translating the teachings of super-resolution fluorescence to other chemical imaging modalities where fluorescent labels are not required and where the materials own physical properties are exploited for optical imaging. We will present an overview of our recent successes in the field (e.g. see Figure 1), specifically addressing our research in (transient) absorption micro-spectroscopy and in mid-infrared imaging [1].

Acknowledgements: The research leading to these results has received funding from the European Community's Seventh Framework Programme (FP7/20012-2015) under grant agreement n°280804. This communication reflects the views only of the authors, and the Commission cannot be held responsible for any use which may be made of the information contained therein.

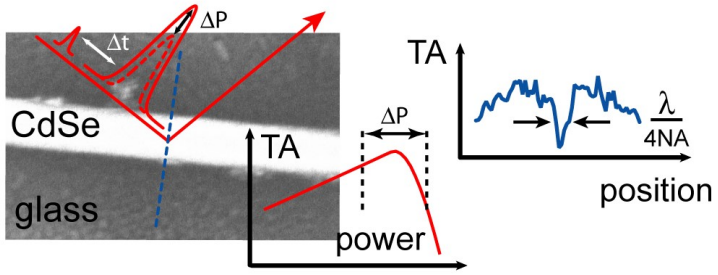

Figure 1: Scheme of super-resolution transient absorption microscopy showing pulse configuration, materials non-linear response and specimen image profile.

[1] N. Liu *et al.*, Far-Field Subdiffraction Imaging of Semiconductors Using Nonlinear Transient Absorption Differential Microscopy, ACS Photonics, vol. 3, pp. 478-485, (2016).

BP-5-2 (Invited)

High Precision, Organelle Targeted Luminescent Probes for Stimulated Emission Depletion (STED) Microscopy

Tia E.Keyes, Aisling Byrne and Chris Burke

School of Chemical Sciences, National Biophotonics and Imaging Platform, Dublin City University, Dublin 9, Ireland

Optical microscopy has played a fundamental role in interrogating live cells, tissues and other biological structures. However, the spatial resolution of classical microscopes is limited due to the light diffraction limit, where features closer than λ/2NA, (where λ is the wavelength of light and NA is the numerical aperture of the imaging lens) cannot be resolved. Stimulated emission depletion (STED) microscopy is one of a number of relatively new optical microscopy methods capable of breaking the diffraction limit. STED and related microscopies makes it possible to non-invasively image organelle structures and molecular dynamics at the nano-scale. However, STED makes a number of important demands on the luminescent contrast agents beyond those of normal fluorescence imaging and probe development for super-resolution microscopy has not kept pace with the evolution of these methods. Currently the fluorescent dyes used for labelling in STED are organic molecules which have short-lived emissive states, are prone to self-quenching at high concentrations, and tend to easily photo-bleach. Key properties associated with transition metal luminophores based on Ruthenium and Osmium such as a large stokes shift, long lived emission states, excellent photostability make them potentially very valuable as STED imaging probes. However, to date they have not been explored in this context, despite the strong need for improved probes. In this contribution we discuss the value of ruthenium (II)Polypyridyl complexes as imaging tools for STED microscopy. We describe reliable routes to specifically targeting such complexes to key organelles by conjugating signal peptides. And, the first STED images of the endoplasmic reticulum (ER) and nuclear DNA in HeLa cells using Ruthenium polypyridyl complexes as probes is described. We compare performance of these probes with a currently recommended probe for STED Alexa Fluor 53 and demonstrate a significant improvement in resolution between conventional confocal microscopy to the STED images, both using CW and pulsed STED. As a proof of principles we demonstrate the application of STED to imaging chromosomal DNA during the difference phases of cell division labelled with a ruthenium complex modified with a nuclear localisation signal.

References;

[1] Aisling Byrne and Christopher Steven Burke &Tia Keyes, Chem. Sci., 2016, DOI: 10.1039/C6SC02588A
[2] Aaron Martin, Aisling Byrne, Christopher S. Burke, Robert J. Forster and Tia E. Keyes, J. Am Chem Soc., 2014, 136, 15300-9.

BP-5-3 (Invited)

Seeing Bone Disease In New Light

A. W. Parker,[1,2,3] K. Sowoidnich[1], J. H. Churchwell[2], K. Buckley,[1,2,3]
J. G. Kerns,[2,3,4] J. Vinton,[3] P. D. Gikas,[2,3], P. Matousek[1,2,3] & A. E. Goodship[2]

1. Central Laser Facility, Research Complex at Harwell, STFC Rutherford Appleton Laboratory, Harwell Oxford, OX11 0FA, U.K.

2. UCL Institute of Orthopaedics and Musculoskeletal Science, London, HA7 4LP, U.K. 3. Royal National Orthopaedic Hospital, Stanmore, HA7 4LP, U.K.

4. Lancaster Medical School, Lancaster University, Lancaster, LA1 4YG, U.K.

In terms of bone disease Raman spectroscopy has several advantages over currently used X-ray based methods. Raman enables chemically specific information to be gained on both the mineral and organic phases of bone as well as being an optical based spectroscopy that avoids ionising radiation. Spatially Offset Raman Spectroscopy (SORS) enables interrogating the chemical make-up of materials beneath a sample surface thus permitting the analysis of bone non-invasively.

At the Royal National Orthopaedic Hospital, Stanmore over the last 5 years we have performed both *in-vivo* and *ex-vivo* investigations of bone using SORS and Raman microscopy. Our studies demonstrate our approach is able to characterise selected bone diseases related to chemical modifications within bone matrix including *osteogenesis imperfecta* (brittle bone disease) osteoarthritis and osteoporosis.[1,2,3] Whilst the task is challenging, and much more work needs to be done, the results demonstrate the potential of SORS to provide a much needed effective clinical diagnostic tool.

In relation to understanding bone disease where mineralisation is disrupted we have performed investigations looking at the structural changes in collagen during mineralisation.[4] Turkey leg tendons (TLTs) are recognised as a model organ for studying distinct regions of mineralised and non-mineralised collagen. This is because at 11 weeks age the extension tendon has no mineralisation, however, at 18 weeks of age there grows distinct sections of mineralisation. We demonstrate how Raman spectroscopy can be used to identify differences in the collagen secondary structure between regions of young TLTs that will remain non-mineralised and those that become mineralised. That is spectra across the transition zone of the mature TLTs and radiographs were used to confirm the presence/absence of mineral corresponding to the mature/young TLTs. Raman analysis of the young TLTs also reveals that collagen becomes more ordered prior to mineralisation, Interestingly, we also observe changes in Amide III:Amide I along the length of the tendon at the predicted transition zones.

Acknowledgments: We thank EPSRC (EP/H002693/1), STFC and UCL for support. We thank the Vesalius Clinical Training Centre, University of Bristol and Watford General Hospital for bone specimens.

References

1. Kerns, JG, Gikas, PD, Buckley, K, Shepperd, A, Birch, HL, McCarthy, I, Miles, J, Briggs, TWR, Keen, R, Parker, AW, Matousek, P, and Goodship, AEArthritis Rheumatol(2014) 66, 1237–46
2. Buckley, K, Kerns, JG, Gikas, PD, Birch, HL, Vinton, J, Keen, R, Parker, AW, Matousek, P, and Goodship, AEIBMS Bonekey (2014) **11**, 602.
3. Buckley, K, Kerns, JG, Vinton, J, Gikas, PD, Smith, C, Parker, AW, Matousek, P, and Goodship, AE. J. Raman Spectrosc (2015) **46**, 610–618.
4. Kerns JG, Buckley K, Churchwell J, Parker AW, Matousek P, Goodship AEAnal Chem (2016) **88**, 1559-63

BP-5-4 (Invited)

Glucose diffusion in colon mucosa – a comparative study between healthy and cancerous tissue

Sónia Carvalho[1], Nuno Gueiral[2], Elisabete Nogueira[2], Rui Henrique[1], L. Oliveira[2], V. V. Tuchin[3,4,5]

1- Serviço de Anatomia Patológica – IPO Porto, Rua Dr. António Bernardino de Almeida S/N, 4200-072 Porto, Portugal

2- CIETI/ISEP – Physics Department, Rua Dr. António Bernardino de Almeida Nº431, 4249-015 Porto, Portugal

1- National Research State University, Research-Education Institute of Optics and Biophotonics, 83 Astrakhanskaya str., Saratov 410012, Russia

2- Laboratory of Laser Diagnostics of Technical and Living Systems of Precision Mechanics and Control Institute of the Russian Academy of Sciences, 24 Rabochaya, Saratov 410028, Russia

3- Interdisciplinary Laboratory of Biophotonics, National Research Tomsk State University, 36 Lenin's av., Tomsk 634050, Russia

Main author email address: lmo@isep.ipp.pt

The possibility of using optical methods to perform noninvasive and early cancer detection is expected with great interest. The study of the optical properties in various human tissues has been made, demonstrating that scattering is significantly higher than absorption in UV, visible and NIR wavelength ranges [1-3]. Such difference potentiates the use of optical clearing treatments to discriminate between healthy and cancerous tissues. Colon cancer is a major health concern worldwide, characterized by high incidence and mortality [4]. A recent study showed that colon mucosa and colon tumor have different refractive index values [5]. Recently, we have estimated the diffusion properties of optical clearing agents in skeletal muscle based on collimated transmittance measurements [6-8]. Those studies have also allowed discriminating between the optical clearing mechanisms and calculating the free water content in the untreated tissues. Glucose diffusion has recently been studied in normal and cancerous mammary tissues as a possible way to establish a diagnosis [9]. Performing similar research in colon mucosa and colon cancer tissues, we were able to calculate the diffusion properties of glucose and differentiate the water content in the two tissue types. Analyzing the differences between glucose diffusion in both samples and correlating them with reflectance measurements, we expect to develop an endoscopic prototype method in the near future to perform noninvasive early colon cancer detection. Such equipment could also be used in ORL applications for larynx, pharynx and esophagus cancer detection.

[1] V. V. Tuchin, Tissue Optics: Light Scattering Methods and Instruments for Medical Diagnosis, 3rd Ed. (Bellingham, WA: SPIE Press), Chapter 1, (2015).
[2] V. V. Tuchin, Optical Clearing of Tissues and Blood (Bellingham, WA: SPIE Press), Chapters 1 and 2, (2006).
[3] A. N. Bashkatov, E. A. Genina, V. I. Kochubey and V. V. Tuchin, Optical properties of human skin, subcutaneous and mucous tissues in the wavelength range from 400 to 2000 nm, J. Phys. D: Appl. Phys, vol. 38, pp. 2543-2555, (2005).
[4]H. Brenner, M. Kloor and C. P. Pox, Colorectal cancer, The Lancet, vol. 383, pp. 1490-1502, (2014).
[5]P. Giannios, S. Koutsoumpos, K. G. Toutouzas, M. Matiatou, G. C. Zografos and K. Moutzouris, Complex refractive index of normal and malignant human colorectal tissue in the visible and near-infrared, J. Biophotonics, to be printed, (2016).
[6] L. Oliveira, M. I. Carvalho, E. Nogueira, V. V. Tuchin, The characteristic time of glucose diffusion measured for muscle tissue at optical clearing, Laser Physics, vol. 23, pp. 075606-1-6, (2013).
[7] L. Oliveira, M. I. Carvalho, E. Nogueira, V. V. Tuchin, Diffusion characteristics of ethylene glycol in skeletal muscle, J. of Biomedical Optics, vol. 20, pp. 051019-1-10, (2015).
[8] L. Oliveira, M. I. Carvalho, E. Nogueira, V. V. Tuchin, Optical clearing mechanisms characterization in muscle, J. Innovative Optical Health Sciences, vol. 9, pp. 1650035-1-19, (2016).
[9] H. Q. Zhong, Z. Y. Guo, H. J. Wei, C. C. Zeng, H. L. Xiong, Y. H. He and S. H. Liu, Quantification of glycerol diffusion in human normal and cancer breast tissues in vitro with optical coherence tomography, Laser Physics Letters vol. 7, pp. 315-320, (2010).

BP-5-5

Laser Techniques for Assessing the Enhanced Aggregation of Erythrocytes in Blood Samples of Diabetic Patients

A.E. Lugovtsov[1], K. Lee[2], A.V. Priezzhev[1,3]

1- International Laser Center of M.V. Lomonosov Moscow State University, 119991, Moscow, Russia
2- Optoelectronics and Measurements Techniques Unit of University of Oulu, 90570, Oulu, Finland
3- Physics Department, M.V. Lomonosov Moscow State University, 119991, Moscow, Russia
anlug@bmp.ilc.edu.ru

Fast development of laser technologies, in particular, optical measurement techniques allow for assessing the optically measured characteristics of biological tissues and cells in norm and pathology.
Diabetes mellitus (DM) is a metabolic disease characterized by high blood sugar levels over a prolonged period and alterations of vitally important systems of the human organism including the cardiovascular system. It is obvious that controling the rheological parameters under DM is very important. The rheological parameters are mostly related to the aggregation properties of red blood cells (RBCs), which are impaired in case of DM. Spontaneous aggregation of RBCs is the process leading to the formation of linear and 3D complex structures. The aggregation process significantly affects the blood viscosity and leads to the alteration of the blood circulation. This work focuses on the aggregation parameters of the RBC that characterize the time and velocity of RBC aggregates formation and can be measured *in-vitro* by laser systems.
The techniques to be discussed are laser scattering aggregometry of RBC [1] and cells trapping and manipulation with laser tweezers (LT) [2].
For measuring the time of spontaneous aggregation in an ensemble of RBC in whole blood we used two commercially available aggregometers – LADE (RheoMedLab, Russia) and Rheoscan-D300 (Rheomeditech, Korea). Operation of these devices is based on measuring the intensity of laser light scattered by whole blood samples. Laser aggregometry allows to study the kinetics of spontaneous aggregation (time dependence of the intensity of light scattered from a sample of whole blood during stasis). Experiments are carried out with samples of whole blood placed in a chamber where shear rate is induced. Shear flow arising in the chamber destroys the aggregates. After halting the flow the process of spontaneous aggregation arises and aggregation kinetics is registered. Computer processing of the obtained kinetic signal yields the characteristic times of linear (T_1) and 3D (T_2) aggregates formation for LADE, and the time of aggregation ($T_{1/2}$) for Rheoscan. To measure the aggregation velocity V_A on cellular level we used a home-made double channeled LT. The laser traps are formed by two single-mode Nd:YAG lasers and a water-immersion objective with high numerical aperture. LT allow for freely manipulating the individual cells with a tightly focused laser beam. To measurement V_A two cells in a suspension highly diluted by autologous plasma are : (1) trapped by LT; (2) attached to each other with well defined linear overlap distance (X ≈ 1 μm) and then released from the trap; (3) the cells spontaneously overlap each other during time Δt with the velocity $V_A = \Delta x/\Delta t$.
All measurements were performed with human blood samples (N=8) drawn from patients with DM and healthy voulonters (N=8, control group) within 3 hours after the blood drawing. The resuts obtined with LADE were $T_1 = 6.2 \pm 1.8\ s$ and $T_2 = 34.0 \pm 11.7\ s$ for the patients with DM and $T_1 = 14.7 \pm 4.9\ s$ and $T_2 = 43.1 \pm 13.9\ s$ for the control group. Aggregation time measured with Rheoscan was $T_{1/2} = 5.3 \pm 1.9\ s$ in case of DM and $T_{1/2} = 9.6 \pm 3.9\ s$ in case of control group. V_A measured with LT in DM group was $V_A = 1.09 \pm 0.31\ \mu m/s$, and in control group was $V_A = 0.54 \pm 0.28\ \mu m/s$. Basing the obtained results we conclude that DM is characterized by enhanced aggregation. It was shown that the characteristic time of aggregates formation is dramatically increased in whole blood of patients with DM relative to the control group. The velocity of spontaneous aggregation of a pair of single RBC is increased too by about two times. Information about alterations of the time of aggregates formation can be considered as an indication of DM as well as for monitoring the patients treatment efficiency.
The work was financially supported by the Russian Scientific Foundation, grant No14-15-00602.

[1] A.V. Priezzhev, N.N. Firsov, J. Lademann, Light backscattering diagnostics of RBC aggregation in whole blood samples, Chapter 11 in Handbook of Optical Biomedical Diagnostics, Editor V. Tuchin, Washington: SPIE Press, pp. 651 – 674 (2012).
[2] K. Lee, M. Kinnunen, M.D. Khokhlova, E.V. Lyubin, A.V. Priezzhev, I. Meglinski, A. Fedyanin, Optical tweezers study of red blood cell aggregation and disaggregation in plasma and protein solutions, Journal of Biomedical Optics, vol. 21(3), pp. 035001 (2016).

BP-5-6

Laser Trapping for the Measurement of Forces at Red Blood Cells Aggregation and Disaggregation

A.N. Semenov[1,2], K. Lee[3], A.E. Lugovtsov[1,2], A.V. Priezzhev[1,2]

1 - Faculty of physics and 2 - International Laser Center of M.V. Lomonosov Moscow State University, Leninskiye Gory, 1-2, 119991, Moscow, Russia
3 - Opto-Electronics and Measurements Techniques Unit, University of Oulu, Erkki Koiso-Kanttilan katu 3, 90570, Oulu, Finland

semenov@physics.msu.ru

Laser trapping systems provide a convenient and very effective opportunity for assessing the mechanisms of interaction on the level of single cells and/or macromolecules [1]. In this study, laser tweezers (LT) were used for trapping the red blood cells (RBC) and measuring the interaction forces between them for studying the process of the RBC aggregation. Spontaneous aggregation of RBCs takes place both *in vivo* and *in vitro* and leads to the formation of first linear and then 3D aggregates, which can be disassembled (disaggregated) when shear stresses in the flow or other external forces are applied. RBC aggregation significantly influences the blood viscosity at low shear stress conditions and affects the blood circulation. With the perspective for the clinical application a number of methods were developed for the quantitative assessment of this property [2]. Recently the LT were introduced to this research and were shown to be a promising tool for the further assessment of the RBC aggregation. In particular LT could characterize the cells interaction strength, which cannot be measured with the conventional methods [3].

We measured the cells aggregation and disaggregation forces (F_A and F_D respectively) using a home-made two-channel LT comprising two Nd:YAG lasers (1064 nm, 200 mW) and a high numerical aperture objective (N.A. = 1.00, x100). One lasers beam could be moved using a motorized-mirror. The measurements were performed in diluted suspension of RBCs (~0.05%) in autologous plasma. The blood for measurements was drawn by venipuncture from patients suffering from Diabetes Mellitus Types I and II (DMI and DMII respectively) and from healthy donors.

F_A – the force leading to overlapping of the two adjacent cells was measured by comparing it with the minimum trapping force (F_T) required for holding the cells from spontaneous overlapping. Measurements were performed in 3 stages: (1) two single RBCs were trapped using different channels of LT; (2) these cells were moved and brought to a point contact; in this position, the cells remain still as long as $F_T > F_A$; (3) F_T was slowly decreased by decreasing the beam power until F_A exceeds F_T and the cell escaped from the trap and overlap. At this point we considered that $F_A$was matching F_T.

F_D – the force that should be applied to separate the cells from each other was measured in 4 stages: (1-2) the aggregate of two RBCs was formed with the same procedure as for F_A measurements; (3) – the cells were separated by moving one of the channels of LT, while the trapping force was slowly decreasing; (4) – the F_T sufficient for separating the cells was found which is equal to F_D.

Each set of F_A and F_D measurements was performed on 15 pairs of RBC for each blood sample and within 3 hours after drawing the blood. Each group of donors included 5-7 persons. The results showed that F_D exceeds F_A by 10-15% in all of the groups. The highest values of the RBC interaction forces were obtained in DMI group (F_A = 6.3 ± 1.5 and F_D = 7.4 ± 2.1 pN). The results in DMII group were F_A = 3.1 ± 0.8 and F_D = 5.0 ± 1.3 pN. The results in the group of healthy controls were F_A = 0.9 ± 0.2 and F_D = 4.9 ± 1.3 pN. We conclude that the cells interaction forces are elevated in the blood of DMI and DMII patients, the highest elevation being observed especially in the former case. The highest difference between F_A and F_D was found for healthy donors. This difference decreases when the cells interaction is enhanced in disease, and finally almost vanishes as in the case of DMI.

The work was partially supported by the RFBR grant № 16-52-51050.

[1] P. Ashokand, K.Dholakia, Optical trapping for analytical biotechnology, Current Opinion in Biotechnology, vol. 23, pp. 16-21 (2012).
[2] O. Baskurt, B. Neu and H. Meiselman, Red Blood Cell Aggregation (CRC Press), Chapter 4 Measurement of Red Blood Cell Aggregation, (2012).
[3] K. Lee, A. Danilina, M. Kinnunen, I. Meglinski and A. Priezzhev, Probing the red blood cells aggregating force with optical tweezers, IEEE Journal of Selected Topics in Quantum Electronics, vol. 22, pp. 7000106 (2016).

BP-5-7 (Invited)

Spectroscopic Imaging of Early Cancer with Scattered Light

L. Qiu[1], L. Zhang[1], V. Turzhitsky[1], Y. Zakharov[1], U. Khan[1], T.M. Berzin[2], M. Sawhney[2], E.U. Yee[3], J.D. Goldsmith[3], E. Vitkin[1], R. Chuttani[2], D.K. Pleskow[2], I. Itzkan[1], and L.T. Perelman[1,4]

[1]*Center for Advanced Biomedical Imaging and Photonics*
[2]*Theodore and Cynthia Berenson Center for Advanced Endoscopy*
[3]*Department of Pathology*
Beth Israel Deaconess Medical Center
[4]*Biological and Biomedical Sciences Program*
Harvard University

ltperel@bidmc.harvard.edu

Optical diagnostic technologies are very valuable tools for studying living tissues inside the human body. While fluorescence and Raman spectroscopy are effective in revealing the molecular properties of tissue, elastic light scattering is capable of characterizing the structural properties of tissue on a cellular and sub-cellular scale. Light scattering in biological tissues originates from tissue inhomogeneities such as cellular organelles, the extracellular matrix, blood vessels, etc. This often translates into unique angular, polarization, and spectroscopic features of scattered light emerging from tissue and therefore information about the tissues macroscopic and microscopic structure can be obtained from the characteristics of the scattered light [1].

In this talk we will discuss how light scattering signatures could be used to remotely and noninvasively detect early precancer in organs which seem to have nothing in common [2,3]. We will show, however, that since precancer in many organs is characterized by certain microscopic changes, such as nuclear sizes, nuclear density, and hyperchromaticity of epithelial cells, their light scattering signatures are also quite similar. A direct connection between the inherent optical properties of diseased tissue and the known pathological features of disease can be provided by light scattering sensitive optical spectroscopy, without the need for exogenous markers.

[1] Perelman LT, Backman V, Wallace M, et al. *Phys. Rev. Lett.* 1998; 80:627-30.
[2] Backman V, Wallace M, Perelman LT, et al. *Nature* 2000; 406:35-36.
[3] Qiu L, Pleskow D, Chuttani R, et al. *Nature Medicine* 2010; 16:603-6.

BP-6-1 (Invited)

Novel graphene oxide/nano-gold platforms for optimized SERS detection

R. Pini[1], P. Matteini[1], M. Banchelli[1], M. de Angelis[1]

1- Institute of Applied Physics "Nello Carrara", National Research Council of Italy, via Madonna del Piano 10, Sesto Fiorentino, I-50019 Italy

R.Pini@ifac.cnr.it

Surface-enhanced Raman scattering (SERS) spectroscopy has emerged as a powerful ultrasensitive analytical technique in biosensing. The SERS effect relies on huge electromagnetic fields concentrated at the nanostructured metal surface to dramatically enhance the Raman signal of molecules when localized surface plasmon resonances (LSPRs) are excited by an external incident electromagnetic wave. Efficient SERS enhancements are typically generated within less than 10 nm from the metal surface and are mostly confined within the so-called "hot spots", i.e. highly curved nanoregions or gaps and junctions between adjacent nanoparticles. The ability to gather molecules in these regions in a homogeneous and reproducible manner represents a current impediment that is still preventing further diffusion of SERS as a systematic analytical tool.

Here we present the use of nonspherical tipped metallic nanostructures with controlled architectural parameters and their assembly into organized bidimensional arrays including a regular distribution of hot spots for protein entrapment and detection [1]. The investigation evidenced that both the contact points between nanoparticle corners and the holes at the interface between nanoparticles are responsible for substantial SERS activity.

A further advancement toward upgrading the performance of SERS technology relies on the combination of plasmonic nanostructures with graphene oxide. Current efforts are taking advantage of a thin graphene oxide coating in drawing and concentrating target molecules as well as in conferring the plasmonic surface with a passivating layer that discards possible disturbances and signal variability induced by metal− molecule interactions. We present an effective graphene oxide/plasmonic substrate with a highly controlled and uniform bilayer structure. The substrate was obtained by fine-tuning in silver nanocubes self-assembly, followed by a controlled adsorption of graphene oxide sheets on the silver layer. Here the graphene oxide coating supplies the signal with additional amplification. The developed system shows a highly uniform signal distribution ascribed to a homogeneous and soft arrangement of graphene oxide sheets over the plasmonic surface, which makes it a reliable tool for detecting different compounds ranging from small molecules to complex biomolecules [2].

[1] P. Matteini, M. de Angelis, L. Ulivi, S. Centi, R. Pini, Concave gold nanocube assemblies as nanotraps for surface-enhanced Raman scattering-based detection of proteins, Nanoscale, vol. 8, 3374-3480, (2015).
[2] M. Banchelli, B. Tiribilli, M. de Angelis, R. Pini, G. Caminati, P. Matteini, Controlled veiling of silver nanocubes with graphene oxide for improved Surface enhcend Raman scattering detection, ACS Applied Materials & Interfaces, vol. 8, 2628-2634, (2016).

BP-6-2 (Invited)

Laser-ablative synthesis of functional nanomaterials for cancer theranostics

A. V. Kabashin

Aix Marseille University, CNRS, LP3 UMR 7341, Campus de Luminy - Case 917, 13288, Marseille, France

The presentation will overview our on-going activities on laser ablative synthesis of some biocompatible colloidal nanomaterials (Au, Si etc) and their testing in biomedical tasks. Our approach is based on ultra-short (fs) laser ablation from a solid target [1] or already formed water-suspended colloids [2] to achieve an efficient control of size characteristics of "bare" ligand-free nanomaterials, or fabricate nanomaterials coated by functional biopolymers (dextran, PEG) to minimize immune response of biological systems. Our experiments in vitro demonstrate an excellent cell uptake of both bare and functional nanomaterials, while the composition of protein corona covering nanoparticles complexes in biological environment promises a good transport of nanomaterials in vivo [3]. In addition, the intravenous administration of Si NPs using small animal model did not reveal any toxicity effects, which was confirmed by behavior of mice, stability of blood content and other biochemical parameters, as well as by histology analyses of all organs and biodistribution of nanoparticles in tissues [4]. Furthermore, the nanoparticles rapidly biodegraded in the organism and were completely cleared 2-3 days after their injection. In general, our tests evidenced a negligible toxicity and much faster clearance of laser-synthesized Si NPs compared to all chemically-synthesized Si NPs counterparts. Laser-synthesized nanomaterials are now actively tested in cancer diagnostics and therapy (theranostics) tasks. In particular, our experiments showed that laser-synthesized nanomaterials can provide a much better efficiency compared to chemically synthesized counterparts in a newly introduced method of mild cancer therapy using Si nanoparticles as sensitizers of radiofrequency radiation-based hyperthermia [5]. Finally, we showed that bare metal nanoparticles synthesized by laser ablation can provide an order of magnitude better response in glucose oxidation tasks, which promises their use as elecrocatalysts in bioimplantable therapeutic devices [6].

[1] A. V. Kabashin, M. Meunier, J. Appl. Phys., Vol. 94, pp. 7941 (2003)
[2] K. Maximova, A. I. Aristov, M. Sentis, A. V. Kabashin, Nanotechnology, Vol. 26, pp. 065601 (2015)
[3] F. Correard, K. Maximova, M.-A. Estève, C. Villard, A. Al-Kattan, M. Sentis, M. Roy, M. Gingras, A. V. Kabashin, D. Braguer, Int. J. Nanomedicine, Vol. 9, pp. 5415 (2014)
[4] T. Baati, A. Al-Kattan, M.-A. Esteve, L. Njim, Y. Ryabchikov, F. Chaspoul, M. Hammami, M. Sentis, A. V. Kabashin, D. Braguer, Scientific Reports, Vol. 6, pp. 25400 (2016)
[4] K. P. Tamarov, L.A. Osminkina, S. V. Zinovyev, K. A. Maximova, J. V. Kargina, A. P. Sviridov, M. Sentis, A. V. Ivanov, V. N. Nikiforov, A. V. Kabashin, V. Yu. Timoshenko, Scientific Reports, Vol. 4, pp. 7034 (2014)
[5] S. Hebié, Y. Holade, K. A. Maximova, M. Sentis, P. Delaporte, K. B. Kokoh, T. W. Napporn, A. V. Kabashin, ACS Catalysis, 5, 6489 (2015)

BP-6-3 (Invited)

Laser Technologies for Complex Studies of Blood Characteristics as Bio-optical Markers of Diseases

A.V. Priezzhev [1,4], A.E. Lugovtsov [4], S.Yu. Nikitin [1,4], K. Lee [1,5], V.D. Ustinov [3,4], V.B. Koshelev [2,4], O.E. Fadyukova [2,4], E.A. Shirshin [1,4], T.N. Tikhonova [1,4], N.G. Zhdanova [1,4], and Yu.I. Gurfinkel [6,4]

1-Faculty of Physics, 2-Faculty of Medicine, 3-Faculty of Computational Mathematics and Cybernetics, and 4-International Laser Center of Lomonosov Moscow State University, Leninskiye Gory, Moscow, Russia;
5-Optoelectronics and Measurements Techniques Unit, University of Oulu, Oulu, Finland;
6-Research Clinical Center of JSC "Russian Railways", Moscow, Russia.

avp2@mail.ru, avpriezz@gmail.com

Search and identification of biomarkers of socially important diseases is one of hot problems of contemporary science. Fast development of laser-optic and biophotonic technologies, in particular, new optical measurement techniques on cellular and molecular levels, recently obtained understanding of tissue optics and fundamental aspects of laser-tissue interactions, allow for introducing new bio-optical markers, as optically measured characteristics of biological structures constituting human organism, which measurable alterations from normal values designate an advent of disease.

This paper focuses at the characteristics of blood that can be measured in-vitro and/or in-vivo by laser-optic techniques, and which alterations can be considered as an indication of disease. The techniques to be discussed are: laser diffractometry of erythrocytes, laser scattering aggregometry of erythrocytes, digital optical capillaroscopy and measurement of the microcirculation parameters, erythrocytes trapping and manipulation with laser tweezers, fluorescence spectroscopy of blood plasma, etc. Experimental protocols and results of measurements performed in-vitro with the samples of whole human and rat blood and blood components will be outlined. Blood for the experiments in-vitro was drawn from clinically healthy human volunteers (control) and from patients suffering from diabetes mellitus, hypertension and other diseases. In-vivo measurements of the microcirculation parameters were conducted with control human subjects and patients suffering hypertension. For the in-vitro experiments with rat blood, the samples were drawn from healthy (control) and sham operated animals, those with experimentally induced diabetes mellitus and/or hypertension. Samples of human and rat blood plasma separated from blood cells were used to study the aggregation of plasma proteins that leads to the loss of their functional properties and is one of the causes of such socially important diseases as the Parkinson and Alzheimer diseases. Fluorescence spectroscopy allows also for identifying other alterations at the molecular level in blood plasma caused by proteins conformational changes that may induce pathological changes at the cellular level and so on up to the level of the whole organism.

The obtained results allow us to conclude that the overviewed laser-optic techniques comprise a powerful tool for efficiently identifying and assessing a set of clinically informative bio-optical markers of diseases.

The work was financially supported by the Russian Scientific Foundation, grant № 14-15-00602.

BP-6-4 (Invited)

Functionalised Red Blood Cells as a Platform for Blood Diagnostics

Kenith E. Meissner[1], Sandra Bustamante-Lopez[1,2], Sarah Ritter[2], Nicholas P.Cooley[3], Mark A. Milanick[3], and Timothy E. Glass[3]

1- Swansea University, College of Engineering, Swansea, UK
2- Texas A&M University, College Station, TX, USA
3- University of Missouri Columbia, Columbia, MO, USA

k.meissner@swansea.ac.uk

Measurement of blood analytes provides crucial information about the health of a patient. Many analytes, such as glucose for diabetic patients, require long-term and/or near- continuous monitoring for proper disease assessment and management. However, standard monitoring techniques are inconvenient, do not allow continuous monitoring and/or only allow periodic sampling. Thus, there is a need for a long-term system platform for in vivo sensing. Red blood cells (RBCs) functionalised with optical sensors provide a microscale platform for this type of minimally or noninvasive sensing. With a 120 day lifespan, human RBCs provide a long-term platform that is both biodegradable and biocompatible, thereby eliminating the immune system response common for many implanted devices. Recently our group demonstrated the ability of low hemoglobin RBCs functionalised with FITC to sense extracellular pH.[1] This talk focusses on our development functionalised RBCs toward blood analyse sensing.

Functionalisation of the RBCs is accomplished by opening lysis pores (~10s of nm) in the RBC membrane and diffusing sensors into the RBCs. Sensors are loaded using a preswelling technique that yields RBCs with near-normal hemoglobin levels.[2-3] Isolated whole bovine RBCs are suspended in Hank's balanced salt solution (HBSS) and centrifuged. Following removal of the supernatant, hemolysate solution containing the NIR sensing dye is added to the RBCs until lysis pores are formed and the dye diffuses into the RBCs. HBSS is then added to reseal the RBCs.

When diffused into RBCs, the dye is responsive to pH in the surrounding medium with the fluorescence displaying both spectral shift and change in quantum yield. The functionalised RBCs do show altered morphology from the loading process. However, the system is promising as a platform for sensing blood analytes that traverse the RBC membrane.

[1] S. Ritter, M. A. Milanick, and K. E. Meissner. (2011). Encapsulation of FITC to monitor extracellular pH: A step towards the development of red blood cells as circulating blood analyte biosensors. Biomed. Opt. Exp. 2. pp. 2012-2021.
[3] H. Tajerzadeh, and H. Hamidi. (2000). Evaluation of hypotonic preswelling method for encapsulation of enalaprilat in intact human erythrocytes. Drug Dev. Ind. Pharm. 26. pp. 1247-1257.
[4] E. Pitt, C. M. Johnson, D. A. Lewis, D. A. Jenner, and R. E. Offord. (1983). Encapsulation of drugs in intact erythrocytes: An intravenous delivery system. Biochem. Pharmacol. 32 (22). pp. 3359-3368.

BP-6-5 (Invited)

Two-photon laser fabrication of scaffolds for tissue engineering and regenerative medicine

V. Bagratashvili[1], S.Timashev[1], B. Chichkov[2]

1- Institute of photon technologies, research center "Crystallography and photonics" RAS, Pionerskaya 2, Moscow, Troitsk, 142190, Russia
2- Laser Center Hannover

Two-photon femtosecond laser polymerization (2PP) technique was used to fabricate biodegradable 3D scaffolds for tissue engineering and regenerative medicine. Two-photon polymerization (2PP) technique is a promising method for 3D scaffold fabrication with high accuracy enabling modelling the cellular interaction and tissue organization with precise structural resolution.
A Ti:sapphire femtosecond laser system (Chameleon, Coherent) delivering 150 fs pulses at an 80 MHz repetition rate, was used for the 2PP fabrication of scaffolds. The experimental setup is similar to one that was previously described [1, 2]. An acoustooptical modulator was applied to trigger exposure of the sample. The beam is then passed through an EC Plan-Neofluar 20× objective (Zeiss, NA¼0.5) and focused into the sample. To fabricate defined scaffold geometry, a custom-written computer code was used.
For the development of 3D scaffolds, different photosensitive materials have been applied: Zr-Si hybrid sol–gel material; synthetic biodegradable star-shaped methacrylate functionalized poly(D,L-lactide) material. We report two different applications of fabricated 3D scaffolds.

3D scaffolds for the analysis of neural network formation and function

3D Zr-Si organic–inorganic scaffolds fabricated by a two-photon polymerization technique were used for the primary culture of mouse embryonic neural cells. We observed that dissociated hippocampal cells adhere to the scaffolds, produce neurites, elongate and differentiate into adult neurons. Neuronal outgrowth and synaptogenesis were confirmed by immunohistochemical staining with antibodies against βIII-Tubulin and synaptophysin. The formation of a functional neural network was assessed by the measurement of spontaneous activity using Ca2+ imaging of dissociated hippocampal cultures grown on Zr-Si scaffolds. The results of this study suggest that two-photon-induced polymerization of organic–inorganic hybrid biomaterials provides a robust model for 3D neuronal tissue engineering studies.

Cross-linked tetrafunctional polylactide scaffolds inducing osteogenic differentiation of mesenchymal stem cells and bone formation

In the presented study, we have developed a synthetic strategy allowing a gradual variation of a polylactide arms' length, which later influences the morphology of the scaffold surface, formed by a two-photon polymerization technique. It has been demonstrated that the highest number of cells is present on the scaffolds with the roughest surface made of the polylactide with longer arms (PLA760), and osteogenic differentiation of mesenchymal stem cells is most pronounced on such scaffolds. According to the results of biological testing, the PLA760 scaffolds were implanted into a created cranial defect in a mouse for an *in vivo* assessment of the bone tissue formation. The *in vivo* experiments have shown that, by week 10, deposition of calcium phosphate particles occurs in the scaffold at the defect site, as well as, the formation of a new bone and ingrowth of blood vessels from the surrounding tissues. These results demonstrate that the cross-linked microstructured tetrafunctional polylactide scaffolds are promising microstructures for bone regeneration in tissue engineering.

[1] A. Ovsianikov, A. Deiwick, S. Van Vlierberghe, M. Pflaum, M. Wilhelmi, P. Dubruel and B. Chichkov, Laser Fabrication of 3D Gelatin Scaffolds for the Generation of Bioartificial Tissues Materials v.4, pp. 288–299 (2011).
[2] A. Koroleva, A. Deiwick, A. Nguyen, S. Schlie-Wolter, R. Narayan, P. Timashev, V. Popov, V. Bagratashvili and B. Chichkov Osteogenic differentiation of human mesenchymal stem cells in 3D Zr-Si organic-inorganic scaffolds produced by two-photon polymerization technique PLoS One v.10, pp. 1–18 (2015).

BP-6-6 (Invited)

Monitoring the Ultrafast Dynamics of DNA Crystals Using Transient Infrared Spectroscopy

James P. Hall[1,2], Fergus E. Poynton[3], Páraic M. Keane[1,3], Sarah P. Gurung[1], John A. Brazier[4], David J. Cardin[1], Graeme Winter[2], Thorfinnur Gunnlaugsson[3], Igor V. Sazanovich[5], Michael Towrie[5], Christine J. Cardin[1], John M. Kelly[3], and Susan J. Quinn[6]

[1]*Department of Chemistry, University of Reading, UK*
[2]*Diamond Light Source, Harwell Science and Innovation Campus, UK*
[3]*School of Chemistry, Trinity College, Ireland*
[4]*Department of Pharmacy, University of Reading, UK*
[5]*Central Laser Facility, Research Complex at Harwell, Rutherford Appleton Laboratory, UK*
[6]*School of Chemistry, University College Dublin, Ireland*
**susan.quinn@ucd.ie*

Knowing the mechanism and dynamics of photo-induced DNA damage is critically important for our understanding of diseases associated with UV-irradiation as well as the development of photosensitised DNA-directed therapies. With photosensitisers, guanine oxidation is often the ultimate site of damage, a process which may be initiated by its one-electron photo-oxidation. The precise dynamics of this process are expected to be sensitive to both the location and the precise orientation of the photosensitiser on the DNA, features which are difficult to define in solution. We show here, for the first time that it is possible to perform ultrafast spectroscopic studies in photosensitiser/DNA crystals, where the spatial arrangement of the photosensitiser and the target guanine are known.[1] By using time-resolved infrared we are able to obtain fingerprint information about both the reduced photosensitiser (a ruthenium polypyridyl complex) and the one-electron oxidised guanine.[2] This work demonstrates that atomic resolution X-ray crystallography can be combined with ultrafast infrared spectroscopic data to define both the geometry of the reaction site and the rates of individual steps in a reversible photo-induced electron transfer process. This allows us to propose an individual guanine as the reaction site.[3]

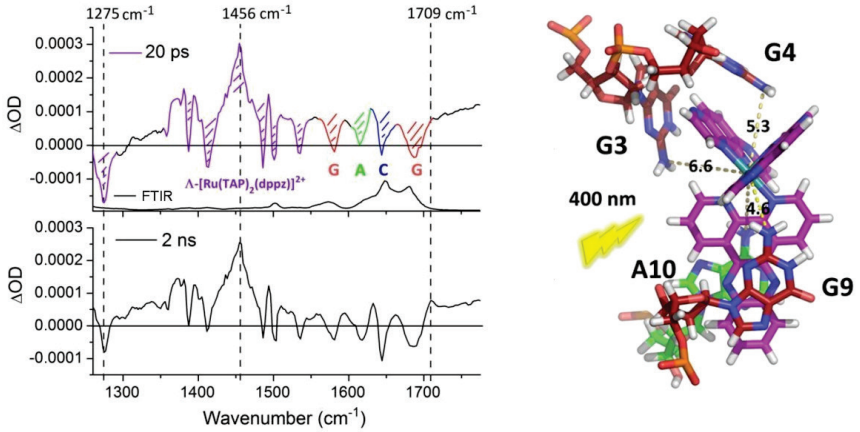

Figure: Transient infrared absorption spectra obtained from D_2O-exchanged crystal samples of Λ-$[Ru(TAP)_2(dppz)]^{2+}$ bound to $(TCGGCGCCGA)_2$.

[1] J.P. Hall, K. O'Sullivan, A. Naseer, J.A. Smith, J.M. Kelly, C.J. Cardin, (2011) Proc. Nat. Sci. Acad. (USA) 108, 17610.
[2] M. Towrie, G.W. Doorley, M.W. George, A.W. Parker, S.J. Quinn, and J.M. Kelly, (2009) Analyst, 134, 1265.
[3] J.P. Hall et al. Monitoring one-electron photo-oxidation of guanine in DNA crystals using ultrafast infrared spectroscopy (2015) *Nature. Chem.*, 7, 961.

BP-P-1

Application of Raman spectroscopy method in assessment of extracellular matrixes based on heart valves

E.V. Timchenko[1], P.E. Timchenko[1], L.T. Volova[2], S.V. Pershutkina[1], P.Y. Shalkovsky[1]

1 - Samara National Research University , 443086, Russia, Samara, Moscow highway, 34

2 - Experimental Medicine And Biotechnologies Institute of the Samara State Medical University, 443079 Russia, Samara, Gagarin Street 20

E-mail: laser-optics.timchenko@mail.ru

Modern development of regenerative medicine predetermines the creation of biomaterials based on the extracellular matrix (EM), including for cardiosurgery. They are obtained from tissues and organs of animals and humans by decellularization process, during which the cells are destroyed and removed, and the main components of the EM - collagen, elastin, glycosaminoglycans - are stored in its native state. An important step in the process of manufacturing of such materials is to control the completeness of removal of cellular components and the safety of matrix [1,2,3,4]. Nowadays for this purpose are used histological, histochemical, biochemical and immunological methods. Their main drawback along with their high cost and labor intensive is the destruction of samples to be analyzed [5]. In this regard, search for non-destructive methods of analysis of extracellular matrixes is an urgent task. From this standpoint, Raman spectroscopy method can be effective in assessing basic components of extracellular matrixes obtained from heart valves.

As the research material were used native and decellularized aortic valves of mature sheep. Decellularization of valves with obtaining extracellular matrix was carried out according to the protocol provided by Professor A. Lichtenberg (Düsseldorf, Germany). Fragments of native and decellularized biomaterial was stored to research in phosphate-saline solution with the addition of antibiotics at 4°C.

Additionally was carried out histological analysis of samples, while material was fixed in 12% formalin, dehydrated and embedded in paraffin. Radial slices of 5-7 microns thick were stained with routine methods and cresyl violet to identify metachromasia of glycosaminoglycans.

Due to the fact that the study samples are multi-component objects, additionally was carried out separation of spectra obtained on spectral lines using deconvolution of Lorentz-Gauss functions in MagicPlotPro software environment. Average value of the coefficient of determination of the result spectrum, generated by spectral contours, from the original Raman spectrum for area 300-220 cm^{-1}, amounted R_2=0,98, average standard deviation of analysis σ = 8,1.

Were obtained and assessed features of Raman spectra in the study of native heart valves and extracellular matrix on their basis.

It was established that the main differences are revealed at 852 cm^{-1}, 935 cm^{-1}, 1062 cm^{-1} and 1340 cm^{-1}, 1450 cm^{-1} wavenumbers, corresponding to amino acid residues of collagen, glycosaminoglycans, lipids and DNA.

To assess quantitative content of main components of heart valves and extracellular matrixes on their basis, the two-dimensional analysis of introduced optical coefficients was carried out, allowing to compare basic components before and after sample preparation.

Raman spectroscopy method allows to carry out qualitative and quantitative assessment of heart valves and biotechnological products on their basis on indicators of content of glycosaminoglycans, collagen, lipids and DNA, that has significant advantages over morphological methods of studies.

1. Zia, S. Hearts beating through decellularized scaffolds: whole-organ engineering for cardiac regeneration and transplantation / S. Zia, M. Mozafari, A. Tan, Z. Cui, A.M. Seifalian, // Informa Healthcare USA. – 2015 doi: 10.3109/07388551.2015.1007.

2. Kifah Shahin, Strategies for Enhancing the Accumulation and Retention of Extracellular Matrix in Tissue-Engineered Cartilage Cultured in Bioreactors [Текст] / Kifah Shahin1 , P.M. Doran. // PLoS ONE. – 2011 – № 6 – P. 1–13.

3. Crapo, P.M. An overview of tissue and whole organ decellularization processes [Текст] / P.M. Crapo, T.W. Gilbert, S. F. Badylak. // Biomaterials. – 2011 – № 32(12) – P. 3233–3243.

4. Assmann, A. Acceleration of autologous in vivo recellularization of decellularized aortic conduits by fibronectin surface coating / A. Assmann, C. Delfs, A. Lichtenberg et al. // Biomaterials. – 2013 – № 34 – P. 6015-6026.

5. He M., Callanan A. Comparison of methods for whole-organ decellularization in tissue engineering of bioartificial organs. Tissue Eng Part B Rev. 2013 Jun; 19(3):194-208. doi: 10.1089/ten.TEB.2012.0340.

BP-P-2

Wavelet analysis of alternating shuttle streaming motility in isolated strand of *P.polycephalum* plasmodium

T.I. Avsievich, S.V. Frolov, S.G. Proskurin

Tambov State Technical University, 106 Sovetskaya St, Tambov, 392000, Russia
email: tiavsievich@gmail.com

Amoeboid motility, inherent for a wide class of cells and plays an important role in the fundamental processes of wound healing, immunity, morphogenesis. Slime mold *Physarum polycephalum* is the classic model unicellular organism for amoeboid motility studying. Actomyosine motor is the force generating system for periodic contractile activity causing shuttle endoplasmic motility in *Physarum* strands. However, the nature and number of oscillators that control the contractile activity of plasmodium remains unknown.

Sign-sensitive laser Doppler system has been used for the registration of shuttle streaming motility in an isolated plasmodium strand of *P. polycephalum*. Alternating velocity time dependencies V(t) were obtained for a horizontally oriented strand (2 cm length) in different conditions [1]: under normal conditions – in buffer solution, after treatment with cellular respiration inhibitors potassium cyanide (KCN) and salicylhydroxamic acid (SHAM) – the complete cessation of plasmodium motility, and after inhibitors were removed – gradual recovery of motility (Fig.1A). Sign-sensitive mode allows to decrease signal to noise ratio, which is almost equal to one (SNR≈1) in the case of absolute magnitude registration. Short-Time Fourier Transform (STFT) of the time dependencies revealed equidistant pairs of harmonic components in the power spectra, regardless of the registration conditions (plasmodium in buffer or treated by inhibitors), and it changes over time. Despite the different values of frequencies ν_1 and ν_2 corresponding to the obtained peaks, their ratio ν_2/ν_1 is equal to two and remains constant for all the dependencies with extremely good accuracy (~2%). The wavelet transform (Fig.1B) of the obtained dependencies confirmed the presence of two harmonic components in each of them, and allowed more accurate visualization of the changes in time.

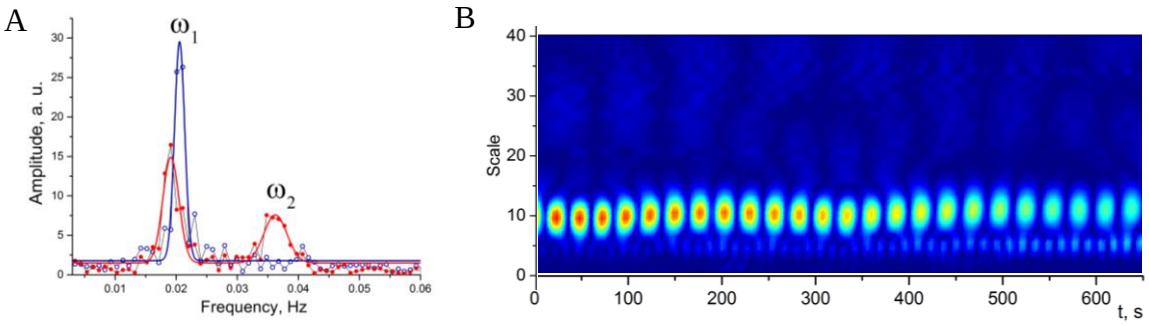

Figure 1. Fourier (A) and Wavelet (B) analysis of time dependency of protoplasmic motility 10 min after treatment by inhibitors.

Mathematical model based on the spectral characteristics obtained by STFT adequately describes the alternating endoplasmic motility in the strand. Significant correlation (R^2~0.95) between experimental and simulated data was observed.

STFT revealed the presence of an internal oscillator, which frequency is doubled and shifted in phase, or the two types of oscillators whose frequencies differ exactly twice [2]. Wavelet analysis allows to visualize changes of harmonic contributions in time more clearly, that is not always possible using Fourier transform.

[1] Avsievich, T.I., Frolov, S.V., Proskurin S. G. Characterization of endoplasmic streaming in Physarum polycephalum using direction sensitive laser Doppler microscopy. Optical and Quantum Electronics. – 2016. vol. 48, № 2. pp. 1-10, (2016)
[2] Wohlfarth-Bottermann, K. E. Oscillatory contraction activity in Physarum. J. Exp. Biol. vol. 81. pp. 15-32, (1979)

BP-P-3

Spectral assessment of influence of lyophilization process in manufacture of implants based on bacterial cellulose

E.V. Timchenko, P.E. Timchenko, E.V. Pisareva, V.V. Revin, A.A. Asadova

Samara National Research University, Samara, Moscow highway 34

laser-optics.timchenko@mail.ru

Bacterial cellulose (BC) is a unique biopolymer based on which can be solved many problems in medicine. Using biocompatible biologically active compounds based on BC is a method of improving pure BC and allows to come closer to the "more perfect" dressing material, that have improved biocompatibility, antimicrobial properties and also capable of retaining water.

Additional processing when creating a BC based on implants can be the process of lyophilization (freeze-drying), which can increase shelf life of biological substances, simplify conditions of storage, marketing and use of the products obtained, process immiscible in liquid phase components. However, the influence of lyophilization on implant structure based on BC is not studied yet.

The objective of research was to study the influence of lyophilization process on composition of hybrid materials based on BC using Raman spectroscopy.

In the work was studied bacterial cellulose (BC), as well as hybrids based on BC, including in composition various combinations of HAP and collagen: BC and HAP, collagen and BC, BC and HAP and collagen. For obtaining BC was used strain Gluconacetobacter sucrofermentas B-11267 [1]. The resulting membrana was washed out with distilled water, dried in drying chamber at 80°C to constant weight. HAP was obtained by the original method [2]. For obtaining composites in environ were added 1% HAP (HAP + BC); 0.5% collagen (collagen + BC), 1% HAP and 0.5% collagen (BC + HAP + collagen). Part of composites further was lyophilized in standard method [3].

Raman spectra of various combined biopolymers based on bacterial cellulose were obtained as results of the studies.

It is shown that during lyophilization process changes the ratio of individual components. So cellulose line is amplified in the normalized spectrum, indicating a decrease in the proportion of individual components. Furthermore for the hybrid samples based on BC with addition of HAP was detected PO_4^{3-} peak intensity increasing in 956 cm^{-1} area with decreasing its width, that indicates a change in degree of HAP crystallinity.

[1] Revin V.V., Liyaskina E.V., Pestov N.A. Preparation of bacterial cellulose and nanocomposite materials. Saransk. Mordovia Universities Press, 128 p. (2014)

[2] Bioimplants to restore the structure and volume of bone tissue. RF Patent № 2372892, app. №2008124263/14, Bull. № 32, 5 p, (2009)

[3] Blankov B.I., Klebanov D.L. Application of lyophilization in microbiology, Medicine, 263 p, (1961).

BP-P-4

Optical methods for assessing the impact of oil on plants

E.V. Timchenko, P.E. Timchenko, E.A. Selezneva, N.V. Tregyb

Samara National Research University, Samara 443986, Russia

laser-optics.timchenko@mail.ru

Nowadays one of the actual problems is prospecting and exploration of oil fields. But existing methods of oil detecting are time-consuming and expensive. At the same time using vegetative biological objects as local integral indicators of oil fields may contribute to the development of rapid detection method of oil fields [1].

Confocal fluorescence microscopy and Raman spectroscopy methods were used as main optical methods.

Raman spectroscopy was implemented using the high-resolution digital spectrometer Shamrock sr-303i with built-in cooling chamber DV420A-OE, providing a spectral resolution of 0.15 nm, with laser module LuxxMaster LML-785.0RB-04 (power up to 500 mW, wavelength 785 nm).

Processing of Raman spectra was carried out in Mathematica'8 software environment. Error of method did not exceed 5.84%.

Microscopic analysis of plant tissue was carried out using laser confocal fluorescence microscopy system made based on Olympus IX71 microscope and laser combine ANDOR. This system provided scanning speed up to 25 layers per second with a resolution up to 400 nm.

Field and laboratory studies were carried out. Pea (*Pisum sativum*) and common wheat (*Tríticum aestívum*) were used as objects of laboratory studies. The samples were divided into two groups, each group was grown in 3 pots. The first group of samples was a control, plants were grown in pure soil without adding hydrocarbons. In pots to the second group of plants in soil was added pure oil at a concentration of 1 g/kg. Such concentration of oil is equal to TLV for pure oil in soil [2]. Also separate studies were carried out on samples of the control group throughout their life cycle in order to eliminate the influence of oil vapor on spectral characteristics of plants. During our experiments, more than 200 samples were studied and were received more than 600 spectra. As objects of field studies were used common dandelion and silver birch. In parallel the control of illumination, humidity and soil acidity was carried out.

The features of Raman spectrum of plants growing under the influence of oil were obtained during the studies. The main changes in Raman spectrum were detected at wavenumbers corresponding to C-Br (605 cm^{-1}) vibrations, aromatic hydrocarbons (840 cm^{-1}) and methane (2120 cm^{-1}).

Microscopic assessment of plants under the influence of oil was carried out.

Based on the results obtained and established spectral relation, was carried out ground mapping, allowing to estimate presence of oil in soil.

[1] Kovalevsky A.L. Biogeochemical exploration of ore deposits. Moscow: Nedra, 1984, 360 p.

[2] Galinurov I.R., Safarov A.M., Kudasheva F.H., Khatmullina R.M., Smirnova T.P. Migration of petroleum hydrocarbons in the profile of alluvial floodplain soils. Tom:16, Number:1, Year: 2011, pp. 47-52.

BP-P-5

EXPERIMENTAL STUDIES OF HYDROXYAPATITE USING RAMAN SPECTROSCOPY METHOD

P.E. Timchenko[1], E.V. Timchenko[1], E.V. Pisareva[1], M. Yu. Vlasov[2], L.T. Volova[2], O.O. Frolov[1]

1- Samara National Research University, Samara, Moscow highway 34

2 -Experimental Medicine And Biotechnologies Institute of the Samara State Medical University, 443079 Russia, Samara, Gagarin Street 20

Main author email address: timpavel@mail.ru

Nowadays for bone restoration in surgical dentistry more and more are widely used biomaterials based on hydroxyapatite. Hydroxyapatite is the main mineral of bone tissue and hard tooth tissues [1]. Due to the ability to form biologically active layers of apatite to interact with natural bone tissue it can successfully be used when restoring damaged bones, as well as part of bioactive layer for better ingrowth of implant [2]. Osteogenic biomaterial based on hydroxyapatites must have undamaged microstructure and architecture of new bone and free of organic phase, in order to avoid antigenic and immunological contamination during implantation. Therefore, to improve the degree of crystallinity of apatite phase, to remove organic phase and other impurities it is carrying out heat treatment of the samples.

The objective of research was to assess the organic and mineral composition of hydroxyapatite, obtained from spongy bone tissue of different animal species with different parameters of demineralization and thermal treatment, using Raman spectroscopy method [3].

As objects of study were used 59 samples of hydroxyapatite obtained from spongy bone tissue of sheep, rabbit, cow, chicken, turkey, duck and goose by recovery from solution during demineralization. Difference of thus obtained biomaterial from synthetic hydroxyapatite is that the final powder besides hydroxyapatite may contain organic components and microelements as well as small concentrations of other apatites existing in bone tissue. For comparison, some samples of hydroxyapatite were subjected to subsequent heat treatment at a temperature of 700ºC for 6 hours.

Results of studies:

- Were experimentally established features of Raman spectra for hydroxyapatite powder samples obtained from bone tissue of different donors during demineralization.
- Hydroxyapatite powder obtained by demineralization comprises protein components remaining in the solution due to the partial destruction of bone tissue during demineralization. With increasing time of demineralization during the preparation of hydroxyapatite powder there is a decrease in concentration of minerals (phosphates 950 cm^{-1} and carbonates 1065–1070 cm^{-1}) in relation to the organic component.

It was established that the heat treatment at a temperature of 700ºC leads to the disintegration of organic components (amide I 1655–1675 cm^{-1}, amide II 1555–1565 cm^{-1}, amide III 1230–1289 cm^{-1}), a relative increase in concentration of mineral substances (phosphate anions 950–962 cm^{-1}) and removing A-type carbonate (1095–1103 cm^{-1}). The observed presence of B-type carbonate and loss of A-type carbonate corresponds to obtaining a biomaterial similar in composition to the young bone tissue.

[1] L. Carlos, J. Carneiro, Basic Histology Text & Atlas (10th ed.) (McGraw-Hill Companies) (2003).
[2] V.I. Savelyev and A.V. Kalinin, The experience of production and application demineralized bone tissue in experiment and clinic, biomedical technology, vol 17, pp. 17-24 (2001).
[3] E.V. Timchenko, P.E. Timchenko, L.T. Volova, Y.V. Ponomareva, L.A. Taskina, Research of organo-mineral structure of bone implants using Raman spectroscopy, Kvant. Electronics, pp. 696–699 (2014).

BP-P-6

Studies of samples of articular surface using Raman spectroscopy method

P.E.Timchenko[1], E.V. Timchenko[1], L.T. Volova[2], D.A. Dolgyshkin[2], M.D.Markova[1]

1- Samara National Research University, Samara, Moscow highway 34
2 -Experimental Medicine And Biotechnologies Institute of the Samara State Medical University, 443079 Russia, Samara, Gagarin Street 20

timpavel@mail.ru

Hyaline articular cartilage is a unique structure that provides functional usefulness of joint [1]. Arthrosis is considered the most common disease of articulation in the world, according to statistics in a varying degree up to 80% of the world population suffer from arthrosis. Defects in hyaline cartilage of the knee joint can occur due to injury, osteochondritis dissecans, osteoarthritis, inflammatory rheumatic diseases, avascular necrosis of subchondral bone and cartilage [2]. It is known that damage of cartilage, regardless of genesis, has no spontaneous cure ability and subsequently it can lead to spread degenerative disease of articulation, progressive loss of cartilaginous tissue and emergence of irreversible secondary arthrotic changes [3]. Therefore, early diagnosis of damaged articular hyaline cartilage is necessary to assign a timely and effective treatment.

This work presents the results of experimental studies of healthy and weared down cartilaginous tissue using Raman spectroscopy method. As objects of study were used 15 fragments of articular surface of human knee, obtained during endoprosthesis replacement surgery carried out on deforming osteoarthritis. On surface of these fragments on the macroscopic picture were conventionally highlited areas of undamaged articular hyaline cartilage, which correspond to unloaded articular surface and zone with progressive deep damage of hyaline cartilage down to the subchondral bone. When happens destruction of hyaline cartilage in the area of its damage there is amplification of peaks at wavenumbers 431 cm^{-1} (PO_4^{3-} (ν2) cholesterol, cholesterol esters), 956 cm^{-1} (PO_4^{3-} (ν1) (P-O symmetric valent)), 1065cm^{-1} (CO_3^{2-}, (C-O planar valent), 1745 cm^{-1} (ν (C=O) lipids) and the weakening of peaks intensity at wavenumbers 1562 cm^{-1} (amide II), 1658 cm^{-1} (amide I), wherein disappears line 1244 cm^{-1} (amide III).

Were introduced optical coefficients for assessing the state of articular surface, allowing verifying areas of cartilage tissue damage on articular surface.

Raman spectroscopy allows carrying out quick non-invasive control of state of articular surface samples with reliable identifying local areas of hyaline cartilage damage that subsequently will allow to develop device for its non-invasive assessment.

[1] Zuev- Ratnikov Sergey Dmitrievich // A new way of articular surfaces autoplasty in the treatment of patients with destructive-dystrophic diseases of the knee joint [Text] - 2015

[2] A.A. Stadnikov, G.M. Kavalersky, S.V. Arkhipov, and etc. // Assessment of modern methods of chondroplasty of defects of the knee joint hyaline cartilage 2008

[3] Denisov-Nikolsky Y.I., Mironov S.P., Omelyanenko N.P., Matveichuk I.V. // Actual problems of theoretical and clinical osteoarthrology. M., 2005.336

LOCALIZATION OF OPTICAL STRUCTURE DISTURBANCES IN BIOLOGICAL TISSUE USING DIFFUSE OPTICAL TOMOGRAPHY

A.Yu. Potlov, S.V. Frolov, T.I. Avsievich, S.G. Proskurin

Tambov State Technical University
Sovetskaya 106, Tambov, Russia
spros@tamb.ru

The key features of the described algorithm are: the initial approximation to the spatial distribution of the absorption and scattering coefficients in an investigated biomedical object is based on the angle-dependent Homogeneity Index $HI(\alpha)$ [1] and the assumption that all the absorbing and scattering inhomogeneities in the object [2] are spherical and have one value of absorption and scattering in all the volume of the inhomogeneity. $HI(\alpha)$ is calculated using normalization of the average flux density of late arriving photons for all Time Point Spread Functions (TPSF). The initial approximation is formed by mapping of the estimated Homogeneity Index into a step function in accordance with the experimentally determined levels of mean values of Late Arriving Photons (LAP). The spatial distribution of the absorption coefficient is formed using analysis of the parts where the step function is equal to –1. For each part of the step function, it is assumed the biomedical object contains a spherical absorbing inhomogeneity with a diameter equal to the half-length of the chord between the angles corresponding to the beginning and the end of the step function. Note that the inhomogeneity center is assumed to be in the point equidistant from the center and the boundary of this object at the angle corresponding to the center of the step function. The initial approximation of the scattering coefficient distribution is calculated similarly. The only difference is that the part where the step function is equal to +1 is analyzed and scattering inhomogeneities are put into correspondence to them.

The suggested algorithm can be used for fast (dialog mode) localizations of absorbing and scattering inhomogeneities in biomedical objects [3, 4] for brain structures diagnostics (fig.1a), traumatology, and mammography using Diffuse Optical Tomography (DOT). Application of this algorithm to the

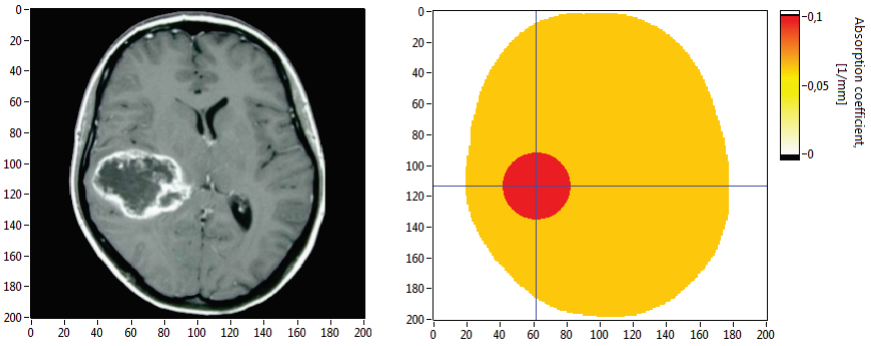

(a) (b)

Figure 1 MRI scan of a patient with a glioblastoma (a), the result of the glioblastoma localization (b)

real biomedical object (Glioblastoma localization) gave the appropriate result (Fig. 1b) for less than 3 sec. Calculation was performed on HP Z640 Workstation (two E5-2620v3c six-core processors, 4GB NVIDIA Quadro K4200 Video Graphics Card, 32 GB DDR4-2133 RAM).

[1] A.Yu. Potlov, S.V. Frolov, S.G. Proskurin Localization of inhomogeneities in diffuse optical tomography based on late arriving photons, Optics and Spectroscopy, Vol. 120, № 1, p. 9 (2016)
[2] A.Yu. Potlov, S.V. Frolov, S.G. Proskurin Movement of the photon density normalized maximum in homogeneous and inhomogeneous media with tissue-like optical properties, Laser Physics, Vol.25, №3, p. 035601 (2015)
[3] H. Dehghani, S. Srinivasan, B. Pogue, A. Gibson Numerical modelling and image reconstruction in diffuse optical tomography, Philosophical Transactions of the Royal Society A., Vol. 367, p. 3073 (2009)
[4] A.B. Konovalov, V.V. Vlasov, A.G. Kalintsev, O.V. Kravtsenyuk, V.V. Lyubimov Time-domain diffuse optical tomography using analytic statistical characteristics of photon trajectories, Quantum Electronics, Vol. 36, № 11, p.1048 (2006)

BP-P-8

Study of different biological tissue absorption spectra in visible and near-IR spectral range.

S.A. Filatova[1,2],I.A. Shcherbakov[1],V.B. Tsvetkov[1,3]

1- General Physics Institute of Russian Academy of Sciences, 119999, Moscow, Vavilov St. 38, Russia;
2-Ulyanovsk State University, 432017, Ulyanovsk, L. Tolstoy St. 42, Russia;
3- National Research Nuclear University MEPhI, 115409, Moscow, Kashirskoe sh. 31, Russia.

E-mail address:filsim2910@gmail.com

Result of the laser radiation impact on biological tissues depends of their optical and thermal characteristics. For therapeutic and surgical application of lasers we have to know optical properties of the biological tissues such as value of water content, absorption coefficient, scattering coefficient and refractive index for biological tissues [1], and thermal conductivity coefficient.

We used skeletal muscle, adipose, spinal cord and dura mater of beef and pork in our study. Such choice is determined by the need for a comparison of tissues with varying degrees of regularity scattering centers and various water saturation. Muscle tissues were selected from different parts of the carcass for comparing the transmission spectra of tissues being different by size, density of the muscle fibers and amount of fat. Measuring of transmission spectra for one sample was repeated several times with intervals of 10 minutes to observe change in the transmission spectrum over time.Transmission spectra were measured by spectrophotometer SHIMADZU UV 3101PC in the spectral range 350-2600 nm.

The absorption spectra were obtained by separation scattering from the extinction spectrum. The absorption spectra of various skeletal muscle tissues are very similar both in position of the absorption bands and value of the absorption coefficient (similarity is observed as well as for beef and pork). They are also similar to the absorption in spinal cord samples and dura mater of pork spinal cord. Absorption of adipose tissues is quite different from all investigated tissues.

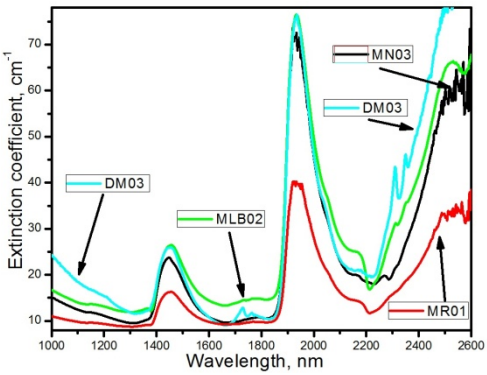

Figure 1. Superposition of extinction spectra of beef (MR01, MN03) and pork (MLB02) muscle tissues, and sample of dura mater of pork spinal cord.All spectra are constructed in the same scale and imposed with a shifton the axis Y.

In summary, we measured extinction and evaluated absorption spectra of beef and pork tissues: skeletal muscle, adipose, spinal cord and dura mater in the range from 350 to 2600 nm. We compared the absorption spectra of biological tissue samples of the same kind, depending on the tissue type.

Acknowledgements.The research was supported by Russian Academy of Sciences in the frames of the program for basic research “Basic and application problems of photonics and the science of novel optical materials” and by the Ministry of Education and Science (project № 14.Z50.31.0015).

[1] A.N.Bashkatov, E.A.Genina,V.V. Tuchin, Optical properties of skin, subcutaneous, and muscle tissues: a review, Journal of Innovative Optical Health Sciences, 4(01), 9-38, (2011).

Optical Coherence Elastography of Porcine Cornea, Sclera, and Cornea/Sclera Transition by Tracking Lamb Waves

F. Zvietcovich[1], J. Yao[2], M. Ramirez[3], M. Buckley[3], J. P. Rolland[2], K. J. Parker[1]

1- Department of Electrical and Computer Engineering, 2- The Institute of Optics, 3- Department of Biomedical Engineering, University of Rochester, Rochester, NY 14627, USA
fzvietco@ur.rochester.edu

Measuring biomechanical properties of the eye such as Young's modulus is fundamental to better understand, diagnose, and monitor degenerative ocular diseases [1]. This research focuses on the study of the propagation of Lamb waves in an *ex vivo* porcine cornea (Fig. 1a), sclera (Fig. 1b), and cornea/sclera transition (Fig. 1c) using phase-sensitive optical coherence tomography (OCT). The phase speed of Lamb waves provides localized information about the shear modulus of the medium which constitutes the foundation of dynamic OCT elastography [2]. A fresh porcine eye was excited with a needle connected to a piezoelectric actuator in order to produce a tone-burst of 1 kHz propagating from left to right. The propagation of the waves was detected using a phase-sensitive OCT system implemented with a swept source laser (HSL-2100-WR, Santec, Aichi, Japan) with a center wavelength of 1318 nm. The tone was sent every 35 ms in order to acquire motion frames at a frame rate of 20 kHz. The region of measurement in the sample consisted of 1024 X 400 elements covering a region of interest 2.5 mm high X 15 mm wide. After the acquisition process was conducted, motion frames were acquired and stored as a video. Subsequently, space-time maps were calculated for each propagation path parallel to the surface of the sample. Herein, the slope of the main peak trajectory of the tone-burst represents the inverse of the Lamb wave speed, which is related to the elasticity of the sample [3].

Porcine cornea reveals differentiated layers as shown in the 2D Lamb wave speed map (Fig. 1d). Moreover, we found a decreasing tendency when a vertical depth-resolved speed profile was analyzed. Similarly, sclera tissue shows defined layers (Fig. 1e) in good agreement with the structural image (Fig. 1b). Finally, the cornea/sclera transition shows two differentiated media in Lamb wave speed (Fig. 1f). Experiments reported an average speed of 1.31 m/s for cornea, and 4.42 m/s for sclera. The sclera/cornea average speed ratio was found to be 3.37. In addition, higher localized speed was found in the cornea/sclera interface which is consistent with the stress concentration generated by the traction in the joint of both tissue types. Further research is required in the area of Lamb waves using new propagation models which take into account the estimation of viscoelastic parameters.

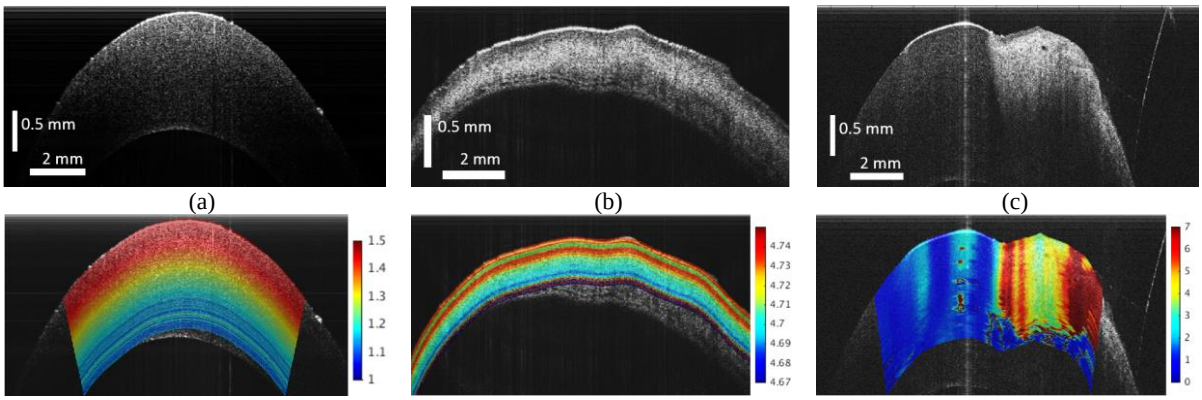

Fig 1. B-mode structural image of a porcine cornea (a), sclera (b), and cornea/sclera transition (c). 2D Lamb wave speed map depicting differentiated layers in cornea (d), sclera (e), and heterogeneous media in cornea/sclera transition (f).

References:

[1] C. Edmund, "Corneal elasticity and ocular rigidity in normal and keratoconic eyes," *Acta Ophthalmol*. (Copenh.) **66**(2), 134–140 (1988).
[2] I. A. Viktorov, *Rayleigh and Lamb waves: physical theory and applications*, New York : Plenum Press (1967).
[3] I. Z. Nenadic, M. W. Urban, M. Bernal *et al.*, "Phase velocities and attentuations of shear, Lamb, and Rayleigh waves in plate-like tissues submerged in a fluid (L)," *The Journal of the Acoustical Society of America*, **130**(6), 3549-3552 (2011).

3D Cell Structure Imaging with Laboratory Scale Cryo Soft X-ray Tomography

Kenneth Fahy[1], Fergal O'Reilly[1,2], Tony McEnroe[1], Jason Howard[1], Aoife Mahon[1], Ronan Byrne[1], Osama Hammad[1] and Paul Sheridan[1]

[1]SiriusXT Ltd., Science Centre North, Belfield, Dublin 4, Ireland.
[2]School of Physics, UCD, Belfield, Dublin 4, Ireland.

Main author email address: kenneth.fahy@siriusxt.com

Cryo-soft X-ray tomography (cryo-SXT) is an extremely powerful technique that allows the imaging of an entire cell in its fully hydrated state with natural contrast. Whole cells up to 10-15 microns thick can be imaged at a 3D resolution approaching 30 nm. Cryo-SXT preserves volatile structures, and since the cell is fully hydrated, avoids artefacts associated with sample shrinkage during dehydration. Cryo-SXT can also image the thickest parts of the cell, including the perinuclear region that contains many of the cell's organelles, which cannot be imaged in 3D by other techniques. Great progress has been made over the last decade in developing cryo-SXT as an imaging technique on synchrotron hosted microscopes [1-4]. Workflows have improved which allow non-synchrotron researchers to access the technique, and significant expertise has been developed in correlating SXT and cryo fluorescence data [5-7]. This amalgamation of techniques integrates 3D molecular localisation data with a high-resolution, 3D reconstruction of the cell. Here we report on the development of a compact lab based microscope that aims to deliver synchrotron performance in a system that will turn cryo-SXT into an affordable, efficient laboratory tool, thus increasing the scope and throughput of possible research projects. The key to this is the development of a sufficiently bright and compact source of soft X-rays.

The technology at the core of the SiriusXT instrument is a high-performance soft X-ray light source based on laser-produced plasma emission with the appropriate size, wavelength and brightness, combined with smart optics whose optical quality is not degraded by the debris generated by the plasma. This unique combination enables the deployment of a lab-scale stable and robust light source suitable for cryo-SXT. We show data on light source performance and first images from our microscope.

[1] C.A. Larabell & K.A. Nugent, Imaging cellular architecture with X-rays, Curr. Opin. Struct. Bio., **20,** pp. 623-631, (2010).
[2] G. Schneider et al, Three-dimensional cellular ultrastructure resolved by X-ray microscopy**,** Nature Methods, **7,** pp. 985-988, (2010).
[3] R. Carzaniga et al, Cryo-soft X-ray tomography: a journey into the world of the native-state cell, Protoplasma, **251,** pp. 449-458, (2014).
[4] J.L. Carrascosa et al, Cryo-X-ray tomography of vaccinia virus membranes and inner compartments, Journal of Structural Biology, **168**, pp. 234-239, (2009).
[5] B.P. Cinquin et al, Putting Molecules in Their Place, Journal of Cellular Biochemistry, **115**, pp. 209-216, (2014).
[6] R. Carzaniga et al, Correlative Cryo-Fluorescence and Cryo-Soft X-Ray Tomography of Adherent Cells at European Synchrotrons, Methods in Cell Biology, **124,** pp. 151- 178, (2014).
[7] K.C. Dent et al, Critical Step-by-Step Approaches Toward Correlative Fluorescence/Soft X-Ray Cryo-Microscopy of Adherent Mammalian Cells, Methods in Cell Biology, **124,** pp. 179-216, (2014).

BP-P-11

Off-axis holographic Laser Speckle Contrast imaging of blood vessels in tissues

A. Abdurashitov[1], O. Semyachkina-Glushkovskaya[1], V. Tuchin[1]

1- Saratov National Research State University, 83 Astrakhanskaya Street, Saratov, 410012

aarkady@me.com

Laser speckle contrast imaging (LSCI) has become the most widely spread tool for functional imaging in tissues [1,2]. Incomplete theoretical description and sophisticated interpretation of measurement results are completely sidelined by a simple hardware, fastness, consistent results and repeatability.
By this study we propose a relatively simple approach to extend capabilities of a typical single-exposure LSCI. It was shown that useful signal in LSCI comes from up to 700 microns from a tissue depth [3]. In this relatively small measuring volume, there is no depth-dependence of the signal. In many tissues the actual penetration depth of light is much greater than the focus depth of an imaging system, especially at imaging of capillaries by high NA objectives.

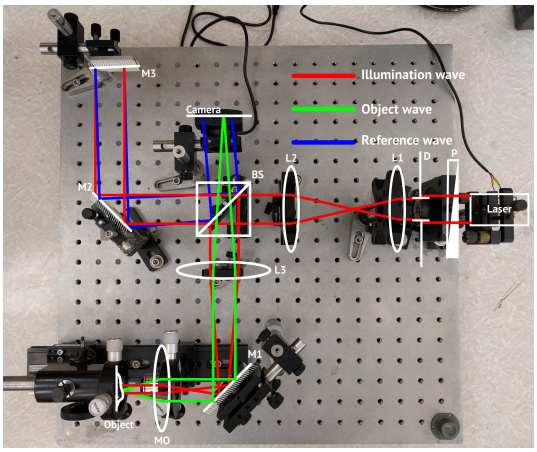

Fig. 1. A single-exposure LSCI setup based on Michelson interferometer.

The focus adjustment can be done mechanically by moving either object or objective lens. But this will limit speed and repeatability of measurements unless there is usage of high precision and high cost hardware. We propose to use off-axis holographic technique (fig. 1) to replace mechanical movements by numerical calculations. After recording of off-axis hologram we can retrieve the information about wave front in a complex form. Next, we can numerically simulate its propagation to a certain distance *z* along the depth axis of an object.
Such technique will allow us to obtain three-dimensional stack from one pre-recorded image. Along with that, single scattering approximation is an accurate estimation of LSCI signals [3] in a case of capillary imaging which makes mathematical formalism easier and intuitive. From this we can conclude that our setup can potentially provide a three dimensional information about *mean velocity* distribution in a capillary net. Which is by far most demanded diagnostic parameter in the study of stroke and over vascular catastrophes.

[1] M. Davis, et al., "Sensitivity of laser speckle contrast imaging to flow perturbations in the cortex", Biomedical optics express, vol. 7.3, pp. 759-775 (2016).
[2] H. Hayashi et al., "Ocular blood flow measured by laser speckle flowgraphy during aortic arch surgery with antegrade selective cerebral perfusion", Journal of Cardiothoracic and Vascular Anesthesia, vol. 30.3, pp. 613-618 (2016).
[3] M. Davis, SM Shams Kazmi and A. Dunn, "Imaging depth and multiple scattering in laser speckle contrast imaging", Journal of biomedical optics, vol. 19.8, pp. 086001-086001 (2014).

BP-P-12

Albumin Conformational Changes in Human Blood Plasma and in Model Solutions Monitored by Means of Capillary Electrophoresis with OD- and LIF-Channels

N. Zhdanova [1a], A. Maydykovskiy [1], E. Shirshin [1], A. Priezzhev [1], E. Prilepskaya [2], P. Rasner [2], V. Fadeev [1]

1- Department of Physics, M.V. Lomonosov Moscow State University, 119991, Leninskie gory, 1/2, Moscow, Russia
2- A.I. Evdokimov Moscow state University of Medicine and Dentistry 127473, Delegatskaya st., 20-1, Moscow, Russia

[a] *zhdanova@physics.msu.ru*

Serum albumin (SA) is the most abundant protein in blood plasma (BP). The main function of SA in blood circulatory is to transport different ligands such as fatty acids, drugs, metabolites, *etc.* and strongly depends on the protein conformation [1].

Optical methods are usually used to characterize SA conformational changes in solutions under different conditions (addition of chemicals, varying temperature, pH), and the results of these studies are extrapolated to human BP. Only a few works are devoted to investigation of SA conformation in BP to indicate pathological processes [2]. The serious limitation of investigation of human BP via optical methods is to separate SA optical response from that of other components.

Here we combine the advantages of optical methods with separation technique (capillary electrophoresis, CE). CE is based on the difference between mobilities of the components in the electric field which depend on the charge to mass ratio [3, 4]. CE setups are usually equipped with a single type of detector, *e.g.*, spectrophotometric [4]. In this work we expanded the opportunities of CE by using simultaneously two types of optical detectors: optical density measurements at 254 nm (OD-channel) and laser induced fluorescence spectra with excitation at 405 nm and registration in the 450 – 750 nm range (LIF-channel).

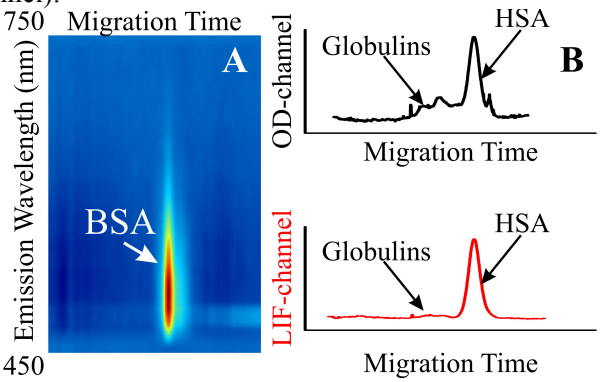

Fig. 1. (A) Spectrophoregramma of aqueous solution of BSA.
(B) Phoregramma of human BP: OD-channel and LIF-channel (the spectra were integrated by wavelength)

Here we investigate model solutions of bovine serum albumin (BSA) as well as human BP. The comparison of signals from OD- and LIF-channels confirms that BSA and human serum albumin in BP have a fluorescence band centered at 525 nm that can be excited at 405 nm (Fig. 1). Though the origin of this 405 nm/525 nm band remains debatable, we suppose that it is due to the interactions between aromatic residues which lead to formation of new low energy excited states. We showed that the migration time of SA as well as the shape of the 405 nm/525 nm fluorescence band strongly depends on the bound ligands that allows one to use CE with OD- and LIF-channels for diagnostics of pathology.

The reported study was supported by Russian Foundation of Basic Research (grant № 16-32-00804).

[1] T. Jr. Peters, Serum albumin, Advanced in protein chemistry, vol. 37, pp. 161-245, (1985).
[2] G. Fanali, A. di Masi, V. Trezza, M. Marino, M. Fasano, and P. Ascenzi, Human serum albumin: from bench to bedside, Molecular aspects of medicine, vol. 33, no 3, 209-290 (2012).
[3] P.D. Grossman and J.C. Colburn, Capillary electrophoresis: Theory and practice (Academic Press), (2012).
[4] P.A.H.M. Wijnen and M.P. van Dieijen-Visser, Capillary electrophoresis of serum proteins. Reproducibility, comparison with agarose gel electrophoresis and a review of the literature, Clinical Chemistry and Laboratory Medicine, vol. 34, no. 7, pp. 535-546 (1996).

BP-P-13

Laser Trapping for the Measurement of Forces at Red Blood Cells Aggregation and Disaggregation

A.N. Semenov[1,2], K. Lee[3], A.E. Lugovtsov[1,2], A.V. Priezzhev[1,2]

1 - Faculty of physics and 2 - International Laser Center of M.V. Lomonosov Moscow State University, Leninskiye Gory, 1-2, 119991, Moscow, Russia
3 - Opto-Electronics and Measurements Techniques Unit, University of Oulu, Erkki Koiso-Kanttilan katu 3, 90570, Oulu, Finland

semenov@physics.msu.ru

Laser trapping systems provide a convenient and very effective opportunity for assessing the mechanisms of interaction on the level of single cells and/or macromolecules [1]. In this study, laser tweezers (LT) were used for trapping the red blood cells (RBC) and measuring the interaction forces between them for studying the process of the RBC aggregation. Spontaneous aggregation of RBCs takes place both *in vivo* and *in vitro* and leads to the formation of first linear and then 3D aggregates, which can be disassembled (disaggregated) when shear stresses in the flow or other external forces are applied. RBC aggregation significantly influences the blood viscosity at low shear stress conditions and affects the blood circulation. With the perspective for the clinical application a number of methods were developed for the quantitative assessment of this property [2]. Recently the LT were introduced to this research and were shown to be a promising tool for the further assessment of the RBC aggregation. In particular LT could characterize the cells interaction strength, which cannot be measured with the conventional methods [3].

We measured the cells aggregation and disaggregation forces (F_A and F_D respectively) using a home-made two-channel LT comprising two Nd:YAG lasers (1064 nm, 200 mW) and a high numerical aperture objective (N.A. = 1.00, x100). One lasers beam could be moved using a motorized-mirror. The measurements were performed in diluted suspension of RBCs (~0.05%) in autologous plasma. The blood for measurements was drawn by venipuncture from patients suffering from Diabetes Mellitus Types I and II (DMI and DMII respectively) and from healthy donors.

F_A – the force leading to overlapping of the two adjacent cells was measured by comparing it with the minimum trapping force (F_T) required for holding the cells from spontaneous overlapping. Measurements were performed in 3 stages: (1) two single RBCs were trapped using different channels of LT; (2) these cells were moved and brought to a point contact; in this position, the cells remain still as long as $F_T > F_A$; (3) F_T was slowly decreased by decreasing the beam power until F_A exceeds F_T and the cell escaped from the trap and overlap. At this point we considered that $F_A$was matching F_T.

F_D – the force that should be applied to separate the cells from each other was measured in 4 stages: (1-2) the aggregate of two RBCs was formed with the same procedure as for F_A measurements; (3) – the cells were separated by moving one of the channels of LT, while the trapping force was slowly decreasing; (4) – the F_T sufficient for separating the cells was found which is equal to F_D.

Each set of F_A and F_D measurements was performed on 15 pairs of RBC for each blood sample and within 3 hours after drawing the blood. Each group of donors included 5-7 persons. The results showed that F_D exceeds F_A by 10-15% in all of the groups. The highest values of the RBC interaction forces were obtained in DMI group (F_A = 6.3 ± 1.5 and F_D = 7.4 ± 2.1 pN). The results in DMII group were F_A = 3.1 ± 0.8 and F_D = 5.0 ± 1.3 pN. The results in the group of healthy controls were F_A = 0.9 ± 0.2 and F_D = 4.9 ± 1.3 pN. We conclude that the cells interaction forces are elevated in the blood of DMI and DMII patients, the highest elevation being observed especially in the former case. The highest difference between F_A and F_D was found for healthy donors. This difference decreases when the cells interaction is enhanced in disease, and finally almost vanishes as in the case of DMI.

The work was partially supported by the RFBR grant № 16-52-51050.

[1] P. Ashokand, K.Dholakia, Optical trapping for analytical biotechnology, Current Opinion in Biotechnology, vol. 23, pp. 16-21 (2012).
[2] O. Baskurt, B. Neu and H. Meiselman, Red Blood Cell Aggregation (CRC Press), Chapter 4 Measurement of Red Blood Cell Aggregation, (2012).
[3] K. Lee, A. Danilina, M. Kinnunen, I. Meglinski and A. Priezzhev, Probing the red blood cells aggregating force with optical tweezers, IEEE Journal of Selected Topics in Quantum Electronics, vol. 22, pp. 7000106 (2016).

BP-P-14

Nano-sensitive optical coherence tomography for the study of structural changes under deformation

G. Lynch[1], S. Alexandrov[1], M. Leahy[1]

1- Tissue Optics and Microcirculation Imaging Group, School of Physics, National University of Ireland Galway, Galway, Ireland

Main author email address: g.lynch9@nuigalway.ie

Optical coherence tomography (OCT) is a rapidly advancing optical imaging technique. It is non-contact, non-invasive and can offer depth-resolved images of highly scattering samples in real time. OCT has myriad applications in the field of biomedical imaging and diagnosis. One such application is optical coherence elastography (OCE). OCE is a promising new method for measuring a sample's mechanical properties. It is performed by applying some mechanical stimulation, or stress, and using OCT to detect the resulting displacement with submicron resolution, usually through speckle tracking or phase detection. The magnitude of the displacement is then related to the mechanical properties of the sample [1].

Nano-sensitive OCT (nsOCT) is a novel label-free imaging technique which has been shown to provide axial structural information with nanometre sensitivity [2]. In nsOCT, the image contrast is based on the spatial frequencies present in a sample. The axial spatial frequencies are directly related to the sample structure. When a sample is illuminated at a fixed illumination angle, the wavelength of the light scattered from a particular sample location depends on the spatial frequency content of the sample. At each sample location, each of the diffracted wavelength components encode a particular spatial frequency component. In Fourier domain OCT (FDOCT), the spectrum at the detector is composed of multiple backscattered wavelengths. Conventional OCT image reconstruction relies on an inverse Fourier transform, during which the spatial information is integrated, which means there is some loss of high frequency information in the reconstructed sample axial profile. In nsOCT, the information is retained by encoding each axial spatial frequency with one unique wavelength [3]. Wavelength is unchanged by the Fourier transform from wavenumber domain to depth domain so the encoded axial spatial frequency is not lost.

This study considers the changes that occur in the structure of a sample under axial deformation. Axial deformation should lead to a change in the axial spatial frequencies. Using nsOCT, the changes in the axial spatial frequency before and after deformation will be investigated and visualised. In contrast to conventional OCE, the spatial distribution of deformations can potentially be reconstructed from just a single frame. Since pathologies such as cancer show structural changes at the nanoscale, the method shows promise as a useful contrast mechanism for elastography.

[1] B. Kennedy, K. Kennedy, D. Sampson, "A Review of Optical Coherence Elastography: Fundamentals, Techniques and Prospects", IEEE Journal on Selected Topics in Quantum Electronics, 20, 2, 7101217, (2014).
[2] S. Alexandrov, H. Subhash, A. Zam, M. Leahy, "Nano-sensitive optical coherence tomography", Nanoscale, 6, pp.3545-3549, (2014).
[3] S. Alexandrov, H. Subhash, M. Leahy, "Nanosensitive optical coherence tomography for the study of changes in static and dynamic structures", Quantum Electronics, 44, 7, 657-663, (2014)

BP-P-15

Doppler MR-OCT angle optimization and depth characterization for flow detection and velocity measurement

Sean O Gorman[1*], Roshan Dsouza[1], Kai Neuhaus[1], Josh Hogan[3], Carol Wilson[3], Paul M. McNamara[1,3] and Martin J. Leahy[1,2]

[1]*Tissue Optics and Microcirculation Imaging group, School of Physics, National University of Ireland, Galway, Ireland.*

[2]*Royal College of Surgeons (RCSI), Dublin, Ireland.*

[3]*Compact Imaging, Inc., 897 Independence Ave., Suite 5B, Mountain View, CA 94043 USA.*

[*]*s.ogorman2@nuigalway.ie*

ABSTRACT

Multiple reference optical coherence tomography (MR-OCT) is a new compact optical imaging device based on a recirculating reference arm scanning optical delay. This technology promises to be a robust, cost-effective semi-solid state design capable of integrating with next generation mobile devices. The re-circulating optical delay utilizes a voice coil actuator and a partial mirror to build up a multiple order interference pattern which can be simultaneously detected with each sweep of the actuator. Our group has recently demonstrated the capability of this method to detect and measure flow using Doppler signal analysis. The MR-OCT system operates at 1310nm with a spatial resolution of ~26 µm and an axial scan rate of 600Hz. Initial studies show a displacement-sensitivity of ~20 nm to ~120 nm for the first 1 to 9 orders of reflections, respectively with a mirror as test-sample. The corresponding minimum resolvable velocity for these orders are ~2.3 µm/sec and ~15 µm/sec respectively. The angle-dependence of the Doppler signal and flow measurements in agar capillary flow phantoms are investigated to examine the depth dependence of velocity measurement in scattering media.

Keywords: *Multiple reference optical coherence tomography, time-domain, wearable devices, biometrics*

Improved signal quality of filtered signals for multiple reference optical coherence tomography (MR-OCT) using a Gaussian window.

Kai Neuhaus[1] ***Sergey Alexandrov***[2] ***Roshan Dsouza***[3], ***Sean O'Gorman***[4], ***Paul McNamara***[5], ***Josh Hogan***[6], ***Carol Wilson***[7], ***Martin Leahy***[8], ***and Hrebesh Subhash***[9]

1-5,8,9 – Tissue Optics and Microcirculation Imaging Group, School of Physics, National University of Ireland, Galway, Ireland
8 – Royal College of Surgeons (RCSI), Dublin, Ireland
3,5-7,9 – Compact Imaging, Inc., 897 Independence Ave., Suite 5B, Mountain View, CA 94043 USA

k.neuhaus2@nuigalway.ie

The growing interest in portable and low-cost optical coherence tomography (OCT) to improve point-of care applications is apparent with increasing research efforts using photonics integrated circuits. MR-OCT is another technology that is using the advantages of well known CD/DVD-ROM technology to build miniaturized and low-cost OCT systems. To separate the the multiple signals originating from the multiple reflections of the partial mirror in the reference arm of Michelson interferometer the filtering can be improved by limiting the signals with a Gaussian window. Additionally a filter using a Gaussian window in the frequency domain is compared to an elliptic and an Chebychev type 2 filter. The SNR is compared on a variety of test signals generated with a mirror in the sample arm at different attenuation levels and the CNR is used to compare the image quality on a layered tape as a scattering sample.

[2]sergey.alexandrov@nuigalway.ie
[3]r.dsouza1@nuigalway.ie
[4]s.orgorman2@nuigalway.ie
[5]pmcnamara@compactimaging.com
[6]jhogan@compactimaging.com
[7]cwilson@compactimaging.com
[8]martin.leahy@nuigalway.ie
[9]hrebesh.mollysubhash@nuigalway.ie

BP-P-17

Thermogenetic activation of individual cells and neurons by infrared and microwave radiation

A.B.Fedotov[1,2], Yu.G.Ermakova[3], I.V.Fedotov[1,2], A.A.Lanin[1,2], V.V.Belousov[3], A.M.Zheltikov[1,2,4]

1 - Physics Department, International Laser Center, M.V. Lomonosov Moscow State University, Moscow 119992, Russia
2 - Russian Quantum Center, ul. Novaya 100, Skolkovo, Moscow Region, 143025 Russia
3 - M.M. Shemyakin and Yu.A. Ovchinnikov Institute of Bioorganic Chemistry, Russian Academy of Sciences, Moscow 117997, Russia
4 - Department of Physics and Astronomy, Texas A&M University, College Station TX 77843, US

a.b.fedotov@phys.msu.ru, zheltikov@physics.msu.ru

Modern technologies enabling precision control over the electrical activity of specific cells or neurons in a living organism offer unique opportunities for the functional analysis of complex biological systems. Thermogenetics is a promising innovative neurostimulation technique, which enables a robust activation of cells and neurons using thermosensitive transient receptor potential (TRP) cation channels [1, 2]. The TRP channels are three orders of magnitude more conductive than conventionally associated with optogenetic channelrhodopsin (ChR) channels and can be activated by heat induced with infrared light [3]. However, a broader application of this approach is hindered by a limited variety of suitable ion channels, as well as by low spatial and temporal resolution.

In the present study, we demonstrate addressed thermogenetic activation of individual cells and neurons using infrared radiation and microwave field. We use TRPA1 channels from snakes as a thermogenetic stimulator of Human Embryonic Kidney 293 (HEK-293) cells, mouse neurons, as well for induction of zebrafish larvae behavioral response. To investigate addressed heating of the transfected cells and neurons by infrared radiation, we used tunable radiation at wavelengths from 1.1 to 1.5 μm that the infrared radiation could be focused to a spot with the diameter about 30 μm, that guaranteed heating of single cell. The neuronal response to the activation by IR laser radiation is fully characterized by means of Ca^{2+} imaging technique. A unique fiber-optic probe that integrates a nitrogen–vacancy diamond quantum sensor with optical and microwave waveguide delivery enables thermometry with a single-cell resolution, allowing neurons to be activated by exceptionally mild heating, thus preventing toxic effects of excessive heat [4]. From the other hand, in specific regimes, this fiber probe can operate as the local source of the heat and microwave radiation enabling changing of the temperature and addressed activation of transfected cells and neurons.

With this arsenal, we carried out a systematic, in-depth characterization of the performance of TRPA1 channels in HEK-293 cells and neurons, including accurate measurements of the pertinent Ca^{2+} dynamics and electrophysiological analysis of the response. Our study demonstrates that the snake TRPA1 channels are ideally suited as a tool for addressed thermogenetics of individual cells, neurons in living animals. The work was supported by Russian Foundation for Basic Research (projects 14-29-07263, 14-29-07182, 16-32-80141). Research into thermogenetic stimulation of TRPA1 expressing cells has been supported by the Russian Scientific Foundation (project No. 14-14-00747).

[1] J.G.Bernstein, P.A.Garrity, E.S.Boyden. Optogenetics and thermogenetics: technologies for controlling the activity of targeted cells within intact neural circuits. Current Opinion in Neurobiology, vol. 22, pp. 61-71 (2012).
[2] E.O.Gracheva, N. T. Ingolia, Y. M. Kelly, et al., Molecular basis of infrared detection by snakes. Nature. vol. 464, pp. 1006-1001 (2010).
[3] D.E.Bath, J.R.Stowers, D.Hormann, A.Straw. FlyMAD: rapid thermogenetic control of neuronal activity in freely walking Drosophila. Nature methods vol. 11, pp. 756-762 (2014).
[4] I.V. Fedotov, N.A.Safronov, Yu.G.Ermakova, et.al., Fiber-optic control and thermometry of single-cell thermosensation logic. Scientific reports. vol. 5, n.15737 (2015).

BP-P-18

In vivo deep-brain imaging with reconnectable neurointerfaces

I.V.Fedotov[1,2], M.S.Pochechuev[3], O.I.Ivashkina[2], M.A.Roshina[2], A.B.Fedotov[1,3], K.V.Anokhin[3], A.M.Zheltikov[1,2,3,4]

1 - Physics Department, International Laser Center, M.V. Lomonosov Moscow State University, Moscow 119992, Russia
2 - Kurchatov Institute National Reseacrch Center, pl.akad.Kurchatova 1, Moscow 123182, Russia
3 - Russian Quantum Center, ul. Novaya 100, Skolkovo, Moscow Region, 143025 Russia
4 - Department of Physics and Astronomy, Texas A&M University, College Station TX 77843, US

a.b.fedotov@phys.msu.ru, zheltikov@physics.msu.ru

Modern optics provides unique opportunities for the investigation of brain and higher nervous activity. The combination of advanced laser technologies and neurosciences is opening a new multi-disciplinary direction of natural sciences — neurophotonics. Neurophotonics is providing the development of a wide spectrum of tools for functional brain diagnostics, stimulation of individual neurons and neural networks, as well as molecular engineering of brain cells aimed at a diagnosis and therapy of neurodegenerative and psychic diseases. Optical fibers suggest unique approaches helping to confront the most challenging problems in brain research, including the analysis of cellular and molecular mechanisms behind memory and cognition. Optical fibers of new generation offer new solutions for the development of fundamentally new, unique tools for neurophotonics and laser neuroengineering — fiber-optic neuroendoscopes and neurointerfaces [1-3]. Neurointerfaces open new horizons for the investigation of the most complex brain functions, enabling a long-term multiplex detection of fluorescent protein markers, as well as photostimulation of neuronal activity in deep brain areas in living, freely behaving animals with an unprecedented spatial resolution and minimal invasiveness [4-6]. This emerging technology opens new horizons for understanding learning and long-term memory through experiments with living, freely behaving mammals.

In the present work, we demonstrate optical reconnectable neurointerface based on bundles of microscaled fibers integrated with scanning fast galvanometric mirrors. We used reconnectable neurointerface and different lines of transgenic mice for low invasive i*n vivo* experiments, that demonstrated multiplex visualization of marker proteins in the brain of freely moving animals with cellular space resolution at long temporal scale. This work was supported by the Program ‘Research and Development in Priority Areas of Development of the Russian Scientific and Technological Complex for 2014–2020’ (Contract 14.607.21.0092 of November 21, 2014; unique identifier of applied research: RFMEFI60714X00.

[1] E.S. Boyden, F. Zhang, E. Bamberg, G. Nagel, and K. Deisseroth, "Millisecond-timescale, genetically targeted optical control of neural activity." Nature Neuroscience, vol. **8**, pp.1263–1268 (2005).
[2] K. Deisseroth, “Optogenetics.” Nature Methods, vol.**8**, pp. 26–29 (2011).
[3] D.R. Sparta, A.M. Stamatakis, J.L. Phillips, N. Hovelsø, R. van Zessen, and G.D. Stuber, “Construction of implantable optical fibers for long-term optogenetic manipulation of neural circuits.” Nature Protocols, vol. **7**, pp.12 – 23 (2012).
[4] L.V. Doronina-Amitonova, I. V. Fedotov, O. I. Ivashkina, M. A. Zots, A. B. Fedotov, K. V. Anokhin, and A. M. Zheltikov, "Implantable fiber-optic interface for parallel multisite long-term optical dynamic brain interrogation in freely moving mice." Scientific Reports. vol. 3, n.3265 (2013).
[5] L.V. Doronina-Amitonova, I.V. Fedotov, O.I. Ivashkina, M.A. Zots, A.B. Fedotov, K.V. Anokhin, and A.M. Zheltikov. “Enhancing the locality of optical interrogation with photonic-crystal fibers.“ Applied Physics Letters. vol.101, pp. 021114 (2012).
[6] L.V.Doronina-Amitonova, I.V.Fedotov, A.B.Fedotov, K.V.Anokhin, A.M.Zheltikov. “Neurophotonics: optical methods to study and control the brain.” Physics-Uspehi. vol. 58, pp. 345–364 (2015).

BP-P-19

Development of a clinical diagnostic decision support expert system for skin melanoma

O.V.Rodionova[1], V. G.Nikitaev[1], V.Yu. Selchuk[2], A.A. Ananskaya[1], E.A. Komochkina[1]

1- National Research Nuclear University MEPhI (Moscow Engineering Physics Institute), Moscow,Russia.
2 - Blokhin Russian Oncological Scientific Center , Moscow, Russia.

olesya2309@inbox.ru

The urgency of melanoma diagnosis is due to the direct relationship between the survival of patients with this tumor and its timely detection at the early stages of development. Both the lack of physicians' oncological vigilance in identifying the background for the occurrence of melanoma tumors and the early stages of melanoma detection in most cases lead to its late diagnosis and high mortality in patients. Generally, at the beginning of the treatment process regional spread of the disease takes place already in 75% of patients, and the five-year survival rate is less than 50%. Although each person on the average has 20 moles, annually only 7 out of 100,000 people fall ill with melanoma Melanoma appears to be a serious problem as annually 10%-30% patients diagnosed with melanoma die [1].
Diagnosis of melanoma during morphological studies of microscopic medications is based on the approach of "bright field" in transmitted light for the analysis of transparent substances. In order to make cells' and tissues' structure perceptible, medications are being labeled with dyes. The pictures of cells' and tissues' structure are got due to light diffraction. Colored pictures, which are got by this approach, allow to analyze the cells' and tissues' structure and judge whether they are sane or they are subject to some pathologic process (cancerous tumor, for example).
Currently, due to the extension of availability of information the diagnostic issues are extremely difficult to solve. Therefore, the use of computer-assisted medical systems and decision support systems (DSS) holds a lot of importance to improve the efficiency of diagnosis of various diseases.
The aim of this work is to develop a computer system for melanoma diagnosis [2], which allows physicians to accurately and quickly diagnose the patients suspected of having the disease.
The structure of a computer expert medical system for melanoma diagnosis Based on light microscopy in the perceptible range of electromagnetic radiation, comprises four main blocks: a knowledge base (KB), a decision-making mechanism consisting of two subsystems: subsystem of analytical and search subsystem, an input mechanism and data output (Figure 1).

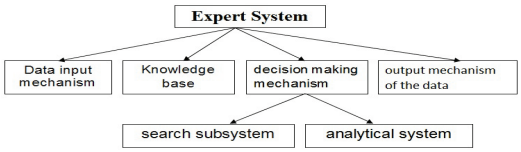

Fig. 1. Conceptual representation of the expert system for melanoma diagnosis

Knowledge base is a principal component of the expert system. It is due to the decision-making mechanism that Knowledge Base is to provide diagnostic information (symptoms, diagnoses) in response to the user requests. You can load, edit and delete symptoms, diagnoses, images in Knowledge Base.
The system under development will help to solve such problems as:
1) An additional level of control. The system will allow making the provisional diagnosis of the patient with a higher level of fidelity (Figure 2)

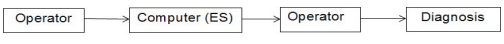

Fig. 2. The block diagram of the diagnosis

2) Comparison of other patients' symptoms by means of the analytical system KB provides an opportunity to study in the process of diagnosing the patient.
The expert system under discussion serves a tool to support the physician's decision making in diagnosing melanoma. In the future the ES developed is expected to be included into the multimedia training complex for skin melanoma for internship doctors and attending physicians.

[1] U. Sharfman, Melanoma, trans. from English. Ed. L.V. Demidova (Garnet) (2015)
[2] A.A. Cherniavsky, Skin melanoma: a teaching aid (NSMA) (2013)

BP-P-20

Design and assembly of a miniature multiple reference optical coherence tomography imaging device

P. M. McNamara[1, 2], C. O'Riordan[3], S. Collins[3], P. O'Brien[3], C. Wilson[2], J. Hogan[2], M. J. Leahy[1]

1- Tissue Optics and Microcirculation Imaging group, National Biophotonics and Imaging Platform, National University of Ireland, Galway, Ireland.
2- Compact Imaging Inc. 897 Independence Avenue, Suite 5B, Mountain View, CA 94043, USA.
3- Irish Photonic Integration Centre (IPIC), Tyndall National Institute, Lee Maltings Complex, Dyke Parade, Cork, Ireland.

Main author email address: paul.mcnamara@nuigalway.ie

Multiple reference optical coherence tomography (MR-OCT) is a new modality of OCT, which is well-suited to low-cost, portable OCT imaging. This modality is a version of time-domain OCT, which utilizes a partial mirror in front of the reference mirror to re-circulate the reference beam allowing extended scanning in depth. A major advantage of this method is that simultaneous depth scanning with a relatively short sweep of a voice coil motor (on which the scanning mirror is mounted) can be achieved. There are numerous potential applications for this technology including biometric security, ophthalmology, dentistry, dermatology and non-destructive testing, all of which have previously been demonstrated using bulk optics configurations [1-3]. This work presents the development of the first iterations of a miniature MR-OCT device. This device utilizes a fibre-coupled input from an off-board superluminescent diode (SLD). The dimensions of the device are 40 mm by 60 mm, but future designs are expected to be smaller in size. All of the miniature components used in the device (i.e. optical components, voice-coil motor and photodetectors) are off-the-shelf which demonstrates the potential for low-cost manufacturing.

This photonic device was assembled as both polarized and non-polarized configurations and can include balanced detection. The device also has an on-board transimpedance amplifier with complimentary outputs. Assembly of the device required extensive planning. In choosing the optical components, Zemax simulations are performed to model the beam characteristics. The layout procedure is modelled using Solidworks and each component is placed and aligned via a well-designed alignment procedure involving an active-alignment 'pick-and-place' automation system.

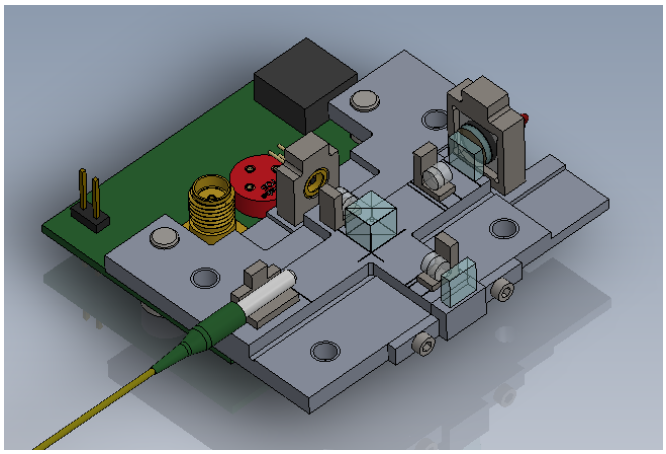

Fig. 1 Solidworks drawing for the unpolarized miniature MR-OCT device.

[1] R. Dsouza, H. Subhash, K. Neuhaus, J. Hogan, C. Wilson and M. Leahy, Dermascope guided multiple reference optical coherence tomography, Biomedical Optics Express, 5(9), 2870-2882, (2014)
[2] R. Dsouza, H. Subhash, K. Neuhaus, R. Kantamneni, P. M. McNamara, J. Hogan, C. Wilson and M. Leahy, Assessment of curing behavior of light-activated dental composites using intensity correlation based multiple reference optical coherence tomography, Lasers in Surgery and Medicine, (2015).
[3] R. Dsouza, H. M. Subhash, K. Neuhaus, J. Hogan, C. Wilson and M. Leahy, 3D nondestructive testing system with an affordable multiple reference optical-delay-based optical coherence tomography, Applied Optics, 54(18), 5634-5638 (2015).

Laser Diagnostics and Spectroscopy

LDS-1-1 (Invited)

Biomedical Applications of Vibrational Spectroscopy: Disease Diagnostics and Beyond

Hugh J. Byrne
FOCAS Research Institute, Dublin Institute of Technology, Kevin Street, Dublin 8, Ireland
Hugh.Byrne@dit.ie

The presentation will describe the efforts of the group in DIT to develop the applications of vibrational spectroscopy for disease diagnostics and beyond, into the realm of in vitro characterisation of the effects of external agents, including chemotherapeutic agents and nanomaterials.

The potential of vibrational spectroscopy, both Raman scattering and FTIR absorption, for label free screening and analysis of disease onset and progression is well established, and applications in cervical tissue biopsies and cytological samples will be described. In cervical cell lines, spectroscopy can discriminate between cells of different degrees of infection with the Human Papilloma Virus, and it is demonstrated that partial least squares regression can be employed to correlate the changes in the spectral profiles to both HPV copy number as well as the upregulation of the protein p16INK4A.

Although the potential of the techniques has been demonstrated by many over the past decades, there is much progress to be made towards the translation to the clinic, and international collaborative efforts to address the identified challenges will be briefly outlined.

Beyond diagnostics, the analytical potential of vibrational screening can also be harnessed for label free screening technologies. In a lung adenocarcinoma cell line, the action of the commercial chemotherapeutic agents doxorubicin, cisplatin and vincristine can be characterised on a subcellular level using Raman spectroscopy. Characteristic spectroscopic signatures of groove binding and intercalation can be identified and differentiated, and the direct chemical effects of the action of the drug can be differentiated from the indirect physiological effects. Multivariate regression models can be established to compare the efficacies of the different chemotherapeutic agents.

In the field of nanotoxicology, Raman spectroscopy can be demonstrated to be an effective monitor of the cellular response, but also as an effective technology to localise and identify the nanoparticles subcellularly, as well as to explore the local environment of the nanoparticle and thus probe the subcellular trafficking and mechanisms of response.

Vibrational spectroscopy is thus demonstrated to represent a truly label free probe of cellular responses beyond the realm of disease diagnostics.

LDS-1-2 (Invited)

Micro-Raman spectroscopy and imaging of group IV semiconductor epitaxial nanolayers for photonic and opto-electronic applications

Tatiana S. Perova

Department of Electronic and Electrical Engineering, Trinity College Dublin, The University of Dublin, Dublin 2, Ireland

perovat@tcd.ie

Raman spectroscopy demonstrates an excellent ability for analysis of stress, composition and defects in groups III-V and II-IV semiconductors, including SiGe, SiC and GeSn alloys. SiGe alloys, for example, were intensively studied for the last quarter of the century and the relationship for different Raman modes depending on Ge content and stress were well established [1]. However, there are only few Raman investigations of GeSn alloys and very thin SiC epitaxial layers published up to date. Furthermore, there are discrepancies of the reported results, related in particular, to the frequency dependence of the main Raman modes versus Sn content for strained and relaxed GeSn layers [2]. In this presentation the results of our recent investigations on ultra-thin SiC layers using micro-Raman mapping (or imaging) technique and on polarized micro-Raman spectroscopy of homogeneous and non-homogeneous GeSn alloys are discussed.

For GeSn alloys it was demonstrated from the comparison of the Raman spectra in two different polarizations, that Ge-Ge and Ge-Sn peaks are more easy to analyze in $z(x,x)\underline{z}$ configuration, while Sn-Sn peak is more pronounced and isolated in $z(x,y)\underline{z}$ configuration. Based on analysis of the aforementioned Raman bands, the dependences of various peaks position vs Sn content (obtained from XRD measurements) were established. It was also shown that the segregates, obtained at higher Sn content as a results of phase separation and Sn diffusion to the surface, are of metallic tin origin.

The thin SiC layers grown by a new method of solid-gas phase epitaxy were also investigated. It is shown that the ultra-thin SiC layers on Si (111) are composed of a cubic polytype of SiC with a small amount of 6H-SiC [3]. The presence of the voids formed in Si under SiC film has been experimentally confirmed by micro-Raman spectroscopy and SEM. Line and area Raman mapping was performed at the voids area. The strong enhancement in the peak intensity of the TO and LO modes is observed for the Raman signal measured in the void area. The intensity of TO Si-C peak increases with void depth (Fig. 1). The enhancement of the electromagnetic field at the voids was also confirmed by theoretical calculation based on Fresnel's equation. The Raman line mapping experiments presented in this work confirm that the voids formed in the Si substrate under the SiC layer cause relaxation of the elastic stress caused by lattice mismatch between the SiC and Si. This enhancement of the Raman signal allows micro-Raman measurements to be used for the detection of different polytypes in ultra-thin SiC layers. It was demonstrated that the quality of GaN layers grown on SiC layers consisting of a mixture of the cubic and hexagonal polytypes is better than that of GaN layers grown on a single SiC polytypes [4].

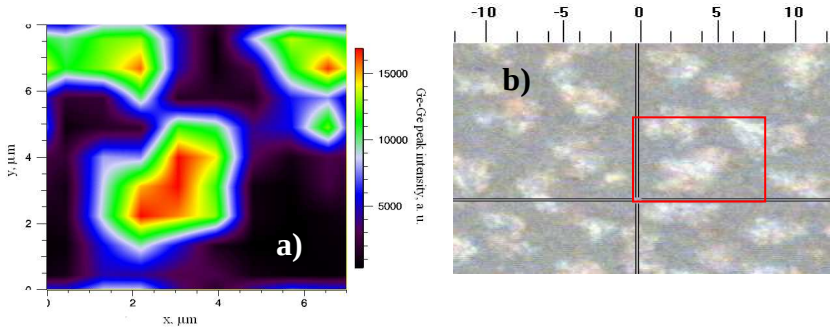

Fig. 1. (a) Raman area map of the Si-C peak intensity corresponding to (b) the optical microscopy image of mapped area (within red square).

[1] T.S. Perova, J. Wasyluk, K. Lyutovich et al., J. Appl. Phys., 109, 033502/1-11 (2011).
[2] M. Oehme, K. Kostecki, M. Schmid et al., Thin Solid Films, 557, 169-172 (2014).
[3] T.S. Perova, J. Wasyluk, S.A. Kukushkin et al., Nanosc. Res. Let., 5, 1507-1511 (2010).
[4] V.N. Bessolov, V.N. Konenkova, S.A. Kukushkin et al., Techn. Phys. Lett., 40, 386-388 (2014).

LDS-1-3 (Invited)

Raman spectroscopy for cytopathology applications

Fiona Lyng

DIT Centre for Radiation and Environmental Science, FOCAS Research Institute, Kevin St, Dublin 8, Ireland

There is an unmet clinical need for new methods to aid clinicians in the early detection of cancer. Current gold standard methods include cytopathology and histopathology but these methods are limited in terms of subjectivity, cost and time. Raman spectroscopy has emerged as a promising new technology for cancer diagnosis and over the past 15 years, there have been numerous reports showing the potential of Raman spectroscopy together with multivariate statistical analysis for the detection of a variety of cancers. This talk will discuss the potential of Raman spectroscopy for cytopathology applications. Studies on the use of Raman spectroscopy for cervical and oral cytopathology will be presented.

Integrated Diffuse Optical Tomography and Hyperspectral Fluorescence System for Tumor Assessment

C.E. Matei[1], M. Patachia[1], S. Banita[1], M. Petrus[1], C. Achim[1], D.C. Dumitras[1]

1- Laser Department, National Institute for Laser, Plasma and Radiation Physics, 077125 Magurele, Romania

consuela.matei@inflpr.ro

Since the 1990s, hybrid imaging has revolutionized the medical diagnosis by means of combined hardware images and software fusion methods allowing complex intrinsic information about functional and anatomical characteristics of soft or hard tissues. The hybrid imaging increased the chances of early diagnosis, improved the accuracy of the anato-metabolic collected data, or allowed the precise monitoring of interventional procedures, while the patients avoid multiple examinations and radiation exposure. The advantages of these methods are mostly to be seen in oncology, where the interest resides in several directions as monitoring the tumor evolution following radiation therapy, improving the discrimination rate between benign and malign nature of tumors in the diagnostic process, or helping the surgeon to assess the tumor spreading during resection procedures. Also, the less invasively the method, the more welcomed by both patients and medical staff.

Starting from these premises, we developed in our laboratory a dual imaging system based on Diffuse Optical Tomography (DOT) and Hyperspectral Fluorescence Spectroscopy (HFS). Typically DOT technique monitors the levels of oxygenated and deoxygenated hemoglobin and could measure redox states of cytochromes by means of carefully selecting the employed wavelengths. HFS brings complementary information based on the autofluorescence of the endogenous tissue fluorophores.

Our DOT system is equipped with two laser diodes (780 nm and 830nm) as light sources, and is built on a 16 optical fiber circular configuration, using two fast 1x8 fiber switches as multiplexors, and a high gain detection chain. The hyperspectral imaging module is working in the spectral range 400 - 1000 nm, with a nominal spectral resolution of 2.73 nm. The CCD camera has a monochrome 2/3" sensor, being able to acquire 1.5 Mega pixel images at 11 fps. For data acquisition and basic processing of the hyperspectral images, the producer's company software SP-SpectralDAQ is used.

Our paper will present in detail the technical construction, considering both optical and electronic aspects, describing the calibration protocol and showing the result of test measurements, followed by several considerations on the reconstruction procedure.

Acknowledgements: This work has been funded by a grant of the Romanian Ministry of Education, CNCS-UEFISCDI, project number PN-II-PT-PCCA-2013-4-2098.

Study of Nitrogen Incorporation into Nanodiamond Films by Multi-wavelength Raman Spectroscopy

M. Veres[1], I. Rigó[1], L. Himics[1], S. Tóth[1], A. Nagy[1], A. Czitrovszky[1], C. Popov[2], V. Ralchenko[3]

1- Wigner Research Centre for Physics, Hungarian Academy of Sciences, 1121 Budapes, Konkoly Thege M. str. 29-33, Hungary
2- Institute of Nanostructure Technologies and Analytics, Center for Interdisciplinary Nanostructure Science and Technology (CINSaT), University of Kassel, Germany
3- Prokhorov General Physics Institute, Russian Academy of Sciences, 119991 Moscow, Vavilov Str. 38, Russia

veres.miklos@wigner.mta.hu

Raman spectroscopy is a routinely used tool for the characterization of nanodiamond structures, giving information on the bonding properties of the diamond grains, the intergrain amorphous carbon phase and the grain boundaries. By using different excitation energies the selective enhancement can be utilized to characterize particular structural units (being excited resonantly with the given excitation photon energy) in more detail [1,2]. In this work multi-wavelength Raman spectroscopy was used to study the effect of nitrogen concentration on the structure of nitrogen containing nanodiamond thin films. Samples were prepared using MW CVD with nitrogen content of the precursor gas ranging from 0% to 20%. Raman spectra were recorded with 244, 488 and 85 nm excitations.

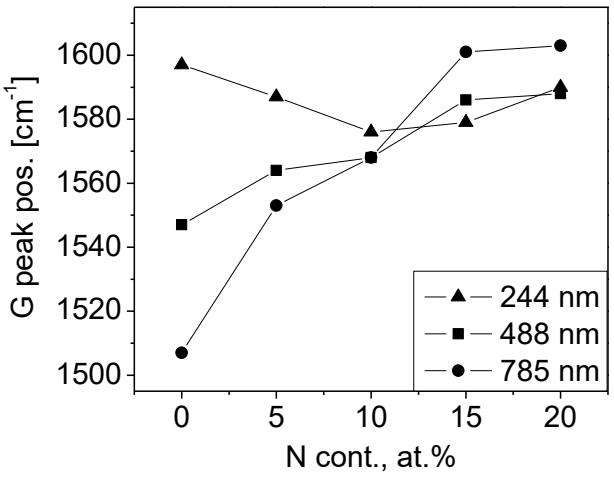

Fig.1.Evolution of the G peak position with nitrogen content in the Raman spectrum of nitrogen containing nanodiamond thin films recorded with different excitation energies.

Fig. 1 shows the evolution of the G peak position with nitrogen content for the different excitation energies. It is known that the incorporation of nitrogen promotes the graphitization of the diamond structure. This causes the shift of the G peak in the Raman spectrum to higher wavenumbers, as it can be seen for the 488 and 785 nm excitations on Fig. 1. However, a completely different behavior was observed for 244 nm excitation, where the G peak has a U-shaped dependence on the nitrogen content: it decreases from 1597 cm^{-1} to 1576 cm^{-1} between 0-10% of nitrogen content, then increases to 1590 cm^{-1}. This is caused by the contribution of different structural units to the Raman spectra excited with different wavenumbers and indicates the non-uniform incorporation of nitrogen atoms into the diamond structure.

[1] M. Veres, S. Tóth, M. Koós, New aspects of Raman scattering in carbon-based amorphous materials, Diamond Relat. Mater. 17 pp. 1692-1696 (2008).
[2] M. Veres, S. Tóth, M. Koós, Grain boundary fine structure of ultrananocrystalline diamond thin films measured by Raman scattering, Appl. Phys. Lett. 91, 031913 (2007).

Surface-enhanced Raman scattering of SiC and diamond nanostructures

I. Rigó[1], M. Veres[1], A. Czitrovszky[1], P.R. Takács, D. Beke[1], L. Himics[1], S. Tóth[1], P. Fűrjes[3]

1 - Institute for Solid State Physics and Optics, Wigner Research Centre for Physics, HAS, Budapest, Hungary
2 - Institute of Technical Physics and Materials Science, Centre for Energy Research, HAS, Budapest, Hungary

rigo.istvan@wigner.mta.hu

Surface-enhanced Raman scattering (SERS) is the only technique capable of detecting a single molecule and simultaneously probing its chemical structure [1]. Surface-Enhanced Raman Scattering is a phenomenon in which the Raman scattering intensity of molecules close to the surface of certain finely divided metals is dramatically enhanced. The SERS enhancement can reach even a level of 10^8–10^{10}. SERS is characterized by surface selectivity and it is a highly sensitive and reliable technique for surface studies that allows the detection of ultra-low amounts of analyses. [2-3] Among others chemical compositions containing carbon are highly sensitive for SERS.
Different SERS substrates were prepared by litographic technique from silicon. Isotropic and anisotropic etching and their combination were applied to the surfaces resulting in formation of arrays of hemispheres, pyramids and rounded pyramids, respectively. All structures were prepared in two sizes: with 1 and 2 micron base, both with 3 micron period. The created structures were coated with a few nanometer thick layer of gold. The SERS-amplification of different nanostructures was determined and compared by Raman measurements on benzene phenol. SERS measurements were carried out on a Renishaw 1000 Raman spectrometer attached to a Leica DM/LM microscope and using 785 nm excitation.

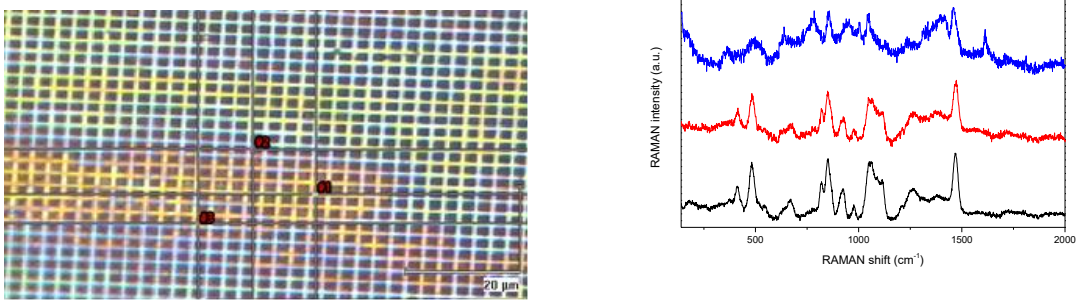

a) b)

Figure 1. a) SERS substrate coveres with SiC suspension; b) SERS spectra of different SiC samples.

The SERS substrates were found to be very sensitive to study silicon carbide (SiC) and ultra-nanocrystalline diamonds. It was possible to differentiate different SiC structures (polytypes), as well as to detect peaks corresponding to surface structural units. In case of nanodiamonds peaks were observed in the low wavenumber region, that can be assigned to surface structural units, too.

Acknowledgment

M. Veres is grateful for the support of the Bolyai János Research Scholarship of the Hungarian Academy of Sciences.

[1] Pedro H. C. Camargo, Leslie Au, Matthew Rycenga, Weiyang Li, and Younan Xia, Measuring the SERS enhancement factors of dimers with different structures constructed from silver nanocubes, Chem Phys Lett. 2010 Jan; 484(4-6): 304–308.
[2] Christy L. Haynes, Adam D. McFarland and Richard P. Van Duyne, Surface-Enhanced Raman Spectroscopy, Anal. Chem., 2005, 77 (17), pp 338 A–346 A
[3] Katrin Kneipp, Martin Moskovits, Harald Kneipp, Surface-Enhanced Raman Scattering: Physics and Applications, Springer Science & Business Media, 2006. jún. 21. - 466 oldal

Characterisation of pharmaceutical inhalers and study of pulmonary drug delivery using lasers and optical methods

A. Nagy, A. Czitrovszky, M. Veres, A. Kerekes, I. Rigo

Department of Applied and Nonlinear Optics, Institute for Solid State Physics and Optics, Wigner Research Centre for Physics of the H.A.S., Budapest, Hungary, Konkoly Thege M. st. 29-33

Main author email address: nagy.attila@wigner.mta.hu

The investigation of the health effects of the inhaled aerosols is in the focus of scientific interest nowadays. Health effects of the inhaled particles are determined mainly by their spatial deposition distribution and local concentration which depends substantially on their transport properties in the multiple-bifurcating human airway system. The delivery of the proper dose to the targeted area and the quantification of the overdose are critical questions during the development of different types of inhalers. In my contribution I present our recent achievements in the field of aerosol drug delivery, I introduce new laser based optical measurement methods and their applications to study the transport and deposition of pharmaceutical aerosol in realistic human airway replicas.

We have developed an optical measurement method based on laser particle counting, which can be used as a replacement of the commonly used analytical methods. A new procedure was developed based on optical image processing for the determination of the amount of deposited particles on the catch plates of cascade impactors. We utilized this method for the investigation of the effect of the humidity on the size distribution of the inhaled drug particles.

We studied the transport of aerosol particles in human airways tracts, and experimentally validated computational fluid dynamics based numerical simulations. The velocity profile of the aerosol drug particles during simulated breathing patterns in the artificial lung model was determined by laser Doppler anemometry.

We developed a new measurement method for the investigation of the deposition of aerosol drug particles in the human airways, where 3D printing technique was engaged for the production of realistic human airway replicas and Raman spectroscopy was utilized to determine the spatial deposition distribution of the particles on the surface of the model. Different medications were tested and compared in terms of particle size distribution and deposition characteristics in idealized and realistic 3D airway models.

All of the above mentioned methods have their own advantages in terms of speed and sensitivity of the measurement. The established theoretical and experimental background and the elaborated methods and tools can be used widely not only for the investigation of aerosol drug delivery, but for studying the deposition properties of natural and toxic aerosols as well.

This work was supported by the National Research, Development and Innovation Office under grant KTIA_AIK_12-1-2012-0019.

[1] Salma I, Balásházy I, Winkler-Heil R, Hofmann W, Záray Gy; Effect of particle mass size distribution on the deposition of aerosols in the human respiratory system; J AEROSOL SCI; 33: 119-132; (2002)

[2] Balásházy I, Hofmann W, Heistracher T; Local particle deposition patterns may play a key role in the development of lung cancer J APPL PHYSIOL 94, 1719-1725 (2003).

[3] A. Kerekes, A. Nagy, A. Czitrovszky, Experimental air flow and deposition studies with hollow bronchial airway models, Journal of Aerosol Medicine and Pulmonary Drug Delivery 22(2)., pp.175-176., (2009)

[4] A. Kerekes, A. Nagy, A. Czitrovszky, Theoretical and experimental investigation of aerosol deposition in realistic human airway model, European Aerosol Conference EAC2012, Sept. 2-7. Granada, Spain, A-WG06S1P30, P253, 1094. (2012)).

LDS-1-8

Simultaneous measurement of physical and optical properties of aerosol particles to determine their origin

Aladár Czitrovszky, Attila Nagy, Miklós Veres, Attila Kerekes

Department of Applied and Nonlinear Optics, Institute for Solid State Physics and Optics, Wigner Research Centre for Physics of the H.A.S., Budapest, Hungary, Konkoly Thege M. st. 29-33

corresponding author: nagy.attila@wigner.mta.hu

Aerosol particle characterization is in the front of scientific interest due to the evident effects of aerosol contamination of the atmosphere on the environment, human health and global climate change as well. The instrumentation is developing rapidly and the number of available methods is increasing, enabling us to perform more accurate characterization of chemical composition and physical properties of the particles. The measured data can be used to characterize the investigated environment which is a critical point in the process of identifying the origin of aerosol contamination in a source apportionment model. Conventional aerosol measuring instruments determine mainly the size distribution and concentration of aerosol particles. In this contribution we propose a new method which applies the DWOPS technique in source identification studies. The Dual Wavelength Optical particle Spectrometer (DWOPS) is capable of simultaneous determination of the real and imaginary part of the refractive index together with the size of the particles with a short sampling time. Performing the measurements in industrial environment the different types of aerosol contaminants could be distinguished.

Using the previously developed instrument [1-3] aerosol contamination measurements were performed in different locations within and around of an industrial facility. A mobile prototype of the instrument was utilized in the study where different metal processing activities were monitored (grinding, cutting, welding, drilling, etc.). In the present contribution we focus on the measurement of the imaginary part of the complex refractive index that relates to the absorption of the particles, which is differing for different types of aerosols. Two measurement campaigns were carried out and the measurements were complemented with other techniques – Raman spectroscopy, optical and electron microscopy and EDAX analysis. To distinguish between different kinds of aerosols the following parameters were derived from the measured data: size distributions, refractive index distributions, size resolved absorbing fractions, size resolved average absorptivity of the measured particles, morphology of the particles based on optical and electron microscopy, chemical composition based on Raman spectroscopy and EDAX analysis.

The main sources of aerosol contamination were identified, and their contribution to the temporal and spatial distribution of the air pollution in the facility and nearby was determined.

This work was supported by the Hungarian TéT_10-1-2011-0725 project.

[1] Szymanski, W.W., Nagy, A., Czitrovszky, A., Jani, P. (2002). A new method for the simultaneous measurement of aerosol particle size, complex refractive index and particle density, Measurement Science and Technology, 13, 303-307.

[2] Nagy, A., Szymanski, W.W., Golczewski, A., Gál, P., Czitrovszky, A. (2007) Numarical and experimental study of the performance of the Dual Wavelength Optical Particle Spectrometer (DWOPS), Journal of Aerosol Science, vol. 38. pp. 467-478. (2007)

[3] Nagy A. et al., Real-time determination of absorptivity of ambient particles in urban aerosol in Budapest, Hungary, Aerosol and Air Quality Research, Vol. 16, pp. 1-10. (2016)

LDS-2-1 (Invited)

Femtosecond Nonlinear Optics in All-Dielectric Nanostructures and Metasurfaces

M.R. Shcherbakov[1], D. Neshev[2], Yu.S. Kivshar[2], and A.A. Fedyanin[1]
[1]Faculty of Physics, Lomonosov Moscow State University, Moscow 119991, Russia
[2]Nonlinear Physics Centre, Research School of Physics and Engineering, The Australian National University, Canberra, Australia
Email: fedyanin@nanolab.phys.msu.ru

Artificially nanostructured materials with novel electromagnetic properties, currently referred to as metamaterials, were originally introduced to enable the on-demand tailoring of their constitutive parameters. Negative refractive indices, epsilon-near-zero phenomena, form birefringence, chirality, and other properties of metamaterials have been reported. Because the constitutive relations for these materials consist of both linear and nonlinear terms, enabling artificial control over electromagnetic nonlinearities is a very feasible task.

The talk surveys the results on the studies of the nonlinear-optical effects in different types of novel planar metamaterials utilizing Mie-type dielectric resonances. First, we discuss the observation enhanced third-harmonic generation from silicon nanodisks exhibiting both electric and magnetic dipolar resonances [1]. Experimental characterization of the nonlinear optical response through third-harmonic microscopy and spectroscopy reveals that the third-harmonic generation is significantly enhanced in the vicinity of the magnetic dipole resonances. Then, we have studied third-harmonic generation from lowloss subwavelength silicon nanodisks arranged in the form of trimer oligomers with varying distance between the nanoparticles. Each of the nanodisks exhibits both electric and magnetic Mie-type resonances that are shown to affect significantly the nonlinear response. We observe the third- harmonic radiation intensity that is comparable to that of a bulk silicon slab and demonstrate a pronounced reshaping of the third-harmonic spectra due to interference of the nonlinearly generated waves augmented by an interplay between the electric and the magnetic dipolar resonances [2].

The ultrafast all-optical switching in subwavelength nonlinear dielectric nanostructures exhibiting localized magnetic Mie resonances is also detected [3]. We employ amorphous silicon nanodisks to achieve strong self-modulation of femtosecond pulses with a depth of 60% at picojoule-per-disk pump energies. In the pump-probe measurements, we reveal that switching in the nanodisks can be governed by pulse-limited 65 fs-long two-photon absorption being enhanced by a factor of 80 with respect to the unstructured silicon film.

References:

1. M.R. Shcherbakov, D.N. Neshev, B. Hopkins, A.S. Shorokhov, I. Staude, E.V. Melik-Gaykazyan, M. Decker, A.A. Ezhov, A.E. Miroshnichenko, I. Brener, A.A. Fedyanin, and Y.S. Kivshar, "Enhanced third-harmonic generation in silicon nanoparticles driven by magnetic response", Nano Letters **14**, 6488 (2014).

2. M.R. Shcherbakov, A.S. Shorokhov, D.N. Neshev, B. Hopkins, I. Staude, E.V. Melik-Gaykazyan, A.A. Ezhov, A.E. Miroshnichenko, I. Brener, A.A. Fedyanin, and Y.S. Kivshar, "Nonlinear interference and tailorable third-harmonic generation from dielectric oligomers", ACS Photonics **2**, 578 (2015).

3. M.R. Shcherbakov, P.P. Vabishchevich, A.S. Shorokhov, K.E. Chong, D.-Y. Choi, I. Staude, A.E. Miroshnichenko, D.N. Neshev, A.A. Fedyanin, and Y.S. Kivshar, "Ultrafast all-optical switching with magnetic resonances in nonlinear dielectric nanostructures", Nano Letters **15**, 6985 (2015).

LDS-2-3 (Invited)

A SENSING MECHANISM FOR FLUORESCENT DETECTION OF CARBON NANOTUBE VIA COMPLEXATION WITH ORGANIC DYES

P. Lutsyk[1,2], M. Shandura[3], O. Kachkovsky[4], Yu. Piryatinski[2], A. Verbitsky[2], A. Rozhin[1]

1- Nanotechnology Research Group and Aston Institute of Photonic Technologies, School of Engineering & Applied Science, Aston University, Aston Triangle, B4 7ET Birmingham, UK
2- Institute of Physics, NAS of Ukraine, 46, prospekt Nauky, 03680 Kyiv, Ukraine;
3- Institute of Organic Chemistry, NAS of Ukraine, 5 Murmanska str., 02660 Kyiv, Ukraine;
4- Faculty of Physics, Taras Shevchenko National University of Kyiv, 4, Academician Glushkov avenue, Kyiv 03127, Ukraine

E-mail: a.rozhin@aston.ac.uk

The physical and chemical properties of carbon nanotubes provide a powerful platform for a variety of practical applications such as reinforced and conductive composites, bio-medical and environmental sensors, nonlinear optical switches, drug delivery systems etc[1,2]. As a result of the rapid advances of nanotechnology, carbon nanotubes present a potential problem as an environmental polluter causing health threats due to confirmed material toxicity[3]. Consequently, an efficient method for their rapid detection must be established.

In this report, we will discuss a novel conception of ionic sensor complexes of single wall carbon nanotubes – organic dye with sensitive and selective response in photoluminescent (PL) signal[4]. As model organic molecules, we have used a family of polymethine dyes with easily tailorable molecular structure and, as a consequence, tunable absorbance and PL characteristics. The complexes are formed due to Coulomb attractions between polymethine dye molecules having uncompensated charge and carbon nanotubes covered by ionic surfactant in water. We have shown that the PL excitation of the dye can be transferred to the nanotubes resulting in selective and strong amplification of the light emission (up to 6 times) from carbon nanotube excitonic levels in the near-infrared spectral range, which was experimentally identified by excitation-emission photoluminescence mapping. The chirality of carbon nanotubes as well as the type of ionic surfactant dispersing the nanotubes strongly affects the PL amplification. Thus the dye complexation provides sensing selectivity towards specific carbon nanotubes, making an efficient probe for carbon nanotube detection.

Acknowledgements
The work was supported by NATO SPS Project (NUKR.SFPP 984189) and by Marie Sklodowska-Curie Research and Innovation Staff Exchanges Scheme (H2020-MSCA-RISE-2015, Project #690945).

[1] M.F. De Volder, S.H.Tawfick, R.H. Baughman, A.J.Hart, Science 339, (6119), 535-539 (2013).
[2] T. Allsop, R. Arif, R. Neal, K. Kalli, V. Kundrát, A. Rozhin, P. Cuvlerhouse, D. J. Webb, Light: Science& Applications, 5, e16036; doi: 10.1038/lsa.2015.36 (2016).
[3] K. Kostarelos, A. Bianco, M. Prato, Nature nanotechnology, 4, 627-633, (2009).
[4] P. Lutsyk , R. Arif , J. Hruby, A. Bukivskyi, O. Vinijchuk, M. Shandura , V. Yakubovskyi, Yu. Kovtun, O. Kachkovsky, Yu. Piryatinski, A. Verbitsky, A. Rozhin, Light: Science& Applications 5, e16028; doi: 10.1038/lsa.2016.28 (2016).

Understanding the Statistics of the Pulse-to-Pulse Phase Coherence from the Spectrum of Optical Frequency Combs

S. P. Ó Dúill, P. M. Anandarajah. and L. P. Barry
The Radio and Optics Communications, Laboratory, School of Electronic Engineering, Dublin City University, Dublin 9, Ireland

Email: sean.oduill@dcu.ie

Optical frequency combs (OFC) are key sources for many photonic applications in fields such as communications, sensing, timing etc.[1]. Ideally, OFCs should have discrete delta-style lines at equi-distant frequencies; though unfortunately noise broadens the discrete comb lines. In the time domain, OFC formation needs *both* amplitude and phase of the field envelope to be periodic for comb lines to appear in the OFC spectrum. A strict requirement is that in spite of inevitable phase disturbances, successive pulses in an optical pulse train need to maintain optical phase coherence in order for the pulse train to form an OFC. Valuable information regarding the pulse-to-pulse phase coherence can be obtained by inspecting the broadening of the comb lines in the OFC spectrum. We use the developed theory to explain the spectral results of OFCs from gain-switched lasers [2], and OFCs from gain-switched lasers are emerging as candidates as transmitter sources for the forthcoming terabit/s networking era of optical communication networks. Typically laser disturbances build up from random spontaneous emission events that perturb the lasing field and therefore the optical phase undergoes a random-walk (Brownian motion, Weiner process). Extending this notion of the random-walk phase coherence to the phase of the pulsations varying as a random walk, then the OFC will have Lorentzian shaped lines [3] and this is shown in Fig. 1(a) indicating discrete comb lines with each line exhibiting Lorentzian line broadening. On the other hand if there is no phase coherence; we take the case that the phase of each pulse varies uniformly over the interval [-π,π], then no OFC is formed and all of the pulse energy is contained within a continuum as is shown in Fig. 1(b) [3]. The absence of pulse-to-pulse phase coherence is the only case that can cause the OFC spectrum to behave in this manner [3] and such information is useful when observing the combs from gain-switched lasers [2]. It should be noted that the effects of pulse timing jitter also affect the OFC spectrum though this just creates a weaker continuum at the expense of the power in the comb lines [3][4].

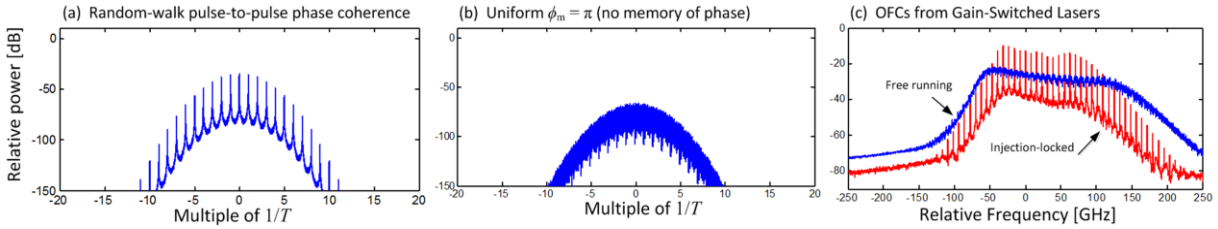

Fig. 1 Various cpectra of optical frequency combs. (a) Comb when the optical pulses have random-walk phase coherence, each line has Lorentzian line broadening. (b) No phase coherence with pulse-to-pulse phase change randomly distributed over [-π,π], hence the absence of comb lines. (c) Optical frequency combs from gain-switched lasers: blue curve without injection locking, red curve with injection locking.

Gain-switched lasers are single-mode lasers modulated with a strong sine-wave such that short optical pulses of a few tens of ps width are created upon every modulation cycle. The spectra of gain-switched lasers with and without injection locking are shown in Fig. 1(c). The blue curve shows the spectrum when the laser is just gain-switched, the continuous spectrum indicates that there is no pulse-to-pulse phase coherence, though when light from an external maser laser is injected into the gain-switched laser the injection locking imposes phase coherence on the pulses and hence a OFC with clearly defined comb lines is formed as is shown by the red curve in Fig. 1(c).

[1] P. J. Delfyett et al., "Optical frequency combs from semiconductor lasers and applications in ultrawideband signal processing and communications," IEEE JLT 24, no. 7, pp. 2701–2719, (2006).
[2] P. M. Anandarajah, et al., "Generation of Coherent Multicarrier Signals by Gain Switching of Discrete Mode Lasers," IEEE Photon. J. 3, no. 1, pp. 112-122, (2011).
[3] S. Ó Duill, et al., "Analytical Approach to Assess the Impact of Pulse-to-Pulse Phase Coherence of Optical Frequency Combs", IEEE JQE 51, no. 11, Article #: 1200208, (2016).
[4] D. A. Leep and D. A. Holm, "Spectral measurement of timing jitter in gain-switched semiconductor lasers," Appl. Phys. Lett. 60, no. 20, pp. 2451–2453, (1992).

Anisotropy of third-harmonic and coherent anti-Stokes Raman scattering signals in silicon nanowire arrays

L.A. Golovan[1], M.M. Kholodov[1], D.E. Presnov[1], A.I. Efimova[1], L.A Osminkina[1], S.V. Zabotnov[1], V.Yu. Timoshenko[1], A.V. Neskoromnaya[2], G.I.Petrov[3], V.V.Yakovlev[3]

[1]Physics Department, M.V.Lomonosov Moscow State University, 119991, Moscow, Russia

[2]Material Sciences Department, M.V. Lomonosov Moscow State University, Moscow 119991, Russia

[3]Department of Biomedical Engineering, Texas A & M University, College Station, TX 77843, USA

golovan@physics.msu.ru

Nowadays, arrays of silicon nanowires (SiNW) of about 100 nm in diameter attract more and more interest. Typically, SiNWs are aligned pillars with the length controlled by the formation procedure [1]. Among their optical properties we can mention extremely high light absorption and enhanced efficiency of various optical processes, including spontaneous Raman scattering, third-harmonic (TH) generation, and infrared interband photoluminescence [2]. These effects are often connected with the light trapping in SiNW arrays caused by effective light scattering in them. However, despite this fact nonlinear-optical effects due to their pronounced dependence on the local field could be able to reveal anisotropy of the SiNW arrays.

In this paper we chose to study features of such nonlinear-optical processes as TH generation and coherent anti-Stokes Raman scattering (CARS) in the SiNW arrays of pronounced anisotropy formed by means of metal-assisted chemical etching process [1] at (110) crystalline silicon (c-Si) wafer. The SiNWs are strongly prolate parallelepipeds of about 100 nm in diameter tilted to the surface at the angle of 45◦ with projection oriented along (110) direction (Fig. 1). Due to effective light scattering in the SiNW arrays demonstrate no orientation effect in linear reflectance measurements.

The broadband CARS signal was generated at the frequency $2\omega_1$ - ω_2, where ω_1 and ω_2 were the frequencies of Nd:YVO4 laser (1064 nm, 10 ps) radiation and a continuum radiation generated in optical fiber, correspondingly. The TH generation was carried out with the help of Cr:forsterite laser (1250 nm, 80 fs). In all cases polarization dependences of the signals were measured.

In contrast to spontaneous Raman, the SiNW arrays exhibit pronounced polarization dependences of the CARS signal. The resonant CARS signal in SiNW ensemble is an order of magnitude less than in c-Si in the case when pumping radiation propagates perpendicular to the SiNWs and the CARS signal is collected in the direction along SiNWs and two orders of magnitude less than in c-Si in another case. The TH signal for SiNW array exceeds one for c-Si in the case of the fundamental radiation incident perpendicular to the SiNWs, whereas in the case of incident wave propagation along the SiNWs it falls several time in comparison with c-Si (Fig. 2). Thus, found in experiments anisotropy of the nonlinear-optical signals evidences the sensitivity of these techniques to the orientation of SiNWs in their highly scattering arrays.

This work is supported by the Russian Foundation for Basic Research grant no. 15-29-01185.

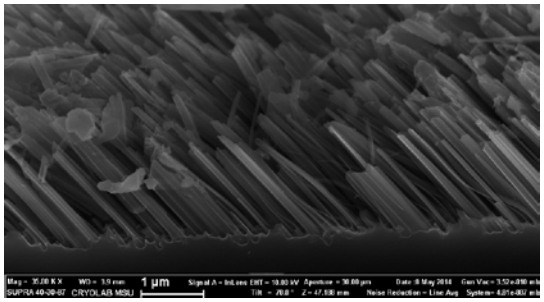

Fig. 1: The SiNW sample cross-section in (100) plane.

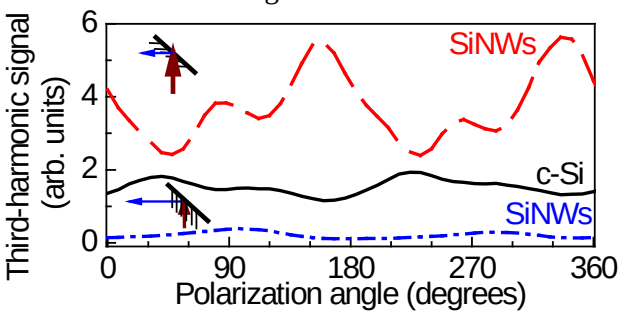

Fig. 2: Orientation dependence of the third-harmonic signals for c-Si and SiNW arrays for pump radiation incident along and perpendicular to the SiNWs.

[1] V.A. Sivakov, G. Brönstrup, B. Pecz, A. Berger, G.Z. Radnoczi, M. Krause, S.H. Christiansen. Realization of vertical and zigzag single crystalline silicon nanowire architectures. J. Phys. Chem. C., vol. 114 pp. 3798–3803, (2010)

[2] S.V. Zabotnov, M.M. Kholodov, V.A. Georgobiani, D.E. Presnov, L.A. Golovan, P.K. Kashkarov. Photon lifetime correlated increase of raman scattering and third-harmonic generation in silicon nanowire arrays. Las. Phys. Lett., vol. 13, pp. 035902–1–035902–5, (2016).

Angle-Resolved Coherent (ARC) Wave-Mixing using a 4 fs White Light Pulse

Ian P. Mercer[1], Tobias Witting[2], Taran Driver[2],

Richard J. Cogdell[3], J.W.G. Tisch[2], J.P. Marangos[2]

1. School of Physics, Centre for Synthesis and Chemical Biology, University College Dublin, Ireland.
2. Biochemistry and Molecular Biology, Faculty of Biomedical and Life Sciences, University of Glasgow, UK.
3. Quantum Optics and Laser Science Group, Blackett Laboratory, Imperial College, London, UK.

ian.mercer@ucd.ie

We recently demonstrated a new coherent multi-dimensional optical wave-mixing technique, Angle-resolved Coherent (ARC) wave-mixing, and we used this to reveal function in a photosynthetic protein [1, 2]. With our approach, features characterizing an arbitrary array of quantum couplings are spatially separated prior to detection.

To date, use of a light source restricted in bandwidth has to 120 nm (0.2 eV) has limited the bandwidth of the resulting ARC maps. Here for the first time, we demonstrate ARC wave-mixing using a light source that spans 550 to 1000 nm (1.0 eV) and we achieve a light pulse duration of just 4 fs at the sample. This allows for the study of coherence in energy transfers over large reorganization energies and the study of fast phenomena in bulk solids and solutions.

Using just a single laser pulse, we show we can record an ARC map of the photosynthetic LL protein complex from Rps palustris in solution at ambient temperature. We observe a bi-exponential energy transfer across a reorganization energy of 0.65 eV in this protein and we propose a mechanism for this.

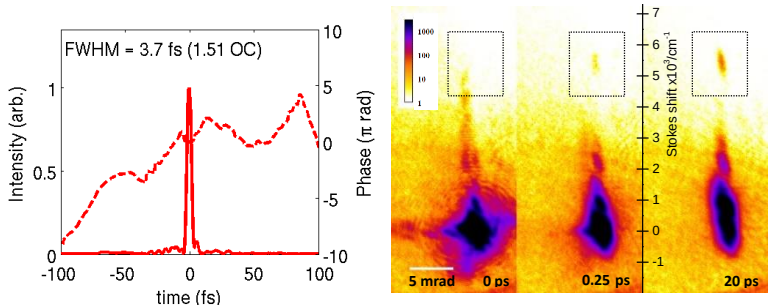

(a) (b)

#

Fig.1 (a) Measured intensity and phase of the light pulse; b) ARC transient grating (TG) maps as measured with the signal filtered for 852 nm for the LL complex from Rps palustris, showing an emerging feature (boxed) for energy transfer over 0.65 eV (5500cm^{-1}).

1. Mercer, I.P., et al., *Instantaneous Mapping of Coherently Coupled Electronic Transitions and Energy Transfers in a Photosynthetic Complex Using Angle-Resolved Coherent Optical Wave-Mixing.* Physical Review Letters, 2009. **102**(5): p. 57402.
2. Mercer, I.P., *Angle-resolved coherent optical wave mixing.* Physical Review A, 2010. **82**(4): p. 043406.

LDS-P-1

NLO spectroscopy of GaSe, GaS and InSe nanoparticles formed via laser ablation

K. R. Allahverdiyev[1,2], M. F. Huseyinoglu[3], Z. Yu. Salaeva

1- Azerbaijan National Academy of Aviation, Bina AZ1045, Baku, Azerbaijan
2- TUBITAK Marmara Research Center, Materials Institute, Gebze, Kocaeli, Turkey
3- Earth System Science Research Center, Girne American University, Girne, Cyprus

kerim.allahverdi@tubitak.gov.tr

Nanoparticles of layered GaSe, GaS, GaS_xSe_{1-x} ($0 \leq 0 \leq 1$) and InSe were fabricated by laser ablation (LA) method by a KrF laser, with 248 nm wavelength, 50 Hz frequency with maximum energy 200mJ and 4 ns pulse duration. Nanoparticles were characterized by XRF, SEM and TEM, optical absorption and Raman spectroscopy (also in confocal geometry). Results were discussed in relation to the particle size. Absorption spectra of particles with diameter 20 nm and less turned out to be blue shifted. This result is explained by a weak confinement effect on Wannier-Mott type excitons. Confocal Raman measurements revealed that by decreasing the particle size, the energy position of the low-frequency Raman active phonons in all three compounds are shifted to lower frequencies (21, 24 and 18 cm^{-1} in bulk GaSe, GaS and InSe, respectively and 8, 11 and 7 cm^{-1} in particles with sizes 5, 6 and 7 nm, respectively). From the low frequency Raman data, decrease of the force constants ~25 % (for GaSe, GaS and InSe) due to the formation of the nanoparticles are estimated, and the origin is suggested. Second harmonic generation (SHG) with 1064 nm line of a mode locked Nd:YAG laser was observed for nanoparticles ablated on different substrates (in case of GaS and solid solutions) the results can be explained by inhomogeneity of ablated particles). Potentials for using these structures (ablated GaSe, GaS_xSe_{1-x} and InSe) for laser light visualizators are discussed.

Keywords: layered crystals, nonlinear optics, laser light visualizator, gallium selenide, indium selenide, Raman scattering, PL, SHG

LDS-P-2

Exploring the uptake mechanism of nanostructures in *Brachionus plicatilis* by the SERS technique

N. Aldaleeli[1](PhD student) and P. Dunstan[2] (Supervisor)

1- Department of Physics, College of Science, Centre for Nanohealth, Swansea University, Singleton Park, Swansea, SA2 8PP

2- Department of Physics, College of Science, Centre for Nanohealth, Swansea University, Singleton Park, Swansea, SA2 8PP

668858@swansea.ac.uk

An important application for surface enhanced Raman Spectroscopy (SERS) is the potential of intracellular analysis based on Raman reporters attached to nanoprobes. SERS is an appropriate technique for identification of molecular species of biological system [1]; measuring local chemical changes at the subcellular level with high spatial and temporal resolution [2, 3]. Measuring pH utilising the enhanced Raman response from pMBA when it has functionalised gold nanoparticles (Au NPs) has attracted significant attention. Thus the application of such a system to the measurement of intracellular pH or organism pH is a key aspect for current development. This study explores the uptake mechanism of functionalised nanostructures into *Brachionus Plicatilis*, firstly to verify that the nanostructures can be taken up by the organism and moreover to identify in which sites the nanoparticles accumulate. Assessing the organism's uptake an internalisation of nanostructures, in this case Rhodamine 6G (R6G) functionalised AuNPs, will assist in developing the methodology in relation to pH-sensing pMBA functionalised AuNPs. Hence establishing a route to predict the intracellular pH measurements accurately. For this purpose Raman mapping based on SERS nanoreporters has been conducted to produce density and contour plots in order to determine the localisation of nanoparticles (R6G functionalised AuNPs) inside the organism. The uptake results show that, after 5 hours incubation of *Brachionus plicatilis* with R6G-AuNPs, the prominent band of R6G, 1508 cm^{-1}, was observed distributes in specific sites within the organism. These sites were identified as the mastax and the stomach which indicates that the NPs have been ingested and the particles accumulated in the ingestion system. We report that further exposure, ~ 24 hours, the plot of the intensity distribution of the 1508 cm^{-1} shows that the peak broadly distributes throughout the organism's body with high localisation in the site of the vitellarium. The evidence here supports the conclusion that the nanostructures start to pass the intestinal tract and enter the tissues, hence there is strong localization at the vitellarium, and the peudocoleom. The wide distribution of the NPs shows the ability of this size of AuNPs to penetrate the ingestion system and distribute into the surrounded tissues without being eliminated by the organism through defecation. Similar results were reported in complementary studies by Flores et al [4]. The fact that the organism is not eliminating the nanoparticles and that they are dispersed in various sections of the organism makes the approach significant in the future reporting of intracellular and organism pH.

[1] W. Xie, L. Su, A. Shen, A. Materny, and J. Hu, "Application of surface-enhanced Raman scattering in cell analysis," *J. Raman Spectrosc.*, vol. 42, no. June 2010, pp. 1248–1254, 2011.

[2] N. Parab and V. Tomar, "Raman Spectroscopy Of Algae: A Review". *J Nanomed Nanotechnol* 03.02 (2012): n. pag. Web.

[3] J. Chan, S. Fore, S. Wachsmann-Hogiu, and T. Huser, "Raman spectroscopy and microscopy of individual cells and cellular components," *Laser Photonics Rev.*, vol. 2, no. 5, pp. 325–349, 2008.

[4] Alvarado-Flores, Jesús et al. "Bioconcentration And Localization Of Lead In The Freshwater Rotifer Brachionus Calyciflorus Pallas 1677 (Rotifera: Monogononta)". *Aquatic Toxicology* 109 (2012): 127-132. Web.

Investigation of the 1.68 eV Near-Infrared Emission Lineshape in Nanodiamond Films by Selective Laser Excitation

L. Himics[1], S. Tóth[1], M. Veres[1], I. Rigó[1] and M. Koós[1]

1- Institute for Solid State Physics and Optics, Wigner Research Center for Physics, Hungarian Academy of Sciences, H-1525 Budapest, P.O. Box 49, Hungary

Main author email address: himics.laszlo@wigner.mta.hu

Color centers (optically active defects) in nanosized diamond constitute an intensively investigated field of research nowadays. Among them the SiV center is a promising candidate for utilization in different fields like quantum computing and cryptography, nanoscopy, medicine or cell biology [1]. This center has a narrow emission band in the near infrared wavelength region around 1.68 eV (738 nm), one photon emission and low electron-phonon coupling, even at room temperatures. Many applications require well detectable (separated from the background) and indistinguishable photons, which means that each individual center emits at the same frequency. Thus the wide spread of the SiV ZPL position and linewidth, and also the asymmetric line broadening toward the lower energy side of the spectrum, observed by many authors, are undesirable.

In this work we investigated the behavior of the 1.68 eV photoluminescence (PL) emission line in series of nanodiamond films containing SiV centers and prepared using different MWCVD deposition parameters (H_2/CH_4 ratio and substrate temperature). The morphology of the samples was investigated by SEM microscopy and average grain size was determined for each sample. PL properties of nanodiamond films having different texture and average grain size were studied by applying different laser excitations (405, 488, 532 and 635 nm).

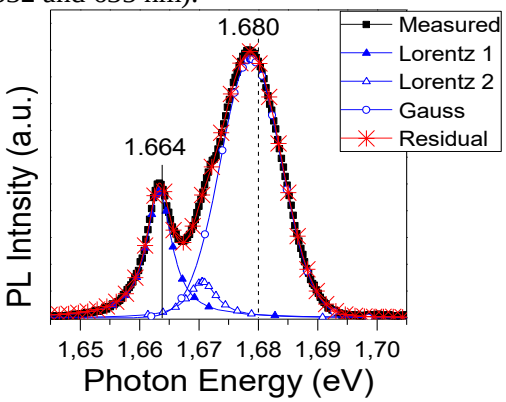

Fig. 1 The fitting procedure of 1.68 eV PL emission line recorded by 635 nm laser excitation.

It was found that the asymmetric tail on the low energy side of the 1.68 eV PL line is changing with average grain size of the nanodiamond film and it is more pronounced in samples having larger grains. We supposed that the asymmetry is caused by the presence of another defect emitting near the SiV emission line, but it has different atomic structure, thus it can be excited with different efficiency by selective laser excitations. It was showed that the contribution of underlying emission line to the 1.68 eV PL peak can be significantly enhanced with 635 nm excitation and this excitation allows the decomposition of the asymmetric ZPL. Based on the peak positions the underlying features were identified as the double line of GR1 defect, emitting at 1.673 and 1.665 eV [2]. Using selective laser excitations we determined that the contribution of the GR1 center emission to the 1.68 eV PL line intensity is more pronounced for nanodiamond samples having larger grain size. This indicates that the defect formation is preferred on the surface of the crystals and in the vicinity of dislocations [2] – a feature being more typical for larger crystals.

[1] T. D. Merson et al., Opt. Lett., 38, pp. 4170-4173 (2013).
[2] A. M. Zaitsev, Optical properties of diamond: a data handbook (Springer Science & Business Media), Chapter 5 (2013).

LDS-P-4

Radiation trapping and pump duration effects on near infrared luminescence of Er:YAG crystal

R. Kostanyan, D. Zargaryan, P. Muzhikyan

1- Institute for Physical Research, National Academy of Sciences, 0203 Ashtarak, Armenia

Main author email address: pmuzhikyan@gmail.com

The eye-safe laser radiation of YAG:Er^{3+} crystal near 1.5 μm is of great interest due to its various applications in optical communications systems, medicine, remote sensing and ranging, etc. Studying the spectroscopic properties and pumping regimes of Er^{3+} ions in YAG:Er^{3+} crystals is important for further improvement of near infrared generation efficiency.

Spectroscopic measurements of luminescence of $^4I_{13/2} \rightarrow {}^4I_{15/2}$ and $^4I_{11/2} \rightarrow {}^4I_{15/2}$ transitions are carried out for 5% and 40% erbium-doped YAG single crystals under pulsed excitations at 445 nm. Observation of time resolved luminescence at 1.5 and 0.98 μm wavelengths is conducted under varying pumping durations changing in the wide range from 20 to 10000 μs. In order to study the influence of radiation trapping effect on the luminescence decay kinetics measurements with pinhole technique as well as without are carried out. The pinhole diameters were 200-1000 microns. The strong dependence of registered luminescence effective decay times of $^4I_{13/2}$ and $^4I_{11/2}$ levels on pumping duration for both registration techniques is discussed. A mathematical model based on modified rate equations is suggested in order to simulate luminescence decay curves. Comparison of results of numerical calculations with measured curves showed better coincidence in case of pinhole presence with increasing accuracy while decreasing the pinhole diameter.

The following nonlinear processes $^4I_{13/2} \rightarrow {}^4I_{15/2} + {}^4I_{13/2} \rightarrow {}^4I_{9/2}$, $^4I_{11/2} \rightarrow {}^4I_{15/2} + {}^4I_{11/2} \rightarrow {}^4F_{7/2}$, $^4S_{3/2}(^2H_{11/2}) \rightarrow {}^4I_{9/2} + {}^4I_{15/2} \rightarrow {}^4I_{13/2}$, $^4I_{11/2} \rightarrow {}^4I_{15/2} + {}^4I_{13/2} \rightarrow {}^4F_{9/2}$ are observed by comparison of experimental and simulated curves.

FTIR-refractometer for scattering liquid analysis

M. Iakimova[1]

[1]Moscow State Technical University n.a. Bauman, Moscow, Russia

e-mail: marya.korotaeva@yandex.ru

A method for measuring the concentration of particles in a liquid by analyzing the distribution of the laser radiation in the direction perpendicular to the "light-shadow" interface formed with the FTIR-refractometer, in combination with radiation attenuation coefficient, measured with a photometer. The milk samples with different concentrations of fat, a predetermined standard chemical control method (the method of Rose-Gottlieb) was used as a model of the environment.

To ensure a low error the high reliability of the results requires high precision optical system with the definite laser beam parameters and manufacturing tolerances of the optical and opto-mechanical components. The mathematical model of the process, taking into account the MTF of the refractometer and the photometer and the experimental sample, allowed us to determine the necessary parameters of laser radiation, providing the ability to determine the mass fraction of fat with an accuracy of 0.01%. In particular, for a photometer with the following parameters: wavelength 808 nm, the diameter of the laser beam - 0.8 ± 0.1 mm; beam divergence - not more than 2 ', the width of the spectrum not more than 20 nm and refractometer with wavelength of 808 nm, beam divergence not more than 1`, the spectral width less than 10 nm, the beam diameter 0.8 ± 0.1 mm; precision manufacturing hypotenuse faces of the measuring prism - $\lambda / 10$. The results was confirmed experimentally on the standard milk samples with the different fat content, as well as the samples of commercially available milk (whole milk and pasteurized milk) (Fig. 1) using a single-mode semiconductor laser with the wavelength of 808 nm.

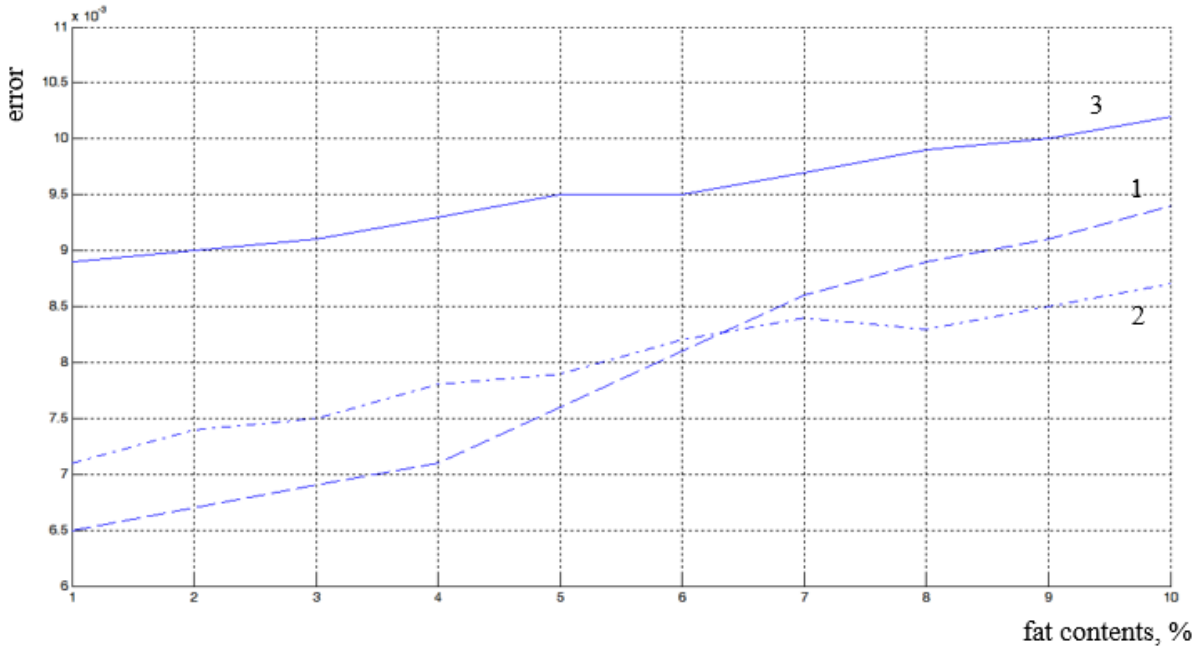

Fig 1. Error in the determination of the mass fraction of fat of milk with different fat contents

1 – standard samples of milk; 2 - whole milk; 3 - pasteurized milk.

LDS-P-6

Viscosity express control of lubricants

D. Melnikov[1]

1- BMSTU, 105005 Moscow, 2-nd Baumanskaya str., 5 (res. 1)

email:Daenoor@gmail.com

The efficiency of the machinery is essentially determined by efficiency of lubrication systems. However, during the operation parameters of lubricants are gradually deteriorating. There are many causes of this phenomenon, but all of them results in decreasing of machinery performance. Wasted lubricant has to be replaced in the end of its resource. But the lifetime of lubricant will depend on the operating conditions of the mechanism. Early replacement increases costs of lubricants, later - may result in damage of mechanism. The solution to this problem is to express control of lubricants parameters directly during operation.

A new nephelometric method of lubricants kinematic viscosity express control was investigated in this work. Basis of method is the laser phase analysis [1,2] – investigation of liquid medium optical parameters while heating/cooling. Viscosity was determined by free flow of liquid in a cuvette. This is express method and it could be easily implemented to a compact stand-alone device. It also has high accuracy for express methods – less than 8 % and the ability of kinematic viscosity rapid measuring over a wide temperature range: -40 to +150 °C. Content of the method lies in the periodically tilting the cell with the liquid sample while scanning the laser beam and heating / cooling. Theory based on the Poiseuille law with a number of assumptions concerning the free flow of liquid in a cuvette. The geometrical parameters of the capillary replaced by the model with corresponding geometrical parameters, and the pressure drop was determined experimentally by the reference samples calibration. Optical measurements were carried out in accordance with [3].

Experimental work had based on testing the reference samples: water and glycerol. Key parameter was the given pressure (pressure divided by density). This parameter was experimentally determined for two different mediums and wide temperature range (10 to 100 ° C). Accuracy was only 3,7 %. Then, the kinematic viscosity of the hydraulic oil has been measured for a temperature range of -40 to +65 °C. Accuracy was 7,6 % – that is permissible for nephelometric measurements.

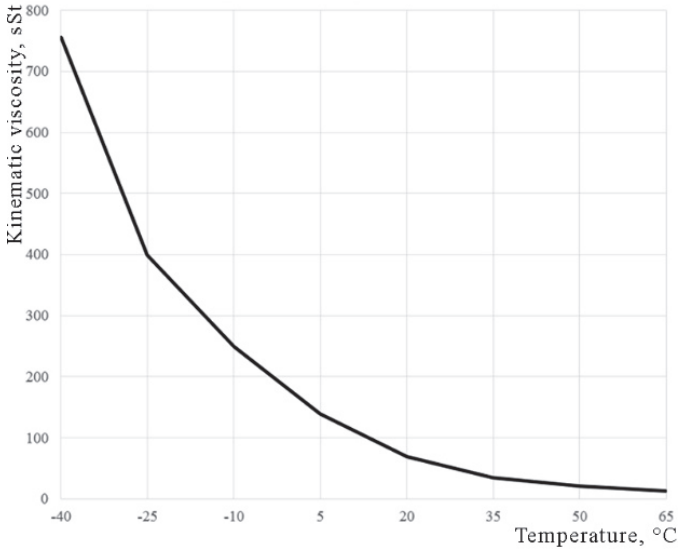

Figure 1. Temperature dependence of viscosity of hydraulic oil

[1] I.Shiganov, D. Melnikov Investigation technical mediums by laser phase analysis // Vestnik Moskovskogo gosudarstvennogo tekhnicheskogo universiteta im. N.E. Baumana. Seriya: Mashinostroenie 2015. №4. P. 100-108

[2] I.Shiganov, D. Melnikov Determination of low-temperature parameters of diesel by express analysis of liquid oils // Technologiya machinostroeniya. 2011. №11. P. 65-67.

[3] M. Korotaeva, V. Alekchnovich, A. Grigoriyants Laser interaction with liquid polydisperse media // Vestnik Moskovskogo gosudarstvennogo tekhnicheskogo universiteta im. N.E. Baumana. Seriya: Mashinostroenie 2012. №5 P. 141-146.

Laser spectroscopy method for non-invasive analysis of breath in subjects with pulmonary disease

M. Bercu (Petrus), C. Achim (Popa), A.M. Bratu, M. Patachia, S. Banita, C. Matei, and D.C. Dumitras

Department of Lasers, National Institute for Laser, Plasma and Radiation Physics,

409 Atomistilor St., PO BOX MG-36, 077125, Bucharest, Romania
E-mail: mioara.petrus@inflpr.ro

Laser Photoacoustic Spectroscopy (LPAS) method is a very powerful investigation technique which is capable of measuring trace gas concentration at sub parts per billion (ppb) level [1]. Oxidative stress in the respiratory system after the normal metabolism of oxygen and production of reactive oxygen species (ROS) increase the production of mediators of pulmonary inflammation and initiate or promote mechanisms of carcinogenesis [2]. The molecules contained in the exhaled breath can provide information about the physiological processes that occur in the body [3,4]. In this study, we present a quantitative analysis of breath ethylene concentrations in non-small cell lung cancer before and immediately after the chemotherapy and in chronic obstructive pulmonary disease (COPD) to illustrate the importance of oxidative stress within these disease, using CO_2LPAS method. Breath ethylene concentrations was monitored in patients with squamous lung-cancer (stages III and IV) under chemotherapy treatment (from 3rd to 6th chemotherapy session) and patients with COPD in advanced stage of the disease. This quantification is superior to the direct measurement of free radical because can be estimated the cellular damage and and the adverse effects. Chemotherapy induced ROS species and their oxidative damage to lipids and cellular membranes and chemotherapeutic treatment is suspected for the toxic side effects [5].
The changes of biochemical pathways proceeded inside cells might be observed in expired air. In the experiment, breath analysis was carried out before and after anticancer therapy. The data showed that cytostatic drugs increase the concentration of ethylene in the breath collected after chemotherapy. Although, chemotherapy improves the survival rates of cancer patients, but oxidative stress in normal tissues increase and decreases the quality of life of patients.
Patients with COPD present a high level of oxidative stress. The sources of the increased oxidative stress in the respiratory compartment of COPD patients derive from the increased burden of oxidants from environmental exposures, such as cigarette smoke in this case, and from the increased amounts of ROS. Oxidative stress lead to defects in tissue repair mechanisms, accelerated apoptosis and enhanced autophagy in lung cells, which have all been linked to the severity and progression of COPD [6]. The results suggest that patients with COPD are characterized by increased systemic and pulmonary oxidative stress breath marker.
Therefore, novel real-time monitoring of endogenous lipid peroxidation in patients with pulmonary injuries provides important details of endogenous production of ethylene.

[1] C. Popa, M. Petrus, A.M. Bratu, Ammonia and ethylene biomarkers in the respiration of the people with schizophrenia using photoacoustic spectroscopy, J. Biomed. Opt.(2015). doi: 10.1117/1.JBO.20.5.057006.
[2] M. W. Lawless, K.J. O'Bryne, S.G. Gray, Oxidative stress induced lung cancer and COPD: opportunities for epigenetic therapy. J Cell Mol Med. 13(9A), 2800-2821 (2009).
[3] Navas MJ, A.M. Jimenez AM. Asuero AG. Human biomarkers in breath by photoacoustic spectroscopy. Clinica Chimica Acta 413, 1171–1178 (2013).
[4] A. Amann, W. Miekisch, J. Schubert, B. Buszewski, T. Ligor, T. Jezierski, J. Pleil, T. Risby, Analysis of exhaled breath for disease detection. Annu. Rev. Anal. Chem. 7, 455-482 (2014).
[5] A. Ulanowska, E. Trawinska, P. Sawrycki, B. Buszewski, Chemotherapy control by breath profile with application of SPME-GC/MS method, J. of Separation Science, 35(21), 2908–2913 (2012).
[6] R.A. Pinho, D. Chiesa, K.M. Mezzomo, M.E. Andrades, F. Bonatto, D. Gelain, F. Dal Pizzol, M.M. Knorst, J.C.F. Moreira, Oxidative stress in chronic obstructive pulmonary disease patinets submitted to a rehabilitation program, Respiratory Medicine 101, 1830-1835 (2007).

LDS-P-8

Development of a high throughput (HT) Raman spectroscopy method for rapid screening of liquid blood plasma from prostate cancer patients.

Dinesh K. Medipally[1, 2], Fiona M. Lyng [1, 2], Jane Bryant[2], John Armstrong[3], Mary Dunne[3] and Aidan D. Meade [1,2].

1. School of Physics, Dublin Institute of Technology, Kevin Street, Dublin 8, Ireland.
2. DIT Centre for Radiation and Environmental Science, Focas Research Institute, Dublin Institute of Technology, Camden Row, Dublin 8, Ireland.
3. Department of Radiation Oncology, Saint Luke's Radiation Oncology Network, St Luke's Hospital, Dublin, Ireland.

Main author email address: dinesh.medipally@mydit.ie

Vibrational spectroscopy has been shown to be a powerful tool with potential clinical applications in the detection and discrimination of a multitude of cancer types. Extensive research has been undertaken on tissue biopsies but fewer studies have focused on less invasive blood samples. Recent studies have shown the ability of Raman and ATR-FTIR spectroscopy to discriminate between non-cancer controls and cancer cases using blood serum or plasma. Vibrational spectroscopic studies of biofluids to date have mainly been performed on dried samples but sample homogeneity and measurement reproducibility can be a problem.

The aim of the present study was to develop a high throughput (HT) Raman spectroscopy method for liquid blood plasma. Blood samples from prostate cancer patients (n = 20) and healthy controls (n = 30) were analysed on a 96 well plate using Raman spectroscopy. The spectra were pre-processed and analysed by principal component analysis - linear discriminant analysis (PCA-LDA). Statistically significant differences were observed between Raman spectra of prostate cancer patients and non-cancer controls and classification could be achieved with high sensitivity and specificity. This study shows the potential of Raman spectroscopy for the screening of prostate cancer.

LDS-P-9

Laser induced mass transport in As-S chalcogenide nanolayers as basis for novel active functional optics and ultrafast photonics

R. Holomb[1], M. Veres[2], A. Czitrovszky[2], O. Kondrat[1], V. Mitsa[1], A. Csik[3], M. Vondráček[4], N. Tsud[5], V. Matolín[5], K.C. Prince[6,7]

1- Uzhhorod National University, Voloshyn 54 str., Uzhhorod 88000, Ukraine
2- Wigner Research Centre for Physics, Hungarian Academy of Sciences, 1121 Budapest, Hungary
3- Institute for Nuclear Research, Hungarian Academy of Sciences, H-4001 Debrecen, Hungary
4- Institute of Physics, Academy of Science of the Czech Republic, Na Slovance 2, CZ-182 21 Prague 8, Czech Republic
5- Charles University, Department of Surface and Plasma Science, V Holešovičkách 2, 18000 Prague 8, Czech Republic
6- Sincrotrone Trieste S.C.p.A., Strada Statale 14, km 163.5, 34149 Basovizza, Trieste, Italy
7- IOM-CNR, 34149 Basovizza, Trieste, Italy

holomb@gmail.com

Nowadays photonics and light technology are already used in information processing systems. Novel photonic and nano-technologies are extremely developing fields indicating that we will depend as much on photonics rather than on electronics in the nearest future. New types of materials are needed to control the light and to access all optical functionality, generally called nanostructured materials with dimensions of their structural elements in the order of tens nanometers.

During the last decades amorphous and glassy chalcogenides containing one or more chalcogen elements (S, Se or Te) have attracted much scientific interest. In addition to their intrinsic infrared properties, the useful combination of optical activity, structural photosensitivity and high third-order optical non-linearity of chalcogenides offer wide possibilities of their applications in domains like information technologies (data storage and ultrafast optical information processing), renewable energy technologies (high efficiency solar cells, solid electrolytes), modern medicine, thermal imaging, sensing and biosensing, etc. The structure and its coupling to the fundamental physico-chemical and optical properties of amorphous chalcogenides has been the subject of intensive studies for decades. In particular, special interest is dedicated to light-matter interactions in various chalcogenide systems.

This report is on the influence of over-bandgap laser irradiation on structural transformations, atomic rearrangements and mass transport in As_2S_3 chalcogenide nanolayers. Amorphous As-S nanolayers were prepared *in-situ* by thermal evaporation of source glasses in ultra high vacuum. In order to investigate the effect of over-bandgap (λ=403 nm) laser irradiation the surface structure of as-deposited, annealed and irradiated stoichometric $As_{40}S_{60}$ nanolayers with realgar-like *r*-As_4S_4 inclusions were studied and characterized by means of photon-energy dependent (E_{ex} = 100, 120, 150, 220, 400, and 650 eV) synchrotron radiation photoelectron spectroscopy. The experimental As 3d core level spectra show that the irradiation of As-S nanolayers with blue laser cause the increase of the concentration of As-rich As-As-2S and 2As-As-S structural units (s.u.) at the surface of As-S nanolayers (Fig. 1). Simultaneously, the rise of the As content at the surface of irradiated nanolayers by about ~2 at.% was also detected from compositional analysis of As 3d and S 2p core level peaks. Photon-energy depended luminescence was also studied and the structure of As_2S_3 nanolayers before and after laser irradiation was characterized by surface-enhanced Raman spectroscopy. The mechanism of laser assisted mass transport in As-S nanolayers through light induced structural rearrangements will be discussed and the possibilities of potential applications of this effect in modern functional optics and nanophotonics will be proposed.

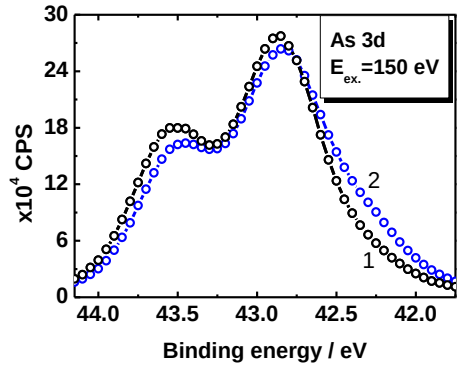

Fig. 1. As 3d core level spectra of as-deposited (1) and laser irradiated (2) As_2S_3 nanolayers.

Acknowledgments. R.H. and O.K. gratefully acknowledge support from the Hungarian Academy of Sciences within the Domus Hungarica Scientiarum et Artium Programme.

LDS-P-10

Spectroscopic study of oriented Tm:SSO crystal

Yu.D.Zavartsev, A.I.Zagumennyi, Yu.L.Kalachev, S.A.Kutovoi, V.A.Mikhailov, I.A.Scherbakov

A.M. Prokhorov General Physics Institute, RAS, Moscow, Russia

kalachev@kapella.gpi.ru

The idea of realization of diode pumped Tm:Sc_2SiO_5 (Tm:SSO) laser was appeared not long ago [1]. It was supposed that Tm:SSO crystal can be effectively used for lasing in 2-mkm range. The Tm:SSO may be classified as multisite material, the kind of crystal with disordered structure, because the scandium ions occupy two different crystallographic positions. This fact leads to complicated absorption spectrum, which in turn depends on optical axis orientation and light polarization. The spectrum broadening may be favorable in obtaining of ultrashort pulses or wavelength tunability is needed to realize devices capable of analyzing different atmosphere compounds with a single laser source.

We grew a laser quality Tm:SSO crystal with 5 at% concentration of Tm^{3+} ions. The crystal sample was prepared as an all faces polished parallelepiped 5.6*4.6*4.5 mm and oriented along optical axis. Polarized absorption spectra were recorded for two polarizations and three orientations of crystal. The full set of data consist of six spectra for each of 6 spectral bands (360,470,680,780,1200,1600 nm). For example, the polarized absorption spectrum of Tm:SSO crystal for one of orientations is shown in Fig1.

Each of 36 spectral set was fitted by a number of Lorentz peaks to obtain the best agreement between experimental data and cumulative fit peak. The typical agreement between fitted and experimental spectrum is shown in Fig2.

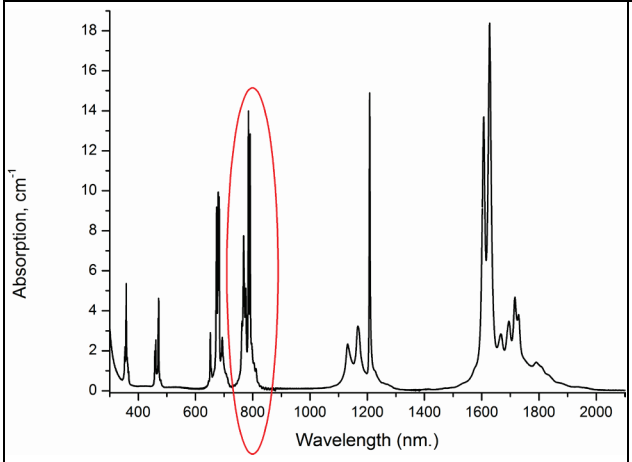

Fig.1. Polarized absorption spectrum of Tm:SSO crystal for one of orientations. Marked spectral band is analyzed in Fig.2.

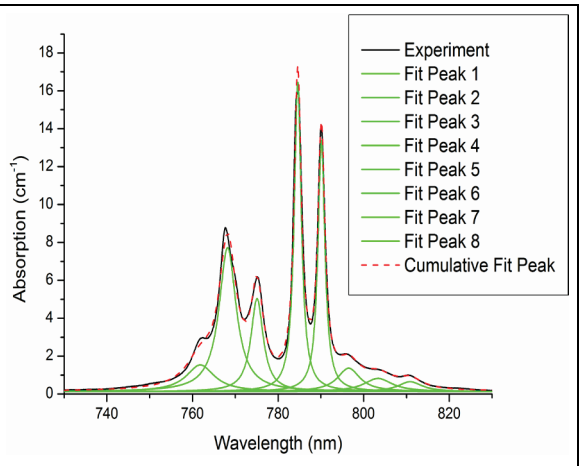

Fig.2. Result of Lorentz-fitting of 780nm absorption line.

As a result the table of the width and height of Lorentz peaks was formed for each polarization and each orientation of sample crystal. It was found, that total amount of parameters may be reduced by 2 times due to experimentally approved fact, that absorption depends mainly on orientation of electric component of light with respect to optical axis of crystal.

This work was supported by the Russian government in the frame of Program of RAS.

[1] Lihe Zheng, Jun Xu, Liangbi Su, Hongjun Li, Witold Ryba-Romanowski, Radoslaw Lisiecki, and Piotr Solars. Crystal structure and optical study of Tm:Sc2SiO5 single crystal. Appl. Phys. Lett. 96, 121908 (2010)

Dual mode diagnostic tool for confocal endomicroscopy and fluorescence lifetime spectroscopy to analyze tissue biochemistry *in-vivo*

Byungyeon Kim, Byungjun Park, Seungrag Lee, and Youngjae Won
Medical device development center,
Osong medical innovation foundation (K-bio)
Cheongju, Republic of Korea
yjwon000@gmail.com

***Abstract*—Confocal endomicroscopy is a powerful tool for *in vivo* real-time imaging at cellular resolution inside a living body without tissue resection. Microscopic fluorescence lifetime measurement can provide information about localized biochemical conditions such as pH and the concentrations of oxygen and calcium. We hypothesized that combining these techniques could assist accurate cancer discrimination by providing both biochemical and morphological information. We designed a dual-mode experimental setup for confocal endomicroscopic imaging and fluorescence lifetime measurement and applied it to a mouse xenograft model of activated human pancreatic cancer generated by subcutaneous injection of AsPC-1 tumor cells. Using this method with pH-sensitive sodium fluorescein injection, we demonstrated discrimination between normal and cancerous tissues in a living mouse. With further development, this method may be useful for clinical cancer detection.**

Keywords— endomicroscopy, Fluorescence lifetime spectroscopy, Fluorescein, Biochemistry, In vivo

I. INTRODUCTION

There has been a growing interest in diagnosing cancer without tissue resection using a minimally invasive and fast approach that can replace immunohistochemical staining [1-4]. Confocal endomicroscopy is a FDA-approved diagnostic tool that enables the minimally invasive discrimination of abnormal lesions from normal tissue surfaces inside a living body by high-resolution cellular imaging. This technique has the advantage that optical biopsy images are displayed in real-time to assist the physician in making immediate patient management decisions. Many studies have demonstrated the use of confocal endomicroscopy for cancer detection in various bodily regions, including stomach, pancreas, colon, alveoli, bladder, and others [5-10]. Despite its powerful advantages, several issues have prevented confocal endomicroscopy from becoming widely accepted in clinical use [11]. In particular, diagnostic efficacy is the most important area in which its reliability has not yet been adequately validated.

The fluorescence lifetime of a molecule is the average time that it spends in the excited state after absorbing extremely short pulsed laser energy [12]. Molecular fluorescence lifetime is not dependent on laser power, the concentration of the molecule, or photo-bleaching, but varies only due to the influence of the local biochemical conditions on energy transfer. Therefore, fluorescence lifetime can be used as an indicator of local biochemical conditions such as pH, the concentrations of oxygen and calcium, and other factors [12-15]. Various fluorescence dyes have been used for in vivo and ex vivo studies of local biochemical conditions to identify abnormal cells or tissues [12]. To avoid side effects of fluorescence dyes, auto-fluorescence naturally emitted by endogenous fluorophores in living tissues can also be applied for fluorescence lifetime measurements [16]. Certain cancer-related auto-fluorescent molecules such as nicotinamide adenine dinucleotide, flavin, and collagen may have altered fluorescence lifetimes due to local perturbations in oxygen concentration and pH. Thus, fluorescent lifetime measurement of auto-fluorescent molecules might present a foundation for the detection of abnormal tissues. The functional information that can be obtained by fluorescence lifetime measurements may help to make confocal endomicroscopy a reliable diagnostic tool for cancer detection.

In this study, we designed a dual-mode experimental setup for confocal endomicroscopic imaging and fluorescence lifetime measurement. A commercially available confocal endomicroscope (Cellvizio, Mauna Kea Technologies, Paris, France) and fluorescence lifetime spectrometer (FluoTime 300, PicoQuant, Berlin, Germany) were linked to the same optical mini-probe. To evaluate the effectiveness of this approach for cancer detection, we subcutaneously injected AsPC-1 activated human pancreatic cancer cells into a living mouse, followed by intravenous injection of sodium fluorescein. Sodium fluorescein is a FDA-approved fluorophore widely used as a diagnostic tool in the fields of ophthalmology and cancer detection. The fluorescence lifetime of sodium fluorescein depends on the local pH [17]. Since pH differs between abnormal and normal tissues, they can be differentiated by measuring the fluorescence lifetime of pH-sensitive sodium fluorescein. We morphologically discriminated abnormal and normal tissues by confocal

endomicroscopic imaging, and then functionally discriminated them by measuring the fluorescence lifetime of injected sodium fluorescein.

II. Material and Methods

A. Experimental setup

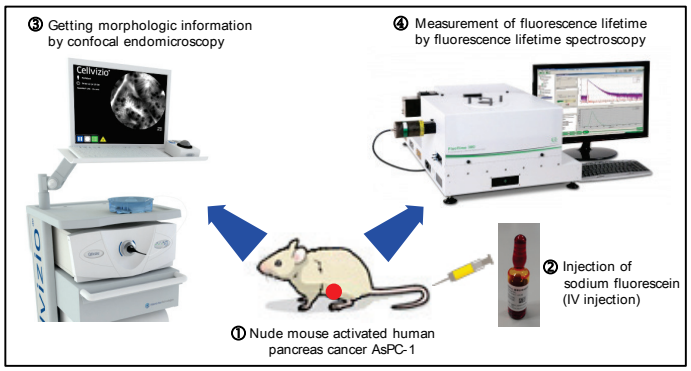

Fig. 1. Experimental concept :① Preparation of nude mouse activated human pancreas cancer AsPC-1 ② Injection of sodium fluorescein (IV injection) ③ Getting morphologic information by confocal endomicroscopy ④ Measurement of fluorescence lifetime by fluorescence lifetime spectroscopy

An experimental concept for the analysis of local biochemical conditions by fluorescence lifetime measurement combined with confocal endomicroscopy is presented in Fig. 1. Nude mouse activated human pancreas cancer AsPC-1 was prepared for the animal test. Sodium fluorescein was used as a fluorescent probe and intravenously injected into the mouse model. Then, the living mouse tissues were morphologically screened by confocal endomicroscopy. When tissues with an unusual morphology were identified by confocal imaging, the distal end of the probe was fixed using a holding jig and the opposite end of the probe was removed from confocal endomicroscopy and connected to the interface module for measurement of fluorescence lifetime. The fluorescence lifetime of sodium fluorescein diffused in that area was measured by fluorescence lifetime spectroscopy. The same process was applied for normal tissue.

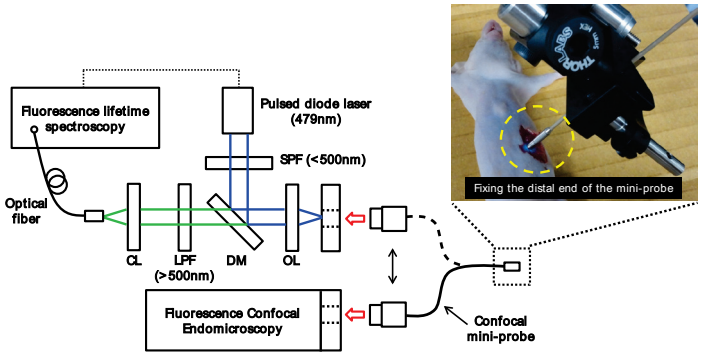

Fig. 2. Dual-mode experimental setup for confocal fluorescence endomicroscopic imaging and fluorescence lifetime measurement

The dual-mode experimental setup for confocal fluorescence endomicroscopic imaging and fluorescence lifetime measurement was shown in Fig. 2. After generating the mouse model, it was morphologically analyzed by confocal endomicroscopy with confocal mini-probe consisted of about 30,000 optical fibers. The confocal endomicroscopy provided the image as a circular pattern. The radius for maximum field of view was 600 um and the lateral resolution was 3.5 um. After morphological analysis, the same mini-probe used for confocal endomicroscopy was applied as a probe for fluorescence lifetime measurements. The fluorescence lifetime of the same region examined by confocal imaging could be measured by fixing the distal end of the mini-probe and moving its opposite end to the specially designed optical interface module. The optical interface module was realized by confocal point measurement setup to perform confocal fluorescence lifetime measurement. A diode pulse laser with a central wavelength of 479 nm was passed through a short pass filter with cutoff wavelength of 500 nm and reflected by a dichroic mirror and injected into the region of interest of the living mouse after passing through an objective lens and the mini-probe. The fluorescence pulse signals from fluorescein inside the mouse were transmitted through the same components in the reverse direction and passed through the dichroic mirror, a long pass filter with cutoff wavelength of 500 nm, and collimating lens. Finally, the fluorescence pulse signals went to the optical fiber of the fluorescence lifetime spectrometer.

B. Preperation of animal model

In vivo tumor xenograft experiments were conducted using 6-week-old male athymic nude mouse (BALB/c-nu) purchased from Central Lab. Animal Inc. (Seoul, South Korea). Tumors were implanted into the abdomens of the mouse by the subcutaneous injection of 1×10^7 AsPC-1 human pancreas cancer cells in 100 μL of serum-free Dulbecco's modified Eagle's medium (Gibco®, Thermo Fisher Scientific, Waltham, MA). The mouse were maintained in a laminar air flow cabinet under specific pathogen-free conditions. All facilities were approved by the Association of Assessment and Accreditation of Laboratory Animal Care, and all animal experiments were conducted under the institutional guidelines established by the Animal Core Facility at The Catholic University of Korea. When the tumor size reached 100–150 mm^3, fluorescein was injected intravenously via the tail vein. Sodium fluorescein (100 mg/mL, 10% [w/v], Novartis, Basel, Switzerland) was diluted to a final concentration of 0.01% (w/v) with phosphate buffered saline, and 200 μl of the diluted solution was injected into the mouse tail vein.

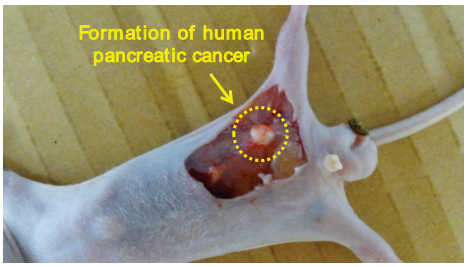

Fig. 3. Formation of human pancreatic cancer in a mouse model following subcutaneous injection of AsPC-1 cells.

III. Results and Discussion

To detect local pH variation between abnormal and normal tissues in a living mouse, sodium fluorescein was injected as described above, and the abnormal and normal tissues of the mouse were screened using standard confocal endomicroscopy. It has been demonstrated that morphological changes such as fibrosis often occur in tissues associated with neoplasia [11]. For confocal endomicroscopy, there is a library of case studies and atlases of normal and disease states available online, which we used for reference. [18] Through confocal fluorescence endomicroscopy analysis, we identified morphological differences such as fibrosis between the cancerous and normal tissues as shown in Fig. 4. Confocal fluorescence images of normal mouse abdominal subcutaneous tissue and the same tissue containing structures associated with the pancreatic cancer structures are shown in Figs. 4(a) and (b), respectively.

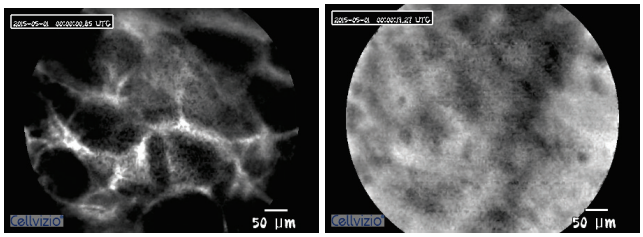

(a) (b)

Fig. 4. Confocal fluorescence imaging of (a) normal and (b) pancreatic cancer infiltrated mouse abdominal subcutaneous tissue

To discriminate abnormal tissues from normal tissues, the fluorescence lifetime of injected pH-sensitive sodium fluorescein was measured by fluorescence lifetime spectroscopy. Fluorescence curves after excitation by laser pulses were measured and plotted as shown in Fig. 5. Since the fluorescence lifetime of sodium fluorescein decreased according to the drop in pH, the widths of the fluorescence curves were shorter in abnormal than in normal tissue, indicating that the pH value of abnormal tissue was lower than that of normal tissue [17]. Curve fitting and calculation of fluorescence lifetimes were performed with FluoFit software (PicoQuant). Fluorescence curves were measured for three different areas in each of the normal and abnormal tissues. The photon numbers used to plot the fluorescence curves were more than 100,000. The measured fluorescence lifetimes of sodium fluorescein inside the normal and abnormal tissues were 3.69~3.81 and 3.09~3.44 ns, respectively. Since the measured fluorescence lifetimes for abnormal tissues were well differentiated from those for normal tissues, the fluorescence lifetime of sodium fluorescein could be used as an indicator to increase the accuracy of cancer detection with confocal endomicroscopy.

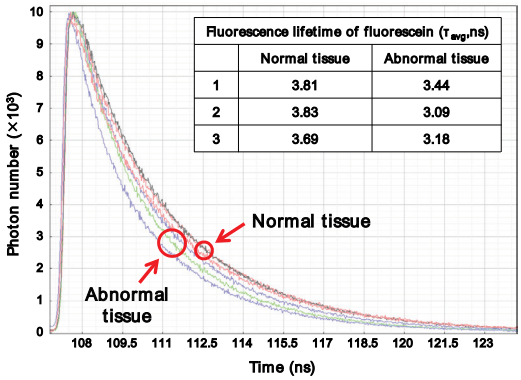

Fig. 5. Confocal fluorescence lifetimes of fluorescein in (a) normal and (b) abnormal tissues screened by confocal endomicroscopy

IV. Conclusions

In this paper, we have demonstrated the application of fluorescence lifetime measurement combined with confocal endomicroscopy for the analysis of tissue biochemistry in a living mouse xenograft model of activated human pancreatic cancer. The abnormal and normal tissues were morphologically analyzed by confocal microendoscopic imaging, then we evaluated the possibility of discriminating between them based on the fluorescence lifetime of sodium fluorescein, which is mainly influenced by the local tissue pH. We successfully discriminated the cancerous and normal tissues, indicating that this method may enable early cancer detection without tissue resection. Subsequent studies are warranted to assess the utility of applying this technique for fluorescent lifetime measurements of endogenous autofluorescent materials or other biocompatible fluorescent materials that are sensitive to changes in parameters such as pH, oxygen concentration, and temperature in the cancer tissue environment.

Acknowledgment

This work was supported by the Industrial Strategic Technology Development Program (10062417) funded by the Ministry of Trade, Industry and Energy (MOTIE) of Korea.

References

[1] R. Shukla, W.M. Abidi, R. Richards-Kortum, S. Anandasabapathy, “Endoscopic imaging: How far are we from real-time histology?” World J. Gastrointest. Endosc. 3 (2011) 183–194.

[2] S. Khondee, T.D. Wang, “Progress in molecular imaging in endoscopy and endomicroscopy for cancer imaging,” J. Healthc. Eng. 4 (2013) 1–21.

[3] S.F. Elahi, T.D. Wang, “Future and advances in endoscopy, J. Biophotonics”, 4 (2011) 471–481.

[4] M.J. Bruno, Magnification endoscopy, high resolution endoscopy, and chromoscopy; towards a better optical diagnosis, Gut 52 (2003) iv7–iv11.

[5] Y.T. Guo, Y.Q. Li, T. Yu, T.G. Zhang, J.N. Zhang, H. Liu, F.G. Liu, X.J. Xie, Q. Zhu, Y.A. Zhao, Diagnosis of gastric intestinal metaplasia with

confocal laser endomicroscopy *in vivo*: a prospective study, Endoscopy 40(7) (2008) 547–553.

[6] M. Giovannini, F. Caillol, F. Poizat, E. Bories, C. Pesenti, G. Monges, J.L. Raoul, Feasibility of intratumoral confocal microscopy under endoscopic ultrasound guidance, Endosc. Ultrasound 1(2) (2012) 80–83.

[7] M.W. Shahid, A. Buchner, V. Gomez, M. Krishna, T.A. Woodward, M. Raimondo, M.B. Wallace, Diagnostic accuracy of probe-based confocal laser endomicroscopy and narrow band imaging in detection of dysplasia in duodenal polyps, J. Clin. Gastroenterol. 46(5) (2012) 382–389.

[8] F.S. Fuchs, S. Zirlik, K. Hildner, M. Frieser, M. Ganslmayer, S. Schwarz, M. Uder, M.F. Neurath, Fluorescein-aided confocal laser endomicroscopy of the lung, Respiration 81(1) (2011) 32–38.

[9] J. Liu, J.J. Liu, W. Adams, G.A. Sonn, K.E. Mach, Y. Pan, A.H. Beck, K.C. Jensen, J.C. Liao, Dynamic real-time microscopy of the urinary tract using confocal laser endomicroscopy, Urology 78(1) (2011) 225–231.

[10] P. Sharma, A.R. Meining, E. Coron, C.J. Lightdale, H.C. Wolfsen, A. Bansal, M. Bajbouj, J.P. Galmiche, J.A. Abrams, A. Rastogi, N. Gupta, J.E. Michalek, G.Y. Lauwers, M.B. Wallace, Real-time increased detection of neoplastic tissue in Barrett's esophagus with probe-based confocal laser endomicroscopy: final results of a multi-center prospective international randomized controlled trial, Gastrointest. Endosc. 74(3) (2011) 465–472.

[11] S.S. Chauhan, B.K.A. Dayyeh, Y.M. Bhat, K.T. Gottlieb, J.H. Hwang, S. Komanduri, V. Konda, S.K. Lo, M.A. Manfredi, J.T. Maple, F.M. Murad, U.D. Siddiqui, S. Banerjee, M.B. Wallace, Confocal laser endomicroscopy, Gastrointest. Endosc, 80(6) (2014) 928–938.

[12] H.C. Gerritsen, M.A. Asselbergs, A.V. Agronskaia, W.G. Van Sark, Fluorescence lifetime imaging in scanning microscopy, in: J.B. Pawley (Ed.), Handbook of Biological Confocal Microscopy, 3rd Ed., Springer, New York, 2006, pp. 516–534.

[13] H.J. Lin, P. Herman, J.R. Lakowicz, Fluorescence lifetime-resolved pH imaging of living cells, Cytometry A 52(2) (2003) 77–89.

[14] H.C. Gerritsen, R. Sanders, A. Draaijer, C. Ince, Y.K. Levine, Fluorescence lifetime imaging of oxygen in living cells, J. Fluoresc. 7(1) (1997) 11–15.

[15] A.V. Agronskaia, L. Tertoolen, H.C. Gerritsen, Fast fluorescence lifetime imaging of calcium in living cells, J. Biomed. Opt. 9(6) (2004) 1230–1237.

[16] J. McGinty, N.P. Galletly, C. Dunsby, I. Munro, D.S. Elson, J. Requejo-Isidro, P. Cohen, R. Ahmad, A. Forsyth, A.V. Thillainayagam, M.A. Neil, P.M. French, G.W. Stamp, Wide-field fluorescence lifetime imaging of cancer, Biomed. Opt. Express 1(2) (2010) 627–640.

[17] M. Hammer, D. Schweitzer, S. Richter, E. Königsdörffer, Sodium fluorescein as a retinal pH indicator? Physiol. Meas. 26 (2005) N9–N12.

[18] Muana Kea Technologies, Cellvizio confocal endomicroscopy case studies library and tissue atlas. http://www.cellvizio.net

Laser–Matter Interaction

LM-1-1 (Invited)

Revealing the mystery of non-reciprocity and polarization spatio-temporal couplings in ultrafast laser direct writing

P. G. Kazansky, A. Patel, R. Drevinskas, A. Čerkauskaitė, F. Zhang

Optoelectronics Research Centre, University of Southampton, SO17 1BJ, United Kingdom
pgk@soton.ac.uk

The nanostructuring of transparent media with ultrafast laser pulses has attracted significant interest due to its unique applications. However, little is understood with respect to the physics of light-matter interaction. While most of the formalisms for ultrashort pulses express the electric field separately in terms of temporal and spatial dependences, one of the major properties of ultrashort pulse generation is spatio-temporal couplings (STC). Studies have shown spatio-temporal induced phenomena with respect to writing direction [1-3] and anisotropic photosensitivity [4] all based around pulse front tilt (PFT), yet they lack the control and understanding of the orientation, direction and quantity of the STC. More recently, a lighthouse-like wavefront rotation (WFR) has recently been exploited to control ultrafast nonlinear processes in the microscale with attosecond resolution (10^{-18} s) [5] emphasizing the need for better understanding of STC in light-matter interaction. Here we show with the control and characterization of STC through the use of grating compressors, we can control and understand ultrafast phenomena associated with material modification. We reveal that the vectorial nature of WFR is manifested on the macroscale introducing non-reciprocity during femtosecond laser writing in transparent media and induces either an isotropic damage-like structure or a self-assembled nanostructure depending on the writing direction; known as the "quill-writing effect" (Fig. 1, left).

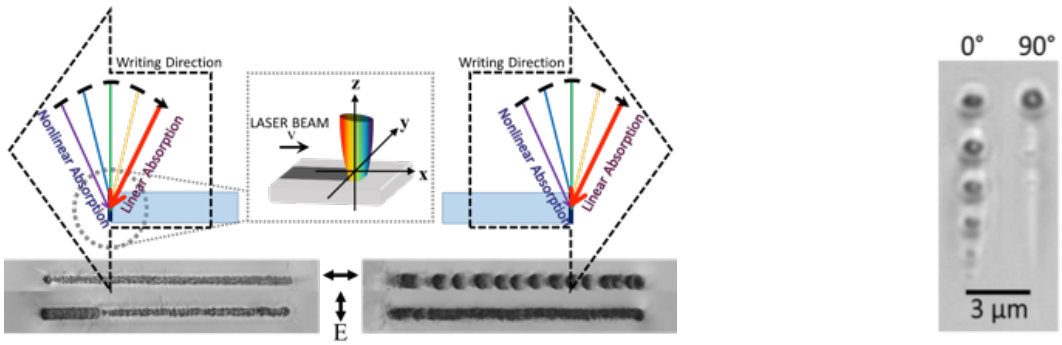

Fig. 1 (Left) The physical interpretation of the quill-writing effect. When the WFR is moving away from the interface, the first half of the beam, responsible for the nonlinear absorption, is unperturbed whereas when moving towards the interface, the light is scattered obstructing it from being absorbed, resulting in the different states of modification based on writing direction. (Right) Optical images od silica modified by transform limited pulses: 10 pulses, E_p = 0.5 µJ, NA= 0.55, τ_p = 300 fs, f = 200 kHz, λ = 1030 nm. When polarization is parallel to STC (0°), chains of nano-voids are observed across the structure and when perpendicular (90) a single void is seen at the top.

We also demonstrate that STC are inherent for all ultrafast laser systems with chirped-pulse amplification and can lead to a strongly anisotropic light-matter interaction that accumulates in multi-pulse irradiation (Fig. 1, right). With tight focusing (NA $\geq$ 0.4), this non-paraxial effect leads to a manifestation of STC in photo-induced modification. In particular, we identify that angular dispersion in the focus leads to the polarization dependent modification, yielding a 200% increase in modification strength by rotating the polarization state with respect to the orientation of the induced STC, introducing a new degree of freedom in ultrafast laser direct writing.

[1] W. Yang, P. G. Kazansky, Y. Shimotsuma, M. Sakakura, K. Miura, and K. Hirao, "Ultrashort-pulse laser calligraphy," Appl. Phys. Lett. 93, 171109 (2008).
[2] W. Yang, P.G. Kazansky, and Yu. P. Svirko, "Non-reciprocal ultrafast laser writing," Nature Photonics 2, 99-104 (2008).
[3] D. Vitek, E. Block, Y. Bellouard, and D. Adams, "Spatio-temporally focused femtosecond laser pulses for nonreciprocal writing in optically transparent materials," Opt. Express 18, 24673–24678 (2010).
[4] P. G. Kazansky, Y. Shimotsuma, M. Sakakura, M. Beresna, M. Gecevičius, Y. Svirko, S. Akturk, J. Qiu, K. Miura, and K. Hirao, "Photosensitivity control of an isotropic medium through polarization of light pulses with tilted intensity front.," Opt. Express 19, 20657–64 (2011).
[5] H. Vincenti and F. Quére, "Attosecond lighthouses: How to use spatiotemporally coupled light fields to generate isolated attosecond pulses," Phys. Rev. Let. 108, 113904 (2012)

LM-1-2 (Invited)

Photons with half a twist: angular momentum and structured light

K. E. Ballantine, J. F. Donegan, P. R. Eastham

School of Physics and CRANN, Trinity College Dublin, Dublin 2, Ireland

easthamp@tcd.ie

Angular momentum is one of light's most fundamental properties, and plays an important role in applications such as optical trapping and quantum information. We expect that, in general, the angular momentum quantum numbers of a photon are integers, so that measuring any aspect of light's angular momentum will give an integer multiple of Planck's constant. In this talk I will describe recent work [1] showing that this is not the case, and that photons can have a half-integer total angular momentum. This arises when, as in a beam of light, there is only a single axis of rotational symmetry. I will explain why this allows a new form of angular momentum, which has a half-itneger spectrum, and show how this half-integer quantization can be demonstrated experimentally. This shows that for light, as is known for electrons [2], reduced symmetry allows for new forms of quantization.

[1] K. E. Ballantine, J. F. Donegan and P. R. Eastham, There are many ways to spin a photon: half-quantization of a total optical angular momentum, Science Advances, 2, e1501748, (2016).
[2] F. Wilczek, Magnetic flux, angular momentum, and statistics, Physical Review Letters, 48, pp. 1144-1146, (1982).

LM-1-3 (Invited)

Novel frequency shift free and polarisation shift free optical phase conjugation scheme

A. Anchal[1], P. Kumar[1], S. O'Duill[2], P. Anandarajah[2], P. Landais[2]

1- Department of Electrical Engineering, Indian Institute of Technology Kanpur, Kanpur 208016, India
2- School of Electronic Engineering, Dublin City University, Dublin 9, Ireland

Main author email address: aanchal@iitk.ac.in

A simple scheme of frequency-shift free and polarisation shift free optical phase conjugation (OPC) presented in inset of Fig 1 is the subject of this communication. It is based on counter-propagating dual pumped four-wave mixing in highly non-linear medium. The two pump frequencies must be symmetrically placed around the signal frequency to ensure that the conjugate wave has the same frequency as that of signal wave [1]. Owing to the counter-propagating nature of pumps, momentum conservation results in conjugate wave counter-propagating to the signal, causes the spatial separation of signal and conjugate waves.

In the first part of the presentation, this new OPC scheme is experimentally demonstrated using a semiconductor optical amplifier as non-linear medium [2].

In the second part, the OPC scheme is numerically studied as a mid-span spectral inversion function in a 40 Gbps QPSK modulated data network over 1000 km standard single mode fiber as depicted in Fig 1. The aim is to mitigate nonlinearity of the single mode fiber. In this numerical investigation, the non-linear medium can be achieved highly non-linear fibre. We examine the performance of mid-span spectral inversion under the effects of design parameters, nonlinear length and pump power. The bit-error rate is evaluated in our mid-span spectral inversion system to assess the performance of our optical phase conjugation. It is carried out as a function of signal power to demonstrate near complete nonlinearity mitigation due to mid-span spectral inversion.

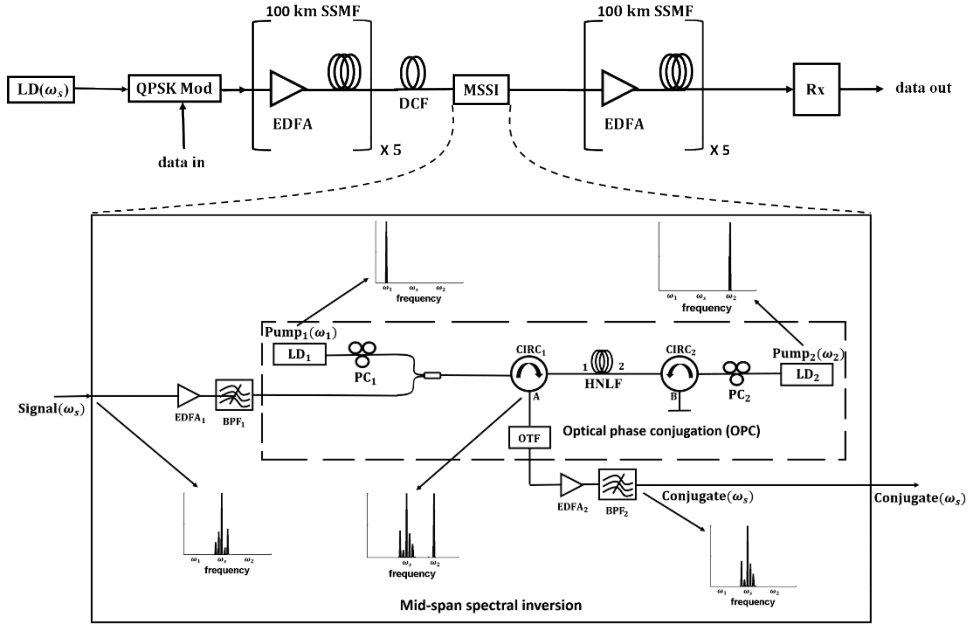

Figure 1: Proposed scheme for nonlinearity compensation of QPSK modulated data transmitted over 1000 km standard single mode fibre (SSMF). The enlarged portion shows frequency-shift free MSSI. Spectrum of input and output to MSSI shows spectral inversion. EDFA = Erbium doped fibre amplifier, DCF = dispersion compensating fibre, LO = local oscillator, $BPF_{1,2}$ = band-pass filter, HNLF = highly nonlinear fibre, $PC_{1,2}$ = polarization controller, $CIRC_{1,2}$ = circulator, $LD_{1,2}$ = laser diode, OTF = optical tunable filter.

[1] A. Anchal, P. Kumar, and P. Landais, Frequency-shift free optical phase conjugation using counter-propagating dual pump four-wave mixing in fiber, Journal of Optics, Volume 18, Number 3, pp. 116-120, (2016)

[2] A. Anchal, P. Kumar, S. O'Duill, P. Anandarajah, and P. Landais, Experimental demonstration of optical phase conjugation using counter-propagating dual pumped four-wave mixing in semiconductor optical amplifier, Optics Communications, Volume 369, pp. 106-110, (2016)

LM-1-4 (Invited)

Nano structuring of metals self-organized by fs double pulse beam

M. Hashida[1], S. Masuno, T. Nishii, H. Sakagami[2], M. Shimizu[3], S. Inoue, S. Sakabe

1- ARCBS, Institute for Chemical Research, Kyoto University, Uji, Kyoto 611-0011, Japan
2- National Institute for Fusion Science, Toki, Gifu 509-5292, Japan
3- Graduate School of Engineering, Kyoto University, Kyoto 615-8510, Japan

Email address: hashida@laser.kuicr.kyoto-u.ac.jp

On metals and semiconductors irradiated by linear polarized femtosecond laser pulses, laser-induced periodic surface structures (LIPSS) are self-organized and oriented perpendicular to the laser polarization direction which might be attributed to the following mechanisms: laser-induced surface plasma waves, the excitation of surface-plasmon polaritons, surface wave induced by parametric decay process, second-harmonic generation, and directional atomic surface diffusion anisotropy arising from plasmon-coupled metallic colloid arrays induced by laser pulses. However, the details of LIPSS orientation for metals produced by femtosecond laser pulses have not yet been investigated and remain debated. In this study, LIPSS formation to investigate the relation between the laser polarization direction and the LIPSS orientation self-organized on the metal surface. In the experiments, the T^6-laser system (λ_L= 805 nm, τ = 40 fs, 10 Hz) was used. The double pulse beam was varied in the time delay from $\Delta\tau$ = 0 to 40 ps. The number of irradiated double pulse beam was N = 50. Laser-produced LIPSS were examined by a SEM. The first-pulse fluence F_1 and the delayed pulse fluence F_2 are kept below the formation threshold F_{TH} = 65 mJ/cm^2 of the periodic grating structure on Ti. We find that periodic grating structures with LIPSS orientation of 45° relative to both polarizations are produced at delay times of 0 and 120 fs. To control LIPSS orientation, a double-pulse beam with a time delay of 0 fs is demonstrated in which a beam composed of a first pulse maintaining constant fluence of F_1 = 70 mJ/cm^2 and a second pulse varying from F_2 = 0 - 70 mJ/cm^2. Figure 1 summarizes the results, which show that LIPSS orientation defined by wave vector can be controlled by changing the second laser fluence. Here, LIPSS orientation of θ = 0° means that the LIPSS direction is characterized by the first laser pulse, while LIPSS orientation of ± 90° means that the LIPSS direction is determined by the second laser pulse. The LIPSS orientations are in a range of 0 - 45° and decrease as the normalized fluence F_2/F_1 decreases [1]. We find that the orientation angle θ of LIPSS produced by double-pulse irradiations can be expressed as $\theta = \tan^{-1}(F_2^2/F_1^2)$. Additionally, ultrafine surface structures which size of < 80nm were produced on titanium surface with appropriate choice of laser irradiation condition.

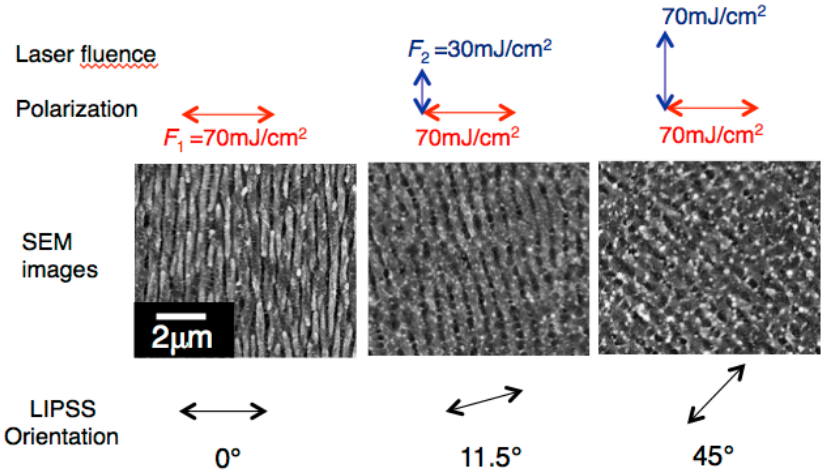

Fig.1 Dependence of LIPSS orientation on the laser fluence of the second pulse F_2 at a first pulse fluence of F_1 = 70 mJ/cm^2

Acknowledgments
This study was financially supported by a Grant-in-Aid for Scientific Research (C)(16K06745) from the Ministry of Education, Culture, Sports, Science and Technology (MEXT), Japan, NIFS Collaborative Research Program (NIFS14KNTS031), and New Energy Industrial Technology Development Organization (NEDO).

References

[1] M. Hashida, T. Nishii, Y. Miyasaka, H. Sakagami, M. Shimizu, S. Inoue, and S. Sakabe, "Orientation of periodic grating structures controlled by double-pulse irradiation", Appl. Phys. A Vol.122., pp. 484-1-484-5, (2016).

LM-1-5 (Invited)

Laser Materials Processing for Energy Storage

Alberto Piqué, Heungsoo Kim, Ray Auyeung and Nicholas A. Charipar

Materials Science and Technology Division, Code 6364, Naval Research Laboratory
Washington, DC 20375

E-mail: alberto.pique@nrl.navy.mil

This talk will present recent work on the fabrication of micro-scale energy storage devices using laser materials processing techniques, such as pulsed laser deposition (PLD), laser-induced-forward transfer (LIFT), and laser structuring. PLD is a versatile technique for depositing high-quality layers of materials for cathodes, anodes and solid electrolytes for thin-film microbatteries. LIFT is a powerful tool for printing complex materials with highly porous structures for the fabrication of micropower sources, such as thick-film microbatteries. In particular, using LIFT it is possible to print thick layers (~100 μm) while maintaining pattern integrity and low internal resistance. As a result, power sources fabricated in this manner exhibit higher energy densities per unit area than those obtained by traditional thin-film growth techniques. In addition, the printed active materials can be modified once printed using laser surface processing techniques, such as laser structuring, to further improve device performance by enhancing the electrodes 3D networked structure and increasing the overall active surface, respectively. This talk will show various examples where these laser techniques have lead to new approaches in the development of micropower sources for microelectronic device applications. We will conclude with a discussion on lessons learned from the characterization of the electrochemical properties of these laser-processed micropower sources.

This work was funded by the Office of Naval Research (ONR) through the Naval Research Laboratory Basic Research Program.

LM-2-1 (Invited)

Experimental investigation of fundamental mechanisms involved in femtosecond laser induced modification of dielectric materials.

Stéphane Guizard[1], Sergei Klimentov[2], Allan Bildé[1], Andrius Melninkaitis[3], Julius Vaicenavicius[3], Balys Momgaudis[3], Nikita Fedorov[4]

(

1. Laboratoire des Solides Irradiés, CEA/CNRS, Université Paris-Saclay, Ecole Polytechnique, 91128 Palaiseau, France,

2. General Physics Institute of the Russian Academy of Sciences, Vavilova St 38, 11991 Moscow, Russia.

3. Institute of Applied Research, Vilnius University, Sauletekio 10, 10223 Vilnius, Lithuania.

4. Laboratoire CELIA, Université Bordeaux-CEA/CNRS, Cours de la Libération, Talence, France.

Main author email address: stephane.guizard@cea.fr

Abstract : Laser processing and machining of dielectrics, like for instance silica or sapphire, is a growing field, involving increasingly complex laser temporal and spatial pulse shaping. The situation is intricate due to the feedback between electronic excitation and pulse propagation. Obviously, a detailed knowledge of all elementary processes involved in the interaction is mandatory for optimizing any laser manufacturing process. In particular, the critical step is energy deposition, which must be controlled to achieve precise laser induced modification. In order to improve our understanding of the interaction, we use three different experimental technique: time resolved holography and interferometry, and double pulse photoelectron spectroscopy. We will show that the combination of these technique allow to get a complete picture of the beam propagation, and to quantitatively characterize in 3D the energy deposition in the solid. Also, we will show that the use of a double excitation scheme allow to control both plasma density and temperature, and gives detailed information on the excitation and relaxation mechanisms, which could not be observed so far. For instance we demonstrate the first direct observation of laser induced avalanche in a solid.

[1] Guizard, S., Klimentov, S., Mouskeftaras, A., Fedorov, N., Geoffroy, G., & Vilmart, G. (2015). Ultrafast Breakdown of dielectrics: Energy absorption mechanisms investigated by double pulse experiments. Applied Surface Science, 336, 206-211

LM-2-2 (Invited)

Laser synthesis of new carbon materials and metal-carbon complexes for photonics applications

A.O. Kucherik, S.V. Kutrovskaya, D.S. Nogtev, A.V. Osipov, S.M. Arakelian,

Stoletov Vladimir State University, Vladimir, Russia
E-mail: kucherik@vlsu.ru

Metal-carbon complexes consisting of noble metal nanoparticles and carbon matrix is a prospective material for photonics applications. One application of these objects is to provide materials for the implementation of Surface Enhanced Raman Scattering (SERS). Carbon stabilizes the metal particles and increases SERS. The control of size and morphology of formed metal-complexes allows to vary its properties. The application of laser ablation materials in a liquid allows to create nanoparticles and clusters with various optical properties. A very perspective carbon material with structural sensitive optical properties is carbyne.

In this work we present the investigation of metal-carbyne clusters formation under the laser radiation of colloidal systems. Colloidal solutions were consisted of carbon and noble metals nanoparticles As a result, there was shown that clusters are forming during the irradiation process. The Raman spectra of those systems depends on the concentration of the particles in the solution and on the laser radiation conditions.

The gold and silver particles were obtained during the cw-irradiation of the targets placed in liquid media. [1]. The power of radiation was 35-50 W, laser beam diameter equaled 30 μm. A target was scanned by the laser beam with the speed of 10-30 μm/s. The irradiation time was 30 min. The average particle size after laser irradiation was 10-30 nm. The size of particles in colloidal system was measured by the Horiba LB-550 (dynamical light scattering particle size analyzer).

Carbon nanoparticles were obtained using the pulse-periodical laser radiation (pulse 2 ms), energy in pulse was from 1 J up to 20 J, pulse frequency – 20 Hz, on the shungite targets placed in water. This kind of method allows to obtain carbon particles with diameters about 100 nm - 2 μm.[2]

The carbon, gold and silver particle colloidal solution was prepared by the intense mixing with concentratration C:Au:Ag 10:1:1 in water (5cl), then the ultrasonic bath was used for about 10 minutes for particle decoagulation. The fiber Yb-laser setup (pulse - 100 ns, repetition rate - 20 kHz, the pulse energy up to 1mJ) was used for the metal-carbyne clusters obtaining [3]. This kind of laser system can realize the particle absorption on the wavelength of 1.06 μm, with short pulse. The colloidal system irradiation was carried out by the scanning of the cuvette volume by focused beam (spot diameter - 50 μm, irradiation time - 15 minutes).

The SERS research by deposited films was performed using Senterra spectrometer (Bruker), with the pump laser wavelength of 532 nm, the power of 0.1 mW and the focal spot diameter of 2 microns (Center for laser and optical materials research, SPbSU).

The standard dye Rhodamine 6G was used as a test molecule. The dye solution in ethanol (10^{-6}M) was placed on a metal-carbon structures using a micropipette. The metal-carbon surfaces are formed on an oxide glass substrates with different composition of metal nanoparticle. The use of films as a substrate of metal-carbon nanostructures under the same measurement conditions allow to detect and identify the dye on the Raman spectra with sureness.

This study was performed within the design part of a government contract for research work with VlSU #2013/14 and RFBR grant #16-42-330531.

[1] S. M. Arakelyan, V. P. Veiko, S. V. Kutrovskaya, A. O. Kucherik, A. V. Osipov, T. A Vartanyan., T. E. Itina Reliable and well-controlled synthesis of noble metal nanoparticles by continuous wave laser ablation in different liquids for deposition of thin films with variable optical properties. J Nanopart Res (2016) 18:155. DOI 10.1007/s11051-016-3468-0.

[2] A.A. Antipov, S.M. Arakelyan, S.V. Garnov, S.V. Kutrovskaya, A.O. Kucherik, D.S. Nogtev, A.V. Osipov: Laser ablation of carbon targets placed in a liquid. Quantum Electronics (2015). doi: 10.1070/QE2015v045n08ABEH015681

[3] S. Arakelian, S. Kutrovskaya, A. Kucherik, A. Osipov, A. Povolotckaia, A. Povolotskiy, A. Manshina Laser-induced synthesis of a nanostructured polymer-like metal-carbon complexes// Proc. of SPIE Vol. 9884, 988425 (2016) doi: 10.1117/12.2225452

LM-2-3 (Invited)

Processing materials beyond diffraction limit using designer ultrafast laser radiation

R. Stoian

Laboratoire Hubert Curien, UMR 5516 CNRS, Université de Lyon, Université Jean Monnet, 42000 St. Etienne, France

Razvan.stoian@univ-st-etienne.fr

Bypassing diffraction limit in laser material structuring is a key issue for a new range of applications in optics and mechanics requiring optical access to the nanoscale. Enabled by the nonlinearity of interaction, ultrafast lasers show remarkable effectiveness in localizing light on subwavelength scales, building up in many cases on a collective carrier response on surfaces and in the bulk. The 3D capability has a particular interest as ultrafast laser interaction with transparent materials can achieve optical functions by space-design of embedded structural transformations with changes of the dielectric function. Control of laser interaction by beam design can drive selected physical paths and geometries, and we will focus here on structural evolutions and dimensional scales enabled by spatio-temporal beam shaping. Essential for refractive index engineering, laser-induced matter transformation can be significantly influenced by the level of the energy deposition, critically dependent on the pulse temporal envelope. Photoionization can be regulated, leading to unprecedented localization of laser energy. Pulse temporal and spatial design can achieve index structures on scales approaching 100 nm, either in direct focusing or self-organization schemes in model fused silica [1,2]. We follow specific dynamics of electronic relaxation in confinement conditions and point out characteristic times of energy deposition, serving as guidelines for control. Fast electronically-induced structural changes or slow thermodynamic transformations can be discriminated. Concepts of non-diffractive beam excitation can additionally take advantage of this localization and achieve unprecedented high aspect ratio structuring. From the application point of view, the mid-infrared spectral range carries a strong potential in sensing and imaging. Extrapolation of controlled laser-induced structural modification towards mid-infrared materials can achieve strong index contrast on micron and submicron scales. We demonstrated linear and nonlinear 3D optical functions in chalcogenide glasses [3,4] where light transport in mid-infrared can be efficiently achieved with large area modes, and the field distributions can be non-perturbatively accessed.

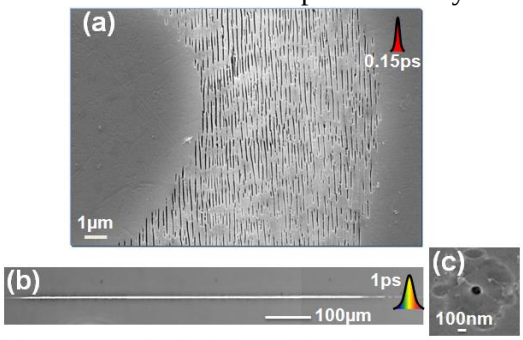

Fig1. (a-c) Examples of bulk nanostructuring in fused silica using self-organization or non-diffractive direct focusing concepts.

[1] K. Mishchik, G. Cheng, G. Huo, I.M. Burakov, C. Mauclair, A. Mermillod-Blondin, A. Rosenfeld, Y. Ouerdane, A. Boukenter, O. Parriaux, and R. Stoian, Nanosize structural modifications with polarization functions in ultrafast laser irradiated bulk fused silica, Opt. Express 18, pp. 24809-24824 (2010).

[2] M. Bhuyan, P. K. Velpula, J. P. Colombier, T. Olivier, N. Faure, and R. Stoian, Single-shot high aspect ratio bulk nanostructuring of fused silica using chirp controlled ultrafast laser Bessel beams, Appl. Phys. Lett. 104, pp 021107/1-4 (2013).

[3] C. D'Amico, G. Cheng, C. Mauclair, J. Troles, L. Calvez, V. Nazabal, C. Caillaud, G. Martin, B. Arezki, E. LeCoarer, P. Kern, and R. Stoian, Large-mode-area infrared guiding in ultrafast laser written waveguides in Sulfur-based chalcogenide glasses, Opt. Express 22, pp. 13091-13101 (2014).

[4] S. Minardi, G. Cheng, C. D'Amico, and R. Stoian, Low-power-threshold photonic saturable absorber in nonlinear chalcogenide glass Opt. Lett. 40, pp. 257-259 (2015).

LM-2-4 (Invited)

High efficiency X-ray K_α laser plasma source for medical imaging and material science

Y. Azamoum, V. Tcheremiskine, R. Clady, A. Ferré, L. Charmasson, O. Utéza, and M. Sentis

Aix Marseille University, CNRS, LP3
163 avenue de Luminy, case 917, 13009 Marseille, France

Sentis@LP3.univ-mrs.fr

Optimization of ultrafast x-ray emission from plasmas produced by femtosecond high intensity laser-solid interaction is still under strong investigation by many groups around the world. Motivation is related to important scientific applications like time-resolved x-ray diffraction or x-ray absorption fine structure spectroscopy for advanced high-resolution diagnostics of materials driven to extreme thermodynamic conditions and societal applications such as phase contrast imaging. Ultrashort K_α X-ray pulses from laser plasmas are studied since decades but the continued improvement of femtosecond laser performances offers today the possibility to explore a wide range of regimes of laser interactions such as intensities > 10^{19} W/cm^2 for pulse duration < 30 fs with controlled high contrast ratios using a unique laser source with moderate affordable peak power (~ 10 TW).
In the present work, Molybdenum K_α line emission produced from ultrahigh intensity femtosecond laser solid interaction is experimentally studied over more than 2 orders of magnitude of temporal pulse contrast ratio as well as over a wide range of pulse intensity using the ASUR laser source [1]. The absolute yield of K_α x-rays is measured as a function of contrast ratio from 6×10^{-8} to 3×10^{-10} (Fig.1a) and for a large intensity range 3×10^{16} - 4×10^{19} W/cm². For intensity I ≥ 10^{19} W/cm², we show that no saturation of the measured K_α yield is observed. Furthermore, K_α conversion efficiency, from laser pulse energy into total energy in K_α line, is measured to be independent of intensity and reaches ~ 2×10^{-4} in 2π solid angle for all the studied contrast ratios (Fig.1b).

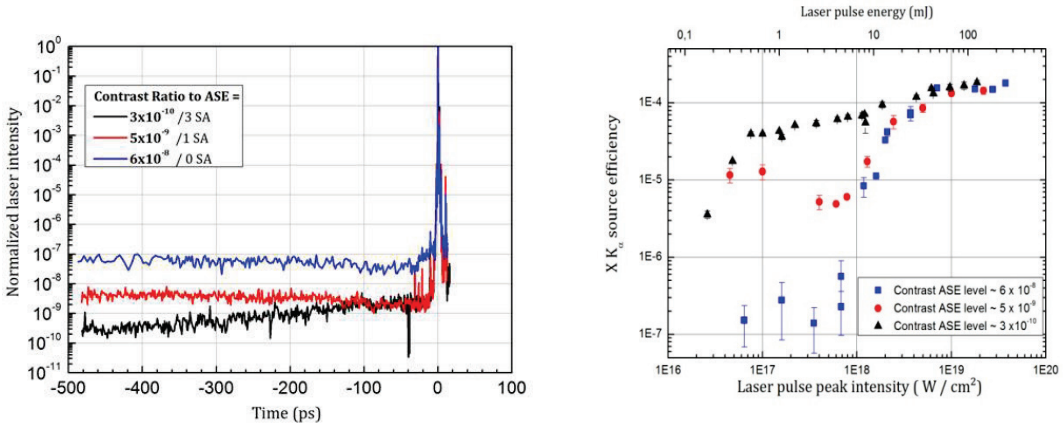

(a) (b)

Fig.1 a) Third order cross-correlation signal for different number of saturable absorbers (SA) inserted inside the laser chain, b) K_α source efficiency as function of laser pulse peak intensity and different contrasts.

The present results bring important information on different interaction regimes of high intensity femtosecond laser radiation with a solid target, since we observe a strong dependence of the K_α emission on both laser pulse contrast and intensity. We will discuss of the interplay of different mechanisms like resonance absorption, vacuum heating (Brunel effect), plasma steepening by radiation pressure and J×B which are present at these different of interactions to explain our experimental results.

[1] R.Clady, V.Tcheremiskine, Y.Azamoum, A. Ferré, et al., Proc. of SPIE Vol. 9726, 97260X-1 (2016).

Reduction of ablation rate by double-pulse laser irradiation with sub-nanosecond interval

Y. Furukawa[1, 2, 3], R. Sakata[1, 2], K. Konishi[1, 2], K. Ono[1, 2], S. Matsuoka[1], K. Watanabe[2, 3], M. Hashida[2, 3], S. Inoue[2, 3], S. Sakabe[2, 3]

1- Faculty of Science, Kyoto University, Kitashirakawa, Sakyo, Kyoto 606-8502, Japan.
2- Graduate School of Science, Kyoto University, Kitashirakawa, Sakyo, Kyoto 606-8502, Japan.
3- Advanced Research Center for Beam Science, Institute for Chemical Research, Kyoto University, Gokasho, Uji, Kyoto 611-0011, Japan.

yfurukawa@laser.kuicr.kyoto-u.ac.jp

The formation of laser-induced periodic surface structure (LIPSS) with femtosecond laser pulse has been studied for metals, semiconductors, and insulators. Interest in LIPSS is increasing for its application to laser micro-fabrication [1]. It has been well confirmed that a femtosecond LIPSS is characterized by a periodic structure with interspace shorter than the laser wavelength and its direction perpendicular to the laser polarization. For LIPSS application, it is desirable to control the LIPSS interspace and the ablation depth separately. However, the physical mechanism of LIPSS is still highly debated and the relation between the LIPSS interspace and the ablation depth has not been studied systematically. To investigate the relation, we study the properties of nanostructure formed with single- and double-pulse femtosecond laser irradiation.

Linearly polarized laser pulses are delivered from the T^6 Ti-sapphire laser system (810 nm central wavelength, 40 fs pulse duration, 10 Hz repetition rate) and are focused on a titanium plate with an inter-pulse interval Δt between the first and second pulses (0.16–1280 ps). The first pulse fluence is set to 70 mJ/cm^2 or 140 mJ/cm^2 while keeping the second pulse fluence at 140 mJ/cm^2. Single pulse irradiation is also done with fluences 140, 210, and 280 mJ/cm^2. Laser-produced craters are imaged with a scanning electron microscope and the depths of craters are measured with a confocal laser-scanning microscope for ablation analysis.

Figures 1 (a) and (b) show examples of single- and double-pulse irradiated surfaces. Total fluence is same for Fig. 1 (a) and (b), but the time interval is 0 ps and 8 ps, respectively. This shows that the morphologies of the nanostructures changes as the time interval is increased. The ablation rate also changes with the increment of time interval as is shown in Fig. 2. Fig. 2 shows the dependence of ablation rate on time interval for double-pulse irradiation with the first pulse fluence 70 mJ/cm^2. The minimum ablation rate (3.3 nm) is smaller than the ablation rate of single-pulse irradiation with fluence 140 mJ/cm^2 (8.3 nm). This indicates that the fist pulse modifies the surface to some extent, reducing ablation by the second pulse.

This study was financially supported by a Grant-in-Aid for Scientific Research (C)(16K06745) from the Ministry of Education, Culture, Sports, Science and Technology (MEXT), Japan and partially supported by and New Energy Industrial Technology Development Organization (NEDO).

[1] B. Wo, M. Zhou, J. Li, G. Li, L. Cai, Superhydrophobic surfaces fabricated by microstructuring of stainless steel using a femtosecond laser, Appl. Surf. Sci. 256, pp. 61-66 (2009).

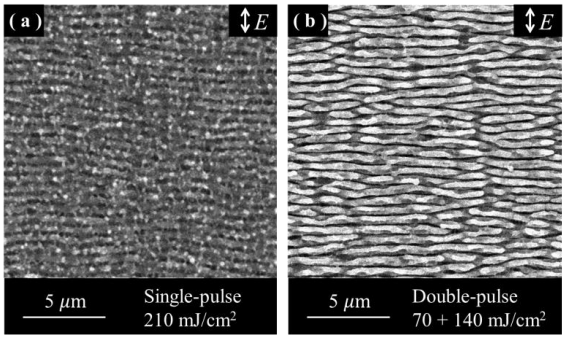

FIG. 1. Examples of SEM images with intervals of (a) 0 ps and (b) 8 ps. The direction of LIPSS growth is perpendicular to the laser polarization (*E*).

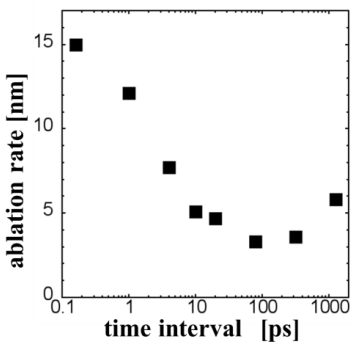

FIG. 2. Dependences of ablation rate on time interval for the first pulse fluence 70 mJ/cm^2.

LM-2-6

Parametric study of microstructure properties at coaxial laser cladding of nickel-based super alloys

M.D. Khomenko, F.Kh. Mirzade, V.G. Niziev

Institute on Laser and Information Technologies - Branch of the Federal Scientific Research Center "Crystallography and Photonics" of Russian Academy of Sciences, 140700, Shatura, Moscow region, Russia

E-mail:hmd@laser.ru

A self-consistent 3-D numerical model including heat transfer, solute transport, melt hydrodynamics and phase change kinetics is developed for laser cladding process with coaxial injection of nickel superalloy powder. Open source Computational Fluid Dynamics package OpenFoam is used for the numerical investigation of additive manufacturing process. S-CLSVOF solver (program) was adopted for numerical modeling of heat conduction, mass transport and free boundary evolution [1] at laser cladding. Population Kolmogorov-Johnson–Mehl-Avrami [2] model is used for phase change modeling with account of non-homogeneous temperature distribution of melt pool [3]. The resulting microstructure of build-up layer is investigated. Influence of self-consistent heat removal and phase change kinetics as well as substrate boundary on phase change process is analyzed. Results show the influence of cooling rate via main processing parameters (powder feed rate, laser power, scanning velocity) on the rapid crystallization at laser cladding and can be used for process map estimation.

This work was carried out with financial State support by the Ministry of Education and Science according to the grant agreement # 14.626.21.0001 (UID RFMEF162614X0001) under the Federal Special-Purpose Program "Research and development on priority directions of scientific-technological complex of Russia for 2014—2020"

1. Albadawi A., Donoghue D.B., Robinson A.J., Murray D.B., and Delauré Y.M.C., "Influence of surface tension implementation in Volume of Fluid and coupled Volume of Fluid with Level Set methods for bubble growth and detachment," *International Journal of Multiphase Flow* , Vol. 53, 2013. pp. 11–28.
2. Crespo D., Pradell T., "Evaluation of time-dependent grain-size populations for nucleation and growth kinetics," *Physical Review B*, Vol. 54, No. 5, 1996. pp. 3101-3109.
3. Khomenko M.D., Panchenko V.Y., Niziev V.G., Mirzade F.K., and Grishaev F.K., *Bulletin of the Russian Academy of Sciences. Physics*, Vol. 80, No. 4, 2016. pp. 381–386.

LM-2-7

Direct Laser Writing in the Regime of Crystal Phase Transition

A.G.Okhrimchuk[1], A.S.Lipatiev[1], E.V. Zharikov[1], V.K. Mezentsev[2], M.P.Smayev[1], P.G. Kazansky[1,3]

1 - D. Mendeleyev University of Chemical Technology of Russia, 9 Miusskaya square, Moscow 125047, Russia
2 - Aston University, Aston Triangle, Birmingham B4 7ET, UK
3 - Optoelectronics Research Centre, University of Southampton, Southampton SO17 1BJ, UK

a.okhrim@yandex.ru

The tightly focused femtosecond laser beam is an effective and non-competitive tool for 3D micro modification of transparent dielectric glasses and crystals. In these 3D micro-structuring the underlying physical phenomena are densification, changes in short-range ordering in glasses and crystal matrixes, ions migration, and phase transition. The last phenomenon is very attractive because it opens possibility to create 3D micro-structures with high contrast of physical properties such as refractive index, electrical conductivity, elastic properties. Up to now only the transitions from glass to crystalline phases and vice versa have been thoroughly investigated [1,2]. Transition from sapphire crystal to super dense aluminum metallic crystal state was detected in nanometers called compressed region around a void. [3].

Here we report of first observation and investigation of phase transition from one dielectric crystal phase to another during laser writing of tracks. Femtosecond laser beam with pulse duration of 180 fs and repetition rate of 1 MHz at wavelength of 1030 nm was focused by microscopic lens (NA=0.65) and cylindrical lens (f=-1000 mm) in the volume of $Y_3Al_5O_{12}$ (YAG) single crystal, which was translated perpendicular to laser beam propagation. Under pulse energy of 500 nJ and translation speed less than 3 mm/s we obtained strongly birefringent tracks with cross-section of few squared micrometers and retardance nearly 100 nm. Raman spectra taken with a confocal setup reveals that mixture of YAG and $YAlO_3$ (YAP) crystal phases present in the laser-modified tracks. No other phases were detected. Appearance of the birefringence has a bistable behavior, when translation speed is changing.

Obviously that the birefringence is due to YAP crystal phase, which is belong to orthorhombic syngony, whereas YAG is a cubic crystal. Numerical solution of heat transport equations shows that the melting point of YAG crystal is reached under our experimental conditions, which is 1970 C. Melting point of YAP crystal is of 100 degrees lower, and we suggest that YAP phase is formed due to specific conditions of rapid cooling, realized in femtosecond laser writing regime.

Acknowlegment: The work was supported by Ministry of Education of Science of Russian Federation, grant #14.Z50.31.0009.

[1] B. Yu, B. Chen, X. Yang, J. Qiu, X. Jiang, C. Zhu, and K. Hirao, "Study of crystal formation in borate, niobate, and titanate glasses irradiated by femtosecond laser pulses," *J. Opt. Soc. Am. B*, vol. 21, no. 1, p. 83 (2004).
[2] S. Juodkazis, K. Nishimura, H. Misawa, T. Ebisui, R. Waki, S. Matsuo, and T. Okada, "Control over the crystalline state of sapphire," *Adv. Mater.*, vol. 18, no. 11, pp. 1361–1364 (2006).
[3] A. Vailionis, E. G. Gamaly, V. Mizeikis, W. Yang, A. V. Rode, and S. Juodkazis, "Evidence of superdense aluminium synthesized by ultrafast microexplosion," *Nat. Commun.*, vol. 2, no. May, p. 445 (2011).

LM-3-1 (Invited)

Laser printing of plasmonic antennas

Yu. Kulchin[1], O. Vitrik[1], A. Kuchmizhak[1,2]

1- Institute of Automation and Control Processes, Far Eastern Branch, Russian Academy of Science, Vladivostok 690041, Russia
2- School of Natural Sciences, Far Eastern Federal University, 8 Sukhanova str., Vladivostok 690041, Russia

alex.iacp.dvo@mail.ru

Resonant plasmonic nanostructures made of noble metals possess pronounced tunable optical resonances in the UV-vis-IR range assosoated with coherent electron plasma oscilations, being a promising platform for advanced light-manipulating and biosensing devices, solar cells, etc. Meanwhile, the present top-down and bottom-up fabrication approaches including chemical syntesis, ion- or electron beam lithography usualy require several consecutive technological steps to produce such nanostructures, making their large-scale fabrication rather time-consuming and costly. Here, we report on controlable and reproducible printing of different functional plasmonic nanostructures – hollow symetry-breaking plasmonic nanovoids [1], isolasated plasmonic nanoring [2], nanorods and nanoring-nanorod ensembles [3] – utilizing direct laser-pulse ablation of a thin noble metal film covering glass or silicon substrate with single short (nanosecond) and ultrashot (femtosecond) pulses. First, direct irradiation of the thin silver and gold films on a glass substrate with a tightly focused femrosecond laser pulse was shown to produce hollow cupola-like nanovoids [1] through the fast melting, acoustic relaxation, deformation and recrystalization of the metal film. The main geometric dimentions of the nanovoids can be readily controled by applied pulse energy, while their geometric shape can be switch between conical and parabolic. The fabricated plasmonic nanostructures demonstrate tuneable size-dependent resonant light scattering in the visible spectral range. These color far-field scattering resonances were attributed to the optical excitation and interference of relevant surface plasmon modes in nanovoid shells, providing a corresponding near-field plasmon-mediated electromagnetic (EM) field enhancement, which was measured experimentally by means of dark-field (DF), photoluminescence (PL) and surface-enhanced Raman microspectroscopy (SERS).
Second, we have demonstrated for the first time that the use of direct single-shot exposure of the metal film by tightly focused nanosecond (ns) laser pulses, followed by slow polishing of the fabricated nanostructures by an accelerated argon ion (Ar^+) of isolated plasmonic nanorods, separated and merged nanorings, as well as more complex nanostructures [2,3]. Within this approach, the ns-laser irradiation of metal film changes its initial thickness through the initiation of fast melting and subsequent hydrodynamic processes, while the following Ar^+ polishing reveals the features of its hidden topography, producing LPR-supporting isolated plasmonic structures on a glass substrate. We experimentally demonstrate that both the shape and the lateral size of the resulting FPNs are determined by ns-laser pulse energy and metal film thickness, while the subsequent Ar+-ion polishing allows varying the height of the resulting nanostructures. Their plasmonic properties were examined by means of DF micro-spectroscopy, SERS and PL measurements and were modeled in the framework of finite-difference time-domain calculations of electromagnetic near-fields.
Finally, we have shown the double-shot technique [4] for femtosecond laser fabrication of an optical nanoantenna with an additional diffraction grating – first pulse can be used to produce main plasmonic nanoantenna of variable shape while the second spatially shifted one imprints radial plasmonic grating near the nanoantenna via constructive interference of the surface plasmon-polaritons with the laser pulse.

[1] A. Kuchmizhak, O. Vitrik, Yu. Kulchin, D. Storozhenko, A. Mayor, A. Mirochnik, S. Makarov, V. Milichko, S. Kudryashov, V. Zhakhovsky, N. Inogamov, Laser printing of resonant plasmonic nanovoids. Nanoscale, (2016). DOI: 10.1039/c6nr01317a
[2] A. A. Kuchmizhak, S.O. Gurbatov, Y.N. Kulchin, O.B.Vitrik, Plasmon mode excitation and photoluminescence enhancement on silver nanoring. Optics Communications, 356, 1-6, (2015).
[3] A. Kuchmizhak, S. Gurbatov, O. Vitrik, Y. Kulchin, V. Milichko, S. Makarov, S. Kudryashov, Ion-beam assisted laser fabrication of sensing plasmonic nanostructures. Scientific Reports, 6, 19410, (2016).
[4] A. Kuchmizhak, A. Ionin, S. Kudryashov, S. Makarov, A. Rudenko, Yu. Kulchin, T. Efimov, Flash-imprinting of intense femtosecond surface plasmons for advanced nanoantenna fabrication. Optics letters, 40(8), 1687-1690, (2015).

LM-3-2 (Invited)

Controlled manipulation and bending of gold nanorods with light

T. Lohmueller[1,2]

1- Photonics and Optoelectronics Group, Department of Physics and Center for NanoScience (CeNS), LMU München, Amalienstraße 54, Munich, 80799, Germany
2- Nanosystems Initiative Munich (NIM), Schellingstraße 4, 80539 Munich, Germany

Email: t.lohmueller@lmu.de

Gold nanorods can be molten and deformed upon irradiation with intense laser light, which allows to change and control their plasmonic properties in solution. Here, we particularly focus on the possibility to bend gold rods with light by a combination of plasmonic heating and optical force. Nanrods in water are irradiated with a laser at a wavelength resonant to their longitudinal plasmon mode. Above a certain laser power, the rods start to melt almost instantaneously as they enter the laser beam. Simultaneously, optical forces are pushing the particles in the direction of the propagating light, which renders it possible to pattern the particles one-by-one on the surface of an underlying substrate. I will show that both the bending angle and the orientation of the printed structures can be controlled by the laser power and polarization. Overall, this approach allows for synthesizing and patterning plasmonic nanoantennas with light on almost any substrate, which hold great potential for the fabrication of flat optics and metasurfaces.

Coupling Between Dielectric and Plasmonic Modes Through Evanescent Coupling for Nano-focusing Applications

Chuan Zhong, Brain David Jennings, Ertugrul Karademir, David McCloskey, John Doneagan*

1- School of Physics, Trinity College Dublin, Dublin 2, Ireland

2- CRANN and AMBER, Trinity College Dublin, Dublin 2, Ireland
Main author email address: zhongc@tcd.ie

Nano-focusing waveguides allows for reducing the cross sections of the propagating optical modes far beyond the diffraction limit. These elements allow for the focusing, guiding and controlling of light in the nanometre scale and have the potential to be applied in a heat assisted magnetic recording (HAMR) system to greatly increase hard drive recording density. A number of methods have been proposed for coupling of light into nano-focusing waveguides for the HAMR system. These include end-fire coupling [1], coupling with a metallic grating [2] and coupling through Yagi-Uda nanoantennas [3].
In this paper, we demonstrate a method using evanescent coupling between a single mode Si_3N_4 dielectric waveguide and a Au taper plasmonic waveguide. As shown in Fig. 1(a), a laser with a wavelength of 840 nm is coupled into a slab Si_3N_4 waveguide by end-fire coupling. Evanescent coupling between the Au and Si_3N_4 interface is used to couple the dielectric modes to plasmonic modes in the plasmonic tapers, the coupling efficiency can reach 50% under suitable momentum matching conditions. Fig. 1(b) show the SEM images of Au tapers with different length made by e-beam lithography. Fig.1 (c) shows the effective refractive index of the plasmonic modes and dielectric modes is 2.1893 and 1.6771 respectively as the thickness of the Si_3N_4 is 165nm. This huge index mismatch induce weak coupling efficiency between the plasmonic modes and dielectric modes which result in a weak enhancement. In this case, a SiO_2 layer with the thickness of 100 nm is needed to achieve an optimized coupling efficiency between these two modes as shown in Fig. 1(d) and the propagation length can reach around 20 μm in this structure.

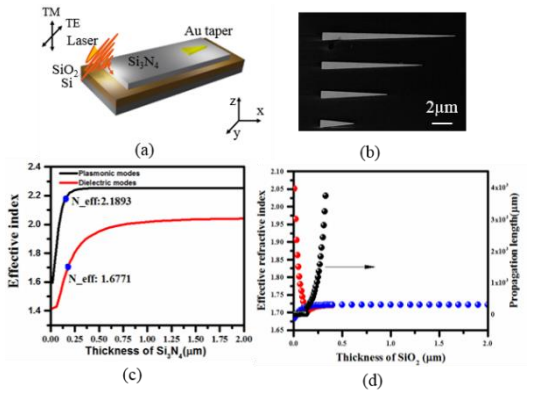

Fig. 1 (a) Schematic of evanescent coupling system. (b) SEM images of the Au tapers. (c) Effective refractive index of the dielectric and plasmonic modes as a function of the thickness of Si_3N_4. (d) Momentum match condition

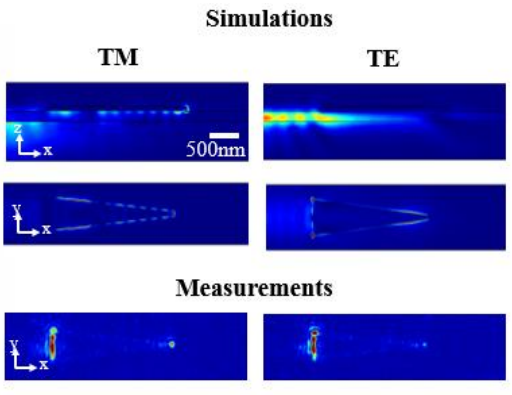

Fig.2 Simulated and experimental results of the taper with the length of 5 μm

The COMSOL simulations in Fig. 2 shows that an effective coupling can be achieved through evanescent coupling with high field enhancement. Far-field measurements show the surface plasmon waveguiding and focusing have been achieved in the tapered plasmonic waveguides. The E-field is mainly located at the interface of Si_3N_4 core and the Au with strong enhancement and high loss for TM modes, while the TE modes have a lower loss but weaker enhancement.

[1] B. C. Stipe, T. C. Strand, Magnetic recording at 1.5 Pb m^{-2} using an integrated plasmonic antenna Nature Photon., 4, 484-488, (2010).
[2] J. Lin, J. Dellinger, and F. Capasso Cosine-Gauss Plasmon Beam: A Localized Long-Range Nondiffracting Surface Wave, Phys. Rev. Lett. 109, 093904 (2012).
[3] Q. Gao, F. H. Ren, and A. X. Wang, Direct and efficient optical coupling into plasmonic integrated circuits, IEEE Photon. Tech. Lett. 28(11), (2016).

LM-3-4

Structural and electrical anisotropy of hydrogenated amorphous silicon films nanostructured by femtosecond laser pulses

D.V. Shuleiko[1], L.A. Golovan[1], S.V. Zabotnov[1], D.E. Presnov[2,1], A.G. Kazanskii[1], P.K. Kashkarov[1]

1- Faculty of Physics, Lomonosov Moscow State University, Leninskie Gory 1/2, Moscow 119991, Russia
2- Skobeltsyn Institute of Nuclear Physics, Lomonosov Moscow State University, Leninskie Gory 1/2, Moscow, 119991, Russia

E-mail: shuleyko.dmitriy@physics.msu.ru

Femtosecond laser pulses with high emission intensity and low photon energy can be used to achieve uniform nanostructuring and modification over the entire volume of siliceous films [1]. This nanostructuring method also leads to anisotropy of structural, electrical and optical properties of processed films. For example, surface periodic structures can be produced [2]. Femtosecond laser radiation also can be used to enhance light absorption and reduce Staebler-Wronski effect in amorphous hydrogenated silicon films (a-Si:H) for potential applications in photovoltaics.

In this paper, a-Si:H films irradiated by femtosecond laser pulses (1250 nm, 100 fs) were investigated. A surface profile with period equal to the laser spot diameter (150 mkm) was formed by means of laser beam movement in the raster mode (Figure 1,a). Scanning electron microscopy also revealed presence of one-dimensional periodic structure, perpendicular to polarization of the incident beam on the treated surface, with 0.36±0.03 or 1.11±0.05 μm period (Figure 1,b). This result is in agreement with the data of [3].

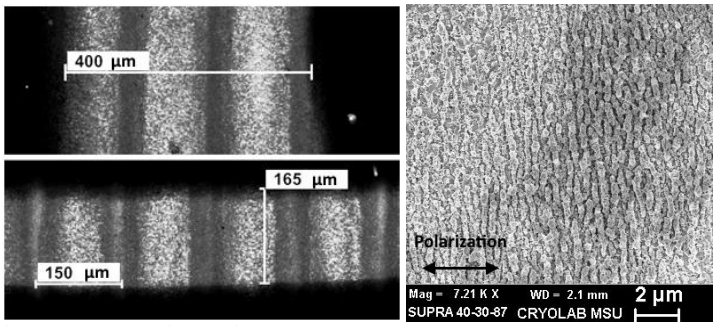

Figure 1. The images of processed a-Si:H film surface, obtained by optical microscopy (a), and scanning electron microscopy (b)

Electrical measurements have shown that the conductivity of a-Si:H film after irradiation with femtosecond laser pulses increased up to 3 orders of magnitude (Table 1) due to dehydrogenation and nanocrystallization of the film [4].

Table 1. Conductivity of a-Si:H film before and after femtosecond laser irradiation

Sample	Specific conductivity σ $(\Omega \cdot cm)^{-1}$
Processed area, the contacts are parallel to scan lines and surface periodic structures	$1{,}58 \cdot 10^{-6}$
Processed area, the contacts are perpendicular to scan lines and surface periodic structures	$4{,}48 \cdot 10^{-6}$
Amorphous silicon	$6{,}73 \cdot 10^{-9}$

The conductivity along the raster lines and periodic structures is almost threefold greater than in the perpendicular direction. A possible explanation of this effect may be given by non-uniform crystallization of amorphous silicon, and the electric field anisotropic depolarization inside the surface periodic structure.

This work was financially supported by the Russian Foundation for Basic Research (project 16-32-80066).

[1] A. V. Emelyanov, M. V. Khenkin, A. G. Kazanskii, et al., Femtosecond laser induced crystallization of hydrogenated amorphous silicon for photovoltaic applications, Thin Solid Films, 556, pp. 410–413, (2014).
[2] G.A. Martsinovsky, G.D. Shandybina, Yu.S. Dementeva et al., Surface electromagnetic wave excitation in semiconductors at femtosecond laser action, Semiconductors, 43, pp. 1339–1345, (2009).
[3] R. Drevinskas, M. Beresna, M. Gecevičius et al., Giant birefringence and dichroism induced by ultrafast laser pulses in hydrogenated amorphous silicon, Appl. Phys. Letters, 106, art. 171106 (2015).
[4] A.V. Emelyanov, A.G. Kazanskii, P.K. Kashkarov et al., Effect of the femtosecond laser treatment of hydrogenated amorphous silicon films on their structural, optical, and photoelectric properties, Semiconductors, 46, pp. 769–774, (2012).

LM-3-5

Nanostructuring of large surfaces of titanium oxide thin films by ultra-short laser beams

A.Talbi[1], C. Tchiffo-Tameko[1], P. Coddet[1], E. Millon[1], A.L. Thomann[1], A. Stolz[1], C. Boulmer-Leborgne[1], GM. O'Connor[2] and N. Semmar[1]

1- GREMI-UMR 7344-CNRS-University of Orleans, 14 rue d'Issoudun, BP6744, 45071 Orleans Cedex2, France
2- NCLA/Inspire Laboratories, School of Physics, National University of Ireland Galway, University Road, Galway, Ireland

abderazek.talbi@univ-orleans.fr

Titanium oxide (TiO_x) has attracted an extensive interest due to its many promising applications in areas ranging from photovoltaics and photocatalysis to photo-/electrochromics and sensors. Enormous efforts have been devoted to the research of TiO_x material in order to improve its properties. Recent progress in this field are focused on the synthesis of TiO_x nanomaterials, including nanoparticles, nanorods, nanowires, and nanotubes [1]. In this work, we aimed to investigate a new route of nanostructuring of large surfaces of TiO_x thin films (25×25 mm²) by ultra-short lasers. Different beams are utilized with varied pulse duration form picosecond to femtosecond and working wavelengths from UV to IR. With 100 fs, 266 nm laser beam, several kinds of LIPSS are formed: high spatial frequency LIPSS (HSFL) with period close to λ/2, low spatial frequency LIPSS (LSFL) with period close to λ and regular droplets (figure1) through self-organization mechanisms by the movement of the molten material forced by driven forces as thermal capillarity and Plateau-Rayleigh instability [2]. The formation of these nanostructures mainly controlled by two parameters: the laser beam fluence (F) and the number of pulses (N), will be discussed in this paper.

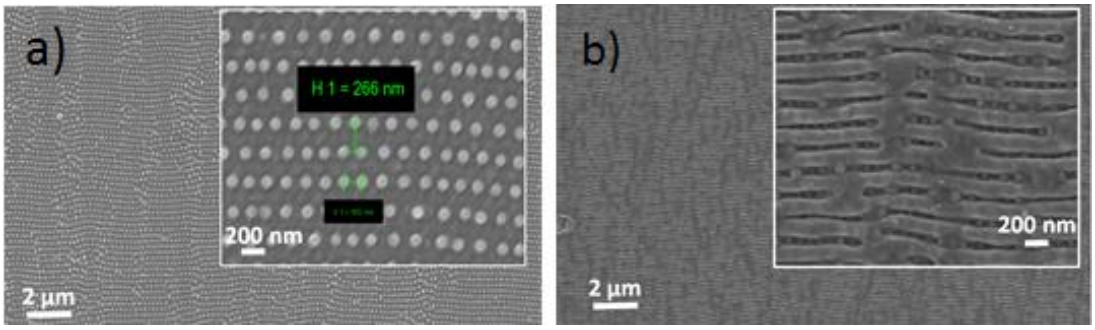

Figure 1. SEM views of larges nanostructured TiOx thin films (5×5 mm²) obtained by fs irradiation: a) regular droplets and b) LSFL organization

[1] Xiaobo Chen et al, Titanium Dioxide Nanomaterials: Synthesis, Properties, Modifications, and Applications. Chem. Rev. **2007,** 107, 2891-2959.
[2] Mindaugas Gedvilas et al, Driving forces for self-organization in thin metal films during their partial ablation with a cylindrically focused laser beam, AIP Conference Proceedings (2012), 1464,229

Role of Nanostructures on the Formation of LIPSS in Platinum Based Stainless Steel Alloys using Multi-Pulse Femtosecond Laser Structuring

G.M. O'Conner[1], C. McDaniel[1]

1- National Centre for Laser Applications, School of Physics, NUI Galway, Ireland

gerard.oconnor@nuigalway.ie

The onset of ripple formation is investigated on a platinum alloy surface for multiple pulses where the applied fluence is less than the single pulse damage threshold fluence. It is proposed that the initiation of Laser Induced Periodic Surface Structure (LIPSS) is a surface effect stimulated by nanostructures formed after the initial pulse. Multiple laser pulses of 500 fs pulse duration, delivered at a moderate (100kHz) repetition rate, and a laser wavelength of 515 nm and 1030 nm were used to generate the LIPSS on a Pt:SS surface with a of roughness value of 2.9 ± 0.2 nm. High-resolution Scanning Electron Microscopy (SEM) and Transmission Electron Microscopy are used to trace LIPSS formation following its initiation nanoparticle and nanopillar structures. The mechanism is interpreted to be due to local enhancement of electric field intensity. The hypothesis is supported using Finite Difference Time Domain (FDTD) simulations. It is proposed that the enhancement of the electric field due to the presence of nanostructures contributes to the sustained formation of the LIPSS structure with subsequent laser pulses.

LM-3-7

Single shot femtosecond laser sub-micron patterning of CVD graphene

A. Gil-Villalba, R. Meyer, L. Froehly, R. Salut, L. Rapp, L. Furfaro, R. Giust,
J.M. Dudley, and F. Courvoisier

Institut FEMTO-ST, UMR 6174 CNRS Université Bourgogne Franche-Comté,
25030 Besançon Cedex, France
E-mail: francois.courvoisier@femto-st.fr

Graphene is an important material for next-generation technologies, but the development of applications in the field of photonics and optoelectronics require micro and nanostructuring of the graphene films [1]. Femtosecond laser ablation is a promising technique because it can process large surfaces at extremely high speed and is easily reconfigurable.
Previous studies of fs-laser ablation of graphene in accumulative thermal regime (burning) have shown high accuracy (down to <100 nm) but it is a slow process [2]. Single shot femtosecond pulse ablation experiments were carried out on graphene but only at scales larger than typically 1 µm [3,4]. We have developed a novel technique to measure the ablation threshold and the ablation repeatability for single shot illumination of CVD graphene, that is size independent. Our technique is based on accurate comparison of a complex beam fluence pattern with the one of SEM image of the damaged graphene monolayer (fig. 1a-b).

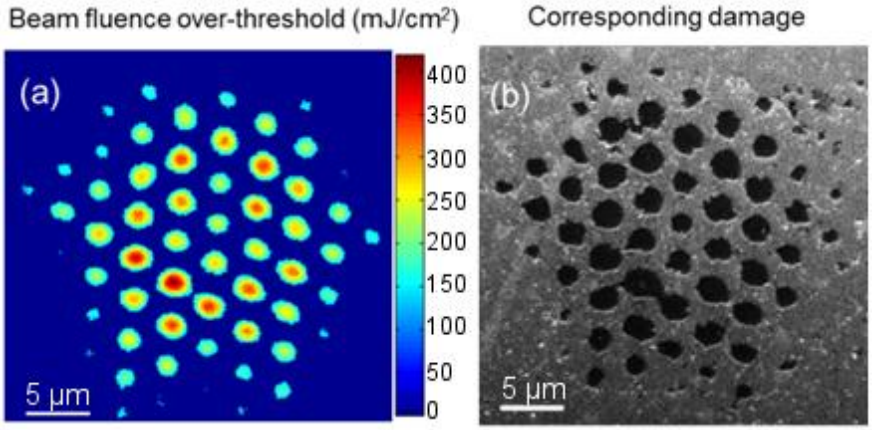

Fig 1. Comparison of fluence distribution over threshold (a) with the SEM image of the damage (b) for a given intensity distribution, pulse duration (130 fs), and input pulse energy (1.3 µJ).

We report a sudden drop of the ablation probability when the over-threshold diameter is below 1 µm. With non-diffracting Bessel beams, we have investigated the limits of nano-drilling with high-angle focusing. We show the diameter limit of ablated holes in CVD graphene using single shot ultrafast laser is approximately 550 nm for both quartz and fused silica substrates.
We also report a strong difference in ablation probability depending on the presence or absence of grain boundary in the vicinity of the illuminated zone, which can be a major constraint when patterning CVD graphene at sub-micron scale.
Our results can be explained by the high free-carrier diffusion in the graphene film and show the needs for more complex strategies for laser structuring of graphene at nanometric scale.

Acknowledgements: The authors acknowledge funding from Region Franche-Comte. This work has been performed in cooperation with the Labex ACTION program (contract ANR-11-LABX-01-01) and from the European Research Council (ERC) under the European Union's Horizon 2020 research and innovation programme (grant agreement No 682032-PULSAR). This work was partly supported by the French RENATECH network.

[1] F. Bonaccorso, Z. Sun, T. Hasan, and A.C. Ferrari, *Nature Photon.* **2010**, 4, 611
[2] R. J. Stohr, R. Kolesov, K. Xia, and J. Wrachtrup, ACS Nano. **2011**, 5, 5141.
[3] J-H.Yoo, J.B. In, J.P. Park, H. Jeon, and C.P. Grigoropoulos, App. Phys. Lett. **2012**, 100,233124.
[4] B. Wetzel, C. Xie, P.-A. Lacourt, J. M. Dudley, and F. Courvoisier, Appl. Phys. Lett. **2013**, 103, 241111.
[5] A. Gil-Villalba, C. Xie, R. Salut, L. Furfaro, R. Giust, M. Jacquot, P. A. Lacourt, J. M. Dudley, and F. Courvoisier, Appl. Phys. Lett. **2015**, 107, 061103

LM-3-8

Coating Alloys Properties of Laser Coating and Thermal Spray Processes

M. Atta Khedr[1], Sameh Akila[1], M. A. Hafez[1], Ali S. Khalil[2]

1- Department of Laser Sciences and Interaction National Institute of Laser Sciences, Cairo University, Giza, Egypt.

2- Institute of mineral Education, Tebin, Helwan, Cairo, Egypt
E mail: makdr@yahoo.com

In our experimental work we describe the difference of laser coating processes during laser surface metal treatment, laser coating processes in comparison with thermal plasma spraying. . High power Nd: YAG laser (1064 nm, 300 – 1600 Watt) has been used in laser coating as coating processes of Stainless Steel S. S. 304 surfaces by different alloys coating materials of ZrO_2- 5% CaO, ZrO_2- 18% to 25% MgO and mix from them. High power Laser for surface treatments, laser modification remitting layer of Ni-Al by lower power 300 W -800 watts on S.S. surface before Zr Composite Alloys coating by high power laser. Different measurements were carried out on the different coated surfaces which obtained by laser coating and plasma tourch arc sprays by measuring the wearing resistance and micro hardening tests, X – Ray diffraction, Scanning electron microscope for determining the morphology of the coating surfaces and film thickness. We reported that the thickness of coating is in the range values 200 t0 300 micrometers. The wear resistance and micro hardness efficiency are increased in laser coating further than plasma thermal spray. The crystalline size structural properties are much improvement in laser coating. That indicates that the bonding forces of crystal lattice are increased by laser coating than thermal spray processes. Laser transformation hardening involves rapid heating and is a novel coating process. Industrial application of laser coating became important branch of advanced laser technology in medical, Environmental applications and space.

LM-4-1 (Invited)

Ship-in-a-bottle integration of biomimetic architecture into lab-on-a-chip by femtosecond laser 3D processing: application to cancer research

Felix Sima[1,2], Dong Wu[2], Jian Xu[2], Katsumi Midorikawa[2], Koji Sugioka[2]

1- Laser Department, National Institute for Lasers, Plasma and Radiation Physics, Magurele, Ilfov, 00175, Romania
2- RIKEN-SIOM Joint Research Unit, RIKEN Center for Advanced Photonics, 2-1 Hirosawa, Wako, Saitama, 351-0198, Japan

Main author email address: felix.sima@inflpr.ro; ksugioka@riken.jp

Due to the high peak intensity which induces multiphoton absorption, ultrafast lasers are able to induce local modifications inside the transparent materials with high precision at micro- and nanoscale. Rapid prototyping technologies using ultrafast lasers for glass or polymer processing have been progressively developed for photonic devices and microfluidic biochip applications.
Herein, we evaluate the potential of developing a new technology by combining subtractive ultrafast laser assisted chemical etching (FLAE) of glasses and two photon polymerization (TPP) additive process [1,2]. This innovative hybrid approach will be described with emphasis on the fabrication of highly functional true 3D biochips.
More concretely, a "ship-in-a-bottle" fabrication concept is introduced in order to integrate 3D polymer structures by TPP inside (in volume) glass micro-channels developed by FLAE (Figure 1). The process allows lowering the size limit of 3D objects created inside channels to smaller details down to the dimensions of several µm or below, and improving the structure stability in the same time as it offers the required robustness for assembling a concrete lab-on-a-chip device.

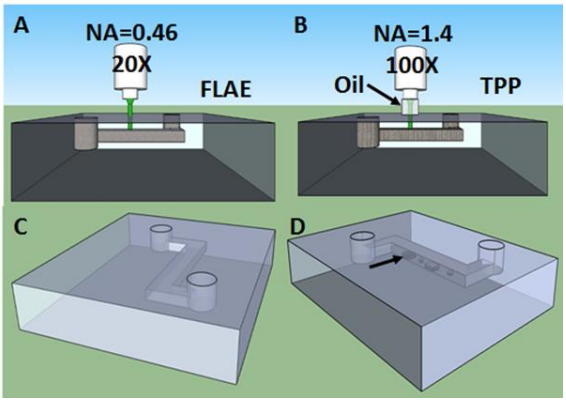

Fig. 1. Schematic of hybrid FLAE-TPP process for "ship-in-a- bottle" polymer integration: FLAE of Foturan glass (A); TPP of SU-8 photoresist inside microchannel (B); Z-shape microchannel fabricated by FLAE (C); Polymeric patterns (indicated by black arrow) developed by TPP inside glass microchannel (D).

Different polymeric geometries has been further proposed as biomimetic architectures [3]. Cancer cell migration was then evaluated by time lapse imagining carried out inside biochip during different time intervals. The cells were found responsive to chemo-gradient concentration created through 2 µm diameter channels of the 3D polymeric scaffold.

[1] D. Wu, S. Z. Wu, J. Xu, L. G. Niu, K. Midorikawa, and K. Sugioka, Hybrid femtosecond laser microfabrication to achieve true 3D glass/polymer composite biochips with multiscale features and high performance: the concept of ship in- a- bottle biochip, Laser & Photonics Reviews, 8(3), 458-467 (2014)
[2] D. Wu, J. Xu, L.-G. Niu, S.-Z. Wu, K. Midorikawa, and K. Sugioka, In-channel integration of designable microoptical devices using flat scaffold-supported femtosecond-laser microfabrication for coupling-free optofluidic cell counting, Light: Science & Applications, 4(1), e228 (2015)
[3] F. Sima, D. Wu, J. Xu, K. Midorikawa, K. Sugioka, Ship-in-a-bottle integratio'n by hybrid femtosecond laser technology for fabrication of true 3D biochips, Proc. SPIE 9350, (2015)

LM-4-2 (Invited)

Fabrication of microdevices using femtosecond laser reductive sintering of metal oxide nano particles

M. Mizoshiri[1], S. Hata[1]

1- Department of Micro-Nano Systems Engineering, Graduate School of Engineering, Nagoya University, Furo-cho, Chikusa, Nagoya, 464-8603, Japan

mizoshiri@mech.nagoya-u.ac.jp

Direct-writing of metal micropatterns has received attention as printed electronics and 3D additive manufacturing techniques. Laser reductive sintering of metal oxide nanoparticles (NPs) is a powerful tool because metal micropatterns enable to be formed in the ambient atmosphere [1]. We have also studied direct-writing using femtosecond laser reductive sintering of CuO NPs. Cu-rich and Cu_2O-rich micropatterns were selectively formed by controlling the laser irradiation conditions such as laser scanning speed and pulse energy [2]. Cu/Cu_2O composite microtemperature sensors were fabricated on a glass substrate using this technique. In this presentation, we introduce the direct-writing technique using femtosecond laser reductive sintering and demonstrate the fabrication of microdevices such as microtemperature sensors and microbridge heaters.

CuO NP solution which included CuO NPs (<50 nm), a dispersant of polyvinylpyrrolidone, and a reductant agent such as ethylene glycol and 2-plopanol was prepared. The materials were mixed using ultrasonic waves. The CuO NP solution was coated on a glass substrate using a spin-coater or a dispenser. Femtosecond fiber laser systems (Toptica, FemtoFiber pro NIP) operating wavelength of 780 nm, pulse duration of 120 fs, and repetition frequency of 80 MHz was used for reductive sintering. Finally, non-irradiated CuO NPs were removed using ethylene glycol and ethanol.

We demonstrated the fabrication of a Cu/Cu_2O composite microtemperature sensor. Cu- and Cu_2O-rich micropatterns, which were selectively formed at laser scanning speed of 15 mm/s and 1 mm/s, and the pulse energy of 0.45 nJ and 0.54 nJ, respectively, exhibited metal-like and semiconductor-like temperature dependence of their resistance. Cu-rich electrodes and Cu_2O-rich temperature detector were directly written by controlling the laser irradiation conditions. Figure 1 shows the temperature dependence of the Cu/Cu_2O composite microtemperature resistance. The negative value of the temperature coefficient of the resistance was consistent with that of Cu_2O-rich micropatterns. The high temperature sensitivity is effective for application of the temperature sensor.

This technique was applied to fabricating 3D microstructures by laminating the 2D micropatterns. CuO NP solution was laminated using a dispenser. Figures 2(a) and 2(b) show an optical microscope and SEM images of a microbridge heater. It was composed of the 1st-3rd layer-electrodes and the 4th layer microbridge. Only the microbridge was heated by applying voltage of 18 V. This direct-writing technique using femtosecond laser reductive sintering is useful to fabricate microdevices with composite materials.

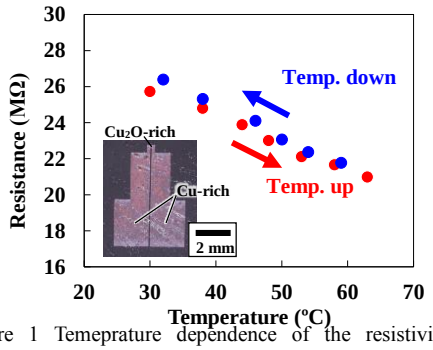

Figure 1 Temeprature dependence of the resistivity of Cu/Cu_2O composite microtemperature sensor.

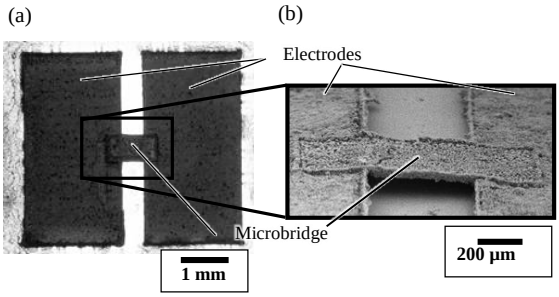

Figure 2 (a) Optical microscope and (b) SEM images of the microbridge heater.

[1] B. Kang, S. Han, J. Kim, S. Ko, M. Yang, One-Step Fabrication of Copper Electrode by Laser-Induced Direct Local Reduction and Agglomeration of Copper Oxide Nanoparticle, The Journal of Physical Chemistry, C115, pp.23664-23670, (2011).
[2] M. Mizoshiri, Y. Ito S. Arakane, J. Sakurai, S. Hata, Direct fabrication of Cu/Cu_2O composite micro-temperature sensor using femtosecond laser reduction patterning, Japanese Journal of Applied Physics, 55, art.no. 06GP05, (2016).

LM-4-3 (Invited)

Laser Beam Propagation

Colin J. R. Sheppard

Department of Nanophysics, Istituto Italiano di Tecnologia, Genova 16163, Italy

The fundamental beam of paraxial optics is the Hermite-Gaussian (HG) (or Laguerre-Gaussian (LG) beam for cylindrical coordinates). The traditional HG or LG beams can be generalized to an arbitrary scaling parameter between the Hermite polynomial and the Gaussian [1], of which the 'elegant HG beam' of Siegman is a particular case [2]. These generalized beams can be further generalized by taking the order of the Laguerre polynomial as complex [3], which are equivalent to the hypergeometric beams, based on confluent hypergeometric functions [4-6].

Paraxial Gaussian beams can be generalized to the non-paraxial domain using the complex source point approach [7-10].

Elegant LG beams of high order tend towards Bessel-Gauss beams [11-13]. Based on the principle of duality, the amplitude given by the product of a Bessel function and a Gaussian can be situated in either the waist or the far field [3].

In propagation of ultra-short pulsed beams, the different spectral components diffract accordingly, and hence the beam behaviour depends on the spatial dependence of the spectrum [14]. For the simplest case of a pulsed Bessel beam we can consider different special cases, including the X-wave and the focus wave mode (FWM) [15-19]. For Gaussian beams, the analogy of the FWM is the isodiffracting beam [20].

[1] R. Pratesi and L. Ronchi, "Generalized Gaussian beams in free space," J. Opt. Soc. Am. **67**, 1274-1276 (1977).
[2] A. E. Siegman, "Hermite-Gaussian functions of complex arguments as optical-beam eigenfunctions," J. Opt. Soc. Am. **63**, 1093-1094 (1973).
[3] C. J. R. Sheppard, "Beam duality, with application to generalized Bessel-Gaussian, and Hermite- and Laguerre-Gaussian beams," Optics Express **17**, 3690-3697 (2009).
[4] M. A. Bandres and J. C. Gutierrez-Vega, "Circular beams," Opt. Lett. **33**, 177-179 (2008).
[5] V. V. Kotlyar, R. V. Skidanov, S. N. Khonina, and V. A. Soifer, "Hypergeometric modes," Opt. Lett. **32**, 742-744 (2007).
[6] E. Karimi, G. Zito, B. Piccirillo, L. Marrucci, and E. Santamato, "Hypergeometric-Gaussian beams," Opt. Lett. **32**, 3053-3055 (2007).
[7] G. A. Deschamps, "Gaussian beam as a bundle of complex rays," Electronics Letters **7**, 684-685 (1971).
[8] C. J. R. Sheppard and S. Saghafi, "Beam modes beyond the paraxial approximation: A scalar treatment," Physical Review A **57**, 2971-2979 (1998).
[9] C. J. R. Sheppard and S. Saghafi, "Electromagnetic Gausssian beams beyond the paraxial approximation," J. Opt. Soc. Am. A **16**, 1381-1386 (1999).
[10] C. J. R. Sheppard and S. Saghafi, "Transverse-electric and transverse-magnetic beam modes beyond the paraxial approximation," Optics Letters **24**, 1543-1545 (1999).
[11] C. J. R. Sheppard and T. Wilson, "Gaussian-beam theory of lenses with annular aperture," IEE J. Microwaves, Optics and Acoustics **2**, 105-112 (1978).
[12] S. Saghafi and C. J. R. Sheppard, "Near field and far field of elegant Hermite-Gaussian and Laguerre-Gaussian modes," J. mod. Optics **45**, 1999-2009 (1998).
[13] M. Porras, R. Borghi, and M. Santarsiero, "Relationship between elegant Laguerre-Gauss and Bessel-Gauss beams," J. Opt. Soc. Am. A **18**, 177-184 (2001).
[14] C. J. R. Sheppard and X. Gan, "Free-space propagation of femto-second light pulses," Optics Communications **133**, 1-6 (1997).
[15] J. Lu and J. F. Greenleaf, "Nondiffracting X waves: exact solutions to free-space scalar wave equations and their finite aperture realizations," IEEE Trans. Ultrasonics, Ferroelectrics and Frequency Control **39**, 19-31 (1992).
[16] J. N. Brittingham, "Focus wave modes in homogeneous Maxwell's equations: Transverse electric mode," J. Appl. Phys. **54**, 1179-1189 (1983).
[17] C. J. R. Sheppard, "Bessel pulse beams and focus wave modes," Journal of the Optical Society of America A **18**, 2594-2600 (2001).
[18] C. J. R. Sheppard and M. D. Sharma, "Spatial frequency content of ultrashort pulsed beams," J. Optics A: Pure and Applied Optics **4**, 549-552 (2002).
[19] C. J. R. Sheppard, "Generalized Bessel pulse beams," J. Opt. Soc. Am. A **19**, 2218-2222 (2002).
[20] S. Feng and H. G. Winful, "Spatiotemporal transformation of isodiffracting ultrashort pulses by nondispersive quadratic phase media," J. Opt. Soc. Am. A **16**, 2500-2509 (1999).

LM-4-4 (Invited)

Advances in laser direct writing of carbon materials for flexible micro-device fabrication

Alexandra Palla Papavlu[1,2], Mihaela Filipescu[1], Thomas Lippert[2], Alexander Wokaum[2], Maria Dinescu[1]

1) Lasers Department, National Institute for Lasers, Plasma and Radiation Physics, 077125 Magurele, Romania
2) Energy and Environment Research Department, Paul Scherrer Institute, 5232 Villigen PSI, Switzerland

E-mail: dinescum@nipne.ro

Nano-sized materials such as carbon nanotubes (CNT) and hybrid CNT i.e. decorated with nanoparticles, due to their unique mechanical and electrical properties, have immediate applications as building blocks for high-performance flexible/transparent electronics. For many applications within the microelectronics field, the challenge is now downsizing the devices, and integrating them onto large-area, flexible and low cost substrates.
In this work, the direct writing of CNT and hybrid CNT materials onto nonconventional substrates, i.e. paper, plastics, tapes, glass, poly(dimethylsiloxane) (PDMS), Al foil, and ultrathin polymer substrates is reported. The direct writing technique is based on laser-induced forward transfer (LIFT), a simple process where a laser beam is focused through a transparent substrate onto a material film to be transferred. Every single pulse promotes the transfer of the thin film material onto a substrate that is usually placed parallel and facing the thin film at very short distances. With LIFT, CNT and hybrid CNT materials are transferred, with a transfer yield of nearly 100%, to fabricate electronic devices. The chemical sensors and thin film transistors maintain their original geometries and electronic properties with high fidelity. For example, the performance, i.e. the sensitivity, resolution, and response time of the laser-printed sensor devices was evaluated by exposure of the sensors to different toxic vapors. Different sensitivities and selectivity to the selected analytes i.e. acetone, ethanol, ammonia, etc. have been measured thus proving the feasibility of LIFT for applications in sensing devices.

Acknowledgements
This work was supported by a grant of the Romanian National Authority for Scientific Research and Innovation, CNCS – UEFISCDI, project number PN-II-RU-TE-2014-4-2311 and a grant from the Commission for Technology and Innovation CTI (project no. 16713.1 PFNM-NM).

LM-4-5

Fabrication of a silicon Fresnel lens for THz range by femtosecond laser ablation

M.S.Komlenok[1, 2], B.O. Volodkin[3], B.A. Knyazev[4, 5], T.V. Kononenko[1, 2], V.I. Konov[1, 2], V.S. Pavelyev[3, 6], V.A. Soifer[3, 6], K.N. Tukmakov[3], Yu.Yu. Choporova[4, 5]

1- A.M. Prokhorov General Physics Institute RAS, 38, Vavilov str., 119991, Moscow, Russian Federation
2- National Research Nuclear University MEPhI (Moscow Engineering Physics Institute), 31, Kashirskoye shosse, 115409, Moscow, Russian Federation
3- Samara University, 34, Moskovskoe shosse, Samara, 443086, Russian Federation
4- Budker Institute of Nuclear Physics SB RAS, 11, akademika Lavrentieva prospect, Novosibirsk, 630090, Russian Federation
5- Novosibirsk State University, 2, akademika Pirogova prospect, Novosibirsk, 630090, Russian Federation
6- Image Processing Systems Institute of the Russian Academy of Sciences, 151, Molodogvardejskaya st., Samara, 443001, Russian Federation

Appearance of the sources of coherent and high power THz radiation [1] has opened new horizons for investigations in this frequency range [2]. Increasing attention is focused on silicon diffractive optical elements (DOE), which are used for the beam manipulation [3, 4]. The common way to form a surface relief is the lithographic etching of a silicon substrate [5, 6]. However the main limitation of this approach is a possibility to form the multilevel DOE, which is more effective than binary one. Here we report on a new method for the microfabrication of silicon diffractive multilevel (4) Fresnel lens for terahertz range based on laser ablation [7]. For this purpose, a high repetition (f = 200 kHz) femtosecond Yb:YAG laser was used. Obtained diffraction optical element was tested in the beam of Novosibirsk Free Electron Laser at the wavelength of 141 μm. The measured diffractive efficiency of the lens is in good agreement with numerical calculations. Specific features and perspectives of the DOE fabrication by short pulsed laser ablation at high repetition rate will be discussed.

This work was supported by the Competitiveness Programm of NRNU MEPhI

[1] B.A Knyazev, G.N. Kulipanov, N.A. Vinokurov, Novosibirsk terahertz free electron laser: instrumentation development and experimental achievements, Measurement Science and Technology, 21 (5), 054017, pp. 1-13 (2010)
[2] G.N. Kulipanov, E.G. Bagryanskaya, E.N. Chesnokov, Yu.Yu. Choporova,V.V. Gerasimov, Ya.V. Getmanov, S.L. Kiselev, B.A. Knyazev, V.V. Kubarev,S.E. Peltek, V.M. Popik, T.V. Salikova, M.A. Scheglov, S.S. Seredniakov, O.A. Shevchenko, A.N. Skrinsky, S.L. Veber, N.A. Vinokurov, Novosibirsk Free Electron Laser—Facility Description and Recent Experiments, IEEE Transactions on Terahertz Science and Technology 5.5 pp. 798-809 (2015)
[3] A.N. Agafonov, B.O. Volodkin, D.G. Kachalov, B.A. Knyazev, G.I. Kropotov, K.N. Tukmakov, V.S. Pavelyev, D.I. Tsypishka, Yu.Yu. Choporova, A.K. Kaveev, Focusing of Novosibirsk Free Electron Laser (NovoFEL) radiation into paraxial segment, JOURNAL OF MODERN OPTICS, 63, 11,pp. 1051-1054 (2016)
[4] B.O. Volodkin, Yu.Yu. Choporova, B.A. Knyazev, G.N. Kulipanov, V.S. Pavelyev, V.A. Soifer, N.A. Vinokurov, Fabrication and characterization of diffractive phase plates for forming high-power terahertz vortex beams using free electron laser radiation, Optical and Quantum Electronics 48, 4, pp. 1-9 (2016)
[5] A.N. Agafonov, B.O. Volodkin, A.K. Kaveev, B.A. Knyazev, G.I. Kropotov, V.S. Pavel'ev, V.A. Soifer, K.N. Tukmakov, E.V. Tsygankova, Yu.Yu. Choporova, Silicon diffractive optical elements for high-power monochromatic terahertz radiation, Optoelectronics, Instrumentation and Data Processing, 49, pp. 189-195 (2013)
[6] A.N. Agafonov, Yu.Yu. Choporova, A.V. Kaveev, B.A. Knyazev, G.I. Kropotov, V.S. Pavelyev, K.N. Tukmakov, B.O. Volodkin, Control of transverse mode spectrum of Novosibirsk free electron laser radiation, Applied Optics, 54, 12,pp. 3635-3639 (2015)
[7] B.O. Volodkin, B.A. Knyazev, V.V. Kononenko, T.V. Kononenko, V.I. Konov, V.S. Pavelyev, V.A. Soifer, K.N. Tukmakov, Yu.Yu. Choporova, Fabrication of a multilevel THz Fresnel lens by femtosecond laser ablation, Quantum Electronics, 45, 10, pp. 933 –936 (2015)

Atomic Force Microscopy Study of Selective Laser Patterning of Indium Tin Oxide Thin Films

N. Farid[1], G.M. O'Conner[1], H. Chan[2], D. Milne[2], P. Rumbsy[2]
1- National Centre for Laser Applications, School of Physics, NUI Galway, Ireland
2- M-Solv Ltd, Oxford United Kingdom

nazar.farid@nuigalway.ie

The ablation properties of ultra-thin (20 nm) and thin (150 nm) Indium Tin Oxide (ITO) thin films, sputtered on glass substrates, is reported for femtosecond (fs) and picoseconds (ps), laser pulses. The effect of parameters such as wavelength, pulse duration, spot radius and laser spot overlap on the film removal properties is reported. An ablative removal mechanism was observed for all wavelengths at both femtosecond and picoseconds time-scales is proposed. Threshold fluence experiments were carried out using both focussed and tilted plane tests. The absorbed threshold fluence values were determined to be 12.5 $mJcm^{-2}$ at 343 nm, 9.68 $mJcm^{-2}$ at 515 nm, and 7.50 $mJcm^{-2}$ at 1030 nm for femtosecond and 9.14 Jcm^{-2} at 1030 nm for picosecond laser exposure. The absorbed threshold fluence was found to be dependent on the applied photon energy. Surface analysis of ablated craters using atomic force microscopy confirms that the selective removal of the film from the glass substrate is dependent on the applied fluence. Film removal is shown to be primarily through ultrafast lattice deformation. The laser absorption and heating process was simulated using a two temperature model (TTM). The interplay between melt driven and ablative processes for selective patterning will be specifically described for picosecond processing using highly overlapped pulses.

LM-4-7

Second harmonic generation in isotropic chiral medium by heterogeneously polarized light pulses

K.S. Grigoriev[1,2], V.A. Makarov[1,2], N.Yu. Kuznetsov[1]

1- Faculty of Physics, Lomonosov Moscow State University, Moscow, Russia
2- International Laser Center, Lomonosov Moscow State University, Moscow, Russia

ksgrigoriev@ilc.edu.ru

Second harmonic (SH) generation is traditionally considered forbidden in centrosymmetric media, however a series of experimental research of the last two decades confirms the appearance of the bulk-generated signal generation at doubled frequency in such media [1, 2]. Several possible mechanism explaining the SH appearance are known today. These include non-locality of the nonlinear optical response of the medium [3], degenerate five-wave [1] and six-wave [4] mixing processes, spatial inhomogeneity of the fundamental field [5] etc.

In the present work it is analytically shown that the appearance of SH signal in the bulk of isotropic chiral medium can be related with the non-locality or frequency dispersion of quadratic medium response in case of certain restrictions on spatial and temporal polarization distributions of the fundamental pulse. The research were carried out within negligible pump depletion approximation, parabolic approximation of diffraction theory and frequency dispersion was taken into account up to the second order. In the case of spatial non-locality of medium quadratic response to generate the SH pulse it is necessary for the fundamental beam to be inhomogeneously polarized in its cross-sections. The polarization distribution in the SH signal is, however, not so inhomogeneous as that in the fundamental pulse. It was also analytically shown that in the case of spatially local, but frequency-dependent quadratic response of the medium the effective second harmonic generation can be achieved by using the fundamental pulse that is heterogeneously polarized in both space and time. The example of such pulse can be a sequence of two pulses that are homogeneously polarized in time but have different polarisation states and the time delay between them should not exceed the length of each pulse. As in the case of the media with non-local quadratic response, the polarization state of the signal pulse at doubled frequency is more homogeneous in space and time compared to the fundamental pulse (fig. 1).

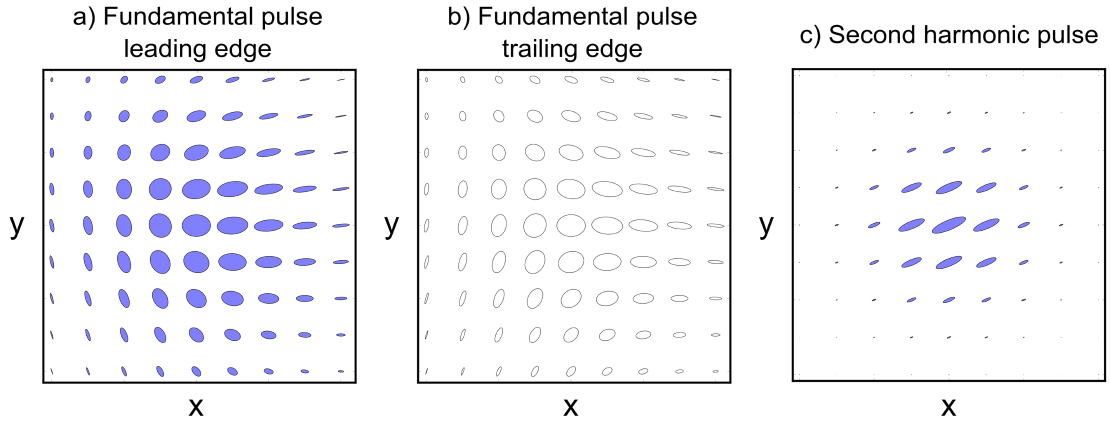

Fig. 1. Transversal polarization distribution in fundamental pulse leading edge (a) and trailing edge (b). The polarization distribution in transversal cross-section of the SH beam is homogeneous in time (c). Filled ellipses are left-hand polarized and empty ellipses are right-hand.

[1] A. V. Balakin, N. I. Koroteev, A. V. Pakulev, A. P. Shkurinov, D. Boucher, P. Masselin, E. Fertein, Experimental observation of the interference of three-and five-wave mixing processes in optical second harmonic generation in a solution of bacteriorhodopsin, JETP Letters, 64, pp. 718-723
[2] A.Savoia, M. Siano, D. Paparo, L. Marrucci, Nonlocal optical second harmonic generation from centrosymmetric birefringent crystals: the case of muscovite mica, J. Opt. Soc.Am., 28, pp. 679–688, (2011)
[3] N.I Koroteev1, V.A Makarov, S.N Volkov, Second-harmonic generation in the bulk of a chiral liquid by a focused laser beam, Opt. Comm., 157, pp. 111-114 (1998)
[4] M. M. Coles, M. D. Williams, D. L. Andrews, Second harmonic generation in isotropic media: six-wave mixing of optical vortices, Opt. Express, 21, pp. 12783-12789 (2011)
[5] A. B. Kozlov, A. V. Andreev, The influence of the spatial inhomogeneity of the field on the nonlinear-optical response of an atom, Quant. Electron. 30, pp. 979-985 (2000)

LM-4-8

GENERATION OF MAGNETO-ACOUSTIC WAVES BY LASER-PLASMA INTERACTION

Karima Annou and Djamila Bennaceur-Doumaz.

Centre de développement des technologies avancées, BP 17, Baba Hassen 16303, Algiers, Algeria.

kannou@cdta.dz

The oblique propagation of ion acoustic waves in magnetized plasma consisting of cold ions and superthermal electrons with kappa distribution is addressed. The combined effects of the external magnetic field, obliqueness (i.e., the propagation angle), and the kappa-electrons, which are found to significantly modify the basic properties of IAW, has been explicitly examined. Using reductive perturbation theory, we have derived a K-dV equation, and its corresponding solitary wave solution. It is pointed out that the superthermality parameter kappa plays a predominant and crucial role in determining the potential polarity of the solitary waves. It is also shown that the properties of solitons are influenced significantly by the plasma parameters. We point out that the results of the present work should also be helpful to explain the basic features of localized electrostatic disturbance in the laboratory, astrophysical and space plasmas, such as laser-plasma interaction, pulsar magnetosphere, the auroral zone and the upper ionosphere, where superthermal plasmas are often present.

Keywords: Nonlinear waves in plasma; Shamel-kappa distribution; Laser-created plasma; Perturbation method.

Effect of Electron spectral indices κ

Figure 1 shows how the amplitude varies with the electron spectral index κ when the angle between the direction of propagation and the magnetic field and the ion cyclotron frequency ($\theta = 10°,\ \omega_{ci} = 0.3$) are held constant.

Effect of angle of propagation θ

Figure 2 depict the effect of the propagation angle θ on compressive and rarefactive solitary waves with fixed plasma parameters, $\kappa = 1.6,\ \omega_{ci} = 0.1$, (for positive potential) and $\kappa = 7,\ \omega_{ci} = 0.1\ and\ M = 1.50$, (for negative potential). It is seen that the angle θ changes slightly the width of the rarefactive waves (negatives solitary structures) while it has no real

effect on their amplitude. By cons, the amplitude and width of compressive waves increase significantly with θ.

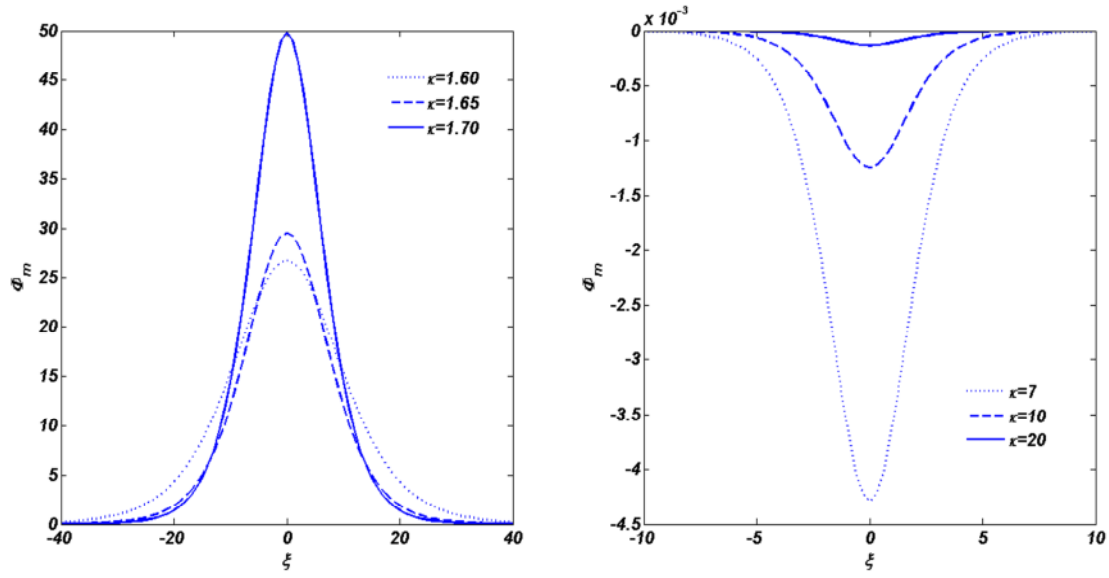

Figure 1. Variation of the solitary wave solution for different Values of κ for $\theta = 10°, \omega_{pi} = 0.3 and\ M = 1.5.$

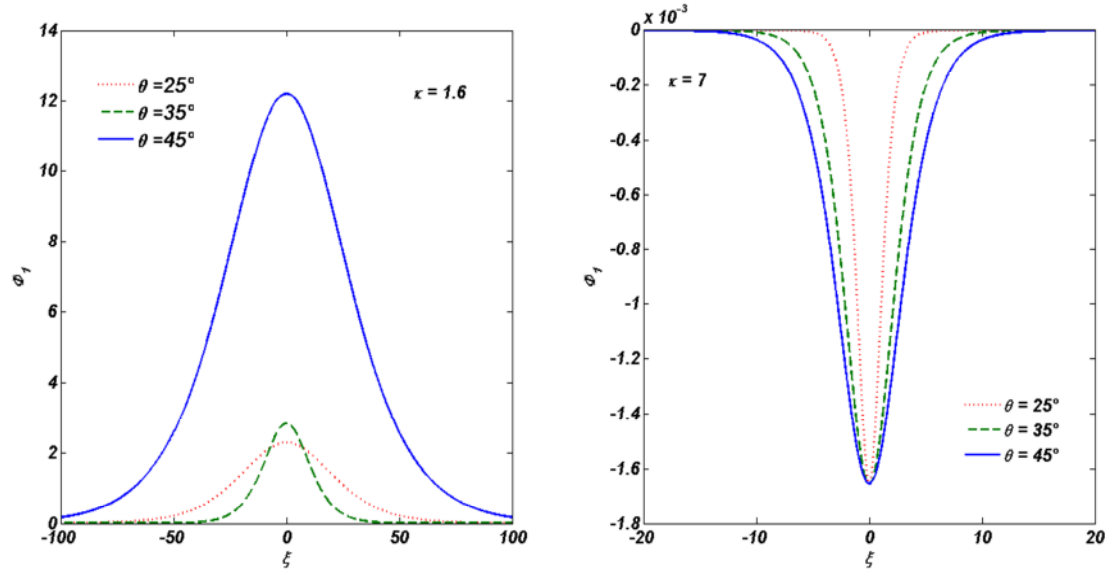

Figure 2. Variation of the solitary wave solution for different Values of θ for $\omega_{pi} = 0.3$, $M = 1.5\ and\ \kappa = 1.6\ for\ positive\ potential\ and \kappa = 7\ \ for\ negative\ potential.$

Laser-Induced MicroPlasma as a tool for transparent materials modification and structuring

V. Veiko, A. Samokhvalov, R. Zakoldaev, M. Sergeev, K. Milyaev
ITMO University, Kronverkskiy Pr. 49, St. Petersburg 197101, Russia
**email address: vadim.veiko@mail.ru*

A few methods for glass structuring are known, where the glass plate contact (direct or indirect) with highly absorb surface (LIPAA, LIBWE, LIBDE etc.) [1-4]. Most of these method based on action of microplasma induced in the interface of glass and absorbing target (so called confinement regime).

We investigated the special mode of these methods called ALIMP (action of laser-induced microplasma), where the graphite plate is placed in the direct contact with the back of the glass surface (Fig. 1 a). Controlled microstructuring of the glass occurs during the laser scanning in contact glass-graphite. The size-shape factor of the future relief highly depends on the characteristic of plasma occurred during the ablation of graphite target.

The ablation of graphite target is obtained by action of laser pulses (λ=1,06 μm, τ=200 ns, E=1 mJ). To investigate mechanism of ALIMP method, we utilized optoacoustic method in the following way: ultrasonic transducer fix on the backside of graphite target to register the amplitude of acoustic signal appeared during the ablation process. As a result of the experiment, the ablation pressure (in case graphite target covered by glass) raise by 5 times in comparison with the ablation at normal atmosphere (Fig. 1 b).

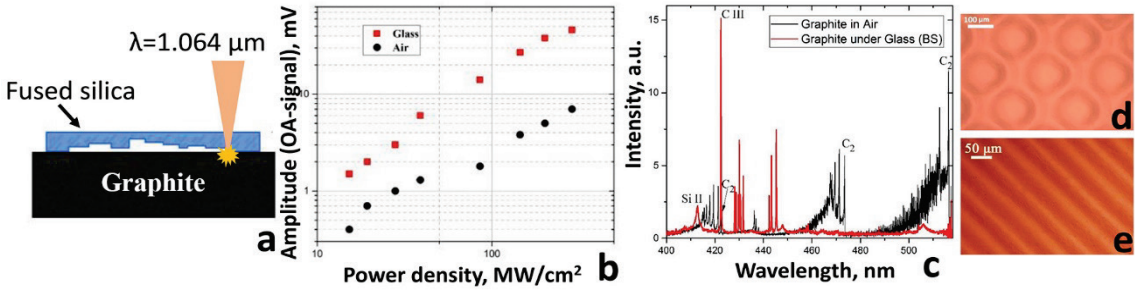

Figure 1 ALIMP method: schematic view of experimental setup (a), the amplitude of acoustic signal at different power density (b), emission spectra of laser plasma (c); formed optical elements: microlens array (d) and phase grating (e).

Besides, we investigated the emission spectra of laser plasma. Some features have been revealed in the confinement regime: ions of CIII, Si II appear in plasma spectra and Swan band C2 (Δν=0,+1,-1) is absence but the last one occurs during graphite ablation at normal atmosphere without covering (Fig. 1 c).The geometry of the relief formed by one pulse defines by the properties of plasma. Thus, the depth and volume of the crater linearly increase at laser power density increasing in the range of 10^7-10^8 W/cm^2. That is quite good correlate with the optoacoustical signal dependence on the power density.

Laser-induced method ALIMP described here gives opportunities for fast and cost-effective microoptical components fabrication on glass surface (microlens array, phase plates or gratings) [5, 6].

Experimental studies have been supported by the grant from leading universities of the RF (subsidy 074-U01) and the RSF agreement № 14-12-00351.

[1] J. Zhang, K. Sugioka, K. Midorikawa, High-speed machining of glass materials by laser-induced plasma-assisted ablation using a 532-nm laser, Applied Physics A, vol. 67 (4), pp. 499-501, (1998).
[2] I.V. Blonsky, A.Y. Danko, V.N. Kadan et al., Influence of the transverse dimension of the torch laser-induced plasma in the material handling processes, Technical Physics, vol. 75(3), pp. 74-80, (2005) - in Russian.
[3] Hopp, B., Cs. Vass, T. Smausz, et al., Production of submicrometre fused silica gratings using laser-induced backside dry etching technique, Journal of Physics D: Applied Physics, vol. **39**(22), pp. 4843-4847 (2006).
[4] J. Wang, H. Niino, A. Yabe, Micromachining of quartz crystal with excimer lasers by laser-induced backside wet etching, Applied physics A, vol. **69** (1), pp. S271-S273 (1999).
[5] G.K. Kostyuk, R.A. Zakoldaev, M.M. Sergeev, et al., Microlens array fabrication on fused silica influenced by NIR laser, Applied Physics B, vol. 122(4), pp. 1-8 (2016).
[6] G.K. Kostyuk, R.A. Zakoldaev, M.M. Sergeev, et al., Laser-induced glass surface structuring by LIBBH technology, Optical and Quantum Electronics, vol. 48(4), pp. 1-8, (2016).

LM-5-2 (Invited)

Laser-induced semiconductor cluster structures on the solid surface; new physical principles to construct the hybrid elements for photonics

S.M. Arakelian, S.V. Kutrovskaya, D.S. Nogtev, A.V. Osipov, A.A. Antipov
A.O. Kucherik, V.I. Emel'yanov*, T. Vartanyan, S. Zimin*****

Stoletovs Vladimir State University, Vladimir, Russia
**Lomonosov Moscow State University, Moscow, Russia*
***Saint-Petersburg National Research University of Information Technologies, Mechanics and Optics, Saint-Petersburg, Russia*
****Demidov Yaroslavl State University, Yaroslavl, Russia*

E-mail: arak@vlsu.ru

Three classes of the study fields are under our consideration: (1) laser-induced surface and thin films nanostructures with controlled topology (background and principal items); (2) optical characteristics of induced nanostructures (for photonic devices fabrication); (3) the quantum states verification in cluster structures; jump electroconductivity and possible mechanisms in nanocluster systems (experiment and theoretical discussion).

In experimental aspect, the laser synthesis technique to produce the nanoparticles (NPs) of different composition [1] in both semiconductor samples (PbTe) and bimetallic film (Au-Ag) [2] is presented by two laser ablation methods consequently: direct laser modification of thin films and laser evaporation of substance from target in liquid to produce the colloidal systems and subsequent deposition of particles from colloidal system on solid substrate (glass). Under a cw-laser radiation a bimodal distribution on PbTe particle size takes place [3]. For such laser-induced nanostructures we demonstrated the superconductivity tendency to increase the electrical conductivity by several times for our case at room temperature in comparison with a homogenous monolithic sample. By drop deposition technique it has been obtained the Au-Ag structures with various topology, and the nanoparticles become quantum dots under some conditions. In the case transmission optical properties are modified in the required manner. Such structures with controlled the optical and electro-physical properties are very principal to construct the elements and devices of optoelectronics and photonics in hybrid circuits on new physical principles.

This study was performed within the design part of a government contract for research work with VlSU #16.440.2014/K and RFBR grant #13-02-97513.

[1] Arakelian S. M., Kucheruk A. O., Prokoshev V. G., Rau V. G., Sergeev A. G., Introduction to femto-nanophotonics:fundamentals and laser methods of controled fabrication and diagnostics of nanostructured materials. Monograph, 744 p., Logos Publ., Moscow (2015).
[2] Arakelyan S. M., Veiko V. P., Kutrovskaya S. V., Kucherik A. O., Osipov A. V., Vartanyan T. A., Itina T. E. Reliable and well-controlled synthesis of noble metal nanoparticles by continuous wave laser ablation in different liquids for deposition of thin films with variable optical properties. J Nanopart Res (2016) 18:155. DOI 10.1007/s11051-016-3468-0.
[3] Arakelian S., Emel'yanov V., Kutrovskaya S., Kucherik A., Zimin S. Laser-induced semiconductor nanocluster structures on the solid surface: new physical principles to construct the hybrid elements for photonics. Journal Optical and Quantum Electronics (2016), 48(6), 1-16. DOI 10.1007/s11082-016-0608-9.

LM-5-3 (Invited)

Interaction of Electromagnetic Waves with Colloidal Nanoparticles: Modeling and Applications

I.N. Zavestovskaya[1,2]

1- N.G. Basov Quantum Radiophysics Department of P.N. Lebedev Physical Institute, Moscow, Russia
2- National Research Nuclear University "MEPhI", Moscow, Russia

INZavestovskaya@mephi.ru

Solid-state nanoparticles (NPs) can efficiently absorb the energy of electromagnetic radio-frequency (RF) radiation and subsequently release it into surrounding medium in the form of heat. A wide variety of materials was proposed to design novel NP-based contrast agents in thermal-related medical technologies. Photoacoustic and thermoacoustic imaging are well-known examples of such technologies. A diversity of materials was used to develop photoacoustic contrast agents, i.e. carbon, gold, cobalt, semiconducting polymers, and various combinations. Photoacoustic contrast agents should efficiently absorb light radiation, generating a required signal-to-noise (S/N) ratio. However, for the same reason, the penetration depth of light is limited by several centimeters.

Therefore, microwave and RF radiations were applied to overcome this limitation. Similarly, the microwave radiation penetrates for several centimeters, and in thermoacoustics the carrier frequencies of electromagnetic fields are near 100 MHz^2. In this frequency range, the radiation absorption by tissues in much smaller, providing a larger penetration depth. The drawback of this approach consists in a low S/N ratio. It is expected that such a problem can be resolved by the employment of NPs as contrast agents.

In present paper, we review our recently obtained data on developing the model of the interaction of spherical colloidal nanoparticles with low-frequency electromagnetic waves. The aim was to describe quantitatively the interaction of NP-electrolyte system with low-frequency electromagnetic waves for medical applications.

We consider the RF heating of a nanoparticle immersed into the electrolyte solutions of varied conductivity. The proposed model allowed us to successfully describe the previously observed effect of strong heating of aqueous suspension of Si and Au NPs under RF irradiation with frequencies varied from 0.1 MHz to 500 MHz. We focused only on the description of heating in MHz region and did not take into account the dielectric losses in water. Our phenomenological analysis shows that presence of NPs can significantly affect the RF heating, especially at low electrolyte conductivities. The model explains the heating dependence on frequency of electromagnetic waves. We also found that optimum particle conductivity for maximum heating is located in range 0.1-1 Sm/m at 30 MHz and -50 mV zeta-potential, while the NP size shows quite insignificant impact on the heating.

We have not considered the ensemble of NPs, but believe that effective medium models can be easily applied for description of the heat release in suspensions of NPs. The developed model can be useful to design and develop new contrast agents for RF-acoustic tomography and solid sensitizers for the RF hyperthermia of cancer.

It should be noted that the observed weak dependence of the RF radiation-induced heating efficiency on conductivity of employed nanoparticle-based sensitizers is a pleasant surprise, which can opens up novel avenues for the development of mild cancer treatment modalities based on the employment of RF radiation. In fact, it means that instead of gold nanoparticles or carbon nanotubes one can explore novel classes of semiconductor nanomaterials, which can offer a better biological compatibility and other functionalities. Silicon nanostructures look as a prominent example of such nanostructures. Si nanoparticles are not only biocompatible, but also biodegradable as in biological tissue they normally decay into orthosilicic acid $Si(OH)_4$, which is naturally excreted from the body through the urine. In addition, Si nanoparticles can be prepared in pure, uncontaminated state by e.g. using methods of laser ablation in gaseous or aqueous ambience, which excludes any secondary biotoxicity related to the contamination of the nanoparticle surface. Finally, Si nanoparticles can exhibit a series of unique properties, including room temperature photoluminescence, singlet oxygen generation under photoexcitation, infrared radiation–induced and ultrasound-induced hyperthermia, which can be applied in parallel to the RF hyperthermia approach.

LM-5-4 (Invited)

Application of UV Filaments for Detecting Oil Products on Water Surface

A.A. Ionin[1], D.V. Mokrousova[1,2], L.V. Seleznev[1], D.V. Sinitsyn[1] and E.S. Sunchugasheva[1,2]

[1]P.N. Lebedev Physical Institute of Russian Academy of Sciences, 53 Leninsky prosp., Moscow 119991, Russia
[2]Moscow Institute of Physics and Technology, Dolgoprudny, Moscow region, Russia
E-mail: aion@sci.lebedev.ru

Detecting and identification of unknown substances is a vital problem for environmental monitoring, which can be carried out with laser spectroscopy. One of the most common procedures of detecting oil spills on water surface is laser fluorescence detection procedure [1] or saturation fluorimetry [2]. Modern detecting laser facilities operate in near-UV wavelength domain with quite long pulses: 12 ns (308 nm) – 6 ns (533 nm) [1]. We propose to excite fluorescence by high-power UV pulses of 100 fs duration. In this case a laser beam propagates in filamentation regime [3], therefore high peak intensity pulses can be delivered to detected substance over a long distance [4]. UV pulses of low energy but high intensity can produce quite a bright luminescence of a target [5]. This presentation will be devoted to a model experiment on detecting the fluorescence of oil products in the form of thin films on water surface excited by femtosecond UV laser pulses.

We used a femtosecond Ti:Sapphire laser facility (100 fs, 248 and 372 nm, 100 and 500 μJ) as a source of UV light in the experiment. Thin films of oil products (oil VM-5, oil 5W-40 and solvent WhiteSpirit) on the water surface were excited by focusing a laser beam. We studied both spectral and energetic characteristics of the films fluorescence for two wavelengths in UV domain.

Fig. 1 demonstrates typical fluorescence spectra of different oil products on water surface for 248 nm laser beam. All spectra have unique and well distinct shapes and extend from 300 to 400-500 nm, which are not overlapped with the laser wavelength. Spectra of oil 5W-40 film fluorescence excited by 370 nm laser pulses covers the same spectral range, but it is harder to select the laser spectral line from the fluorescence spectrum. Films of oil VM-5 and WhiteSpirit are transparent for this laser wavelength. Therefore, shorter UV laser pulse wavelength is more preferable for fluorescent spectroscopy than commonly used ones.

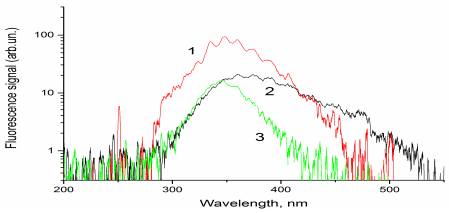

Figure 1. Typical fluorescence spectra of different oil products excited by 248 nm laser beam:
1) oil VM-5, 2) oil 5W-40 and 3) solvent WhiteSpirit.

Integrated over the whole spectrum fluorescence signal increases with enhancement of pulse power, but the signal begins to saturate when pulse power exceeds critical power of self-focusing for the corresponding wavelength – single filament regime. Propagation of laser beam in multifilamentation regime (pulse power corresponds to hundreds of critical power) will result in much higher integral fluorescence signal because of additive contribution from every filament. This regime could enhance useful signal of fluorescence crucial for long range detection of oil spills. Thus, we experimentally studied an opportunity of applying UV femtosecond laser pulses as spectroscopic means for oil and oil products films on water surface. It was shown that shorter UV wavelengths are more suitable for fluorescence detection. Multifilamentation regime seems to be very effective for fluorescence detection of oil products. This research was supported by RFBR grants 14-02-00489 and 14-22-02021

[1] T. Hengstermann, R. Reuter, “Lidar fluorosensing of mineral oil spills on the sea surface,” Appl. Opt., vol. 29, pp. 3218-3227, 1990.
[2] V. V. Fadeev, S. A. Dolenko, T. A. Dolenko, Ya. V. Uvenkov, E. M. Filippova, V. V. Chubarov, “Laser diagnostics of complicated organic compounds and complexes by saturation fluorimetry,” Quant. Electron., vol. 27, pp. 571-574, 1997.
[3] A. Couairon, A. Mysyrowicz, “Femtosecond filamentation in transparent media,” Phys. Rep., vol.441, pp. 47-189, 2007.
[4] V D Zvorykin, A A Ionin, et al., "Production of extended plasma channels in atmospheric air by amplitude-modulated UV radiation of GARPUN-MTW Ti : sapphire—KrF laser. Part 2. Accumulation of plasma electrons and electric discharge control", Quant Electron, vol. 43 (4), pp. 332-338, 2013.
[5] A.A. Ionin, D.V. Mokrousova, L.V. Seleznev, D.V. Sinitsyn, E.S. Sunchugasheva, N.A. Fokina, “Spectroscopy based on target luminescence caused by interaction with UV filaments,” Las. Phys. Lett., vol. 12, pp. 065701, 2015.

LM-5-5 (Invited)

On some problems of laser interferometers for the direct detection of gravitational waves

V.I. Pustovoit

Scientific and Technological Centre of Unique Instrumentation RAS

vladpustovoit@gmail.com

Contents of the report

1. Metody assessment of observed events.

2. About the problem of the creation of mirrors with high reflectivity and radiation resistance.

3. Geterogennye environment (metamaterials) to create highly reflective laser mirrors.

LM-5-6 (Invited)

Luminescent properties of bismuth-doped alumino- and phosphosilicate fibers under two-step excitation

S.V. Firstov[1], K.E. Riumkin[1], V.F. Khopin[2], S.V. Alyshev[1], E.G. Firstova[1], M.A. Melkumov[1],·A.N. Guryanov[2], E.M. Dianov[1]

1- Fiber Optics Research Center, Russian Academy of Sciences, 38, Vavilov str., Moscow 119333, Russia
2- Institute of Chemistry of High-Purity Substances, Russian Academy of Sciences, 49, Tropinin str., Nizhny Novgorod 603600, Russia

E-mail: riumkin@fo.gpi.ru

The attractive feature of bismuth-doped glasses and fibers is broadband long-lifetime luminescence covering the spectral region from 1000 to 2000 nm [1]. It is well known that near infrared luminescence is caused by optical transitions between energy levels of Bi-related laser-active centers (BACs). However, exact nature of BACs and the structure of their energy levels still remain unclear because of capability of Bi to exist in various valences and to form complexes different from BACs. Therefore, two-step excitation spectroscopy which is highly sensitive and selective tool for the detection of various Bi forms is highly appropriate of available methods to investigate the Bi-doped fibers.This approach was successfully used to determine low-lying excited levels of BACs in silicate and germanosilicate fibers [2]. In this summary, we present a series of results on study of BACs in Bi-doped alumino- and phosphosilicate fibers under two-step excitation. The use of radiation source with tunable wavelength allows selective excitation of BACs with subsequent registration of anti-Stokes luminescence (λ_{em}) at 750 and 770 nm in alumino- and phosphosilicate fibers, correspondingly (Figure 1, c). It was shown that these bands arise due to BACs responsible for lasing. The anti-Stokes luminescence intensity as a function of excitation wavelengths (λ_{ex1}, λ_{ex2}) in various types of fibers was obtained (Figure 1, a). For comparison, the similar results for Bi-doped silicate fibers are also presented. It is seen that transitions energies strongly depend on glass host (Figure 1, b).

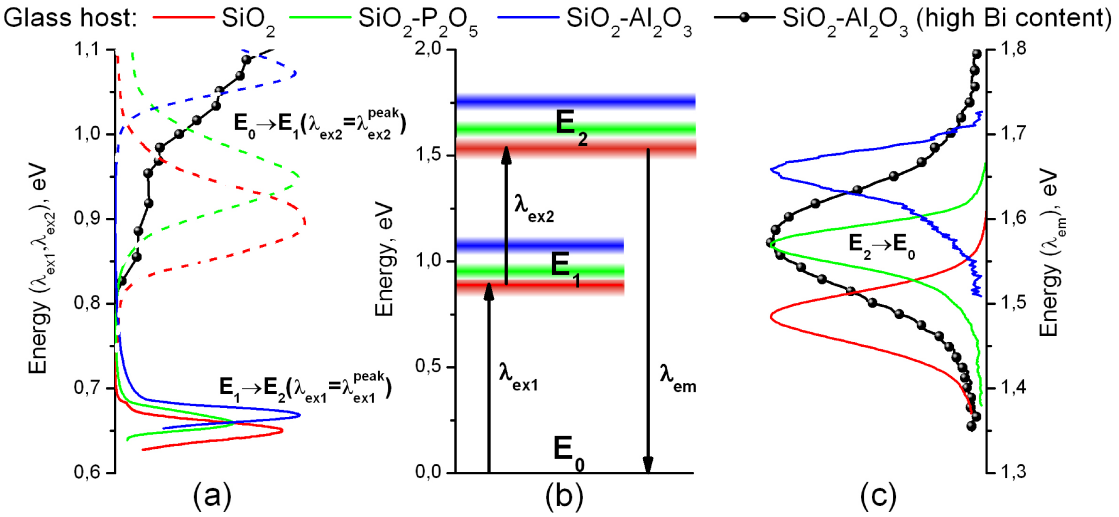

Figure 1. The dependence of the anti-Stokes luminescence intensity on excitation wavelength (two-step excitation) (a); energy level scheme of BACs (b); anti-Stokes luminescence spectra (c).

Analyzing the luminescent properties of heavily Bi-doped aluminosilicate fibers, it was shown that an increase of Bi led to the disappearance of laser-active centers and generation of new luminescent centers with broader anti-Stokes luminescence at 780 nm and unstructured excitation spectrum (Figure 1, a,c). It should be noted that in contrast to BACs this luminescence band could be excited by one-wavelength (>1000 nm) cascade excitation. Moreover, distinctive feature of this type of luminescent centers is that they are characterized by upconversion and high-intensive excited state absorption processes [3].

The study was supported by the Russian Foundation for Basic Research (grant 16-02-00440).

[1] I. Bufetov, M. Melkumov, S. Firstov, K. Riumkin, A. Shubin, V. Khopin, A. Guryanov, E. Dianov, Bi-Doped Optical Fibers and Fiber Lasers, IEEE J. Select. Top. Quantum Electron., vol. 20, no. 5, pp. 111-125 (2014).
[2] S. Firstov, V. Khopin, V. Velmiskin, E. Firstova, I. Bufetov, Anti-Stokes luminescence in Bismuth-doped silica and germania-based fibers, Opt. Express, vol. 21, pp. 18408-18413, (2013)
[3] K. Riumkin, M. Melkumov, I. Varfolomeev, A. Shubin, I. Bufetov, S. Firstov, V. Khopin, A. Umnikov, A. Guryanov, E. Dianov, Excited-state absorption in various bismuth-doped fibers, Opt. Lett., vol. 39, pp. 2503-2506 (2014)

LM-P-1

High-conductivity SnO_2:Sb films produced on flexible organic substrates

L. S. Parshina, O. A. Novodvorsky, O. D. Khramova, A. A. Lotin, V. A. Mikhalevsky, E. A. Cherebilo

ILIT RAS, Branch of the Federal Scientific Center «Crystallography and Photonics» RAS, 140700, Shatura, Russia

ParshinaLiubov@mail.ru

Tin oxide (SnO_2) films have been widely used as a transparent conducting thin film material for application in various fields such as display technology, organic light-emitting-diodes, thin-film solar photovoltaics, low emissivity windows in buildings, defrosting windows, electrochromic windows, static dissipation coatings and gas sensors [1, 2].

The varying of the erosive plume energy spectrum due to variation of wavelength of ablative radiation and energy density on the target in the pulsed laser deposition (PLD) method opens the prospects of flexible control of the grown films properties [3]. The properties of the obtained films depend on energy of the deposited particles because of a nonequilibrium of the deposition process [4]. The employment of the PLD method with plume energy control in synthesis of the SnO_2:Sb thin films allows applying these materials on flexible organic substrates thanks to the possibility of considerable decrease in the temperature of the films growth at the expense of particle energy increase in the plasma plume of that earlier, as far as we know, it wasn't carried out. Application the droplet-free mode of films deposition provides the production of the high-quality smoothness uniform films at the room substrate temperature thanks to removing of the drops which are taking off from the target on the substrate in process of film deposition.

In the present work the high-conductivity transparent in the visible region SnO_2:Sb films on flexible organic polyethyleneterephthalate (PET) substrates have been produced at low substrate temperatures up to room temperature by the droplet-free PLD method under ablation of ceramic targets by radiation of different wavelength (248 nm, 532 nm, 1064 nm). The obtained films were exposed to the post-growth laser annealing with wavelength of 248 nm for the goal of the increase in the film conductivity. Structural, optical and electric properties of the obtained films have been investigated from deposition parameters such as wavelength of the ablative radiation, energy density on the target, oxygen pressure during the deposition, and the laser annealing. XRD analysis indicated that the films grown at room temperature of substrate were amorphous. After laser annealing they became partially crystallized. It was established that the post-growth laser annealing with the energy density on the film from 20 mJ/cm^2 to 40 mJ/cm^2 reduces the resistivity of the SnO_2:Sb low-resistance films by 20 times, and of the high-resistance films by 300 times. The optimum energy density and the radiation dose of the SnO_2:Sb film without a damage of the substrate were determined. The SnO_2:Sb films possessed a high transparent in the visible region from 400 nm to 700 nm. The SnO_2:Sb films minimum resistivity of $6{,}5 \cdot 10^{-3}$ Ohm·cm was reached on PET organic substrates without the post-growth laser annealing. The SnO_2:Sb films minimum resistivity of $1{,}2 \cdot 10^{-3}$ Ohm·cm was reached by using the post-growth laser annealing.

This work has been supported by grants RFBR № 14-07-00688, 14-47-03605, 15-38-20369, 15-29-01171, 15-07-04142, 15-07-03331, 15-07-03580, 16-29-05385, 16-07-00842.

[1] G. P. Crawford, Flexible flat panel displays (John Wiley and Sons Ltd.), (2005).

[2] T. M. Lee, H. C. Choi, J. H. Noh, D. S. Kim, EL display printed on curved surface, Micro Electro Mechanical Systems, IEEE 22th International Conference, pp. 943-946, (2009).

[3] L. S. Parshina, A. A. Lotin, D. A. Zuev, E. V. Khaydukov, O. D .Khramova, A. V. Shorokhova, O. A. Novodvorsky, V. Ya. Panchenko, Influence of the energy spectrum of the plume ions on the thin films parameters of metals and semiconductors, Russian Journal of Perspective Materials, vol. 14, pp. 255-261, (2013).

[4] L. S. Parshina, O. A. Novodvorsky, O. D. Khramova, I. A. Petukhov, A. A. Lotin, V. A. Mikhalevskiy, A. V. Shorokhova, Influence of the plume energy on the SnO_2:Sb films characteristics by using the PLD droplet-free method, Computational nanotechnology, vol. 1, pp. 62-67, (2014).

LM-P-2

Theoretical modeling of laser metal nanoparticles fragmentation in water

A. A. Ananskaya[1,2], I. N. Zavestovskaya[1,2], A. P. Kanavin[1,2], O. V. Rodionova[2]

1- P.N. Lebedev Physical Institute of RAS, Moscow, Russia
2 - National Research Nuclear University MEPhI, Moscow, Russia

korolek2512@yandex.ru

Due to the unique optical, physical and chemical properties, metal nanoparticles become more and more popular, and find wide applications in optics, electronics, biomedicine, analytical chemistry and photochemistry. Gold nanoparticles are of special interest because of their chemical stability. There are various methods to produce the nanoparticles. Of special note is the laser ablation [1]. Laser ablation in liquids is an effective physical method to produce the nanoparticles in the form of colloids. However, ablation in water and other solutions in the absence of chemically active components results in the formation of rather large-sized nanoparticles with a wide size spectrum. In this connection, to reduce the size of nanoparticles their colloids are additionally treated by ultrashort laser pulses, and this results in the fragmentation of produced nanoparticles [2]. For example, Werner et al [3] investigated femtosecond fragmentation of the aqueous solution of gold nanoparticles with a diameter of 60 nm. Using in situ microscopy and transmission electron microscopy thresholds of fragmentation were identified: (7.3±1.5) mJ/cm^2 for irradiation at a wavelength of 400 nm and (3.6±0.5) mJ/cm^2 for 532 nm.

The aim of this work was to study the physical model of the processes of electrization and fragmentation of gold nanoparticles in water under the action of femtosecond laser pulses. To test this model, we also needed to identify thresholds of fragmentation of gold nanoparticles and compare them with experimental data.

All numerical calculations in this study were conducted in the MATLAB software environment. For approximation of obtained dependencies, Origin8 was used.

The considered physical model of metal nanoparticle fragmentation is based on the electrization of metal nanoparticles heated by a laser pulse, and their division under the development of instability of a charged liquid metal drop. As a mechanism of electrization we have considered the process of hot electrons' emission from the surface of a nanoparticle and further solution in water [4]. A numerical solution has been performed of the problem of gold nanoparticle heating under the absorption of femtosecond laser pulses. A system of equations which describe the propagation of electrons in the dielectric medium taking into account their spatial self-charge was formulated and numerically solved.

The estimates of the potential gained by the nanoparticle due to the electron thermionic emission and their further solution have been obtained. On the basis of the Rayleigh drop model, the criterion of nanoparticle fragmentation has been found, as well as the dependence on the nanoparticle size. It has been shown that at the moment of nanoparticle complete melting the potential gained by the particle due to the electron thermionic emission turns to be significantly higher than the stability threshold of the gold charged drop, and the particle disintegrate. The calculated critical values of laser radiation F_{melt} needed to completely melt the 60 nm nanoparticles for τ_{pul} =150 fs and λ=400 nm and 532 nm are in good agreement with the critical values of such nanoparticles' disintegration obtained experimentally and confirmed by numerical calculations in [3]. Thus as soon as the gold nanoparticle goes into a liquid state it turns to be Rayleigh unstable. The discussed mechanism of gold nanoparticle fragmentation does exist in practice.

[1] Zavestovskaya I. N., Eliseev P. G., Krokhin O. N., and Men'kova N. A., Appl. Phys. A **92**, 903 (2008)
[2] Besner S., Kabashin A.V., Meunier M., Appl. Phys. Lett. **89**, 233122 (2006)
[3] Werner D., Furube A., Okamoto T., Hashimoto S., J. Phys. Chem. C **115**, 8503 (2011)
[4] Zavestovskaya I.N., Kanavin A.P., Makhlysheva S.D., Bulletin of the Lebedev Physics Institute, **40**, 335-338 (2013)

LM-P-3

Micro-optical components fabrication by laser-induced micro plasma

V. Koval, V. Rymkevich, G. Kostyuk, R. Zakoldaev*, M. Sergeev, V. Veiko, A. Samokhvalov

ITMO University, Kronverkskiy Pr. 49, St. Petersburg 197101, Russia

**email address: zakoldaev@gmail.com*

The development of laser technology determined the appearance of the various methods for micro-optical elements fabrication. Combined laser-induced technologies based on strong absorption of laser radiation by different materials [1, 2] contact with the back side of the glass plate are widely spread today and present particular interest among reputable methods. Their advantage is the speed during the components fabrication and the possibility of automation the manufacturing process.

Thus, in this work we consider the design, manufacture and testing of micro-optical elements, as diffractive phase gratings and random phase plates. The method called laser-induced black-body heating (LIBBH) [3] is used for the elements fabrication. This type of elements are widely used to change the phase of the wavefront of laser beam. A lot of applications can be found at laser beam transformation with high efficiency. For instance, diffractive phase gratings (Fig. 1a) are an effective beam splitter in the scheme of multi-beam interference. Random phase plates (Fig. 1b) are an integral part of laser beam homogenizing.

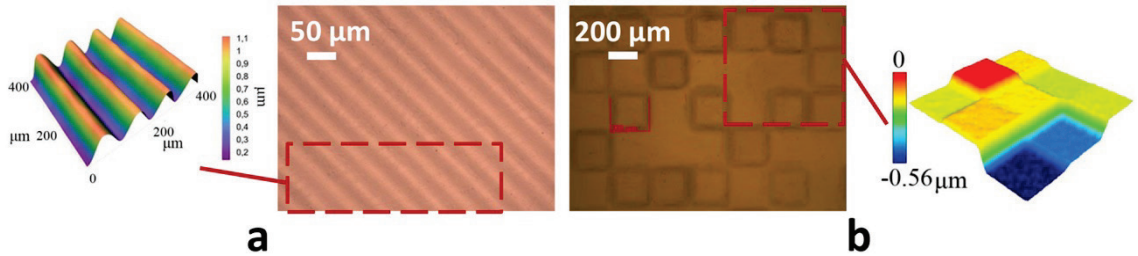

Figure 1 Optical images and measured 3D profiles of microoptical elements fabricated on fused silica surface by LIBBH method: periodical diffractive grating (a) and random phase plate (b).

Fabricated diffractive phase gratings have been pre-calculated to achieve high diffractive efficiency. That allowed us to use them in multi-beam interference scheme for metal films microstructuring. As for laser beam homogenization, special algorithm (microrelief of the elements has complex distribution with a multi-level architecture – Fig. 1b) was developed to achieve the lowest intensity modulation in the area of homogenization. All main steps of micro-optical elements fabrication by LIBBH method have been investigated and automated.

Experimental studies have been supported by the grant from leading universities of the RF (subsidy 074-U01) and the RSF agreement № 14-12-00351.

[1] J. Zhang, K. Sugioka, K. Midorikawa, High-speed machining of glass materials by laser-induced plasma-assisted ablation using a 532-nm laser, Applied Physics A, vol. 67 (4), pp. 499-501, (1998).
[2] I.V. Blonsky, A.Y. Danko, V.N. Kadan et al., Influence of the transverse dimension of the torch laser-induced plasma in the material handling processes, Technical Physics, vol. 75(3), pp. 74-80, (2005) - in Russian.
[3] G.K. Kostyuk, R.A. Zakoldaev, M.M. Sergeev, et al., Laser-induced glass surface structuring by LIBBH technology, Optical and Quantum Electronics, vol. 48(4), pp. 1-8, (2016).

LIPSS formation from nanoparticles produced by picosecond and femtosecond laser shots on mesoporous silicon

A. Talbi[1], A. Petit[1], S Kaya-Boussougou[1], A. Stolz[1], C. Boulmer-Leborgne[1], N. Semmar[1]

1- GREMI-UMR 7344-CNRS-University of Orleans, 14 rue d'Issoudun, BP6744, 45071 Orleans Cedex2, France

This work deals with a comparative study of Laser-Induced Periodic Surface Structures (LIPSS) formation on mesoporous silicon following two laser regimes: picosecond and femtosecond. The formation of LIPSS from nanoparticles by different mechanisms mainly coalescence and agglomeration has been evidenced by Scanning Electron Microscopy (SEM) images (figure1). The formation of a liquid phase during both laser interaction at low fluence (~20 mJ/cm^2) and after a large number of laser pulses (~ up to 10000) has been also shown (see figure 1 and figure2) [1]. Transmission Electron Microscopy analyses have been conducted to investigate the molten phase structures below and inside LIPSS. Finally it is concluded that LIPSS are composed of amorphous silicon when mesoporous silicon is irradiated by laser beam in picosecond and femtosecond regime. Nevertheless mesoporous silicon located between LIPSS stays crystallized.

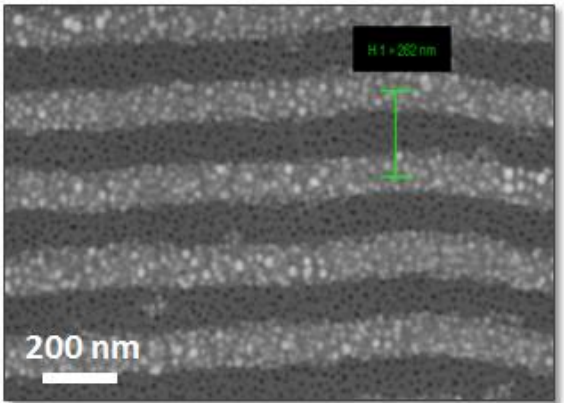

Figure 1. Nanoparticles based LIPSS formed on mesoporous silico by ps irradiation at 20 mJ/cm² and after 12000 shots

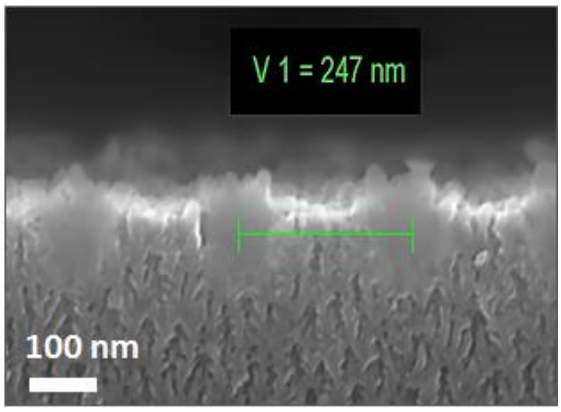

Figure 2. SEM cross section view of LIPSS formed by ps irradiation at 20 mJ/cm² and after 12000 shots

[1] A. Talbi et al. Nanoparticles based laser-induced surface structures formation on mesoporous silicon by picosecond laser beam interaction, Applied Surface Science 374, 31–35 (2016).

LM-P-5

Optoacoustic investigations of formation mechanism of silicon nanoparticles synthesized by pulsed laser ablation in liquid

A. Aryshev, V. Veiko, S. Kudryashov, A. Samokhvalov

National Research University of Informational Technologies, Mechanics and Optics, Saint-Petersburg, Russia

samokhvalov.itmo@gmail.com

Laser ablation of solids in liquid is a quick, easy, versatile and green method for nanoparticles synthesis. Most importantly it provides with opportunity to obtain impurity free colloidal solutions of synthesized nanoparticles without using any surfactants or chemical reagents. Due to this advantages laser ablation synthesis of nanoparticles in liquid media gained increasing interest in recent years. This method is successfully using to fabricate various nanoparticles with novel morphologies and possibility to control shape, size and material phases, however the mechanism of nanoparticles formation hasn't been much studied and there is no consensus on this problem.

In this work we report the research of the Si nanoparticle synthesis by pulsed laser ablation in liquid media. For the investigation of nanoparticles formation mechanism, we used optoacoustic method of acoustic pressure measurements, based on analysis of the silicon target acoustic response on the laser irradiation depending on laser fluence value.

To register an acoustic signal, the pressure transducer (lithium niobate crystal), attached to the bottom side of silicon wafer, was used. The forward side of this target was irradiated by single fiber laser pulse (1 mJ, 1.06 μm, 200 ns). This experiment was performed in the air medium and in the distilled water as well (thickness of the water layer was 1,5 mm above target surface).

Results show that amplitude of optoacoustic signal is nonmonotonically increasing. It experiences a spike near the 10 J/cm^2 value of laser fluence and then levels off with further increasing of energy density. Moreover, in case of ablation in liquid, the acoustic pressure is two-orders higher than in the air (Fig. 1 – a).

Single pulsed craters were studied by optical microscopy and light white interferometry to explain this characteristic curve. Comparing the acoustic signal trend and the craters shape, it is possible to conclude, that the mechanism of nanoparticles formation below the 10 J/cm^2 value of laser fluence is caused by the processes of normal evaporation and nucleation in supersaturated steam, while the increasing of laser fluence over this value provides the generation of laser plasma plume, which causing the change of nanoparticles synthesis kinetic (Fig. 1 – b,c).

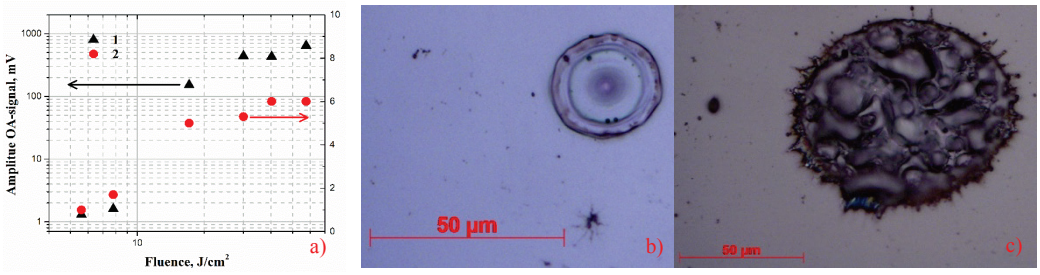

Figure 1. – a) Optoacoustic signal amplitude dependence on laser fluence in case of ablation in 1 – distilled water, 2 – air medium. Difference in craters shape on laser ablation of silicon wafer in liquid, b) – below 10 J/cm2, c) – above the threshold.

It is worth noting that further increasing of laser fluence didn't have a significant effect on ablated mass, so nanoparticles mass yield attains the saturation above the 10 J/cm2 of laser fluence.

Thus, nanoparticle formation mechanism during laser ablation in liquid was studied by using the optoacoustic method. It was shown, that, in case of technological process of nanoparticles synthesis, there is a threshold for effective laser fluence. Using energy densities above this threshold is impractical.

LM-P-6

3D printing of gradient polymer nanocomposites via laser-assisted sintering

I. Shishkovsky, V. Scherbakov, S. Kudryashov, A. Ionin

P.N. Lebedev Physical Institute of Russian Academy of Sciences, Leninskiy prospect 53, 119991 Moscow, Russia
Main author email address: shiv@fian.smr.ru, aion@sci.lebedev.ru

Direct fabrication of multilayered nanosystems is a difficult technological task. As is known, sintering is a thermally activated process that is accompanied by coagulation of nanoparticles into micro-sized conglomerates. Stabilization of nanoparticles in a polymeric matrix makes possible [1] to arrange a desired distribution of nanoparticles in polymer and thus to protect them from oxidation and even to design functionally graded (FG) structures.

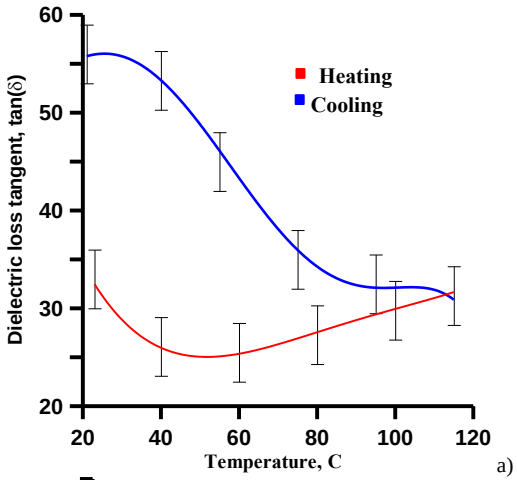

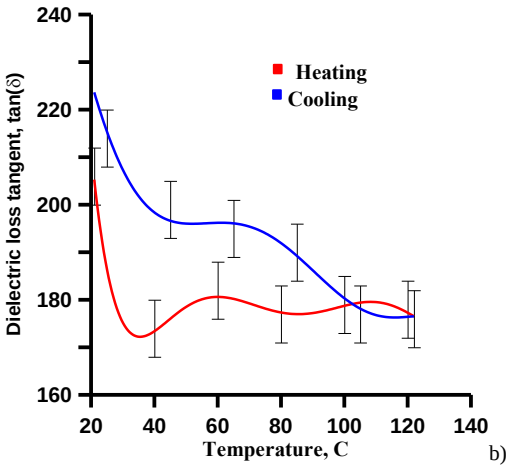

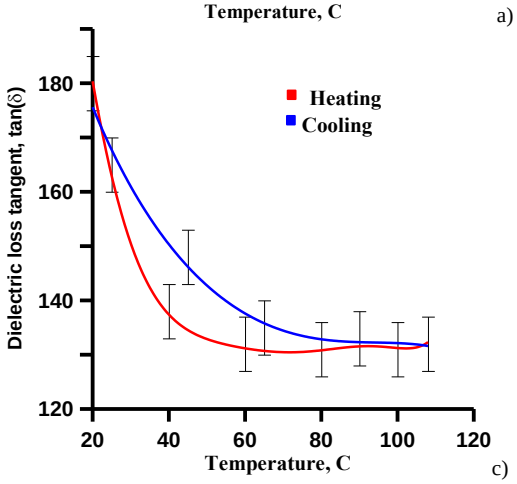

Fig. 1 Temperature dependencies of dielectric loss tangent - tan δ for 3D FG samples (10 layers, mixtures 1:10) with sequences: a) Cu + PEEK / Ni + PEEK / Cu + PEEK; b) Ni + PEEK / Cu + PEEK / Ni + PEEK; c) Ni + PEEK / Cu + PEEK. Red curves- heating stage, blue curves- cooling stage. Laser influence regime - P = 6.2 W, V = 40 mm/s. PEEK – polyether ether ketone.

Selective laser sintering (SLS) is a promising technique for fabrication of the functionally graded structure with nano additives. Recently [1, 2], the laser-assisted 3D synthesis was used to fabricate polycarbonate structures containing encapsulated nickel and/or copper nanoparticles, chemically active and uniformly distributed over the sintered polymer.
In this communication, we report on electrophysical properties of functionally graded Cu + PEEK/Ni + PEEK layers prepared by SLS. It was shown (fig.1) that with the layer number growing a figure of merit for multilayer system grows. At the layer interleaving most growing of Q factor into 3D samples was observed at the order of interleaving Ni+ PEEK / Cu + PEEK, rather then on the contrary.
This work was supported by the Russian Science Foundation (project no. 15-19-00208).

[1] I. Shishkovsky and Y. Morozov, Electrical and magnetic properties of multilayer polymer structures with nanoinclusions as prepared by selective laser sintering, Journal of Nanoscience and Nanotechnology, vol. 13, pp. 1440-1443, (2013).
[2] I. Shishkovsky, V. Scherbakof, I. Volyansky, Low-dose laser sintering of Cu nanoparticles on the ceramic substrate during ink-jet interconnection,. Proc. SPIE, Vol. 9065, 90650I. (2013).

LM-P-7

Frequency domain thermoreflectance techniques for quantifying heat flow in nanostructured devices, films and interfaces

D. McCloskey[1]

1- School of Physics, CRANN and AMBER, Trinity College Dublin, Dublin 2, Ireland.
Email: mccloskd@tcd.ie

We present recent work on frequency domain techniques for mapping temperature and thermal properties in thin films and devices developed at Trinity College Dublin. Thermal wave spectroscopy is a method by which a periodic heat source is applied to the surface of a sample and the result and amplitude and phase of the temperature is monitored. A common implementation is the 3ω technique, where a periodic current in a surface resistive heater is used as a heat source, and the temperature is monitored through the change in heater resistance [1]. In this work we concentrate on optical techniques which use either electrical or optical power to generate the heat source, and monitor the temperature rise through a change in reflectivity [2-4].

Solving the 1D heat diffusion equation with a periodic surface heat flux in a semi-infinite medium gives a periodic temperature distribution $\Theta(x)$ with form

$$\Theta(x) = \frac{Q_0}{2\varepsilon\sqrt{\omega}} \exp\left(-\frac{x}{\mu}\right) \exp\left[-i\left(\frac{x}{\mu} + \frac{\pi}{4}\right)\right], \quad (1)$$

where $\mu = \sqrt{2\alpha/\omega}$ is the thermal penetration depth, and $\varepsilon = \sqrt{k\rho c_p}$ is the thermal effusively of the sample. Q_0 is the amplitude of the surface heat flux, and k, ρ and c_p have their usual meanings of density, thermal conductivity and specific heat capacity.

We see that this has the form of a critically damped wave. The amplitude of the temperature oscillation decays exponentially to 1/e its value in a distance μ, and the phase lag in the sample will also depend on μ. The amplitude of the temperature at the surface will decrease with $\sqrt{\omega}$. So by measuring this amplitude as a function of frequency we can extract the thermal effusively. In practice a more complicated thermal model is used allowing us to extract thermal properties of multilayer films and thermal interface resistance [4]. The phase only is fitted as it is less sensitive to sources of noise than the temperature amplitude.

Two techniques are discussed. The first, known as CCD thermoreflectance (CCD-TR) [3], employs a lock-in technique with a standard microscope system and CCD camera to take high resolution (~250nm) temperature maps of devices. Higher resolution temperature maps are possible compared to IR imaging with a significantly reduced cost. The second technique, known as frequency domain thermoreflectance (FDTR) [4], works by sweeping the modulation frequency between 100Hz and 200MHz. Fitting the phase lag of the surface temperature oscillation allows us to a to extract the thermal conductivity and interface thermal resistance of multilayer thin film structures. We use this technique to explore thermal properties of materials relevant for heat sinking of microelectronics, integrated photonics, and to probe novel nanomaterials for thermoelectric applications.

[1] D.G. Cahill, “Thermal conductivity measurement from 30 to 750 K: the 3ω method, Rev. Sci. Instrum,” 61, 802-808 (1990)
[2] D. G. Cahill, et al.,"Nanoscale thermal transport", *J. Appl. Phys.* 93, 793 (2003),
[3] M. Farzaneh,, et al. "CCD-based thermoreflectance microscopy: principles and applications,” J. Phys. D: Appl. Phys. **42**(14): 143001 (2009).
[4] Schmidt, A. J., et al. (2009). "A frequency-domain thermoreflectance method for the characterization of thermal properties," Rev. Sci. Instrum., **80**(9): 094901.

This work is funded by the Irish Research Council (IRC) under grant number: GOIPD/2015/259

LM-P-8

Phase field model for stress/strain evolution during laser sintering of metal powders

F.Kh. Mirzade

Institute on Laser and Information Technologies - Branch of the Federal Scientific Research Center "Crystallography and Photonics" of Russian Academy of Sciences, 140700, Moscow region, Russia

E-mail: fmirzade@rambler.ru

Laser metal powder sintering is an additive manufacturing process for rapid prototyping of fully dense metal components. It involves the supply of powders into a laser-heated spot where the powder is melted and forms a melt pool which quickly solidifies. During the laser sintering (LS) process, several complex phenomena occur as the laser beam interacts with both incoming powders material and the substrate material. These phenomena include thermal transport, fluid flow, mass transport, and solidification, as well as others. Macroscopic temperature, concentration and fluid velocity fields have been studied by many researchers [*A. F. A. Hoadley and M. Rappaz, Metall. Trans. B* ***23****B 631 (1992)*]. However, the modeling of microstructure evolution of the solidification (mesoscale process) during the LS has received a little attention. The phase field modelling (FPM) [*I. Steinbach, Model. and Simul. in Mater. Sci. and Eng.,* ***17*** *073001 (2009)*] is one of the most powerful methods for such purposes.

In this contribution, a FPM is developed to examine the effects of elastic stresses on solidification microstructures during LS of metal powders. Governing equations considering the coupling effects among phase variable, an orientation variable, temperature and stress/strain have been derived based on thermodynamic laws. Thermal expansion, transformation dilatation, and effect of stresses/strains on phase transformation are included in the formulation. Using these equations, a linear stability analysis of solidification front is carried out, to find dispersion relationships and a spectrum of wave numbers of unstable perturbations. Our study showed that, in addition to the thermal and mass transfer processes, the elastic field generated by the stresses is another important factor that controls the mode of instability. An increase in stress values increases the maximally wavelength of the unstable perturbations. Characteristic scale of growing crystalline structures is also obtained.

A multiscale model for the LS process has been developed by coupling the microscale model based on the FPM with the macroscale model taking into account the macroscale temperature and fluid velocity fields. Linking of macroscale process and microstructure evolution by considering the relationship of micro - and microparameters, including laser and powder parameters (laser power, scanning velocity, powder feed rate) will lead to a better understanding of the solidification patterns formation mechanisms during LS process.

LM-P-9

The structural features of germanium and silicon nanoparticles formed by means of laser ablation in gases and liquids

F.V. Kashaev[1], T.P. Kaminskaya[1], S.V. Zabotnov[1], L.A. Golovan[1]

[1]- Department of Physics, M.V. Lomonosov Moscow State University, 119991, Moscow, Russia

Email: kashaev.fedor@gmail.com

Laser nanostructuring of semiconductor materials is important in many technological applications. The great interest of scientists in researching of nanodimensional structures is caused by their variety of possible applications in optoelectronics, photonics and biomedicine. Ultrafast pulsed laser ablation is one of the most promising methods for producing nanoparticles. The advantages of this method include chemical purity of the fabrication process and possibility of changing the structural, optical and electronic properties of the nanoparticles produced by ablation of varying conditions (such as the type of buffer medium or medium pressure) [1].

In this study the monocrystalline silicon and germanium was irradiated by ultrashort laser pulses in gases (helium and nitrogen) and liquids (water and liquid nitrogen). The choice of silicon as material of research is caused by biocompatibility and biodegradability of silicon nanoparticles, which in turn allows using it in biomedical field as contrasting agents in optical coherence tomography [2]. Ablation of germanium is interesting due to its high refractive index, possessing small effective mass and high mobility as compared to Si. [3]. Ge nanometer-sized structures have attracted tremendous attention due to their quantum confinement effects.

Determination and comparison of the structural properties of silicon and germanium nanoparticles formed by means of laser ablation is very important due its influence on optical and electrical properties of the particles. Raman spectra indicated the presence of mainly crystalline phase in the formed nanoparticles. The size of nanocrystals was determined by atomic-force microscopy (AFM). Fig. 1 demonstrates the Raman spectrum of germanium nanoparticles, fabricated by picosecond laser ablation (1064 nm, 30 ps, 10 Hz, 17 J/cm^2) in liquid nitrogen in comparison with initial germanium spectrum. The broadening and shifting of the peak evidenced about the phonon confinement [4]. Using the calibration curve, it is possible to determine the size of nanoparticles by shift of peak. The size of nanoparticles corresponding to shift 2 cm^{-1} is equal to 6 nm, as confirmed by AFM studies.

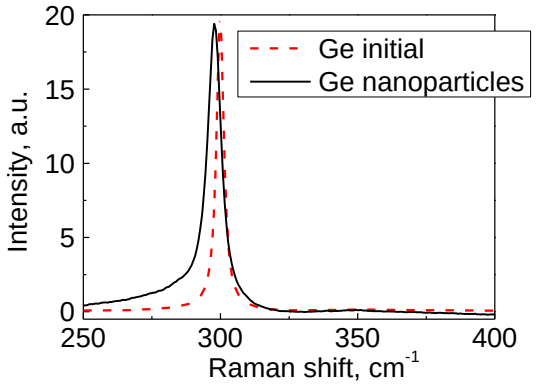

Fig. 1 The Raman spectrum of germanium nanoparticles, formed by laser ablation in liquid nitrogen.

This work was supported by RFBR grant nos. 14–22–01086.

[1] G.N. Makarov, Laser application in nanotechnology: receiving nanoparticles and nanostructures by methods of laser ablation and laser nanolithography, Physics-Uspekhi, vol. 183, pp. 673-718 (2013).
[2] A.D. Krainov, P.D. Agrba, E.A. Sergeeva et al., Study of contrasting properties of nanoparticles for optical diffuse spectroscopy problems, Quantum Electronics, vol. 44, pp. 757-762 (2014).
[3]A.F. Khan, M. Mehmood, A.M. Rana et al. Effect of annealing on structural, optical and electrical properties of nanostructured Ge thin films, Applied Surface Science, vol. 256, pp. 2031-2037 (2010).
[4] V.A. Volodin, V.A. Sachkov, The improved model of localization of optical phonons in silicon nanocrystals, JETP, vol. 143, pp. 100-108 (2013).

LM-P-10

Numerical simulation of heat and mass transfer processes during laser cladding of metal powders

A.V. Dubrov, F.Kh. Mirzade, V.G. Niziev

Institute on Laser and Information Technologies -
Branch of the Federal Scientific Research Centre "Crystallography and Photonics"
of Russian Academy of Sciences.
1, Svyatoozerskaya st., Shatura, Moscow Region, 140700, Russia

dubrov.av@gmail.com

Numerical simulation of the thermo- and hydrodynamic processes, accompanying the technological process of laser cladding of metal powders, was performed using the final volume method in the parallel computing environment. To obtain the resulting surface profile consideration was also given to the mass transfer between the nozzle and the surface of the substrate, the laser radiation absorption by the surface of the cladded layer and by the powder being transported, the capillary effects, which govern substantially the shape of the molten metal surface. The influence of process parameters (laser power, scanning velocity, powder feed rate and material) on the molten pool and cladded track geometry as well as on the temperature distribution in the material has been studied. It is shown that the numerical model used permits simulating the common practical defects such as the balling effect and the pores formation in the interlayer regions. The results obtained are useful for selecting the technological process parameters, and could be taken into account for the simulation of microstructure formation and residual stresses in the cladded layers.

Optical studies on laser-induced oxidization in Cu thin films

William M. Abbott[1,2], and David McCloskey[1,2]

[1]Department of Physics, Trinity College Dublin, College Green, Dublin 2, Ireland

[2]AMBER Research Centre, CRANN Institute, Trinity College Dublin, Dublin 2, Ireland

abbottw@tcd.ie

Copper is already a highly important material in microelectronics, and may also become just as vital in emerging plasmonic technologies[1]. The use of copper in current and future devices is limited, however, by its tendency to oxidize even at ambient conditions[2]. Hence, it is crucial to understand the oxidation behavior in nanoscale Cu materials in order to devise strategies to prevent its occurrence. In this work we investigate the oxidation dynamics of Cu thin films irradiated by a 488nm Ar-ion cw-laser. Through the use of a customized microscope set-up, we were able to induce oxidation with varying spot-size, and measure the reflectivity change in the affected area in order to determine the timescale at which oxide formation occurs. Initially, a layer of Cu_2O is formed. The sudden decrease in reflectivity is attributable to formation of CuO at the beam center, which then grows radially. The oxidation is power dependent, occurring more readily at higher powers. The oxide composition was confirmed through Raman spectroscopy and EDX measurements, showing a central area of CuO, surrounded by Cu_2O. Hence, the Cu_2O is entirely converted to CuO by laser heating. This opens up the possibility of laser-written electronic circuits[3,4].

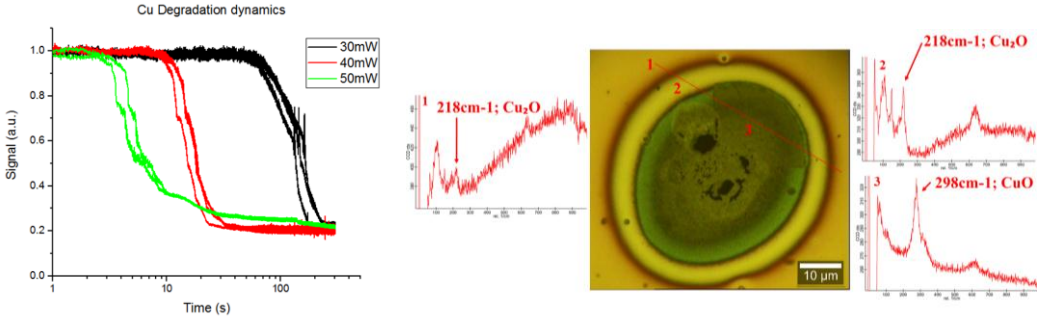

Fig 1(a); reflectivity change in Cu thin film after irradiation with laser at various powers, (b); Raman spectra of laser irradiated area, showing growth of CuO and Cu_2O

REFERENCES

1. Sun, Q.-C. *et al.* Copper plasmonics and catalysis: role of electron–phonon interactions in dephasing localized surface plasmons. *Nanoscale* **6,** 12450–12457 (2014).
2. Li, J., Mayer, J. W. & Colgan, E. G. Oxidation and protection in copper and copper alloy thin films. *J. Appl. Phys.* **70,** 2820 (1991).
3. Figueiredo, V. *et al.* Effect of post-annealing on the properties of copper oxide thin films obtained from the oxidation of evaporated metallic copper. *Appl. Surf. Sci.* **254,** 3949–3954 (2008).
4. Erdoğan, İ. Y. & Güllü, Ö. Optical and structural properties of CuO nanofilm: Its diode application. *J. Alloys Compd.* **492,** 378–383 (2010).

LM-P-12

Coating Alloys Properties of Laser Coating and Thermal Spray Processes

M. Atta Khedr[1], Sameh Akila[1], M. A. Hafez[1], Ali S. Khalil[2]

1- Department of Laser Sciences and Interaction National Institute of Laser Sciences, Cairo University, Giza, Egypt.

2- Institute of mineral Education, Tebin, Helwan, Cairo, Egypt
E mail: makdr@yahoo.com

In our experimental work we describe the difference of laser coating processes during laser surface metal treatment, laser coating processes in comparison with thermal plasma spraying. . High power Nd: YAG laser (1064 nm, 300 – 1600 Watt) has been used in laser coating as coating processes of Stainless Steel S. S. 304 surfaces by different alloys coating materials of ZrO_2- 5% CaO, ZrO_2- 18% to 25% MgO and mix from them. High power Laser for surface treatments, laser modification remitting layer of Ni-Al by lower power 300 W -800 watts on S.S. surface before Zr Composite Alloys coating by high power laser. Different measurements were carried out on the different coated surfaces which obtained by laser coating and plasma tourch arc sprays by measuring the wearing resistance and micro hardening tests, X – Ray diffraction, Scanning electron microscope for determining the morphology of the coating surfaces and film thickness. We reported that the thickness of coating is in the range values 200 t0 300 micrometers. The wear resistance and micro hardness efficiency are increased in laser coating further than plasma thermal spray. The crystalline size structural properties are much improvement in laser coating. That indicates that the bonding forces of crystal lattice are increased by laser coating than thermal spray processes. Laser transformation hardening involves rapid heating and is a novel coating process. Industrial application of laser coating became important branch of advanced laser technology in medical, Environmental applications and space.

LM-P-13

The preparation of nanoparticles by laser ablation in water of crystalline laser active element $YAlO_3:Nd^{3+}$

Vitaly Krasovskii[1,2], Vladimir Pustovoy[1], Vladimir Svetikov[1]

1-A.M.Prokhorov General Physics Institute of the RAS. 38, Vavilov st., Moscow, 119991, Russia
2-National Research Nuclear University MEPHI. 31, Kashirskoe sh., Moscow, 115409, Russia

pustovoy@nsc.gpi.ru

Nanoparticles containing rare earth elements are considered to be promising for biomedical applications [1]. The problem with this is the difficulty in radiation of nanoparticles with a size less than 1 micron. As a rule, mechanical mill applied for nanoparticles producing [2].
In the present work an attempt was made for producing nanoparticles using pulsed laser ablation in waterof the crystalline active laser element $YAlO_3:Nd^{3+}$. Ablation was carried out using radiation of a mode-locked Nd laser at the wavelength of 1.06 μm, pulse duration 15 ns, the energy of the impulse of 10 mJ and a repetition rate of 5 Hz. The radiation is focused on surface YAP crystal under the layer of deionized water with a lens with focus length of 3 cm. The radiation power on the sample surface was 0.6 KW, at an intensity of about 23 GW. Processing was carried out for 20 min. To precipitate coarse particles, which are formed by the spallation mechanism [3], the samples were centrifuged at 4000 rpm for 10 min.

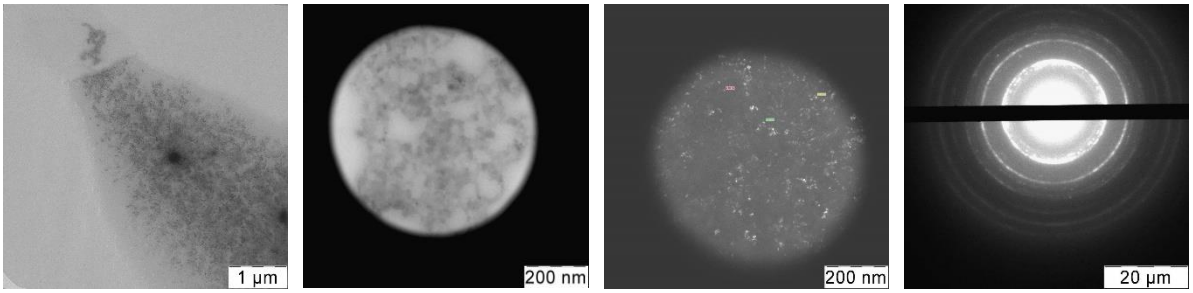

Fig.1. TEM results of nanoparticles obtained by laser ablation in water of laser active element. (a) area with a high concentration of nanoparticles in the scale of 1 μm (b) 200 nm scale, (c) dark-field (scale 200 nm, (d) electronic diffraction pattern

Sample preparation for TEM studies were carried out by applying drops of an aqueous colloid on the standard graphite grid, followed by drying. The results of electron microscopy and electron diffraction (Fig.1 (a,b)) showed enough presence of nanoparticles with a diameter of 5-20 nm. Electron microscopy in dark field shows the presence of metallic nanoparticles with a diameter of 5-8 nm, Fig.1 (c). Results of electronic diffraction plot with a high concentration of nanoparticles showed the presence of crystalline lattice in the non-metallic particles (Fig.1(d)).
This work was supported by The Russian Foundation for Basic Research (Grants 16-32-80032, 16-02-00694) and Program of fundamental researches of the Presidium of the Russian Academy of Sciences I.39P.

[1] D.J. Naczynski, C. Sun, S. Türkcan et al. Nano Lett. 15(1), 96-102, 2015.
[2] G.Chernik, E.Fokina, N.Budim, M.XHuller, V.Kochnev, Nanoindustria, vol.5, pp.32-35 (2007).
[3] K. Sokolowski-Tinten, J. Bialkowski, A. Cavalleri et al, Phys. Rev. Lett. vol. 81, p224, (1998).

Selective structuring of molybdenum-aluminium-molybdenum multi-layered thin film using short and ultra-short laser

P. Das Gupta[1], N. Farid[1], G. M. O'Connor[1]
1- National Centre for Laser Applications, School of Physics, NUI Galway, Ireland

p.dasgupta1@nuigalway.ie

Molybdenum-Aluminium-Molybdenum multi-layered thin film, commonly known as MAM has a special interest in touch panel devices fabrication. In this study, selective structuring of MAM has been performed using short and ultra-short laser sources. A Hippo Mid-Power Q-switch laser with 1064 nm wavelength generates 9 ns pulses (FWHM) and after passing through second and third harmonic crystal, it produces second and third harmonics wavelength of 532 nm and 355 nm, respectively. An ultra-short pulse laser (Amplitude Systems S-PULSE HP), centred at 1030 nm, with second and third harmonic are used to produce 500 fs (at FWHM) pulses. Both laser beams are linearly polarized and Gaussian both spatially and temporally. These laser beams were focused using a galvanometer scanning lens of focal length 100 nm on an XYZ stage. The energy of laser pulses was varied using a combination of the polarizer and half wave plate. Scanning electron microscope (SEM) and atomic force microscope (AFM) were used for surface morphology and measurement of surface profile and dispersive X-Ray (EDX) spectroscopy employed to characterize the depth wise elements distribution and different laser treated zone.

Different laser fluence regimes for MAM processing were identified both for femtosecond and nanosecond laser ablation. Different threshold fluence of MAM was determined using Liu's method. Primary experiments result in a variation of threshold fluence with incident laser wavelength and four different threshold fluence were determined for femtosecond laser processing. Femtosecond laser ablation results absorbed threshold fluence required for complete removal of top molybdenum layer are 0.089±0.009 Jcm^{-2}, 0.2040±0.001 Jcm^{-2} and 0.091±0.001 Jcm^{-2} for using 1030 nm, 515 nm and 343 nm laser wavelength respectively. Nanosecond laser processing shows a much higher threshold value compared to femtosecond case. Results shows threshold fluences for nanosecond laser processing are from 0.133±0.001 Jcm^{-2} (1064 nm) to 0.162±0.004 Jcm^{-2} (532 nm) and 0.117±0.009 Jcm^{-2} (355 nm). Figure 1 represents an optical microscopic image on MAM surface after single pulse nanosecond and femtosecond laser interaction.

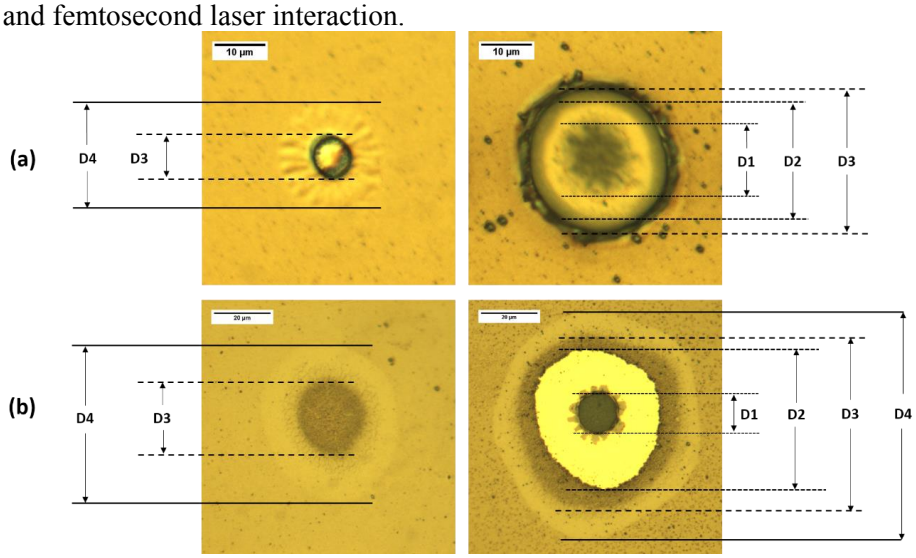

Figure 1: Ablation regime on Mo-Al-Mo (MAM) after (a) nanosecond and (b) femtosecond laser ablation at low (left images) and high fluences (right images)

To understand these fluence regimes, a heat diffusion and a two temperature based finite element method were used to simulate nanosecond and femtosecond ablation process respectively. It has found that these fluences correspond to different ablation mechanism. A full analysis and demonstration of MAM ablation by nanosecond and femtosecond laser and dependence of wavelength and absorbed laser fluence will be presented.

Laser Systems and Materials

LSM-1-1 (Invited)

Progress in diode-pumped Alexandrite lasers: status and future potential

G. M. Thomas[1], A. Minassian[2], W. R. Kerridge-Johns[1], X. Zheng[1], A. T. Coney[1], and M. J. Damzen[1]

1 Photonics Group, Blackett Laboratory Physics, Imperial College London SW7 2AZ, UK
2 Unilase Ltd. Imperial College Incubator, Bessemer Building, Prince Consort Road, London SW7 2AZ, UK
gmt03@ic.ac.uk

Broadly tunable lasers find application in a diverse range of applications, including remote sensing, atomic physics and biomedical imaging. Lasers operating in the near-infrared region attract a lot of interest due to well-established technology available in this wavelength region. Alexandrite is a solid-state laser material that was first developed in the 1970's and has been shown to operate ~700—850nm [1]. In comparison to the most widely used solid-state laser in this wavelength region, Ti:sapphire, Alexandrite has a number of superior properties that make it an interesting, and potentially cheaper alternative [2]. These include good thermal and mechanical properties, as well as a long room-temperature fluorescence lifetime (τ_f ~260μs) and the notable capability for extraordinarily high power direct diode-pumping using red laser diodes (Fig. 1(a)) [3]. Despite this capability, reports of diode-pumping Alexandrite have been so far limited [4]. Here, we review some recent successes in diode-pumping Alexandrite lasers, including high power continuous-wave (CW) operation, both active and passive Q-switching, and cavity-dumped Q-switching, for a fully versatile laser source.

We will review diode-pumping Alexandrite crystals in various pumping geometries, including rod and slab designs. Highlights of this include end-pumping of Alexandrite rods, demonstrating record CW output powers (> 26W). Active Q-switching using a BBO Pockels Cell was also demonstrated from end-pumped geometries, with pulse energy scaled to 3mJ with 70ns pulse duration (Fig. 1(b)), by dual-end-pumping, efficiently distributing the inversion along the length of the rod. Again using a BBO Pockels Cell, cavity-dumped Q-switching was investigated, demonstrating pulse energy of 0.5mJ with 3ns pulse duration. Most recently, passive Q-switching has been obtained using a saturable absorber, generating few-100ns pulses. Finally, some discussion of future potential of diode-pumped Alexandrite technology will conclude this paper.

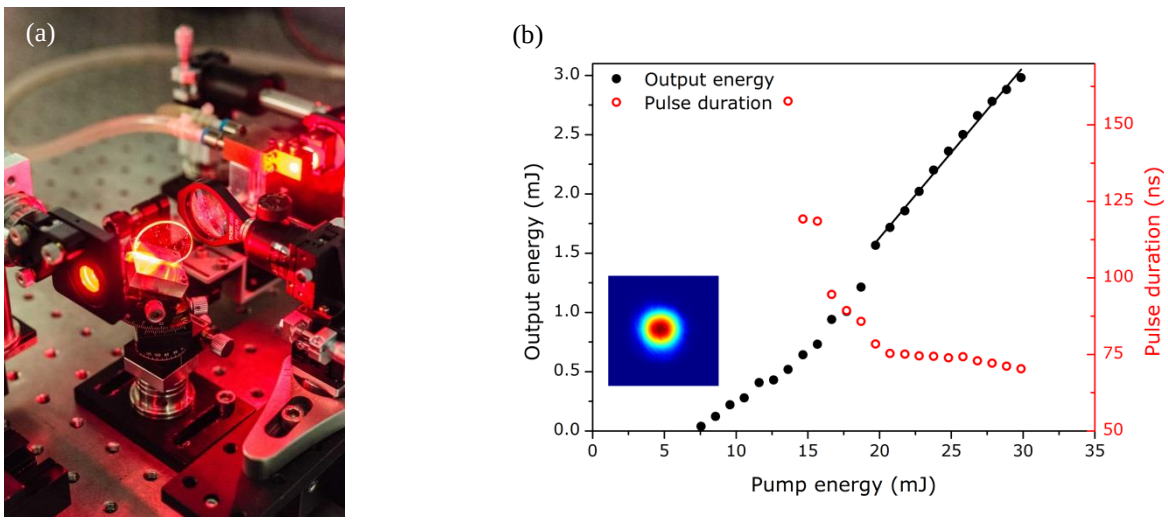

Figure 1: (a) Diode-pumped Alexandrite laser in operation; (b) Q-switched dual-end-pumped Alexandrite laser results with 3mJ pulse energy and pulse duration 70ns.

[1] J. Walling *et al*. "Tunable alexandrite lasers: Development and performance," IEEE J. Quantum Electron. **21**, 1568-1581 (1985).
[2] R. C. Powell, *et al*. "Spectroscopic properties of alexandrite crystals," Phys. Rev. B Condens. Matter **32** (5), 2788–2797 (1985).
[3]A. Teppitaksak *et al*. "High efficiency >26 W diode end-pumped Alexandrite laser," Opt. Express **22**, 16386-16392 (2014).
[4] E. Beyatli *et al*."Tapered diode-pumped continuous-wave alexandrite laser," J. Opt. Soc. Am. B **30**, 3184-3192 (2013).

LSM-1-2 (Invited)

CMOS-Compatible Integrated Rare-Earth Doped Lasers

A. Baldycheva[1,2]

[1]*Photonic Microsystems Group, Research Laboratory of Electronics, Massachusetts Institute of Technology, 77 Massachusetts Avenue, Cambridge, Massachusetts 02139, USA*
[2]*Optoelectronic Systems Group, Department of Engineering, University of Exeter Harrison Building, North Park Road, Exeter EX4 4QF, UK*

On account of the low cost, scalability and compatibility with standardized CMOS electronics, Si microphotonics is an enabling technology for applications ranging from high-speed communications to biomedicine. In fully integrated photonic systems, coherent light generation from miniature low-noise on-chip laser sources is of critical importance. In this talk, we present recent developments in on-chip silicon lasers integrated within the 300 mm silicon photonics platform. Using a novel integration approach that combines rare-earth-doped glasses with silicon-compatible silicon nitride waveguides, the high-power and low threshold monolithic lasers integrated on Si chip are demonstrated.

Distributed Bragg reflector (DBR) lasers are demonstrated on-chip across a broad range of wavelengths, within both the C- and L-bands of the erbium gain spectrum[1]. The grating features of the DBR cavities are defined in silicon nitride waveguide by wafer-scale immersion lithography. A top erbium-doped aluminum oxide layer is deposited using physical vapor deposition (PVD) technology during the final step in the fabrication process. Phase shifted distributed feedback (DFB) structures are created using varying grating periods and strengths with a quarter wavelength defect in the center Lasers with the highest grating strength shows a slope efficiency of 7% and the highest achieves on-chip power of 75 mW[2].

An alternative approach for denser integration of lasers is to use microring resonators[3]. A series of microrings are defined in silicon nitride and a trench in the cladding oxide allows the rare-earth-doped glass to be deposited as the cladding layer. Adjusting the coupling gap between the bus waveguide and the resonator permitted efficient delivery of the pump laser without compromising the quality factor of the cavity. The microtrench sidewall contains the mode and makes tight bends and small resonators possible even though the mode is not highly confined to the high index silicon nitride layer. Microrings proved to be a very versatile laser platform, lasing at wavelengths ranging from 1043 nm to 1560 nm depending on the doping type.

Finally, integrated components necessary for a mode-locked laser are demonstrated on a platform that allows for monolithic integration with active silicon photonics and CMOS circuitry. CW lasing and Q-switched mode-locking are observed in the full structures[4].

1. Purnawirman *et al.* C-and L-band erbium-doped waveguide lasers with wafer-scale silicon nitride cavities. *Opt. Lett.* **38,** 2–5 (2013).
2. Hosseini, E. S. *et al.* CMOS-compatible 75 mW erbium-doped distributed feedback laser. *Opt. Lett.* **39,** 3106 (2014).
3. Purnawirman *et al.* Compact Rare-Earth-Doped Microring Lasers Monolithically Integrated on Silicon Chips. in *CLEO Europe: 2015* CK_12_2 (OSA, 2015).
4. Sorace-Agaskar, C. M. *et al.* Integrated Mode-Locked Lasers in a CMOS-Compatible Silicon Photonic Platform. in *CLEO: 2015* SM2I.5 (OSA, 2015). doi:10.1364/CLEO_SI.2015.SM2I.5

Coherence properties of frequency swept laser sources

Guillaume Huyet

Cork Institute of Technology, Cork, Ireland

LSM-1-4 (Invited)

Visible and IR laser sources based on fluoride hosts doped with rare earths

Stefano Veronesi [1], Alberto Sottile [1,2], Daniela Parisi [1], Eugenio Damiano [1], Zhongan Zhang [1], Alberto Di Lieto [1,2], Mauro Tonelli [1,2],

1- NEST- Istituto Nanoscienze – CNR, Piazza S. Silvestro 12, Pisa, 56127, Italy,
2- Dipartimento di Fisica, Università di Pisa, Largo B. Pontecorvo 3, Pisa, 56127, Italy,

Fluoride hosts represent one of the most important classes of crystalline materials in developing solid state lasers. Notwithstanding their long career as laser media, research is still running in order to obtain best performing materials, cheaper and reliable growth methods or doping solutions which could allow the access to selected wavelengths. Fluoride hosts have been successfully utilized to develop solid state lasers in a wide wavelength range starting from UV to mid IR (300 nm – 4 μm) [1]. They mainly benefit from low phonon energy, usually in the 350-500 cm^{-1} range, which reduces the detrimental non-radiative contributions and weak thermal lensing. Rare earths ions in fluoride hosts exhibit generally long lifetime of their levels, especially in the IR region, making them ideal media for lasers operating in the Q-switched regime.

Focusing our attention on the visible and IR region the most important emitters are Pr^{3+} and Nd^{3+}, Yb^{3+}, Er^{3+}, Tm^{3+}, and Ho^{3+}, respectively. In particular Pr is the most known and widely used visible emitter which can be utilized for a number of laser lines having both technological and/or fundamental relevance. As a dopant in isotropic, uniaxial or biaxial hosts it provides a wide choice of laser wavelengths, starting from blue-green to deep red, quasi diffraction limited beams and high slope efficiencies, up to 38% [2,3]. Few laser results obtained with fluoride hosts grown with both Czochralski and μ-pulling-down methods will be presented. Moreover, fluorides have been successfully utilized to obtain waveguide lasers operating at 604 and 720 nm [4]. Another relevant spectral region for solid state lasers is the IR. Confining our attention to the 2 μm window, the most popular optically active ions are Tm^{3+} and Ho^{3+} as single active ions or in co-doped configurations. Their emission is roughly 100 nm apart, but this difference is essential. In fact Tm emission overlaps a water absorption band, while Ho is almost outside this absorption. In this region the low phonon energy of fluorides and their long living levels (around 14 ms) allow one to obtain very efficient laser emission and high peak power in Q-switched operation. Considering singly doped Tm^{3+} samples, the upper laser level is populated trough the cross relaxation process $(^3H_4, {}^3H_6) \rightarrow (^3F_4, {}^3F_4)$. In hemispherical or microchip cavity configurations slope efficiency (in CW regime) up to ~ 70%, pulse durations (in passively Q-switched regime) as short as 7.6 ns and peak powers up to ~160 kW can be achieved [5]. Holmium doped materials are in band pumped around 1940 nm delivering high slope efficiency and multiwatt emission around 2050 nm [6].

[1] A. Kaminskii, "Laser crystals and ceramics: recent advances," Laser & Photon. Rev. **1**, 93–177 (2007).
[2] A. Sottile, Z. Zhang, S. Veronesi, D. Parisi, A. Di Lieto, and M. Tonelli, "Visible laser operation in a Pr^{3+}:$LiLuF_4$ monocrystalline fiber grown by the micro-pulling-down method," Opt. Mater. Express. **6**, 1964-1972 (2016).
[3] F. Cornacchia, A. Di Lieto, M. Tonelli, A. Richter, E. Heumann, and G. Huber, "Efficient visible laser emission of GaN laser diode pumped Pr-doped fluoride scheelite crystals," Opt. Express **16**, 15932–15941 (2008).
[4] S. Müller, T. Calmano, P. Metz, N.O. Hansen, C. Kränkel, and G. Huber, "Femtosecond-laser-written diode-pumped Pr:$LiYF_4$ waveguide laser," Opt. Lett. **37**, 5223-5225 (2012).
[5] H. Yu, V. Petrov, U. Griebner, D. Parisi, S. Veronesi, and M. Tonelli, "Compact passively Q-switched diode-pumped Tm:$LiLuF_4$ laser with 1.26 mJ output energy," Opt. Lett. **37**, 2544-2547 (2012).
[6] S. Veronesi, Y. Zhang, M. Tonelli, and M. Schellhorn, "Efficient laser emission in Ho^{3+}:$LiLuF_4$ grown by micro-pulling down method," Opt. Express **20**, 18723–18731 (2012)

2.5 kW CW Narrow Linewidth Yb-doped all-fiber Amplifiers for Beam Combining Application

Yunfeng Qi[1],* Yifeng Yang[1], Bing He[1], Jun Zhou[1]

1- Shanghai Key Laboratory of All Solid-State Laser and Applied Techniques, Shanghai Institute of Optics and Fine Mechanics, Chinese Academy of Sciences, Shanghai 201800, China

Main author email address: dreamer_7@mail.siom.ac.cn

Beam combining of fiber lasers has attracted much interest as a practical means to power scale fiber laser/amplifiers beyond the limitations of a single mode output from an individual fiber. [1] Almost all of these high power combining process (coherent or spectral) impose more strict limitations to those individual fiber lasers, especially operation of no more than dozens of GHz level. [2-4] It's hard for those narrow linewidth fiber lasers operation beyond kilowatt output power due to the limitation of nonlinear effects(NLE) and/or degradation of beam quality due to thermo-optical effects.[5,6]

In this paper, we present results on an all fiber master oscillator power amplifier (MOPA) structure with commercially available LMA-YDF-20/400 main fiber seeded by a 50 GHz spectral linewidth master-oscillator. With the optimum mode control and effective cooling technology, 2.52kW cw output power at 1064.1nm is obtained. The slope-efficiency is about 86%, the ASE suppression is about 55 dB and the beam quality is near-diffraction limited around M^2=1.19 at the maximum power. The laser system operated quite stably and no saturation or mode-instability phenomena were observed, which means higher output laser power could be obtained if injecting higher pumping power.

[1] Richardson, D. J., Clarkson, W. A., "High power fiber lasers: current status and future perspectives [Invited]," Opt Soc Am B, Papers 27(11), B63-B92(2010).

[2] Jeong, Y., Sahu, J. K., Payne, D. N., "Ytterbium-doped large-core fiber laser with 1 kW continuous-wave output power," OSA Technical Digest, Advanced Solid-State Photonics, Santa Fe, No. 26 Mexico: PDP13(2004).

[3] Jeong, Y., Sahu, J. K., Payne, D. N., "Ytterbium-doped large-core fiber laser with 1.36 kW continuous-wave output power," Opt Express, Papers 12(25), 6088-6092(2004).

[4] Bonati, G., Voelckel, H., Gabler, T., "1.53kW from a single Yb-doped photonic crystal fiber laser," Late Breaking Developments San Jose: Photonics West, 5709-2a(2005).

[5] Wirth, C., Schreiber, T., Rekas, M., "High-power linear-polarized narrow linewidth photonic crystal fiber amplifier," Proc. of SPIE Vol. 7580 1H(2010)

[6] Eidam, T., Wirth, C., Jauregui, C., "Experimental observations of the threshold-like onset of mode instabilities in high power fiber amplifiers," Opt Express, Papers 19(14), 13218-13224 (2011).

Widely tunable repetition-rate and pulse-duration nanosecond pulses from two spectral beam combined fiber amplifiers

Y. Yang[1], Man Hu[1], B. He[1], Y. Qi[1], and J. Zhou[1]

1- Shanghai Key Laboratory of All Solid-State Laser and Applied Techniques, Shanghai Institute of Optics and Fine Mechanics, Chinese Academy of Sciences, Shanghai, China

Main author email address: bryanho@siom.ac.cn, and yfyang@siom.ac.cn

Repetition-rate-tunable and duration-adjustable high power nanosecond laser sources are of great interest for material processing, remote sensing, telecommunications and laser-matter interactions [1-3]. We demonstrate a spectral beam combining (SBC) work on two pulse Yb-doped fiber amplifier chains. The repetition-rate of the single channel is tuned from 1 MHz to 100 MHz and the pulse-duration can be changed from 4 ns to 400 ns. By setting a proper temporal delay value between two pulse lasers, both the tuning range of repetition-rate and pulse-duration can be twice broadened. The precise adjusting of temporal delay can be realized directly by a common waveform generator. For SBC with more pulse amplifier channels, the tuning range of combined laser can be broadened wider, which makes a significant contribution for many applications in industrial processing and biomedicine areas. It is also worth noting that, when realize the temporal overlap of pulses from the two channels, pulses with doubled average and peak powers are obtained and the tunable characteristics of single pulse channels are remained for the combined pulse laser.

[1] B. R. Washburn, R. W. Fox, N. R. Newbury, J. W. Nicholson, K. Feder, P. S. Westbrook, and C. G. Jørgensen, "Fiber-laser-based frequency comb with a tunable repetition rate," Opt. Express 12, 4999 (2004).
[2] Fabio Di Teodoro, Paul Belden, Pavel Ionov, Nicolette Werner, "High-power ns-pulse fiber laser sources for remote sensors," Optics Fiber Technology 20, 688 (2014).
[3] Chris B. Schaffer, Nozomi Nishimura, Eli N. Glezer, Albert M. T. Kim, and Eric Mazur, "Dynamics of femtosecond laser-induced breakdown in water from femtoseconds to microseconds," Opt. Express 10, 196 (2002).

Prospects of ytterbium-doped, monoclinic magnesium tungstate crystal for optical vortex laser

Wei-Dong Chen[1], Jie-Ling. Lu[1], Li-Zhen Zhang[1] Ge Zhang[1] and Yung-Fu Chen[3]

1- Key Laboratory of Opto electronic Materials Chemistry and Physics, Fujian Institute of Research on the Structure of Matter, Chinese Academy of Sciences, Fuzhou, Fujian 350002, China
2- Department of Electrophysics, National Chiao Tung University, 1001 Ta Hsueh Road, Hsinchu, Taiwan
3- Max-Born-Institute for Nonlinear Optics and Ultrafast Spectroscopy, 2A Max-Born-Str., Berlin D-12489, Germany
Main author email address:chenweidong@fjirsm.ac.cn

Optical vortex, signifying light field endowed with orbital angular momentum (OAM) known as the helical wave, represents a fundamentally new optical degree of freedom [1]. The OAM of light field is regarded as a useful description of spatial degree freedom of light, which comes from spatial distribution of the intensity and phase structure of the optical field, even down to the single photon limit [2, 3].

Ytterbium-doped laser gain media is preferred to the neodymium-doped materials in the spectra range of 1 μm mainly due to the very simple electronic level structure of Yb^{3+} ion eliminating most of the parasitic effects, prolonging energy storage lifetime, extremely low quantum defect and the broadband absorption and emission spectra. Very recently, we developed a new monoclinic crystal, namely ytterbium-doped magnesium tungstate ($Yb:MgWO_4$), by using the method of Top Seeded Solution Growth (TSSG). $Yb:MgWO_4$ crystal possessed the features of very high values of absorption and emission cross section, broader emission and absorption linewidths and the strong anisotropy due to the low-symmetry structure, which making it a promising laser gain medium in the spectra range of 1 μm [4].

Here we present the optical vortex laser demonstration of using an ytterbium-doped, monoclinic magnesium tungstate ($Yb^{3+}:MgWO_4$) crystal, with scaling to the 2.7 W via zero-phonon line pumping. The robust first-order Laguerre-Gaussian doughnut beam with well-determined spiral phase-front trajectory was selectively excited without using any specific intracavity spiral chirality selection components, which signified the promising prospects of the $Yb:MgWO_4$ crystal for generation of optical vortex laser beam. The power scaling and phase front characteristics of $Yb:MgWO_4$ were presented in Fig.1.

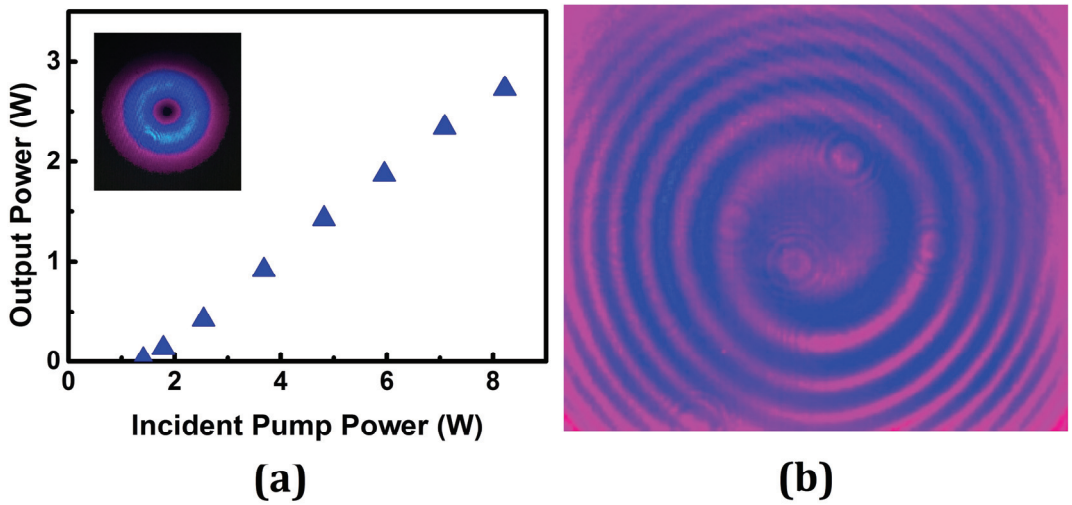

Fig. 1. (a) Power scaling characteristics of $Yb:MgWO_4$ vortex laser and its far-field beam intensity profile of first-order Laguerre-Gaussian beam; (b) the phase front infromation of $Yb:MgWO_4$ vortex laser beam.

[1] X.L. Wang, X.D. Cai, Z.E. Su, M.C. Chen, D. Wu, L. Li, N.L. Liu, C.Y. Lu, and J.W. Pan, Nature **518**, 516-519 (2015).
[2] M. Padgett, J. Courtial, and L. Allen, Phys Today **57**, 35-40 (2004).
[3] S. Franke-Arnold, L. Allen, and M. Padgett, Laser Photonics Rev **2**, 299-313 (2008).
[4] L. Zhang, W. D.Chen, J. L.Lu, H.F. Lin, L.Z. Li, G.F. Wang, G. Zhang, and Z.B. Lin, Opt Mater Express **6**, 1627-1634 (2016).

LSM-2-2 (Invited)

Tm-doped crystalline liquid-phase-epitaxy layers for high power femtosecond lasers at 2 µm

R. Soulard[1], M. Salhi[1], G. Brasse[1], J.L. Doualan[1], A. Braud[1], R. Moncorgé[1], M. Laroche[1], A. Tyazhev[2], T. Godin[2], A. Hideur[2], P. Camy[1]

1- Centre de Recherche sur les Ions, les Matériaux et la Photonique (CIMAP), UMR 6252 CEA-CNRS-ENSICAEN, Normandie Université, 6 Bd Maréchal Juin, 14050 Caen, France
2- CORIA UMR 6614, CNRS-INSA-Université de Rouen, Normandie Université, Av de l'université, B.P. 12, 76801 Saint Etienne du Rouvray, France

remi.soulard@ensicaen.fr

Femtosecond laser sources emitting around 2 µm are raising a great interest for various applications like medical surgery and atmospheric sensing and monitoring thanks to the strong absorption of water and human tissues in this "eye safe" spectral range [1, 2]. These 2 µm laser sources can be also used to pump optical parametric oscillators based on chalcogenide materials emitting in the mid-IR [3].

Among 2 µm lasers systems based on fluorides, there is only few papers using saturable absorbers [4-7] and specially SESAMs [7]. The latter are optical devices that enable very simple self-generation of passive mode-locking and they are commercially available at rather low prices. Our goal is to use them in a short cavity to develop compact and efficient high repetition rate mode-locked 2µm sources. The main interest in using Tm doped materials as active medium in the form of thin disks is because of the efficient thermal management, which can be easily achieved with this type of geometry.

Active structures developed in our group, can indeed be advantageously used in a perpendicular configuration to form so called thin-disks. Until very recently, thin-disk laser devices were made with disks that were mechanically thinned down to few hundreds of microns. The original approach proposed here, is to grow such disks by using the liquid phase epitaxy (LPE), technique in order to solve the problem of mechanical strains inherent to the usual "top-down" thin disk configuration. With the LPE technique, a doped layer of a few hundreds of microns thick can be grown on single crystalline substrates having thicknesses in the millimeter range. In the route towards a multi-pass thin disk configuration, we report here for the first time on the fabrication of a highly doped Tm:LiYF4 layer and its laser operation around 1.9 µm when the layer is pumped perpendicularly to the surface in one single pass.

We also used our samples as one dimensional asymmetrical waveguides exhibiting high gain while keeping good spatial properties. Higher gain can even be obtained when the waveguides are structured as a ridge. In a first step towards waveguide mode-locking operation, we produced short pulses at a 180 MHz repetition rate in a Tm^{3+}: YLF bulk sample using a SESAM. Stable continuous mode-locking has been obtained with good efficiencies with respect to the absorbed pump power. And we will present in this communication the first mode-locking operation in a Tm:YLF waveguide grown by the LPE technique.

[1] K. Scholle, S. Lamrini, P. Koopmann and P. Fuhrberg, 2 µm Laser Sources and Their Possible Applications, LISA laser products OHG-Germany
[2] I.T. Sorokina and K.L. Vodopyanov (eds), Solid-State Mid.Infrared Laser Sources (Springer-verlag, Berlin Heidelberg,2003)
[3] H. Bai, X. Xiong, Y. Wei, W. Pan, S. Gao, Mid-infrared fiber optical parametric oscillator using a three- hole suspended-core chalcogenide fiber, Journal of Physics: Conference Series, vol 679, 012017 (2016).
[4] Y. Bai, M. Qi, S. Wang, R. Shi, D. Li, Z. Ren, and J. Bai, CW Mode-Locked 1.908_m Tm:LiYF4 Slab Laser Based on an Output-Coupling Graphene Saturable Absorber Mirror, Applied Physics Express, 102701 (2013)
[5] A. Schmidt, D. Parisi, S. Veronesi, M. Tonelli, W.B. Cho, S.Y. Choi, J. H. Yim, S. Lee, F. Rotermund, U. Griebner, V. Petrov, Passive mode-locking of a Tm:YLF Laser, CLEO, CMY5 (2011)
[6] X. Zou, Y. Leng, Y. Li, Y. Feng, P. Zhang, Y. Hang, J. Wang, Passively Q-switched mode-locked Tm:LLF laser with a MoS2 saturable absorber, Chines Optics Letters, 13, 081405 (2015)
[7] N. Coluccelli, G. Galzerano, D. Gatti. A. Di Lieto · M. Tonelli · P. Laporta, Passive mode-locking of a diode-pumped Tm:GdLiF4 laser, Appl. Phys. B, 101, 75–78 (2010)

High-Peak-Power Picosecond Lasers with the Dynamical Operation Control

N.G. Mikheev, V.B. Morozov, A.N. Olenin, I.V. Tulin, D.I. Ustinov, D.V. Yakovlev

International Laser Center and Physics Faculty of M.V. Lomonosov Moscow State University, Moscow 119991, Leninskiye Gory

morozov@phys.msu.ru

Picosecond lasers with single pulse energy of a few millijoules, controllable repetition rates within kilohertz, in a compact and reliable design, are claimed in satellite and lunar laser ranging, remote 3d-imaging, time-resolved laser spectroscopy, material processing, driving photoinjectors etc. Advanced pulse-diode-pumped lasers generating ultrashort, mainly picosecond, pulses may utilize dynamical operation control schemes based on active and passive mode-locking, negative feedback and adjustable loss level in the oscillator cavity [1]. Such lasers providing high energy and peak power levels just at the laser output, radiation stability, reasonably low optical jitter [2], enhanced tolerance to environmental conditions, can be easily power scaled and integrated into complicated measuring systems and technological complexes.

In the present paper we demonstrate picosecond pulse-diode-pumped Nd:YAG laser with one amplifier stage operating at repetition rate up to 400 Hz and providing output single pulse energy up to 3 mJ. Both laser and amplifier use diode end-pumping by means fiber coupled laser diode arrays.

At high repetition rates generation conditions strongly depend on thermal lens induced in the laser crystal [3]. Increase of average pump power at longitudinal geometry may result in aberrational lens formation and increasing radiation losses. To provide operation at high repetition frequencies, special efforts should be paid to compensate spherical part of the thermal lens and to minimize the aberrational one.

Using removable Fabry-Perot etalons inside oscillator cavity allows varying output pulse width which can take several different values from 25 and up to 280 ps.

Similar schemes were realized with Nd:YLF lasers providing shorter pulse width within 15 ps.

To describe evolution of time pulse profile a universal model specially aimed at numerical calculation of generation process in advanced pulse-periodic high-peak-power picosecond lasers [4] is used. The model describes pulse formation governed with active and passive mode locking, negative feedback, adjustable loss level in the resonator, and also taking into account the pulse profile modifying due to amplification. Further development of the model is presented.

[1] M.V.Gorbunkov, A.V.Konyashkin, P.V.Kostryukov, V.B.Morozov, A.N.Olenin, V.A.Rusov, L.S.Telegin, V.G.Tunkin, Yu.V.Shabalin, D.V.Yakovlev. Pulsed-diode-pumped, all-solid-state, electro-optically controlled picosecond Nd:YAG lasers. *Quantum Electron.*, **35** (1), 2-6 (2005).

[2] A.A.Karnaukhov, V.B.Morozov, A.N.Olenin and D.V.Yakovlev. *J. Phys.: Conf. Ser.* **414,** 012027 (2013).

[3] V.B.Morozov, A.N.Olenin, V.G.Tunkin, D.V.Yakovlev. Operation conditions for a picosecond laser with an aberration thermal lens under longitudinal pulsed diode pumping. *Quantum Electron.*, **41** (6), 508–514 (2011).

[4] N.G.Mikheev, V.B.Morozov, A.N.Olenin, D.V.Yakovlev. Picosecond lasers with the dynamical operation control. *Proc.of SPIE*, **9917**, 99170A1-9 (2016).

Q-Switched Microchip Laser Development for Range Finding in Space Environment

B. Couto[1], H. Abreu[1], P. Gordo[1], A. Amorim[1]

1- CENTRA-SIM, Dpt. De Física da Faculdade de Ciências da Universidade de Lisboa

bac@sim.ul.pt

In recent years, the number and relevance of unmanned scientific missions to celestial bodies has gained momentum. Reliable and small sized altimetry solutions are of crucial importance for the small landing platforms involved in such missions. In this context, miniature sized pulsed lasers are a strategic asset for ESA.

CENTRA-SIM, in consortium with EFACEC-Space is developing a Q-Switched Microchip laser in the 1550nm region, an atmospheric window both in Earth and in Mars. Preliminary link budget calculations [1] allowed to predict that 200 μJ pulses would provide adequate range for time of flight altimetry.

Er^{3+} doped active media emit in the above mentioned wavelength range and efficient performance is obtained through co-doping with Yb^{3+} to better absorb the pumping light between 0,9 μm and 1 μm [2]. The improvement of Yb-Er:glass properties has allowed a combination of lasing efficiency with mechanical resilience that favours this type of host when compared to crystalline media [3-5]. The desired pulse energy favours passive Q-switching with doped crystalline media, as their semiconductor counterparts are more suited for lower energy ranges [6]. The absorption cross section of Co^{2+} doped spinels has proven to combine well with the emission cross section of Yb-Er:glass for Q-switching applications in the 1,5μm region and so these two materials have been selected as a baseline for our development.

A numerical model was implemented that connects microscopic parameters with the rate equations, along the approaches of Zolotovskaya et al. [7] and Spuhler et al. [8] and preliminary dimensioning of the laser system matching the desired pulse energy was achieved. Experimental confirmation of these results is currently under way.

A robust small size mechanical design for a diode pumped Q-switched microchip laser has been developed. The design allows for careful alignment and positioning while monitoring laser system output. Adequate materials for space operation [9] have been considered and thermal simulations indicate that the design should withstand a wide range of temperatures.

Acknowledgments: This work is partially supported by Fundação para a Ciência e a Tecnologia that provides a PhD scholarship in the frame of the Daephys Doctoral Progam.

[1] J. Abshire, X. Sun, R. Afzal “Mars Orbiter Laser Altimeter: Receiver Model and Performance Analysis” APPLIED OPTICS, Vol. 39, No. 15, 2000

[2] E. Snitzer and R. Woodcock, “Yb3+–Er3+ GLASS LASER,” Applied Physics Letters, vol. 6, no. 3, pp. 45-46, 1965.

[3] S. Jiang, J. Myers, D. Rhonehouse, M. Myers, R. Belford, S. Hamlin, "Laser and Thermal Performance of a New Erbium Doped Phosphate Laser Glass", SPIE Vol. 2138, Longer-Wavelength Lasers and Applications, 1994

[4] G. Karlsson, F. Laurell, J. Tellefsen, B. Denker, B. Galagan, V. Osiko and Sverchkov, “Development and characterization of Yb-Er laser glass for high average power laser diode pumping,” Applied Physics B-Lasers and Optics, vol. 75, pp. 41-46, 2002.

[5] J. MŁYŃCZAK, K. KOPCZYŃSKI, Z. MIERCZYK, M. MALINOWSKA and P. and OSIWIAŃSKI, “Pulse generation at 1.5-μm wavelength in new EAT14 glasses doped with Er3+ and Yb3+ ions,” OPTO−ELECTRONICS REVIEW, vol. 20, no. 1, pp. 14-17, 2012.

[6] U. Keller, “Ultrafast solid-state laser oscillators: a success story for the last 20 years with no end in sight,” Applied Physics B- Lasers and Optics, vol. 100, pp. 15-28, 2010.

[7] S. Zolotovskaya, V. Yumashev, N. Kuleshov and A. Sandulenko, “Diode-pumped Yb,Er:glass laser passively Q-switched with a V3:YAG crystal,” Applied Optics, vol. 44, no. 9, pp. 1704-1708, 2005.

[8] G. Spühler, R. Paschotta, R. Fluck, B. Braun, M. Moser, G. Zhang, E. Gini and U. Keller, “Experimentally confirmed design guidelines for passivelyQ-switched microchip lasers using semiconductor saturable absorbers,” J. Opt. Soc. Am. B , vol. 16, no. 3, pp. 376-388, 1999.

[9] EUROPEAN COOPERATIONFOR SPACE STANDARDIZATION, Space product assurance- Data for selection of space materials and processes, ECSS-Q-70-71A rev. 1- ESA Publications Division, ESTEC.

Sub-THz acousto-optic modulation of chirped femtosecond laser pulses

K.B. Yushkov[1], V.Ya. Molchanov[1]

1- Acousto-Optical Research Center, National University of Science and Technology "MISIS",4 Leninsky Prospekt, 119049 Moscow, Russia

Email address: aocenter@misis.ru

Ultrawide-bandwidth modulation of laser pulses is required in many high-power applications. Bulk electro-optic modulators provide direct modulation with frequencies of the order of 10 GHz. Electro-optic pulse shaping is used in the front-end systems of NIF and LMJ facilities.

In this report, we proposed a new method for adaptive modulation of chirped ultrashort laser pulses with frequencies of the order of 100 GHz. We achieved the progress in pulse shaping by using a high-resolution quasicollinear acousto-optic (AO) Bragg cell. This type of AO interaction is widely used in AO dispersive delay lines (AODL) for femtosecond pulse shaping [1,2]. Ultrasonic waves induce a chirped Bragg grating with spatially-distributed phase matching in a lengthy AO crystal. Diffraction of chirped laser pulses by such grating results in direct time-domain modulation.

The experimental shown in Fig.1 setup consists of a femtosecond laser with the spectrum width of 130 nm centered at 795 nm. Folded Martinez stretcher with the transmission window of 100 nm the was used to obtain chirped pulses with duration of ≈600 ps. Custom homemade AODL had the passband of 0.24 nm the for collimated light [3]. Picosecond streak camera PS-1/S1 with pulse response width of 1.2 ps was used for direct measurement of temporal pulse shape [4].

We measured temporal shape of chirped pulses after rectangular spectrum modulation by the AODL. An example of experimental modulation step response is shown in Fig. 2. Modulation rise/fall time was measured to be 5.0±0.6 ps that corresponds to the bandwidth of 70 GHz.

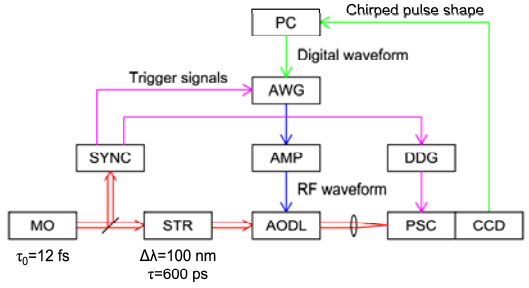

Fig.1 Scheme of the experimental setup: AMP – RF power amplifier; AWG – RF arbitrary waveform generator; DDG – digital delay generator; MO – master oscillator; PSC – picosecond streak camera; STR – stretcher; SYNC – electronic synchronization unit.

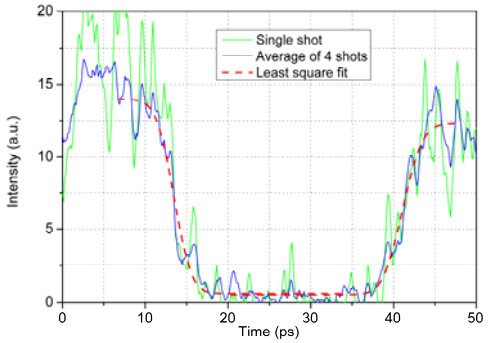

Fig. 2. Temporal response to rectangular spectral modulation: rise/fall time equals to 5 ps. Least square fit was made using the error function as model.

Time-bandwidth product of modulation in our experiment was equal to approximately 45. We estimate that it can be improved up to almost 150. Corresponding estimated modulation bandwidth exceeds 0.15 THz. The bandwidth can be upscaled to the THz frequency region using a stretcher with smaller linear chirp or partial compensation of the second-order dispersion by the compressor.

We expect AO modulation of chirped laser pulses as a promising method for obtaining multi-GHz and THz arbitrary temporal pulse shaping.

[1] V.Ya. Molchanov, S.I. Chizhikov, O.Yu. Makarov, N.P. Solodovnikov, V.N. Ginzburg, E.V. Katin, E.A. Khazanov, V.V. Lozhkarev, I.V. YakovlevAdaptive acousto-optic technique for femtosecond laser pulse shaping. Applied Optics, vol. 48, pp. C118–C124, (2009).
[2] S.I. Chizhikov, S.G. Garanin, L.V. Goryachev, V.Ya. Molchanov, V.V. Romanov, N.N. Rukavishnikov, S.V. Sokolovskii, I.N. Voronich, K.B. Yushkov. Acousto-optical adaptive correction of chirped laser pulse spectral profile in Nd-phosphate glass regenerative amplifier. Laser Physics Letters, vol. 10, p. 015301 (2013)
[3]K.B. Yushkov, V.Ya. Molchanov. MTF formalism for measurement of spectral resolution of acousto-optical devices with synthesized transmission function. Optics Letters, vol. 38, pp. 3578–3580, (2013).
[4] M.Ya. Shchelev. Pico-femto-attosecond photoelectronics: looking through the lens of half a century. Physics–Uspekhi, vol. 55, pp. 607 – 614 (2012).

Time domain thermoreflectance method for measurement of thermal properties of layered materials

***Ertugrul Karademir*[1], *David McCloskey*[1], *Ryan Enright*[2], *Graeme Cunningham*[2], *John Donegan*[1]**

[1] *School of Physics and CRANN, Trinity College Dublin, College Green, Dublin 2, Ireland*
[2] *Nokia Bell Labs Ireland, Blanchardstown Business & Technology Park, Dublin, D15 Y6NT, Ireland*

Main author email address: karademe@tcd.ie

Heat management of lasers is a current and urgent issue in telecommunications. New material research is being done for designing materials that are suitable for controllable heat dissipation during the operation of the laser. However, we are limited with the methods to measure thermal conductivity (TC) of complex materials such as layered thin films which are quite commonly used in telecommunication lasers. Time domain thermoreflectance (TDTR) [1] is pump-probe technique to extract TC of various materials. Here the surface temperature of a material is recorded as a function of time by monitoring the reflectivity of the surface. The method is instrumental in investigation of thermal properties of various material systems. TDTR has been successfully applied to study thermal transport in thin films [2], bulk materials [3], liquids [4], and across interfaces [5,6]. TDTR is also useful for measuring thermal transport across multi layered structures [7]. In our implementation of the method we measure the thermal quality the active device and design novel devices with better heat dissipation, thus increase the efficiency of it. Thus far, we have implemented our version of the setup and measured TC of thin AlN films. Initial results indicate order of magnitude decrease in TC of AlN, from 130 W/m/K to 14 W/m/K.

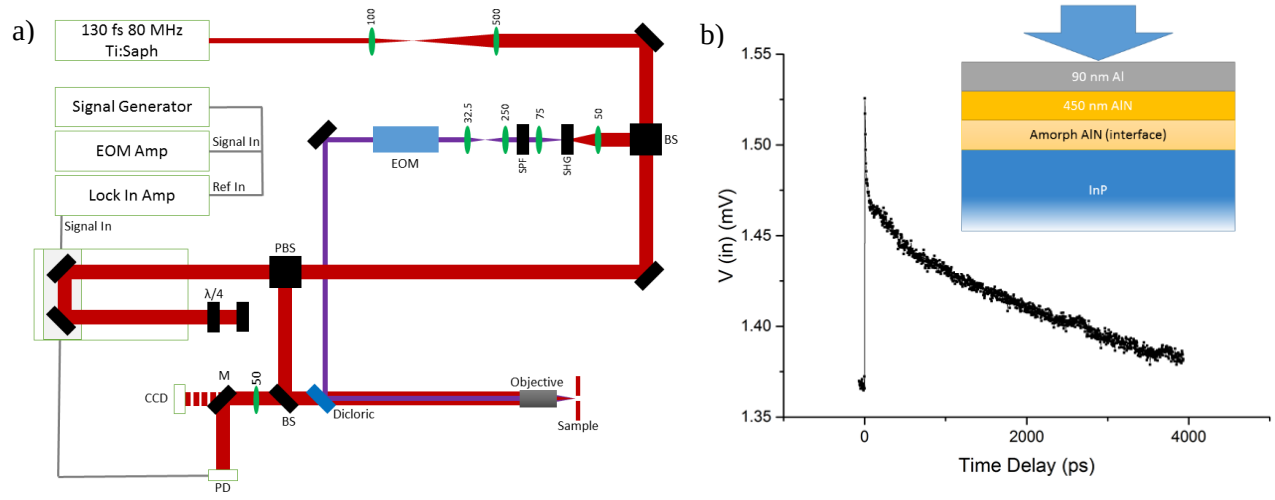

Figure 1 a) The TDTR setup that is built in TCD. Pump wavelength is 415 nm generated by second harmonic crystal and the probe wavelength is 830 nm. b) Time domain response of reflectivity signal. The sample under investigation is presented in the inset.

[1] C. A. Paddock and G. L. Eesley, J. Appl. Phys. 60, 285 (1986).
[2] S. Huxtable, D. G. Cahill, V. Fauconnier, J. O. White, and J.-C. Zhao, Nat. Mater. 3, 298 (2004).
[3] W. S. Capinski, H. J. Maris, T. Ruf, M. Cardona, K. Ploog, and D. S. Katzer, Phys. Rev. B 59, 8105 (1999).
[4] A. Schmidt, M. Chiesa, X. Chen, and G. Chen, Rev. Sci. Instrum. 79, 064902 (2008).
[5] R. M. Costescu, M. A. Wall, and D. G. Cahill, Phys. Rev. B 67, 054302 (2003).
[6] B. C. Gundrum, D. G. Cahill, and R. S. Averback, Phys. Rev. B 72, 245426 (2005).
[7] D. G. Cahill, Rev. Sci. Instrum. 75, 5119 (2004).

LSM-3-1 (Invited)

2D broadband saturable absorbers for Q-switched lasers

X. Mateos[1,2,*], J.M. Serres[1], P. Loiko[1,3], K. Yumashev[3], V. Petrov[2], U. Griebner[2], M. Aguiló[1], F. Díaz[1]

1-Física i Cristal·lografia de Materials i Nanomaterials (FiCMA-FiCNA), Universitat Rovira i Virgili (URV), Campus Sescelades, c/ Marcel·lí Domingo, s/n., E-43007 Tarragona, Spain

2-Max Born Institute for Nonlinear Optics and Short Pulse Spectroscopy, Max-Born-Str. 2a, D-12489 Berlin, Germany

3-Center for Optical Materials and Technologies, Belarusian National Technical University, 65/17 Nezavisimosti Ave., 220013 Minsk, Belarus

Main author email address: xavier.mateos@urv.cat, mateos@mbi-berlin.de

The Q-switching technique enables the generation of short and high energy laser pulses. Compared to active Q-switching, passive Q-switching (PQS) in more compact laser cavities with reduced roundtrip time provides shorter pulses, down to picosecond pulse duration [1]. Such short laser pulses are of special interest at wavelengths around 2 µm for applications in medicine (due to the high water absorption), remote sensing (water and CO_2) and for pumping of mid-IR OPOs.

Since graphene has been used as a SA for lasers [2], other 2D materials such as transition metal dichalcogenides (MoS_2, WS_2 and $MoSe_2$) and black phosphorus emerged [3]. Such 2D materials are attractive for photonic and electronic devices. Among the photonic applications, they are especially important as broadband SAs to cover broad spectral ranges due to their unique band structure, for instance, graphene with zero bandgap or MoS_2 with a transition from indirect to direct bandgap when transforming from bulk to monolayers. Such SAs show very broad linear absorption with absorption saturation from the visible to the near infrared (NIR), as well as low saturation intensity, low non-saturable losses and high damage threshold, desirable characteristics of the SAs. For this reason, new SAs satisfying these requirements are being intensively studied.

The microchip laser concept consists of sandwiching the laser active medium between two plane mirrors or depositing dielectric coatings with proper transmission/reflection for laser oscillation at the desired wavelength directly on the active medium. Such a configuration, only under the condition of positive thermal lens in the active medium, ensures laser mode stabilization and very low intracavity losses. The latter increases the laser efficiency and the pulse energy. The extremely short cavity length provided by the microchip results in further shortening of the roundtrip time, and consequently, of the pulse duration.

In the present work, we report on the application of graphene (and few carbon layers, n = 1, 2, 3 and 4) as well as few-layer MoS_2 SAs in Yb (at ~1 µm) and Tm (at ~1.9 µm) microchip lasers.

Stable Q-switching was achieved with all the SAs. The output characteristics of the PQS Yb and Tm microchip lasers are summarized in Table 1. For the sake of brevity, we present in Table 1 only the results with MoS_2 and n = 3 carbon layers SAs. The latter provided the best results among all the n_i carbon nanostructured SAs studied in this work.

Table 1. Output characteristics of Yb and Tm:KLuW microchip lasers PQS with MoS_2 and graphene SAs

Crystal	SA	P_{out}, mW	η, %	λ_L, nm	τ, ns	PRF, kHz	E_{out}, µJ	P_{peak}, W
Tm:KLuW	MoS_2	1270	43	1929	175	170	7.5	42.7
	graphene	1030	39	1926	190	260	4.0	20.9
Yb:KLuW	MoS_2	147	7	1030	220	300	0.5	2.2
	graphene	315	12	1032	140	320	1.0	7.0

Where P_{out} denotes average output power, η slope efficiency, λ_L the laser wavelength, τ the pulse duration, PRF the pulse repetition frequency, E_{out} the pulse energy and P_{peak} the peak power.

[1] E. Mehner, B. Bernard, H. Giessen, D. Kopf, and B. Braun, Sub-20-ps pulses from a passively Q-switched microchip laser at 1 MHz repetition rate, Opt. Lett., vol. 39, 2940-2943 (2014).

[2] Q. Bao, H. Zhang, Y. Wang, Z. Ni, Y. Yan, Z. X. Shen, K. P. Loh, and D. Y. Tang, Atomic-layer graphene as a saturable absorber for ultrafast pulsed lasers,"Adv. Funct. Mater., vol. 19, 3077–3083 (2009).

[3] S. Wang, H. Yu, H. Zhang, A. Wang, M. Zhao, Y. Chen, L. Mei, and J. Wang, Broadband few-layer MoS_2 saturable absorbers, Adv. Mater., vol 26, 3538-3544 (2014).

LSM-3-2 (Invited)

Cascaded intracavity frequency down-conversion of 1 µm laser radiation to the mid-IR

Valentin Petrov[1], Nadezhda Y. Kostyukova,[1,2,3] Andrey A. Boyko,[1,2,3] Georgi M. Marchev,[1] Valdas Pasiskevicius,[4] Andrius Zukauskas,[4] and Dmitry B. Kolker[3]

1- Max-Born-Institute for Nonlinear Optics and Ultrafast Spectroscopy, 2A Max-Born-Str., D-12489 Berlin, Germany,
2- Special Technologies, Ltd., 1/3 Zeljonaja gorka Str., 630060 Novosibirsk, Russia,
3- Research Laboratory of Quantum Optics Technology, Novosibirsk State University, 2 Pirogova Str., 630090 Novosibirsk, Russia,
4- Department of Applied Physics, Royal Institute of Technology, 10691 Stockholm, Sweden,
e-mail: petrov@mbi-berlin.de

Cascaded or tandem optical parametric oscillators (OPOs) for down conversion of laser radiation into the mid-IR spectral range using non-oxide nonlinear crystals in the second stage have rarely been realized with intracavity pumping [1]. In addition to the more compact and robust design such schemes profit from the higher (intracavity) pump power for the OPO second stage provided by the signal or idler wave of an oxide crystal based OPO first stage, in turn pumped as a rule at 1.064 µm by a Nd:YAG laser system. Compared to pumping inside the cavity of a ns laser, demonstrated in the past with CdSe, $ZnGeP_2$ (ZGP) and orientation-patterned GaAs (OPGaAs) in gain-switched or Q-switched lasers, the cascaded OPO approach offers the flexibility of selecting the most suitable pump wavelength for broadband tunability of the second stage based on a specific non-oxide nonlinear crystal [1]. Previous demonstrations of intracavity pumped (or coupled) tandem OPOs were characterized by limited tunability, maximum up to about 8 µm [2] determined by the doubly-resonant OPO (DRO) scheme and the crystal choice in the second stage. We investigated a singly-resonant OPO (SRO) based on a $AgGaSe_2$ (AGSe) crystal intracavity pumped at ~1.85 µm by the signal pulses of a Rb:PPKTP DRO. Both the choice of a SRO design and the transparency of the AGSe crystal enabled coverage of much broader portions of the mid-IR spectral range. With two AGSe samples cut for type-I and II phase-matching, an extremely broad tuning range for the non-resonated idler was achieved, extending from 5.8 to ~18 µm [3].

Depending on the interaction type in the two nonlinear crystals, by suitable adjustment of the polarizations, the coupled cavity set-up of such a cascaded intracavity pumped OPO can be easily transformed into a self-seeded mid-IR OPO where the two nonlinear crystals share exactly the same doubly-resonant cavity. We studied also such a scheme, equivalent to intracavity difference-frequency generation (DFG) due to the high seed level, employing a similar set-up with the same nonlinear crystals and a dichroic half-wave plate [4]. It is simpler, the overall insertion loss due to the AGSe crystal is reduced and the extraction of the mid-IR radiation can be more efficient. This novel scheme relies on the Rb:PPKTP based DRO as a first stage aiming at high depletion of its signal wave in the second (DFG) stage based on type-I AGSe. Consequently DFG radiation is created in both directions. Notwithstanding expected complications related to relative phases of undepleted waves, we employed a double pump pass. With this scheme, we achieved an average power of 67 mW (100 Hz) at 7 µm equivalent to an overall conversion efficiency from the 1.064 µm pump of 1.2%. The output energy of the mid-IR ns pulse (0.67 mJ) is comparable with the best results achieved by extracavity DFG at 5 Hz [5] but the overall conversion efficiency is two times higher.

[1] V. Petrov, ”Frequency down-conversion of solid-state laser sources to the mid-infrared spectral range using non-oxide nonlinear crystals,“ Progress Quantum Electron. **42**, 1-106 (2015).
[2] P. B. Phua, K. S. Lai, R. F. Wu, and T. C. Chong, “Coupled tandem optical parametric oscillator (OPO): an OPO within an OPO,” Opt. Lett. **23**, 1262-1264 (1998).
[3] A. A. Boyko, G. M. Marchev, V. Petrov, V. Pasiskevicius, D. B. Kolker, A. Zukauskas, and N. Y. Kostyukova, “Intracavity-pumped, cascaded $AgGaSe_2$ optical parametric oscillator tunable from 5.8 to 18 µm,” Opt. Express **23**, 33460-33465 (2015).
[4] A. A. Boyko, N. Y. Kostyukova, G. M. Marchev, V. Pasiskevicius, D. B. Kolker, A. Zukauskas, and V. Petrov, “Rb:PPKTP optical parametric oscillator with intracavity difference-frequency generation in $AgGaSe_2$,” Opt. Lett. **41**, 2791-2794 (2016).
[5] R. Utano and R. J. Ferry, “8-12 µm generation using difference frequency generation in $AgGaSe_2$ of a Nd:YAG pumped KTP OPO,” Advanced Solid-State Lasers, 1997, Vol. 10 of OSA TOPS, paper PC11, pp. 267-269.

LSM-3-3 (Invited)

Megawatt continuous wave intracavity power thin disk laser for the alignment of molecules

C. Kränkel[1,2], B. Deppe[1,2,3,4], G. Huber[1,2,3], J. Küpper[2,3,4]

1. Institut für Laser-Physik, Universität of Hamburg, Luruper Chaussee 149, 22761 Hamburg, Germany
2. The Hamburg Centre of Ultrafast Imaging, Luruper Chaussee 149, 22761 Hamburg, Germany
3. Department of Physics, University of Hamburg, Luruper Chaussee 149, 22761 Hamburg, Germany
4. Center for Free-Electron Laser Science, DESY, Notkestraße 85, 22607 Hamburg, Germany

kraenkel@physnet.uni-hamburg.de

Investigations on the structural dynamics of molecules by time resolved X-ray diffractive imaging in synchrotrons or free-electron lasers [1,2] are greatly simplified by the availability of molecules fixed-in-space aligned or oriented [3]. Free-electron lasers with very large photon fluxes such as the European XFEL or LCLS II, but also synchrotrons, operate at kHz to several MHz repetition rates, sometimes in burst modes. The alignment of gas-phase ensembles of molecules exploits the interaction between the anisotropic polarizability of the molecule and polarized electric fields. Due to the high electric field strengths for strong adiabatic alignment of gas-phase ensembles of molecules in the order of 10^{10}-10^{11} W/cm^2 required over a duration of hundreds of picoseconds or even nanoseconds [4], easily several kW of average power or even MW of continuous wave laser power are needed to provide aligned molecules at synchronized frequencies or even continuously. Therefore, up to now, aligned molecules can only be supplied at few Hz to few kHz frequencies [4], i.e. most of the X-ray pulses are not used effectively.

Here, we propose to provide the necessary field strength in an intracavity focus of a continuous wave thin-disk laser resonator [5] with low output coupler transmission. For this purpose, a TEM_{00} resonator is to be set up, which enables to focus the beam with reasonable Rayleigh lengths to focal beam radii in excess of ω_0 = 10 µm. At this beam diameter, the required field strengths are achieved at intracavity power levels of several 100 kW.

In first proof-of-principle experiments, we investigated a Yb(7%):YAG disk and a Yb(3%):Lu_2O_3 disk [6] in a short linear resonator. In this configuration we obtained more than 100 kW of intracavity power at moderate pump powers in the order of 50 W and a pump spot diameter of 1.2 mm [7]. At higher pump powers we observed a strong heating of the disks and damage in some cases. However, a further scaling of the intracavity power to MW intracavity power levels should be possibly by increasing the pump and laser mode area to realistic values of about 4 mm.

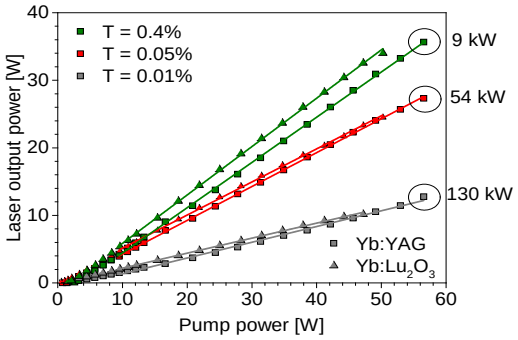

Fig. 1: Laser characteristics of Yb :YAG and Yb:Lu_2O_3 thin disk lasers at low output coupler transmissions T. For the values in circles the continuous wave intracavity power is stated.

[1] P. Emma et. al., "First lasing and operation of an ångstrom-wavelength free-electron laser", Nature Photonics **4**, 641-647 (2010)
[2] J. Küpper, "X-Ray Diffraction from Isolated and Strongly Aligned Gas-Phase Molecules with a Free-Electron Laser", Phys. Rev. Lett. **112**, 083002 (2014)
[3] H. Stapelfeldt and T. Seideman, "Colloquium: Aligning molecules with strong laser pulses", Rev. Mod. Phys. **75**, 543 (2003).
[4] S. Trippel et al.,"Strongly aligned and oriented molecular samples at a kHz repetition rate", Mol. Phys. **111**, 1738 (2013).
[5] A. Giesen et al., "Scalable concept for diode-pumped high-power solid-state lasers", Appl. Phys. B **58**, 363 (1994)
[6] C. Kränkel, "Rare-earth-doped sesquioxides for diode-pumped high-power lasers in the 1-, 2-, and 3-µm spectral range", IEEE J. Quantum Electron. **21**, 250–262 (2015).
[7] B. Deppe et al., "High intracavity-power thin-disk laser for the alignment of molecules", Opt. Express **23** (22), 28491-28500 (2015)

LSM-3-4 (Invited)

Dynamics of color-centers in $KTiOPO_4$ isomorphs induced by picosecond blue-ultraviolet pulses

S. Tjörnhammar[1], V. Maestroni[1,2], A. Zukauskas, C. Canalias[1], F. Laurell[1] and V. Pasiskevicius[1]

[1] *Royal Institute of Technology, Roslagstullsbacken 21, 106 91 Stockholm, Sweden.*

[2] *Politecnico di Milano, Piazza Leonardo da Vinci, 32, 20133 Milano, Italy.*

vp@kth.se

Flux-grown $KTiOPO_4$ (KTP) isomorph family nonlinear crystals, including $RbTiOPO_4$ (RTP), $KTiOAsO_4$, $RbTiOAsO_4$ (RTA) gained widespread use as optical frequency converters and electrooptic modulators in visible and near infrared spectral ranges owing to large nonlinear coefficients and apparent absence of photorefractive beam distortion. Moreover, the arsenate isomorphs KTA and RTA have extended transmission range in the mid-infrared due to lower phonon energy of phonons. Periodic poling using external electric field further increased usability of the crystals, to the point where large aperture high-quality periodically poled Rb:KTP (PPRKTP) structures can be used for high energy parametric devices [1]. Recently, PPKTA has been demonstrated to have excellent performance as high power CW frequency converter to the green spectral range [2]. It has been known that KTP, like most of nonlinear crystals, exhibit color center formation or so called "grey-tracking" when exposed to high-intensity blue and ultraviolet radiation [3]. Although several possible physical mechanisms have been hypothesized, the origin of the color centers in KTP isomorphs, however remained unclear. Here we systematically investigated dynamics of the color-centers induced by picosecond pulses at 398 nm in different periodically poled KTP isomorphs using high-sensitivity thermal-lens spectroscopy [4]. In this technique, the picosecond pulses at 398 nm were used for generation of free carriers primarily by linear absorption into Urbach tails of the electronic bands, while the induced absorption was measured at the wavelength of 1.04 μm. The linearity of the blue-light absorption was determined from the independence of the color center concertation on the blue-light intensity in the intensity range between 37 MW/cm^2 and 733 MW/cm^2. The photo-generated electrons and holes induce electronic polarization on the Ti-O bonds which are mostly contributing to the density of states at the Γ point of the conduction and valence bands. The polarization elicits local distortion of the TiO_6 octahedra resulting in self-trapping of the free carriers, therefore forming polarons. It has been shown that in TiO_6 structural groups the self-trapped electrons and holes form Ti^{4+}/Ti^{3+} and O^{2-}/O^- centers, respectively [5]. Such centers, however, are not stable at room and higher temperatures and require charge compensation in order to produce long-lived absorption centers. Our measurements show that such stabilization is provided by native mobile defects in KTP isomorphs – potassium and oxygen vacancies, making the color center accumulation sensitive to the ionic conductivity of the crystal. This stabilization mechanism competes against the destabilizing action of the polar lattice vibrations. In arsenate isomorphs such as PPKTA, the phonon energy is lower than in PPKTP and there is thermal population of the strongest mode of vibration even at room temperature. This results in drastically faster relaxation of the induced absorption in arsenates and virtually absent accumulation of the absorbing centers. The results of this work provide understanding of the underlying mechanisms behind the color center formation in KTP isomorphs and suggest ways to decrease their effect and to further improve performance of the periodically poled KTP-family crystals.

[1] A. Zukauskas, N. Thilmann, V. Pasiskevicius, F. Laurell, and C. Canalias "5 mm thick periodically poled Rb-doped KTP for high energy optical parametric frequency conversion" Optical Mat. Express, **1**, 201-206 (2011).

[2] P. Zeil, A. Zukauskas, S. Tjörnhammar, C. Canalias, V. Pasiskevicius, and F. Laurell, "High-power continuous-wave frequency-doubling in $KTiOAsO_4$.," Opt. Express **21**, 30453–9 (2013).

[3] M. P. Scripsick, D. N. LoIacono, J. Rottenberg, S. H. Goellner, L. E. Halliburton, and F. K. Hopkins, "Defects responsible for gray tracks in flux-grown $KTiOPO_4$," Appl. Phys. Lett. **66**, 3428 (1995).

[4] J. Hirohashi, V. Pasiskevicius, S. Wang, F. Laurell "Picosecond blue light-induced absorption in single-domain and periodically poled ferroelectrics," J. Appl. Phys., **101**, 033105 (2007).

[5] C. Di Valentin and A. Selloni, "Bulk and Surface Polarons in Photoexcited Anatase TiO_2," J. Phys. Chem. Lett. **2**, 2223–2228 (2011).

LSM-3-5 (Invited)

Research on functional graphene photonic devices and their application to ultrafast fiber laser systems

Dong-Il Yeom

Department of Physics & Department of Energy Systems Research, Ajou University, 443-749, Suwon, Republic of Korea

diyeom@ajou.ac.kr

Graphene, a single atomic layer of carbon atoms arranged in a hexagonal lattice, has been widely investigated with great interest because of its extraordinary optical and electrical properties [1-2]. In particular, its huge Kerr-nonlinearity with ultrafast nonlinear response over broad spectral range facilitated its applications to the nonlinear optic fields. One of the successful applications of the graphene in nonlinear optics includes saturable absorbers (SA), i.e., optical components used for initiating and stabilizing the pulsed laser operation. Indeed there are a number of demonstrations on ultrafast solid-state and fiber lasers based on SAs with layered graphene and graphene related materials such as reduced graphene oxide. Another interesting features of the graphene material is its optical properties can be readily controlled through electrical [3, 4] or optical means [5] by shifting the Fermi level of the graphene, which opens new possibility to realize tunable nonlinear optic devices based on graphene.

In this presentation, we report our recent works about tunable nonlinear photonic devices based on graphene and their application to ultrafast fiber laser system. First, we introduce all-fiber graphene devices that show strongly enhanced nonlinear interaction between evanescent field and mono-layer graphene. Their applications as SAs for stable mode-locking of the fiber lasers are also presented both at normal and anomalous dispersion regimes of the laser cavity over broad spectral ranges from 1 μm to 2 μm [6, 7]. In addition, we show that the saturable absorption properties of the SA can be optically tuned through cross absorption modulation, leading to manipulation of the fiber laser operation to different pulsed laser modes. Secondly, we report the electrical control of all-fiber graphene devices by integrating the graphene field effect transistor onto the side-polished fibers [8]. We simultaneously studied the electrical transport and optical absorption properties of the fabricated device where we observed that the nonlinear absorption properties such as modulation strength and non-saturable loss of the device can be significantly changed with applied voltage of less than few volts. The application of our devices as electrically tunable SAs will also be discussed for ultrafast fiber laser control.

[1] F. Bonabboroso, Z. Sun, T. Hasan, and A. C. Ferrari, “Graphene photonics and optoelectronics,” Nat. Photonics 4, pp.611-622 (2010)

[2] P. Avouris and M. Freitag, “Graphene Photonics, Plasmonics, and Optoelectronics,” IEEE J. Sel. Top. Quantum Electron. **20**(1), 6000112 (2014).

[3] F. Wang, Y. Zhang, C. Tian, C. Girit, A. Zettl, M. Crommie, and Y. R. Shen, “Gate-Variable Optical Transitions in Graphene,” Science **320**(5873), 206–209 (2008).

[4] Z. Q. Li, E. A. Henriksen, Z. Jiang, Z. Hao, M. C. Martin, P. Kim, H. L. Stormer, and D. N. Basov, “Dirac charge dynamics in graphene by infrared spectroscopy,” Nat Phys. **4**(7), 532–535 (2008).

[5] W. Li, B. Chen, C. Meng, W. Fang, Y. Xiao, X. Li, Z. Hu, Y. Xu, L. Tong, H. Wang, W. Liu, J. Bao, and Y. R. Shen, “Ultrafast all-optical graphene modulator,” Nano Lett. **14**(2), 955–959 (2014).

[6] N. H. Park, H. Jeong, S. Y. Choi, M. H. Kim, F. Rotermund, and D.-I. Yeom, “Monolayer graphene saturable absorbers with strongly enhanced evanescent-field interaction for ultrafast fiber laser mode-locking,” Opt. Express **23**(15), 19806–19812 (2015).

[7] H. Jeong, S. Y. Choi, M. H.Kim, F. Rotermund, Y.-H. Cha, D.-Y. Jeong, S. B. Lee, K. Lee, and D.-I. Yeom, "All-fiber Tm-doped soliton laser oscillator with 6 nJ pulse energy based on evanescent field interaction with monoloayer graphene saturable absorber," Opt. Express 24, 14152-14158 (2016).

[8] E. J. Lee, S. Y. Choi, H. Jeong, N. H. Park, W. Yim, M. H. Kim, J.-K. Park, S. Son, S. Bae, S. J. Kim, K. Lee, Y. H. Ahn, K. J. Ahn, B. H. Hong, J.-Y. Park, F. Rotermund, and D.-I. Yeom, “Active control of all-fibre graphene devices with electrical gating,” Nat. Comm. **6,** 6851 (2015).

LSM-3-6 (Invited)

Study Effects of Lasing Degradation and Windows Damage in Diode Pumped Alkali Lasers

B.V. Zhdanov, M.D. Rotondaro, M.K. Shaffer, and R.J. Knize

US Air Force Academy, Laser and Optics Research Center
2354 Fairchild Dr., Ste. 2A31, USAF Academy, CO 80840, USA

Boris.zhdanov.ctr@usafa.edu

Experiments on power scaling of Diode Pumped Alkali Lasers (DPALs) revealed some limiting parasitic effects such as alkali cell windows and gain medium contamination and damage, output power degradation in time and others causing lasing efficiency decrease or even stop lasing [1]. These problems can be connected with thermal effects, ionization, chemical interactions between the gain medium components and alkali cells materials. Study of all these and, possibly, other limiting effects and ways to mitigate them is very important for high power DPAL development.

In this talk we present results of our experiments on temperature measurements in the gain medium of operating Cs DPAL at different pump power levels in the range from lasing threshold to the levels causing damage of the alkali cell windows. For precise contactless in situ temperature measurements, we used an interferometric technique, developed in our lab [2]. In these experiments we observed that damage of the lasing alkali cell starts in the bulk at definite critical temperatures of the gain medium. At this critical temperature, the hydrocarbon and the excited alkali metal begin to react producing the characteristic black soot and, possibly, some other chemical compounds, which both harm the laser performance and significantly increase the harmful heat deposition within the laser medium. This soot, being highly absorptive, is catastrophically heated to very high temperatures that visually observed as bulk burning. This process quickly spreads to the cell windows and causes their damage.

[1] B.V. Zhdanov, M.D. Rotondaro, M.K. Shaffer, and R.J. Knize, "Power Degradation Due to Thermal effects in Potassium Diode Pumped Alkali Laser ", Opt. Comm., 341, 97-100 (2015).
[2] M. K. Shaffer, T. C. Lilly, B.V. Zhdanov, R. J. Knize, "In situ non-perturbative temperature measurement in a ^{133}Cs alkali laser", M. K. Shaffer, T. C. Lilly, B.V. Zhdanov, R. J. Knize, Optics Letters, Optics Letters, Vol. 40, Issue 1, pp. 119-122 (2015)

LSM-3-7 (Invited)

Structural, spectroscopic and lasing properties of $SrMoO_4:Tm^{3+}$single crystals

M.E. Doroshenko[1], L.I. Ivleva[1], G.M. Kuz'micheva[2], E.E. Dunaeva[1], A.G. Papashvili[1]

1-A.M. Prokhorov General Physics Institute RAS, Moscow, Russia
2-Lomonosov Moscow State University of Fine Chemical Technologies

Email address:ivleva@lst.gpi.ru

Strontium molibdate crystal is well-known and highly efficient Raman medium [1]. The development of $SrMoO_4$ crystals doped with Tm ions can provide the oscillation at laser wavelength around 1900 nm which can be further self converted to 2.2 μm spectral ranges at the first Stokes component. The optical quality crystals were grown in the air using Czochralski method and characterized by high absorption cross section of Tm^{3+} ions at $^3H_6$-$^3H_4$ transition [2]. In Tm^{3+} doped matrix the thulium ions can be excited around 800 nm from the ground state to the $^3H_4$ energy level. The upper laser level $^3F_4$ is then populated by a cross relaxation process that occurs between two thulium ions. The efficiency of the cross relaxation process depends on the doping concentration of the thulium ions since the involved dipole-dipole interaction depends on the ion spacing. It is also possible to pump the $^3F_4$ energy level directly between 1700 nm and 1800 nm.

In our work we investigated a series of $SrMoO_4:Tm^{3+}$ samples grown from the melt with different $TmNbO_4$ concentration (from 0.5 to 2.0 wt.%). Taking into account effective segregation coefficient K_{Tm}=0.3 in the medium, maximum concentration Tm^{3+} ions in doped $SrMoO_4$ crystal was 0.08 at.% ($5x10^{19}$ cm^{-3}). The structure peculiarities of the material were studied by X-ray diffraction method. Comparison of spectroscopic and laser properties was carried out for samples under 795 and 1700 nm laser diode pumping.

Following the rules of isomorphous substitution, the sample composition should be (Sr^{2+}, Tm^{3+})(Mo^{6+}, Nb^{5+})O_4. Taking into account the electroneutrality of the system its refined composition must be written as $0 \rightarrow Tm^*_{Sr} + Nb'_{Mo}$. But according to our data its refined composition is supposed to be $0 \rightarrow Tm_i^{n\bullet} + V_{Sr}^{m'} + Nb_i^{p\bullet} + V_{Mo}^{q'}$, what can be explained by the strong difference of 21.4 % for ionic radii Sr^{2+} and Tm^{3+} (r_{Sr2+} =1.26 Å, r_{Tm3+} =0.99 Å). The presence of Nb^{5+}ions at tetrahedral positions which have a larger ionic radius as compared to the ionic radius of Mo^{6+} (r_{Mo6+} = 0.41 Å, r_{Nb5+} = 0.48 Å) could leads to an increase in the size of the tetrahedron. At the same time vacancies were found in Mo positions and Nb ions occupy interstitial positions close to V_{Mo} . Such structural peculiarities cause the specific spectroscopic properties of the material.

Spectroscopic and lasing properties of $SrMoO_4:Tm^{3+}$ crystal were investigated and low efficiency of 790 nm excitation was demonstrated due to negligible contribution of cross-relaxation process to population of upper $^3F_4$ laser level even for $5x10^{19}cm^{-3}$ thulium concentration. It was shown that $^3H_6$-$^3F_4$ absorption and $^3H_4$-$^3H_6$ fluorescence spectra are not overlapped even at room temperature which requires phonon assistance for cross-relaxation process to take place. The gap between fluorescence and absorption spectra is about 1000 cm^{-1} which is very high despite the existence of high energy phonons (887 cm^{-1}) in $SrMoO_4$. Up-conversion fluorescence from $^3H_4$ level under 1700 nm excitation was shown to originate from phonon assisted excited state absorption of pump radiation. Under 1700 nm laser diode pumping efficient room temperature lasing was obtained with slope efficiency up to 18%. Broad oscillation wavelength tuning within 1840-1980 nm spectral range was demonstrated. Thus, $SrMoO_4:Tm^{3+}$ crystal can be considered as a perspective material for development efficient tunable near 2 μm lasers under 1700 nm diode laser pumping.

[1] T.T .Basiev and V.V. Osiko, New materials for SRS lasers, Russian Chemical Reviews,v.75, No. 10, pp. 847-862, (2006).
[2]. E.E. Dunaeva, P.G. Zverev, M.E. Doroshenko, A.V. Nekhoroshikh, L.I. Ivleva, V.V. Osiko, Growth and spectral-luminescent study of SrMoO4 crystals doped with Tm3+ ions, Doklady Physics, Vol. 61, No. 3, pp. 119–123, (2016).

LSM-P-1

The investigation of magnetoresistive effect in thin films of InSb:Mn at room temperature by the I-V characteristics method

V. A. Mikhalevskiy[1], O.D. Khramova[1], O.A. Novodvorsky[1], A.A. Lotin[1], L.S. Parshina[1], E.A. Cherebilo[1], S.F.Marenkin[2], A.N.Aronov[2]

[1]ILIT RAS, Branch of the Federal Scientific Center "Crystallography and Photonics" RAS, 1 Svyatoozerskaya St., 140700, Shatura, Moscow Region, Russia

[2]Kurnakov institute of general and inorganic chemistry of the Russian Academy of Sciences, 31 Leninsky prospect, 119991, Moscow, Russia

Email: uhr@inbox.ru

Ferromagnetic semiconductors (A^{III} - B^{V}):Mn are of great interest for magnetoelectronic and spintronic applications. Theoretical models that describes the characteristics of an ideal transition in a magnetic field, based on the diffusion of carriers through the potential barrier, predict a large magnetoresistance (MR) of ferromagnetic heterojunction **[1]**. Curie temperature of the narrow bandgap semiconductor p-InMnSb achieves 600 K. Heterojunctions p-InMnSb/n-InSb show significant MR and a high degree of spin polarization of the carriers (~ 48% at zero field and 298 K) **[2].** The PLD method allows to produce uniform thin films InSb:Mn from the InSb-MnSb alloy targets with a concentration of manganese up to 20%. In the diode heterostructures p-(InSb:Mn)/n-InSb, produced by PLD the positive MR at 298 K in a magnetic field of 0.15 T was observed **[3].**

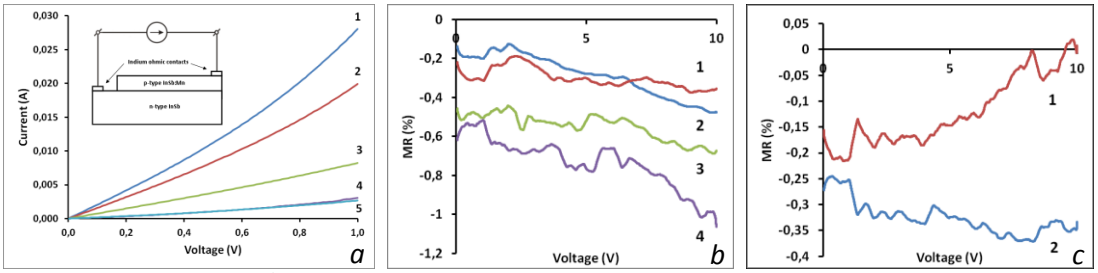

Fig. 1. *a* – I-V characteristics of the p-(InSb:Mn) / n-InSb heteroostructure with B = 0,15 T (1 – **B** = 0, 2 - **E**↑↓**B,** 3 - **E**↑↑**B,** 4 – **B** was oriented from bottom to top of the film, 5 – **B** from top to bottom) and schematic of the structure as insert; *b* – MR of the film vs voltage measured with different out-of-plane magnetic fields (1 – **B** = 0,15 T from bottom to top, 2 – **B** = 0,15 T from top to bottom, 3 – **B** = 1 T from bottom to top, 4 – **B** = 1 T from top to bottom); *c* – MR of the film vs voltage measured with magnetic and electric fields collinear (1 - **E**↑↓**B**, 2 - **E**↑↑**B**).

In this paper, the I-V characteristics of the p-(InSb:Mn) / n-InSb diode heterostructures were measured under different orientations magnetic fields (in the plane of the structure and perpendicular to it) at room temperature (Fig. 1a). Under the collinear direction of the electric and magnetic fields we found different behavior of the p-(InSb:Mn)/n-InSb diode heterostructures I-V characteristics when changing the direction of the magnetic field to opposite, which may be caused by the MR effect in the p-(InSb: Mn) layer. By the method of the I-V characteristics we investigated the effect of MR in InSb:Mn thin films containing 4%, 5%, 10% and 20% MnSb for various orientations of the magnetic field relative to the current direction at room temperature. The I-V characteristics were measured from 0 to 10V, with the different collinear directions of the magnetic field. The R (V) curve was determined from the I-V characteristics. According to the formula (R (H) - R (0)) / R (0) * 100% MR was calculated for each value of V. Dependence of MR (V) are shown in Fig.1b and Fig.1c. The possible reasons for the behavior of dependencies MR (V) in a collinear direction fields are under discussion.

The research was supported by the Russian Foundation for Basic Research projects № 15-07-03331, 15-29-01171, 15-38-20369, 15-07-03580, 16-29-05385, 16-07-00842, 16-29-11719, 16-29-11800.

[1] I. Zutic, J. Fabian, and S. Das Sarma, Spintronics: Fundamentals and applications, REV. OF MOD. PHYS., 76, 323-410, (2004).
[2] J.A. Peters, N. Rangaraju, C. Feeser and B. W. Wessels. Spin-dependent magnetotransport in a p-InMnSb/n-InSb magnetic semiconductor heterojunction, Appl. Phys. Lett., 98, 193506, 2011.
[3] O. D. Khramova, V.A. Mikhalevsky, L. S. Parshina, O. A. Novodvorsky, S. F.Marenkin, A. A. Lotin, E. A. Cherebilo, B. A. Aronzon, A. N. Aronov, V. Ya. Panchenko, Magnetoresistance of the p-(InSb+MnSb)/n-InSb diode structure, 2016, DOI: 10.1007/s11082-016-0609-8

Compact All-Fiber Infrared Broadband Source Based on High-Concentration Er/Yb Composite Optical Fiber

B.I. Galagan[1], O.N. Egorova[2], B.I.Denker[1], V.A. Kamynin[1], A.A. Ponosova[1], S.E. Sverchkov[1], S.L. Semjonov[2], V.B. Tsvetkov[1]

1- General Physics Institute, Russian Academy of Sciences, 119991, Moscow, 38 Vavilova St.
2- Fiber Optics Research Center, Russian Academy of Sciences, 119333, Moscow, 38 Vavilova St.
E-mail: denker@lst.gpi.ru

1. Introduction

Infrared broadband fiber light sources are essential for such applications as fiber-optic gyros, optoelectronic components testing, optical tomography and etc. Rare-earth-doped fibers with phosphate host matrix attract much research interest due to excellent rare-earth ions solubility in contrast to silica matrixes and better physical properties compared to tellurite or fluorite glasses. To the best of our knowledge only one research paper [1] devoted to development of broadband phosphate fiber source, but presented scheme includes bulky optical components.

We report experimental results on a compact all-fiber single-pass forward-signal broadband light source based on high-concentration erbium-ytterbium-codoped composite optical fiber, which takes advantages of both phosphate and silica glasses.

2. Experiment

A highly Er/Yb-doped phosphate-core silica-cladding double-clad fiber was used as source gain medium. The small-signal absorption was about 0,3 dB/m at pump wavelength 971 nm. Output power and emission spectra were measured with varying the pumping power and length of a composite cladding pumped Er/Yb co-doped phosphate core silica cladding optical fiber. The fibers were from 40 to 60 cm long. The output beam from the phosphate fiber end was coupled into single-mode fiber pigtail with angle polished connector.

3. Results

Maximum output power was achieved about 24 mW with the composite fiber just 40 cm long, and was equal to 18 mW for source with the fiber 60 cm long. Spectra of light sources are presented on figure 1. Increasing of active fiber length from 40 cm to 60 cm provide increase of spectral width at the level of -10 dB.

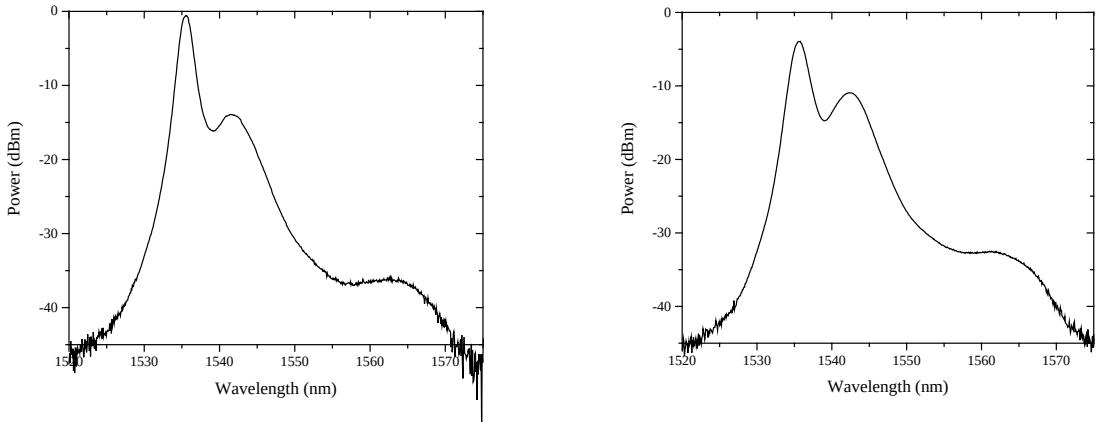

a b

Figure 1 - Output spectra of broadband fiber light sources: a – 40 cm; b – 60 cm.

In summary, we demonstrate the operation of a compact all-fiber broadband high-concentration Er/Yb-codoped phosphate core silica cladding source by employing the conventional forward-signal single-pass configuration. This study was supported by RFBR, the project 14-29-08168 ofi_m.

References:

[1] Feng Song, Zhenzhou Cheng, Changguang Zou, et.al., Compact high power broadband Er3+-Yb3+-codoped superfluorescent fiber source, Appl. Phys. Lett., 93, 091108, (2008).

LSM-P-3

Optical Properties of $Gd_3Al_2Ga_3O_{12}:Ce^{3+}$ Crystals

O. Buzanov[1], V. Kasimova[2], N. Kozlova[2], A. Kozlova[2], V.Shayapov[3], D. Spassky[4], E. Zabelina[2]

1- "Fomos-Materials" Ltd.,. Buzheninova street 16, Moscow, 107023 Russia
2- National University of Science and Technology "MISiS", Leninskii pr. 4, Moscow, 119049 Russia
3- Nikolaev Institute of inorganic chemistry SB RAS, 3, Acad. Lavrentiev Ave., 630090, Novosibirsk, Russia
4- D.V. Skobeltsyn Institute of Nuclear Physics, M.V. Lomonosov Moscow State University, Leninskie gory, GSP-1, 119991, Moscow, Russia

Main author email address: kozlova_nina@mail.ru

Cerium-doped gadolinium–gallium–aluminum garnet ($Gd_3Al_2Ga_3O_{12}:Ce^{3+}$, GGAG:Ce) is a promising new scintillation material which was synthesized for the first time in 2011 [1].
The structure of this crystal belongs to the cubic system, sp. gr. *Ia*3*d* . GGAG:Ce is proposed for use in medical visualization equipment as a sensor element in a positron emission tomograph (PET).
Scintillation properties of GGAG:Ce crystals have been studied intensively. However, an analysis of the data in the literature showed that some fundamental characteristics of this material (in particular, the refractive index) have not been measured.
Thus, the purpose of this study was to determine the optical characteristics of GGAG:Ce crystals by optical spectrophotometry on the UV-Vis-NIR spectrophotometer Cary-5000 (Agilent Technologies) with the accessory "UMA" and the luminescent characteristics.
GGAG:Ce crystals were grown at "Fomos-Materials" Ltd. by the Czochralski method on an upgraded Kristall-3m system. The initial material for growth was a stoichiometric charge prepared by solid-phase synthesis from a mixture of initial oxides of 99.99% purity grade.
The crystals were grown from an iridium crucible 80 mm in diameter in a mixture of argon with 1–2% oxygen.
The spectral dependences of the absorption coefficient of this material were obtained under normal incidence of naturally polarized light in the wavelength range of 250–800 nm; three absorption bands can be observed: in the range $\lambda \sim 420$–460 and near $\lambda \sim 340$ and 270 nm.
Excitation and luminescent spectra were obtained with a deuterium lamp at T = 79 K. The broad emission band with a maximum at the wavelength $\lambda = 530$ nm can be observed.
The reflectance and transmittance spectra were measured for p, s-polarized light in the wavelength range of 300–800 nm at the angle of light incidence of 10º– 75° with a step of 5°; based on these data, the spectral dependences of the absorption coefficient were calculated taking into account the reflection. For obtaining the refractive indices were used two spectrophotometric methods: 1. definition the Brewster angles; 2. measurement of the reflection spectra from one surface at the angle of incidence close to normal [2].
We calculated the refractive indices, plotted the dispersion dependence, and approximated the experimental data using the Cauchy equation. The refractive indices are listed in Table 1[2].

Table 1. Refractive indices of GGAG:Ce

λ, nm	400	425	589	650	700	800
n	1.950	1.937	1.903	1.899	1.898	1.897

[1] K. Kamada, T. Yanagida, T. Endo, et al., 2-inch size single crystal growth and scintillation properties of new Scintillator; Ce:$Gd_3Al_2Ga_3O_{12}$" IEEE Nuclear Science Symposium Conference Record., pp. 1927 , (2011).
[2] N. S. Kozlova, O. A. Busanov, E. V. Zabelina, A. P. Kozlova, and V. M. Kasimova Optical Properties and Refractive Indices of $Gd_3Al_2Ga_3O_{12}:Ce^{3+}$ Crystals, Crystallography Reports, vol. 61, No. 3, pp. 474–478, (2016)

Repetitively Pulsed Cryogenically Cooled Slab RF Discharge Q-switched CO Laser

A.A. Ionin, A.Yu. Kozlov, D.V. Mokrousova, L.V. Seleznev, D.V. Sinitsyn, E.S. Sunchugasheva

P.N. Lebedev Physical Institute of Russian Academy of Sciences, 53 Leninsky prosp., Moscow 119991, Russia
E-mail: aion@sci.lebedev.ru

We previously reported the results on study of physics and engineering of cryogenically cooled slab RF discharge first-overtone CO laser [1]. In this presentation quasi sealed-off operation of the laser was demonstrated by using an active gas mixture with extremely high content of oxygen – up to 50% with respect to CO concentration. The first-overtone CO laser generated up to ~ 2 W of averaged output power within 2.55÷3.90 μm wavelength range with pulse repetition rate from 300 up to 7500 Hz. Of course, the laser setup described in [1] could also operate as a typical fundamental band CO laser within the spectral range of 5÷6 μm. We performed experimental test series using a hybrid waveguide-unstable laser resonator and obtained ~12 W of averaged output power with ~10% efficiency. But the multi-parametric research of this mode of operation was out of our interest, because there are fundamental band CO lasers of different designs including commercial ones.

Nevertheless, for some sort of applications, for instance, for IR laser radiation conversion in non-linear crystal [2], laser pulses with high peak power but not very high pulse energy (to prevent thermal breakdown of the crystal) are needed. The only way for the CO laser to effectively meet these requirements is applying Q-switching or/and mode-locking techniques because of specific features of the laser active medium kinetics: typical laser pulse duration in free-running mode of lasing under pulsed pumping could not be made shorter than a few dozens of microsecond.

In this presentation we will report results of our study of cryogenically cooled fundamental band RF discharge slab CO laser equipped with an external Q-switching system, which is non-traditional for slab lasers and has not been presented elsewhere. The experiments were made with the laser setup described in [1] using V-type double-path resonator with a rotating mirror (Fig.1a).

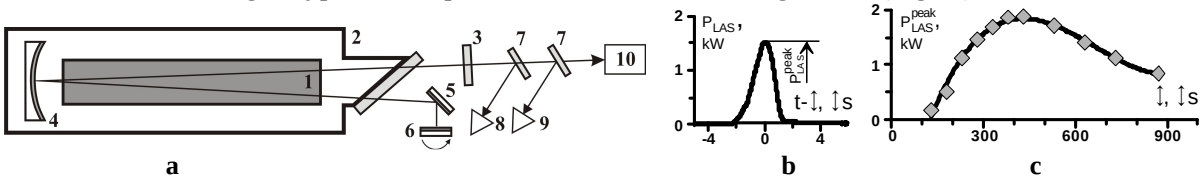

Fig.1. Experimental setup (a), typical Q-switched CO laser radiation pulse waveform (b), and the laser pulse peak power vs. delay time τ between RF pump pulse and Q-switching moment. 1 - electrode system (slab volume 400x16x3 mm^3), 2 - laser chamber, 3 - output coupler, 4 - concave retroreflector, 5 - plane mirror, 6 - rotating mirror, 7 – beam splitter, 8 - photodetector, 9 - power meter, 10 - spectrograph.

The rotating mirror (6000 rpm) was synchronized with RF power supply (carrier frequency 60 MHz, output RF power up to 1 kW) by additional optical sensor (not presented in Fig.1) through the special manually regulated electronic delay driver. Q-switched CO laser pulse repetition rate was 100 Hz with individual pulse duration (FWHM) of ~2 μs (typical waveform is presented in Fig.1b). The laser radiation pulse peak power obtained in the experiments was up to 2 kW (integrated over the whole output spectrum) near the optimal delay time τ~400 μs between RF pump pulse and Q-switching moment (Fig.1c). The laser radiation spectrum covered the interval 5.0÷6.9 μm and consisted of ~70 spectral lines. About half of them (~40 lines) had 20÷80 W of individual peak power. Our analysis of the temporal behavior of each spectral component demonstrated for them to be generated simultaneously unlike in the case of pulsed free running mode when lasing on different spectral lines is typically time mismatched. The results obtained are enough for starting experiments on frequency conversion of the fundamental band Q-switched slab CO laser radiation in non-linear crystals.

The research was supported by the Russian Science Foundation (Grant #16-19-10619).

[1] A. Ionin, A. Kozlov, D. Sinitsyn, Physics and Engineering of Cryogenically Cooled Slab RF Discharge First-Overtone CO Laser, The 23-th Annual International Conference on Advanced Laser Technologies (ALT'15), Faro, Portugal, 2015: Book of Abstracts, p.154 (2015).
[2] O.V. Budilova, A.A. Ionin, I.O. Kinyaevskiy, Yu.M.Klimachev, A.A.Kotkov, A.Yu.Kozlov, G.V. Lanskii, Broadband two-stage frequency conversion of CO laser in $AgGaSe_2$ crystal, Optics Letters, vol.41(4), pp.777-780, (2016).

LSM-P-5

The memristive effect observed in vanadium dioxide at room temperature

L.S. Parshina, O.A. Novodvorsky, A.A. Lotin, O.D. Khramova, V.A. Michalevsky, E.A. Cherebilo, M. N. Esaulkov

ILIT RAS, Branch of the Federal Scientific Center "Crystallography and Photonics" RAS, 1 Svyatoozerskaya St., 140700, Shatura, Moscow Region, RUSSIA

parshinaliubov@mail.ru

The memristors are elements on the basis of which, it is expected, computing and memory devices of new generation and neuromorphic systems will be designed. The memristive effect (change and "storing" of material resistance in the course of current flowing through it) has been revealed in many binary oxides and nitrides of metals and the list of such materials is constantly extending [1]. One of these oxides is vanadium dioxide, the memristive properties of which are demonstrated at the temperature of phase transition [2] or at room temperature under pressure [3]. In our work the structures of Au/VO_2/VO_{2-x}/Au synthesized on the *c*-cut sapphire substrates located on bulk copper foundation at room temperature have been investigated (figure 1a).

In the process of the structures' synthesis by the pulsed laser deposition method the oxygen vacancies *x* were varied by changing of buffer oxygen pressure in the vacuum chamber that allowed reaching the desired conductivity in the depleted injection VO_{2-x} layer [4]. As illustrated in figure 1*b* under the influence of short voltage pulses the resistance of the structure decreases significantly, demonstrating the memristive effect. The typical I-V characteristic of such structure is presented in figure 1*c*.

It is seen that with increasing of the amplitude of voltage pulses (the blue line, the arrow up) and further decreasing of their amplitude (the red line, the arrow down) the structure returns to its initial state, but current magnitude is not the same as primary**,** that illustrates the memristive effect. Thus, a possibility of the use of vanadium dioxide as a working material for creation of memristors at room temperature is demonstrated for the first time.

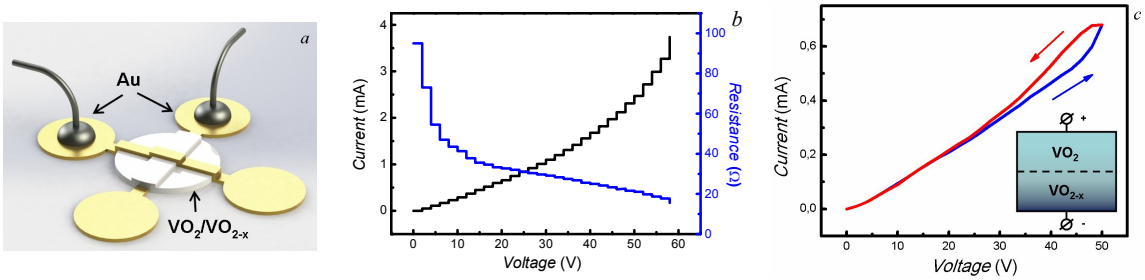

Fig. 1. *a* – The schematic image of the Au/VO_2/VO_{2-x}/Au structures synthesized on the *c*-cut sapphire substrates thermo stabilized at room temperature by copper plate. *b* – Changing of the resistance and current of the structure under the influence of short voltage pulses. *c* – I-V characteristics of the Au/VO_2/VO_{2-x}/Au structure. The inserts represents the schematic image explaining the principle of memristor operation.

The research was supported by the Russian Foundation for Basic Research projects № 15-07-03331, 15-29-01171, 15-38-20369, 15-07-03580, 16-29-05385, 16-07-00842, 16-29-11719, 16-29-11800.

[1] J.J. Yang, D.B. Strukov and D.R. Stewart, Memristive devices for computing, Nature nanotech., vol. 8, pp.13-24 (2014).
[2] Giwan Seo, Bong-Jun Kim, Hyun-Tak Kim, Yong Wook Lee. Thermally- or optically-biased memristive switching in two-terminal VO_2 devices Current Applied Physics, vol. 14, pp.1251-1256, (2014).
[3] Z. You, Y. Zheng, S. Ramanathan, Multi-resistance states through electrically driven phase transitions in VO2/HFO2/VO2 heterostructures on silicon, IEEE Electron Device Lett. vol. 33, pp. 101-103, (2012).
[4] O.A. Novodvorskii, L.S. Parshina, O.D. Khramova, V.A. Mikhalevsky, K.D. Shcherbachev, and V. Ya. Panchenko, Influence of the conditions of pulsed laser deposition on the structural, electrical, and optical properties of VO_2 thin films, Semiconductors., vol. 49(5), pp,577-583 (2015).

LSM-P-6

Kinetic of valence transformation Cr^{4+} ions in Cr-doped YAG ceramic

M. Chaika, O. Vovk, N. Dulina, A. Doroshenko, S. Parkhomenko, O. Tolmachov.

Institute for Single Crystals of National Academy of Sciences of Ukraine, Nauky ave. 60 Kharkiv, 61001 Ukraine

prometeicom@gmail.com

Yttrium-aluminum garnet ceramics doped with Cr^{4+} in tetrahedral coordinate state, (Cr^{4+}:YAG) has the unique characteristics being a saturated absorber for the 1.06 μm laser emission of Nd:YAG [1] as well as being a tunable mid-IR laser in the spectral range of 1.3 to 1.6 μm [2]. As a single dopant Cr incorporated into YAG as a Cr^{3+} in octahedral site. Ionic radius Cr^{3+} is too large to occupy tetrahedral coordinated state. Cr ion should be oxidised to Cr^{4+} to be transfer into tetravalent state a YAG crystalline lattice.

The objective of this study is investigating the kinetics of oxidative transfer Cr^{3+} to Cr^{4+} under the air annealing.

To study the oxidative transferring ions of Cr^{3+} to Cr^{4+}, the garnet ceramics of Ca0.15Y2,85Cr0.05Al4.95O12 was synthesized by reaction sintering at high temperature. Divalent additives of CaO or MgO were used for charge compensation. The phase composition was determined as YAG structure. Average size of the grains of obtained ceramics was 2.2 μm distributed from 0.5 to 5 μm. The ions of Cr^{4+} were no presented initially in the ceramic samples. The concentration changing of these ions under annealing was performed by measuring optical absorbance of one. The time dependence of ion concentration Cr^{4+} at four evaluated temperatures was carried out to determine activation energy.

Time dependence concentration of Cr^{4+} ion in octahedral and tetrahedral crystallographic position shows same behaviour. That indicating formation of Cr^{4+} in these positions limited same stage. To describe oxidative kinetic of Cr^{4+} ions were used Jander model. According to this model recharging Cr^{3+} ions is controlled by diffusion process (Figure 1a). The value of activation energy process of recharging Cr was calculated. Obtaining activation energy has been estimated of 2,67 ± 0.21 eV (Figure 1b), which coincides with literature data for energy of activation oxygen into YAG ceramics [3]. As results was establish that oxidative transfer Cr^{3+} to Cr^{4+} in ceramics Ca0.15Y2.85Cr0.05Al4.95O12 is limited by diffusion of oxygen into ceramics.

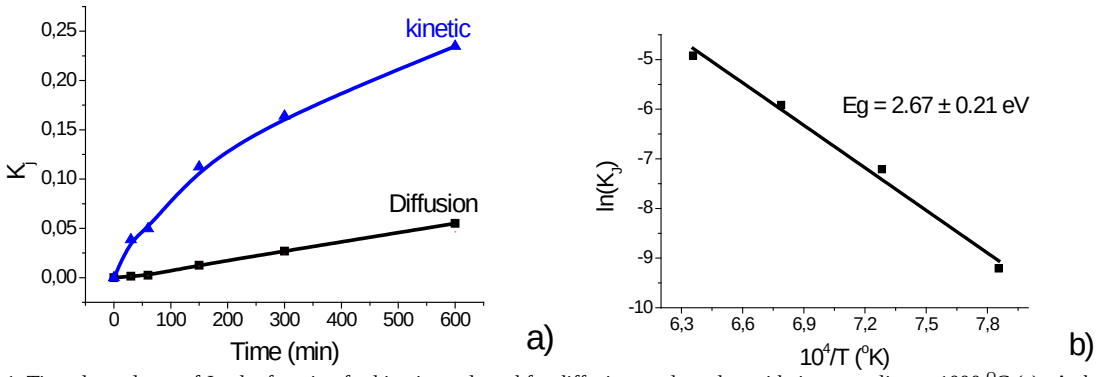

Figure 1. Time dependence of Jander function for kinetic mode and for diffusion mode under oxidative annealing at 1000 ^{O}C (a), Arrhenius plot of oxidation of Cr^{4+}ions (b).

[1] ZHU, Siqi, et al. High average power passively Q-switched laser diode side-pumped green laser by using Nd:YAG/Cr^{4+}:YAG/YAG composite crystal. Journal of Laser Applications, 26.3, 032009, 2014.

[2] Angert, N. B., Borodin, N. I., et al. Lasing due to impurity color centers in yttrium aluminum garnet crystals at wavelengths in the range 1.35–1.45 μm, Soviet Journal of Quantum Electronics, 18.1, 73, 1988.

[3] Li, Zhen, et al. Mechanism of Intrinsic Point Defects and Oxygen Diffusion in Yttrium Aluminum Garnet: First Principles Investigation, Journal of the American Ceramic Society 95.11, 3628-3633, 2012.

LSM-P-7

Radiation dynamics of a singly-resonant intracavity optical parametric oscillator pumped by a semiconductor disk laser

Yu. A. Morozov

Kotelnikov Institute of RadioEngineering & Electronics (Saratov Branch), Russian Ac. Sci.
38 Zeleonaya Str. 410019, Saratov, Russia

yuri.mor@rambler.ru

Nonlinear optical frequency conversion is proved to be an effective method for generating coherent emission in wide spectral region including the mid- and far-infrared [1]. Among the most suitable devices for implementation of optical frequency conversion, continuous-wave optical parametric oscillators (OPOs) have to be mentioned. Singly-resonant OPOs (SROs) are known to be more simple and easy-to-use devices than their doubly- and triply-resonant counterparts. It should be noted, however, that SROs typically need tens-of-watt lasers to overcome the threshold of stimulated parametric generation. At the same time, power oscillating in a high-finesse cavity of a laser is known to be greatly enhanced in comparison with output power of the laser. Hence, in order for a SRO to be a subject of enhanced power it would be located in the laser cavity. Such an intracavity SRO (ICSRO) was demonstrated first with a titanium sapphire laser [2] and subsequently with a neodymium laser [3]. Unfortunately, an ICSRO based on a neodymium laser shows pronounced relaxation oscillations of output wave intensity due to its long-lived upper-state of gain media. To eliminate this disadvantage, pumping of an ICSRO by a vertical external cavity surface-emitting laser (VECSEL), which is also referred to as a semiconductor disk laser, has been proposed a few years ago by D.J.M. Stothard *et al.*[4]. In their device, the pump and signal optical fields have wide spectral separation (the wavelength of the pump field is 1.05 μm and that of the signal is 1.6 μm). This allows for using a dichroic beamsplitter for spatial separation the pump and the signal cavities. For an ICSRO with closer wavelengths of the pump and signal fields, making a suitable beamsplitter appears to be a challenging task.

Recently, we have proposed the continuous-wave ICSRO pumped by a semiconductor disk laser with the joint cavity for the both pump and signal radiation [5]. An application of this conception allows to avoid using a dichroic beamsplitter thus making the device more compact (the cavity may be as short as 15-20 mm) and easy-to-use. For closely spaced wavelengths of the pump (1.98 μm) and signal (2.25 μm), their cavity mode separation is approximately the same. This makes the pump and signal to be multi-mode optical fields because they could effectively interact in a nonlinear crystal via idler emission. The mathematical model of the intracavity parametric generation should thus be built with consideration this multi-mode nature of the pump and signal emission. Our model improves that of Ref.[6], where single-mode signal emission has been assumed. Using the multi-mode model, we numerically analyze the transient dynamics of the ICSRO [5] and determine the conditions for single-mode steady-state operation of the device. The nonlinear optical interaction in the laser cavity was shown to have a strong impact on the dynamics. The main manifestation of this impact consists in transfer of emission intensity from a center of laser (pump) line to its edges thus resulting in multi-mode oscillations. It was shown that inserting an additional frequency selective element (e.g. a Fabry-Perot etalon) makes the ICSRO emit single-mode in a steady-state operation.

[1] Solid-state mid-infrared laser sources, T. Sorokina, K. L. Vodopyanov, Eds.(Springer-Verlag Berlin Herather idelberg), Chapter 11, (2003).

[2] F. G. Colville, M. H. Dunn, M. Ebrahimzadeh, Continuous-wave, singly resonant, intracavity parametric oscillator, Opt. Lett., vol.22, pp.75-77, (1997).

[3] D. Stothard, M. Ebrahimzadeh, M. Dunn, Low pump threshold, continuous-wave, singly resonant, optical parametric oscillator, Opt. Lett., vol.23, pp. 1895-1897, (1998).

[4] D. Stothard, J. Hopkins, D. Burns, M. Dunn, Stable, continuous-wave, intracavity, optical parametric oscillator pumped by a semiconductor disk laser (VECSEL), Opt. Express, vol.17, pp. 10648-10658, (2009).

[5] Yu. A. Morozov, M. Yu. Morozov, V. I. Kozlovsky, O. G. Okhotnikov. Compact intracavity singly-resonant optical parametric oscillator pumped by GaSb-based vertical external cavity surface-emitting laser: Concept and the main operational characteristics. IEEE Journ. of Sel. Top. in Quantum Electronics, vol.21, pp.1603105-1—1603105-5, (2015).

[6] G. A. Turnbull, M. H. Dunn, M. Ebrahimzadeh, Continuous-wave, intracavity optical parametric oscillators: an analysis of power characteristics. Appl. Phys. B, vol.66, pp.701-710, (1998).

LSM-P-8

Athermal performance of single mode slotted high-order semiconductor lasers

M. Wallace[1,2,3], D. McCloskey[1,2,3], R. Meehan[4], R. Enright[1], E. Karademir[1,2,3], G. Jain[1,2,3], J. F. Donegan[1,2,3]

1- School of Physics, Trinity College Dublin, Dublin 2, Ireland
2- Centre for Research on Adaptive Nanostructures and Nanodevices (CRANN), Trinity College Dublin, Dublin 2, Ireland
3-Advanced Materials and BioEngineering Centre (AMBER), Trinity College Dublin, Dublin 2, Ireland.
4- Efficient Energy Transfer Department (ηET), Bell Labs, Nokia Ireland Ltd., Dublin, Ireland

wallacmj@tcd.ie

An athermal bias current control procedure is demonstrated for three section slotted single mode laser in which the laser wavelength and power does not vary with changes in temperature. This control procedure leverage's separate gain, grating and semiconductor optical amplifier (SOA) sections to achieve wavelength stability of ±0.04 nm / ±5 Ghz and output power stability of ±0.1 mW over a 40°C temperature range. Athermal wavelength and power performance is achieved with a three section design as seen in figure 1. The design allows individual control over separate sections of the laser making it possible to maintain both stable power and wavelength by applying the appropriate currents for a given temperature. In addition the control scheme does not require any wavelength or power feedback, relying only on the bulk temperature measurement of the system and pre-calibration. Such a control procedure allows one to run lasers un-cooled – eliminating or reducing the dependence on Peltier coolers, which represent a large proportion of energy consumption.

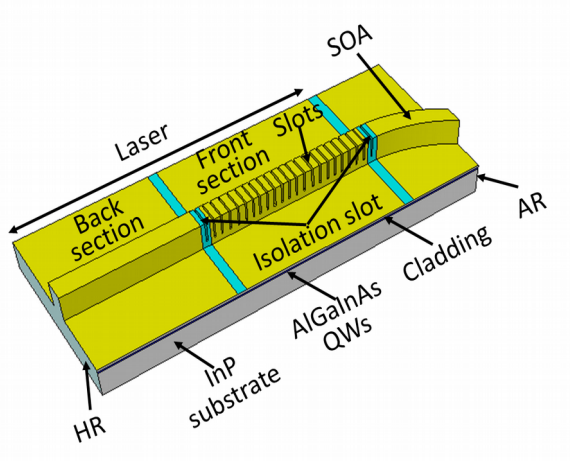

Figure 1: Slotted Fabry Pérot design.

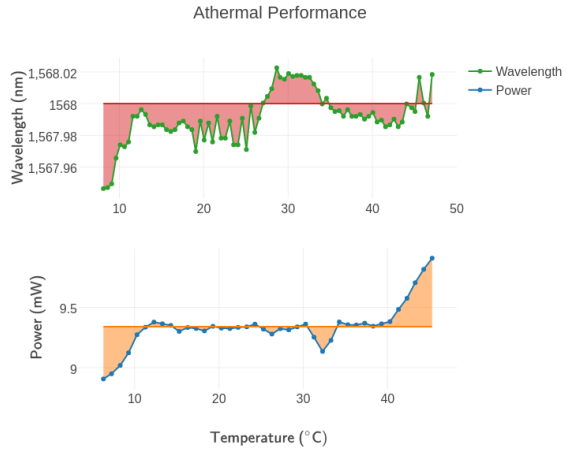

Figure 2: Wavelength and output power with temperature.

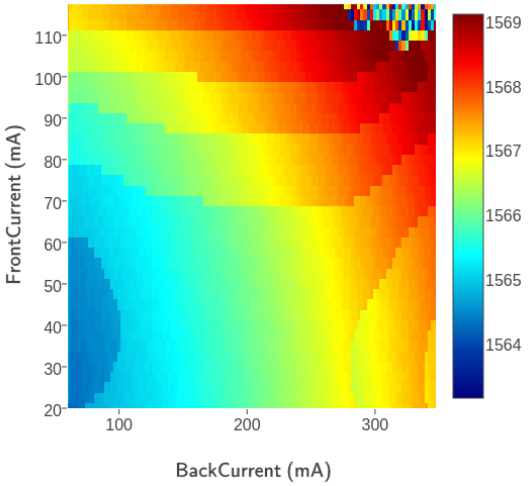

Figure 3: Wavelength tuning map.

LSM-P-9

High Power Fiber Lasers and Beam Combining Technology in SIOM

B. He[1], Y. Yang[1], Y. Qi[1], and J. Zhou[1]

1- Shanghai Key Laboratory of All Solid-State Laser and Applied Techniques, Shanghai Institute of Optics and Fine Mechanics, Chinese Academy of Sciences, Shanghai, China

Main author email address: bryanho@siom.ac.cn,and yfyang@siom.ac.cn

Fiber amplifier has been established as reliable and promising high-power laser architecture owing to its advantages like compactness, high conversion efficiency and excellent heat dissipation [1]. The increasing demand for high power laser sources with diffraction-limited beam quality has led to a significant scaling in output power [2]. Spectral beam combining (SBC) and coherent beam combining (CBC) technology has been developed to upgrade the power level while maintaining excellent beam quality, at the same time, avoid some limitation of monolithic fiber amplifier, such as thermal damage, nonlinear effects, and modal instability [3]. SIOM have been working for more than 15 years committing to build narrow linewidth single mode fiber laser and high brightness beam combining system. A record of 50 GHz linewidth 2.5 kW fiber amplifier with integration design is achieved lately. An 8 channel 10.8 kW SBC system is established by 1.5 kW-level all-fiber superfluorescent sources. A 4 channel 5.4 kW passive CBC system is established by an all-optical feedback loop.

[1] A. Tünnermann, T. Schreiber, F. Röser, A. Liem, S. Höfer, H. Zellmer, S. Nolte, J. Limpert, J. Phys. B 38, S681-S693 (2005).
[2] J. Limpert, F. Röser, S. Klingebiel, T. Schreiber, C. Wirth, T. Peschel, R. Eberhardt, and A. Tünnermann, IEEE J. Sel. Top. Quantum Electron. 13(3), 537-545 (2007).
[3] T. Y. Fan, IEEE J. Sel. Top. Quantum Electron. 11(3), 567-577 (2005).

LSM-P-10

Optical Parametric Generation in Orientation-Patterned Gallium Arsenide

B. Donelan[1], C. Kneis[1], G. Scurria[1], B. Cadier[2], T. Robin[2], E. Lallier[3], A. Grisard[3], B. Gérard[4], M. Eichhorn[1], C. Kieleck[1]

1- French-German Research Institute of Saint-Louis, 5 Rue du Général Cassagnou, 68301 Saint Louis, France
2- iXFiber, Rue Paul Sabatier, 22300 Lannion, France
3- Thales Research and Technology France (TRT), RD 128, 91767 Palaiseau Cedex, France
4- Alcatel-Thales 3-5 Lab, RD 128, 91767 Palaiseau Cedex, France

brenda.donelan@isl.eu

There is a necessity for development of mid-infrared coherent sources for applications such as spectroscopy, medicine, and material processing. Orientation-Patterned Gallium Arsenide (OP-GaAs) is an attractive material for non-linear conversion in the infrared regime, owing to its broad transparency from 0.8 μm - 18 μm, and high effective non-linearity. Using 2 μm pump sources, high output power, high efficiency and excellent beam quality can be reached. Previously, we reached with OP-GaAs, in Optical Parametric Oscillator (OPO) experiments, output powers of 7.7 W (Ho^{3+}:YAG pump) and 2.2 W (Tm^{3+},Ho^{3+}-codoped fiber pump) [1]. Optical Parametric Generation (OPG) has been achieved in OP-GaAs before, using a regeneratively amplified Ti:sapphire laser down-converted through optical parametric amplification and difference-frequency generation pump [2].

Here, we employ a very simple pump source, consisting of a single oscillator fiber laser, to directly pump OPG in OP-GaAs. The pump source is a novel Q-switched mode-locked (QML) Tm^{3+}:silica fiber laser, wherein the train of mode-locked (ML) pulses is modulated by a Q-switched (QS) envelope. This allows for higher pulse energy and peak power than either ML or QS alone [3]. The QML laser has a fiber length of 2.2 m, and the cavity was closed with a grating, giving feedback at 1.99 μm. The laser has achieved output power of 25 W in QML (180 kHz QS). It was operated at a QS repetition rate of 40 kHz and a ML rep. rate of 40 MHz. The slope efficiency was 25%. The OPG experiments were performed at a pump power of 7 W, with a total pump pulse energy of 175 μJ distributed over the ML sub-pulses within the QS envelope. The duration of each ML sub-pulse is <2.5 ns. The OP-GaAs crystal is 34 mm long, has a period of 63.8 μm and an OP height of ~500 μm.

In Figure 1(a), the OPG output power versus incident pump power is shown. The total conversion slope efficiency reached was 4.1%, with a slope efficiency of 3.5% and 0.7% for signal and idler, respectively. The threshold for the OPG process was 35 μJ. The maximum output energy reached was greater than 2.0 μJ (82 mW) for the combined signal and idler. The spectrum of the signal at 2.81 μm and idler at 6.88 μm can be seen in Figure 1(b). Attenuation of the idler was present due to strong water absorption lines in this spectral region, which can be seen as dips in the emission spectrum.

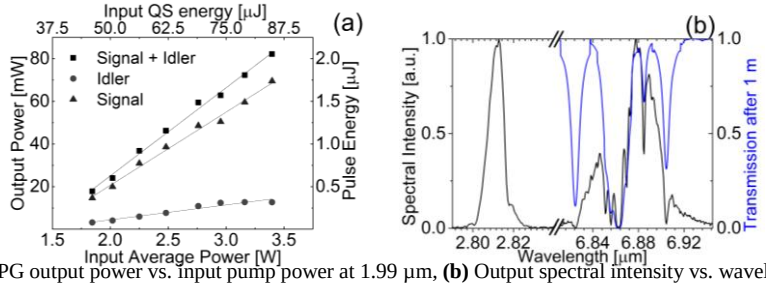

Fig. 1 (a) OPG output power vs. input pump power at 1.99 μm, **(b)** Output spectral intensity vs. wavelength of the OPG process with overlay of atmospheric transmission spectrum in blue, water responsible for attenuation

To the best of our knowledge, we have demonstrated the highest output energy from OPG in OP-GaAs by a factor of 25 [2].

[1] C. Kieleck, A. Hildenbrand, M. Eichhorn, D. Faye, E. Lallier, B. Gérard, S. D. Jackson, "OP-GaAs OPO pumped by 2μm Q-switched lasers: Tm;Ho:silica fiber laser and Ho:YAG laser", Proc. SPIE 7836, 783607 (2010).

[2] P. S. Kuo, K. L. Vodopyanov, M. M. Fejer, D. M. Simanovskii, X. Yu, J. S. Harris, D. Bliss, and D. Weyburne, "Optical parametric generation of a mid-infrared continuum in orientation-patterned GaAs", Opt. Lett. 31, 71-73 (2006)

[3] C. Kneis, B. Donelan, A. Berrou, I. Manek-Hönninger, B. Cadier, T .Robin, M. Poulain, F. Joulain, M. Eichhorn, C. Kieleck, "4.5 W mid-infrared supercontinuum generation in a ZBLAN fiber pumped by a Q-switched mode-locked Tm^{3+}-doped fiber laser", Proc. SPIE 9342, 93420B (2015).

LSM-P-11

The acousto-optically Q-switched Tm:Ho:YbAG laser pumped at 1678 nm

Yu.D.Zavartsev, A.I.Zagumennyi, Yu.L.Kalachev, S.A.Kutovoi, V.A.Mikhailov, I.A.Scherbakov

A.M. Prokhorov General Physics Institute, RAS, Moscow, Russia

mihailov@kapella.gpi.ru

The first experiments with Tm:Ho:YbAG (Tm:Ho:$Yb_3Al_5O_{12}$) crystal demonstrated its high laser efficiency in CW regime in 2 um spectral range under pumping by Raman shifted Erbium fiber laser at 1678 nm [1].

Here we report results of study of the laser characteristics of the acousto-optically Q-switched Tm:Ho:YbAG laser. These experiments have been fulfilled at conditions analogical to [1]. Active element was cut out along [100] in form of cube with an edge length of 3 mm without coatings. The concentration of Tm^{3+} and Ho^{3+} ions in the active elements was 6,4% and 0,8%, respectively. Tm:Ho:YbAG crystal was pumped by a Raman shifted Erbium fiber laser at 1678 nm ($^3H_6$-$^3F_4$ Tm^{3+} ions transition). Hemispherical laser cavity was formed by a high reflection flat mirror and 50 mm radius of curvature of output coupler with ~97% reflectivity. The crystal was grown by the Czochralski method from an iridium crucible.

An acoustic optical modulator with the effective length ~ 30 mm and driving frequency 80 MHz was inserted in the laser cavity to realize stable Q-switched laser operation. Radio frequency power was ~ 10 W. Both parallel surfaces of the quarts modulator were antireflection coated for 2 um. A stable Q-switched regime of laser operation was realized (Fig.1).

Slope and total laser efficiencies reached the highest values ~ 20 - 30% and ~11% at pulse repetition rates > 50 kHz. Laser pulses duration reduced with increasing of absorbed pump power up to lowest value ~ 40 ns at 740 mW of pumping (Fig.2).

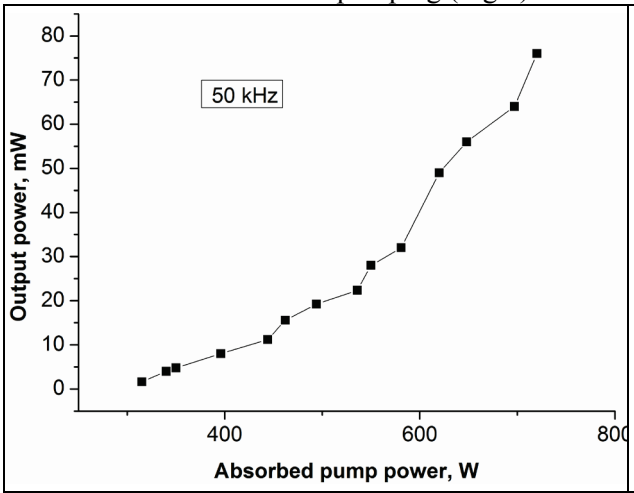

Fig.1. Laser output power versus absorbed pump power.

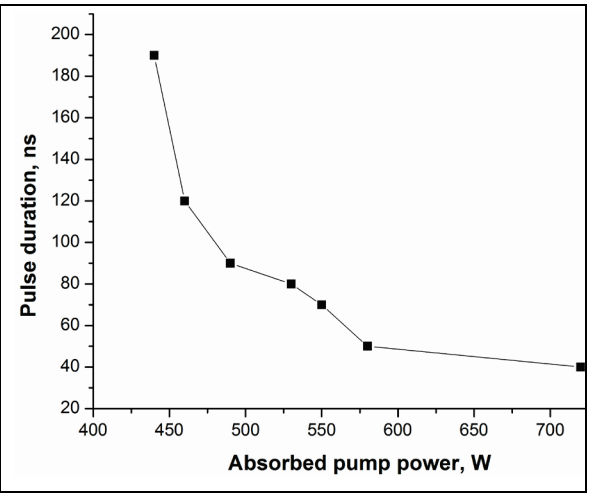

Fig.2. Pulse duration versus absorbed pump power..

Reduction of pulse repetition rates lower 50 kHz under the same incident pump power leads to reduction laser efficiency. This fact allowed to estimate under this experimental conditions luminescent lifetime ~ 20 us. Such lower experimental value of lifetime can be explain as result of energy transfer in result of upconversion effect. The central wavelengths of laser emission for CW and Q-switched modes of operation were the same ~ 2,1 um.

This work was supported by the Russian government in the frame of Program of RAS.

[1] V.A.Mikhailov, Yu.D.Zavartsev, A.I.Zagumennyi, Yu.L.Kalachev, S.A.Kutovoi, I.A.Shcherbakov. "Laser operation of Tm:Ho:YbAG crystal pumped at 1678 nm" International Conference ALT-2014, 6-10 October, 2014, Cassis, France, Book of Abstracts, p.P30, 2014.

LSM-P-12

N_2-laser with electrohydrodynamic flow circulation system

Yu. V. Khomich[1], I. E. Rebrov[1], V. A. Yamshchikov[1]

1- Institute for Electrophysics and Electric Power RAS, Dvorzovaya Naberezhnaya 18, 191186, Saint-Petersburg, Russia

Re_i@rambler.ru

Electrohydrodynamic system for electric discharge N_2-laser integrated in gas circulation and cooling contour was investigated. Experimental studies and mathematical modeling of gasdynamic processes in EHD flow considering configuration of circulation chamber and the area of discharge gap of 200 cm^3 were carried out.

EHD circulation system consists of multiple plasma emitters (PE) and ion collectors. To determine the optimal parameters of the system computer simulation was used. The amount of cascade stages, number of emitters in each stage and their mutual position were varied to achieve maximum flow. The operation of the device, depending on the supply voltage and the amount of plasma emitters was studied.

Calculation model was based on a system of equations describing the dynamics of the ions in a gaseous medium in an external electric field. On the basis of Poisson, electric potential, continuity equation for current, Navier-Stokes equations for steady state incompressible gas flow equations was calculated distribution of an electric field, space charge density and EHD flow velocity in two spatial coordinates in a plane transverse to the electrodes. The model has the following assumptions: plasma emitter is a cylinder with uniform distribution of surface charge; the thickness of the plasma layer at the emitter is negligible; model takes into account only the particles of one charge.

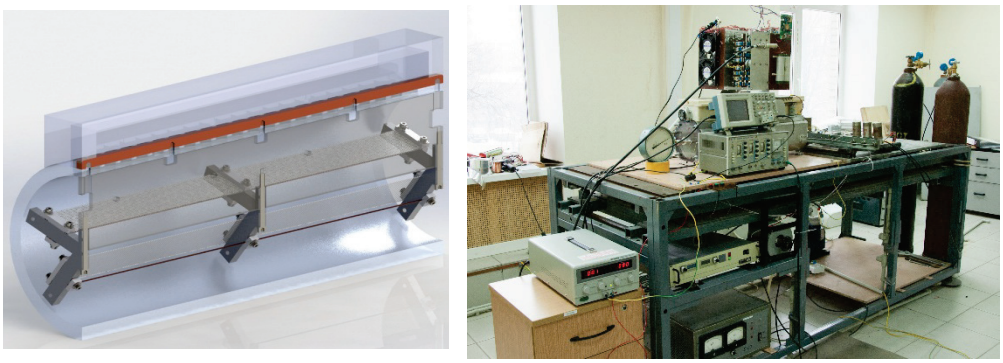

Fig. 1. a) Circulation chamber of electric discharge laser with four stage (cutaway). b) Experimental setup for the study of gas-discharge laser with EHD pumping system.

Based on numerical simulation the experimental setup for the formation of flow EHD in a gaseous environment with plasma emitters and ion collectors was designed and created (Fig 1 a, b). The system consisted of a series of individual devices, allowing you to perform a consistent increase in the number of stages and a parallel increase in the number of plasma emitters to achieve maximum flow rates. The possibility of increasing the volume flow by increasing sequential stages up to 7 and a parallel increase in the number of plasma emitters up to 6 was demonstrated experimentally. The gas at atmospheric pressure is reached the flow quantity of more than 15 l/s and the velocity of 5.2 m/s. 4 cascade EHD flows formation system was integrated in a cylindrical electric-discharge laser chamber.

[1] Rebrov I.E., Khomich V.Y., Yamshchikov V.A., Simulation of Intense Electrohydrodynamic Flow Based on Dielectric Barrier Discharge // Journal of Physics: Conference Series, Vol. 652, P. 12036, (2015).
[2] Nebogatkin S.V. et al., Powerful electrohydrodynamic flow on the basis of the high-frequency barrier discharge in gas, Advances in Applied Physics, Vol. 2, № 6. P. 595–603, (2014).
[3] Gamirullin, M.D. et al., The experimental setup for study of plasma actuators generating an electrohydrodynamic flow, Applied Physics, Vol. 5, P. 95–101, (2015).
[4] Moshkunov S.I. et al., High Voltage IGBT Switches for Electro-optical Shutter Control, Advances in Applied Physics, Vol. 1, P. 630–635, (2013).
[5] Rebrov I.E., Yamshchikov V.A., Khomich V.Y., Electrohydrodynamic flow induced by dielectric barrier discharge for gas laser circulation system, Hakone, Zinnowiz, Germany, Vol. 1/1, P. 78, (2014).

SOA-based All optical wavelength conversion of 40 Gb/s pol-mux DQPSK

Sepideh T. Naimi, Seán P. Ó Dúill, and Liam P. Barry

The RINCE Institute, School of Electronic Engineering, Dublin City University, Ireland
Author email address (Sepideh.Tayebnaimi2@mail.dcu.ie)

In order to increase the bit rate in modern wavelength division multiplexed (WDM) fiber systems, future optical networks will rely on all optical wavelength conversion (WC) of advanced modulation formats. Quadrature amplitude modulation (DQPSK) and Optical quadrature amplitude modulation (M-QAM) are the most promising advanced modulation formats in the next generation of optical communication networks to achieve greater spectral efficiency and maximize the overall network capacity [1,2]. One approach to perform all-optical WC is to employ the four-wave mixing (FWM) process within semiconductor optical amplifiers (SOAs) due to transparency to modulation format and transparency to baud rate of FWM in SOA‘s [1,2]. In this paper, we extend our previous works, in [1,2] and investigate the simulation scheme to design an all-optical wavelength converter for pol-mux modulation formats [4]. For the first time, we calculate the linewidth limits for the pump laser for wavelength conversion of a 10 Gbaud pol-mux DQPSK at the forward error correction threshold using detailed simulations of FWM conversion of such signals in an SOA with various pump linewidths. The system schematic is shown in Fig.1(a). The modulated signal from the transmitter (Tx) is coupled with two CW pumps and then amplified in an SOA. Two parallel pumps are used and the polarization of DQPSK signal is arbitrary. The wavelength converted signal (idler) is then filtered out using an optical band pass filter (OBPF) and then detected using an ideal coherent receiver. In [2,3], we explained the details of modelling wavelength conversion using SOAs based on interband carrier density pulsations (CDP), intraband carrier heating (CH), and spectral hole burning (SHB) effects.

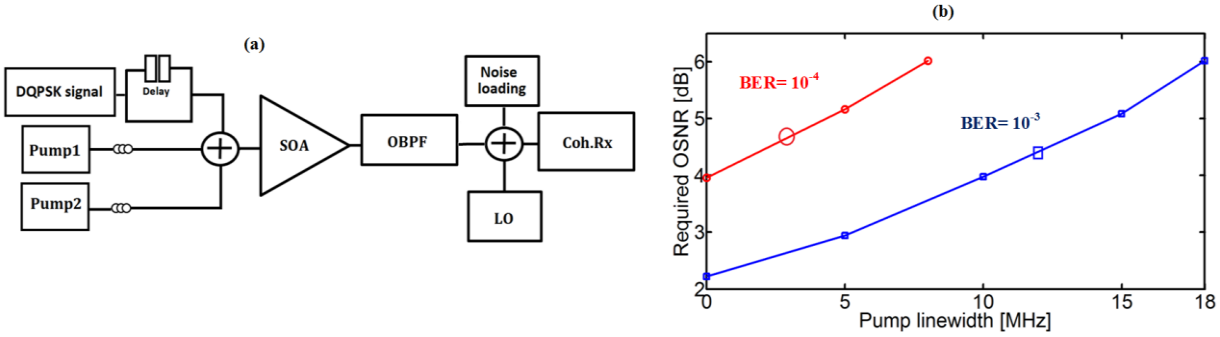

As is clear from Fig.1 (b), the maximum allowable pump linewidth are of the order of 18 MHz at BER of 10^{-3} and 9MHz for BER values of 10^{-4}, in order to perform wavelength conversion of 10 Gbaud pol-mux DQPSK. Some fast tuning lasers exhibit smaller linewidths than 9MHz [4], though careful characterization and control would be necessary for their use as pumps in FWM-based wavelength converters.

References

[1] S. T. Naimi, S. P. O Duill, and L. P. Barry, “Simulations of the OSNR and laser linewidth limits for reliable wavelength conversion of DQPSK signals using four-wave mixing,” *J. Opt. Commun*., vol. 310, no. 1, pp. 150–155, 2014

[2] S. T Naimi, S. P. O Duill, and L.P. Barry, “Detailed Investigation of the pump phase noise tolerance for the wavelength conversion of 16-QAM signals using FWM,” *IEEE/OSA J. Opt. Commun. Netw*, vol. 6, no. 9, pp. 793–800, 2014

[3] A. P. Anthur, R. Zhou, E. Martin, S.O. Duill and L. P. Barry “ Wavelength conversion of Nyquist Pol-Mux QPSK superchannel using four-wave mixing in SOA“,in *Proc. Optical Fiber Communication Conf*., 2016, paper Tu2K.6.

[4] S. P. O Duill and L. P. Barry, “Improved reduced models for single-pass and reflective semiconductor optical amplifiers,” *J. Opt. Commun*., vol. 334, no. 1, pp. 170–173, 2015.

LSM-P-14

Green synthesis of Dy-doped Ag nanoparticles

L.A.Apresyan[1], V.I. Krasovskii[1,2], V.I.Kryshtob[1], V.I.Pustovoy[1], S.I.Rasmagin[1], T.V.Vlasova[1]

[1]A.M.Prokhorov General Physics Institute of the Russian Academy of Sciences. 38, Vavilov st., Moscow, Russia, 119991
[2]National Research Nuclear University MEPHI. 31, Kashirskoe sh., Moscow, Russia, 115409

pustovoy@nsc.gpi.ru

It is known that plasmon resonance can be observed in silver nanoparticles, which results in a significant increase in the local field intensity, and is accompanied by new optical effects, such as increased absorption and luminescence of light, Raman scattering, up-conversion and others similar phenomena related to plasmonics [1]. The study of the important question of plasmonic effects impact on the optical properties of rare-earth metals at the moment is just beginning (see recent review [2], which reflects primarily results on plasmon-enhancement of up-conversion in $NaYF_4$ nanoparticles doped by Yb^{3+} and Er^{3+} ions). Under certain conditions, a plasmon resonance can reduce the pump threshold of up-conversion in the particles with rare earth elements [2,3].

This work reflects the first phase results of the authors study of the plasmon resonance influence on combined transitions in rare-earth elements functionalizing Ag nanoparticles. For this purpose, by the method of "green" synthesis [4] using an peppermint leaf extract [5], and crystalline menthol (which is expected to replace the above extract during synthesis), colloids of net silver nanoparticles and the same nanoparticles, functionalized by dysprosium were created. The optical absorption spectra of silver nanoparticles were obtained and analyzed by the method of [6] (see. Fig. 1), the data analysis of the electronic spectroscopy of silver nanoparticles (Fig. 2) and silver nanoparticles with dysprosium (Fig. 3) was carried out, and estimates of their structural parameters (form and dimensions) were given.

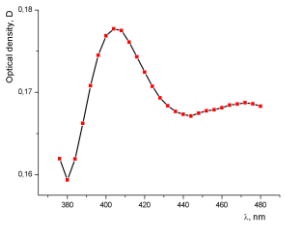

Fig. 1

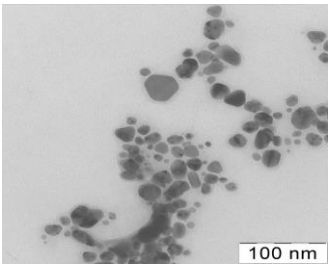

Fig. 2

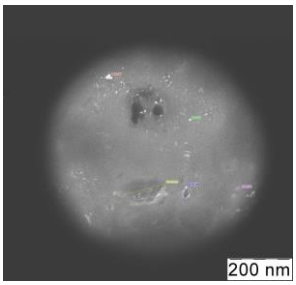

Fig. 3

The form (mainly spherical) and the size of silver nanoparticles (d = 18-29 nm) and shell (dobol = 36 nm), the volume fraction of the silver colloidal solution f = 6x10-5 were experimentally determined, which are in good agreement with theoretical predictions based on the model [6]. The peppermint extract creats essentially monodisperse and menthol - polydisperse silver nanoparticles. Functionalizing of silver nanoparticles by dysprosium by the methodology can easily be extended to other rare earth elements.

This work was supported by The Russian Foundation for Basic Research (Grants 16-32-80032, 16-02-00694) and Program of fundamental researches of the Presidium of the Russian Academy of Sciences I.39P.

[1]. B. Di Bartolo, J. Collins and L. Silvestri, Eds. Nano-Structures for Optics and Photonics, Springer, 586 pp. (2015).
[2]. W. Park, D. Lu and S. Ahn. Plasmon enhancement of luminescence upconversion Chem. Soc. Rev. ,44, 2940 (2015).
[3]. W.Xu, et al., Ag-SiO2-Er2O3 Nanocomposites: highly effective Upconversion Luminescence at high power excitation and high temperature. Sientific Reports 4, 5087, pp.1-9 (2014).
[4]. V.A.Basiuk,_E.V.Basiuk, Eds., Green Processes for Nanotechnology From Inorganic to Bioinspired Nanomaterials., Springer, pp.446 (2015).
[5]. U.K.Parashar, P.S.Saxena, A.Srivastava. Bioinspired synthesis of silver nanoparticles. Digest J.Nanomater. Biostructures.vol.4, 1, pp.159-166 (2009).
[6]. V.A. Karavanskii, A.V. Simakin, V.I. Krasovsky, P.V. Ivanchenko. Nonlinear optical properties of colloidal silver nanoparticles produced by laser ablation in liquids. Quantum Electronics. vol.34, 7, pp. 644-648 (2004).

LSM-P-15

Synthesis, optical fibre fabrication and investigations of luminescent tin containing glasses

B. I. Denker[1], R. P. Ermakov[1,2] B. I.Galagan[1], L. D.Iskhakova[2], S. E. Sverchkov[1], V. V. Velmiskin[2], E. M. Dianov[2]

1. A.M.Prokhorov General Physics Institute of RAS, Vavilov str. 38, 119991, Moscow, Russia
2. Fiber Optics Research Center of RAS, Vavilov str.38, 119991, Moscow, Russia

Our recent paper [1] described the wideband infrared photoluminescence in divalent tin-containing silicate glass. Its relatively long (~100 μs) lifetime and good overlapping of its excitation spectra with the wavelengths of common laser diodes have made it a new promising material for tunable fiber lasers and amplifiers. Nevertheless, SnO-SiO_2 glass system is very difficult from technological point of view. The main difficulty of the glass synthesis is the partial disproportionation of SnO into SnO_2 and metallic tin, both insoluble in the glass melt. We have tried to overcome this difficulty by total or partial substitution of SiO_2 by GeO_2 as a more fusible oxide. Starting from SnO-GeO_2 mixture, a set of glass samples with SnO content variable from 0% to 40% mol. was prepared in alumina and silica crucibles. In contrast to tin-silicate glasses, all the tin-germanate ones showed no traces of tin disproportionation: the glasses had no metal tin or SnO_2 inclusions.

All the tin-germanate glass samples showed photoluminescent properties resembling those of tin-silicate glasses, but with certain differences. The emission band of tin-germanate glasses (when excited at 950 nm) was peaking at 1.6 μm, while tin-silicate glass emission peaks at 1.5 μm, see **Fig.1**. The e-fold emission decay lifetimes of tin-germanate glasses varied from 150 for the glass with 40%mol SnO to 450 μs for the glass with 5%mol SnO, see **Fig.2**).

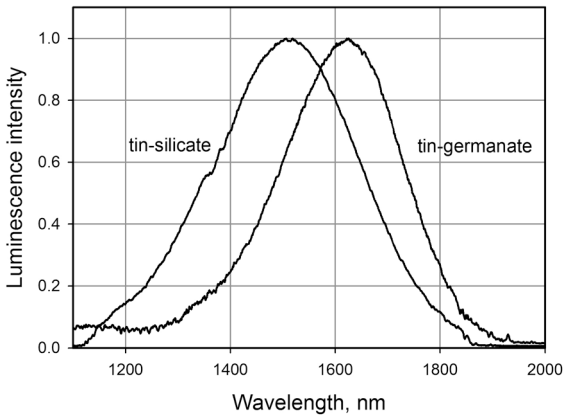

Fig.1.Luminescence spectra of glass samples excited at 950 nm

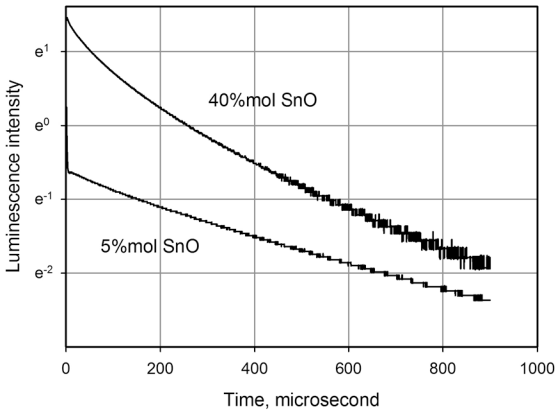

Fig.2.Luminescence decay of the tin-germanate gasses excited by OPO pulse at 950 nm

It is interesting to note, that the samples prepared in silica glass crucibles contained large amounts (tens of percent) of SiO_2, but were free of SnO_2 or metal Sn inclusions typical for tin-silicate glasses. We have tried to use this opportunity to prepare a clear SnO and SiO_2 containing glass and to develop an original way of manufacturing an optical fiber with divalent tin-containing core. In the first stage the SnO-GeO_2charge was placed in the Heraeus Suprasil F300 silica tube tightly sealed from one end. The tube was filled with ultra-pure argon and passed through a hot zone of the drawing tower. In this process the molten charge and the support tube formed respectively the core and the cladding of fiber preform. In the second stage, the preform was jacketed with another F300 tube. The multimode optical fiber with polymer protection coating was drawn from the fabricated preform at 1820 °C. Its outer diameter was 120 μm and the core diameter - 10 μm.

Due to strong mutual diffusion of the core and cladding components the concentrations of tin and germanium in the fiber core were much less than those in the charge. The silicon content even in the core center was about 20 times higher than that of germanium. Thus the core consisted of mostly silicate, and not germanate glass. Using cleaved fiber pieces of 1 and 3 m in length we have directly determined its numerical aperture as NA = 0.486. Thus, fiber fabrication procedure starting from SnC_2O_4 – GeO_2 powders mixture in a silica tube resulted in multimode fiber with mostly silicate core composition.

References

[1]B. I. Denker, B. I. Galagan, L. D. Iskhakova, S. E. Sverchkov and E. M. Dianov, " Infrared luminescent properties of tin-silicate oxide glass," Appl. Phys. B **120**, 13 (2015)

Photoacoustics

PA-1-1 (Invited)

Simultaneous in vivo imaging of diffuse optical reflectance, optoacoustic pressure and ultrasonic scattering

Pavel Subochev[1], Anna Orlova[1], and Ilya Turchin[1]
(List of authors in 11 point, centred and bold: the presenting author underlined)

1- The author affiliation and full address should be located here in 10 point, centred and in italics
ilya@ufp.appl.sci-nnov.ru

We present reflection-mode bioimaging system providing complementary optical, photoacsoutic and acoustic measurements by acoustic detector after each laser pulse. When the laser pulse interacts with the sample, there are two types of photons important for trimodal visualization. Photons that reach optical absorber generate OA signal. Back-scattered photons being absorbed by metalized surface of acoustic detector provide both the DR signal and the probing US pulse. Therefore, single laser pulse allows complementary measurement of diffuse optical reflectance (DR), optoacoustic (OA) pressure and ultrasonic scattering (US). The lateral resolution of OA/US modalities 50μm/35μm was provided by focal spot of spherically-focused 35MHz polyvinylidene fluoride (PVDF) detector with a 30MHz bandwidth, F = 6.8 mm focal distance, and 0.6 numerical aperture. The lateral resolution of DR modality 3.5 mm was majorly provided by focal spot of light delivery system consisting of 77 optical fibers with 0.12 numerical aperture [1].

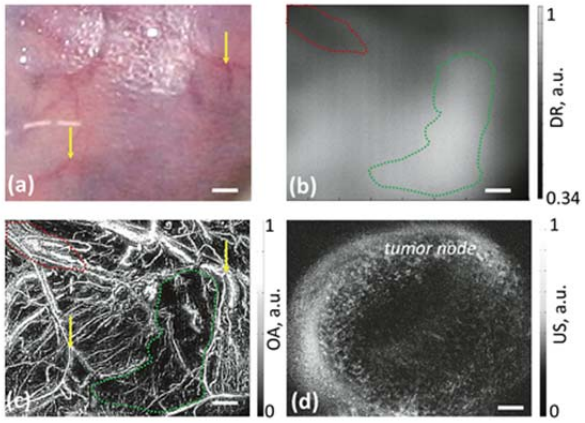

Figure 1. The results of simultaneous DR/OA/US imaging of the SKBR3 tumor, all bars are 1 mm. (a) – photograph of tumor in vivo, (b) – MIP DR image; (c) – MIP OA image; (d) – MIP US image. Yellow arrows indicate superficial blood vessels, red and green dots indicate the regions with high and low hemoglobin content correspondingly

To demonstrate the in vivo capabilities of the system we present the results of complementary DR/OA/US imaging of a mouse SKBR3 tumor model (Figure 1), head of a newborn rat, and the back of a newborn rat with 3.5mm/50μm/35μm lateral resolution. Zones with low DR signal (Figure1b) can be presented by haemorrhages or by areas with high vessels density. OA image (Fig.2c) demonstrates the spatial distribution of individual blood vessels located at different depths of the tumor (with superficial vessels marked by yellow arrows) and characterizes the same zones as the regions with high vessels density. US image (Fig. 1d) represents the contours of the tumor node. Structural information provided by US image complements functional information provided by DR and OA images and allows to differentiate blood supply of normal and tumor tussues.
Along with the imaging of the optical and acoustic heterogeneities, we propose to use the developed method of trimodal DR/OA/US registration for quantitative measurements. However, to reconstruct tissue chromophore concentrations it is important to provide multispectral DR/OA/US measurements and use proper Monte-Carlo simulation for non-homogeneous tissues and the geometries of the light delivery and detection.

[1] P. Subochev, "Cost-effective imaging of optoacoustic pressure, ultrasonic scattering, and optical diffuse reflectance with improved resolution and speed," Optics letters, 41, 1006-1009 (2016)

PA-1-2 (Invited)

Two labeling concepts for deep tissue optical imaging: upconverting nanoparticle or ultrasound

S. Andersson-Engels[1,2], M. Mousavi[2], A. Walther[2], L. Rippe[2], and S. Kröll[2]

1- IPIC, Tyndall National Institute, Lee Maltings Complex, Dyke Parade, Cork T12R5CP, Ireland
2- Department of Physics, Lund University, P.O. Box 118, SE-221 00 Lund, Sweden

stefan.andersson-engels@tyndall.ie

The authors are working along two concepts to develop optical macroscopical imaging at increased depth in biological tissue. The first concept is based on using upconverting nanoparticles as an exogenous contrast agent and analysing the luminescence signal, while the second concept is based on acousto-optical imaging, here also called ultrasound optical tomography.

Upconverting nanoparticles provide several advantages as compared to conventional fluorescence dyes for deep tissue imaging. It can be excited and emit light at wavelengths with low tissue attenuation, thus yielding good light penetration. The concept also avoids any background fluorescence from tissue autofluorescence, as the emission from the upconverting nanoparticles ís anti-Stokes shifted, and thus at a different wavelength than any tissue autofluorescence. It is thus straight forward to filter it out without any superimposed autofluorescence background. In addition due to the non-linear behaviour of the emission as a function of excitation fluence rate, the obtained spatial resolution will also be better than for conventional fluorophores as a contrast agent. Recent advances and plans for the new Biophotonics@Tyndall team starting will be provided at the presentation.

The second approach the authors are working along to develop techniques for deep tissue optical imaging is ultrasound optical imaging. This is based on a focussed ultrasound pulse providing spatial resolution for the optical imaging. When light at a very narrow frequency is diffusely transmitted through the tissue, a fraction of the light passing the ultrasound focus will be frequency shifted with the ultrasound frequency. The idea is to filter out that fraction of the light before the detection, thus providing the spatial information given by the ultrasound focus. Several challenges arise in doing this. The first is to obtain sufficiently good optical filtering, as the frequency shift defined by the ultrasound is typically low, in the MHz region. At this, for optical radiation, small frequency shift, one needs to have a sufficiently good optical filtration to suppress the un-shifted light not passed through the ultrasound focus, while transmitting the ultrasound shifted light. Such optical filtering can be obtained in optically pumped rare-earth metal doped crystals. Another challenge is to obtain a sufficiently high signal to allow deep tissue imaging. Simulations suggest that ultrasound optical tomography has a potential to be several orders of magnitude more sensitive than photoacoustic imaging, being the spear head for deep tissue imaging with high spatial resolution today [1]. The results of these simulations and the plans for the future will be presented at the presentation.

[1] A. Walther, L. Rippe, S. Kröll, S. Andersson-Engels, “Non-invasive optical oxygenation imaging of the heart using Ultrasound Optical Tomography (UOT)”. Manuscript (2016)

PA-1-3 (Invited)

OPTOACOUSTIC DIAGNOSTIC MODALITY: FROM IDEA TO CLINICAL STUDIES WITH HIGHLY-COMPACT LASER DIODE-BASED SYSTEMS

Rinat O. Esenaliev

Laboratory for Optical Sensing and Monitoring,
Center for Biomedical Engineering,
Department of Neuroscience and Cell Biology,
Department of Anesthesiology
University of Texas Medical Branch,
301 University Blvd., Galveston, Texas 77555-1156, USA

riesenal@utmb.edu

Optoacoustic (photoacoustic) diagnostic modality is a novel technique which combines high optical contrast and ultrasound spatial resolution. It utilizes time-resolved detection of thermoelastic waves generated in tissues by short optical pulses. We proposed to use the optoacoustic technique for noninvasive biomedical applications. Most important applications include noninvasive monitoring of cerebral blood oxygenation in patients with traumatic brain injury, neonatal patients, fetuses during late stage labor, central venous oxygenation monitoring, total hemoglobin concentration monitoring as well as hematoma detection and characterization. We developed and built optical parametric oscillator (OPO)-based systems tunable in a wide NIR spectral range (700-2400 nm). Recently, we built a multi-wavelength, highly-compact, laser diode-based system for optoacoustic imaging, monitoring, and sensing. The system is fiber-coupled and has high pulse energy at 150-ns duration and 1-kHz repetition rate. To provide sufficient output pulse energy, a specially-designed fiber-optic system was built and incorporated in ultra-sensitive, wide-band optoacoustic probes. Each probe was designed and built for a specific application: noninvasive probing of important blood vessels in adults, neonates, or fetuses. We performed clinical tests of the systems and the optoacoustic probes in backward (reflection) and forward (transmission) modes. In the backward mode, both optical irradiation and ultrasound detection are performed from the same hemisphere, while in the forward mode ultrasound detection is performed from the opposite hemisphere. The high pulse energy and repetition rate allowed for rapid data acquisition with high signal-to-noise ratio from cerebral blood vessels such as the superior sagittal sinus, central veins such as the internal jugular vein, peripheral veins and arteries, as well as from intracranial hematomas. The laser diode-based system was capable of automatic, real-time, continuous measurements of blood oxygenation in these blood vessels and total hemoglobin concentration measurements in the radial artery. The high pulse energy and repetition rate of the system allows for rapid optoacoustic imaging as well.

The authors acknowledge support of these studies by the NIH (Grants # U54EB007954, R01EB00763, R01NS044345, R41HL103095, R43HD075551, and R41HD076568), Noninvasix, Inc., John Sealy Memorial Endowment Fund for Biomedical Research, Moody Center for Traumatic Brain Injury Research, industrial partners, UTMB Business Acceleration Program, and Texas Emerging Technology Fund. Drs. Esenaliev and Prough are co-owners of Noninvasix, Inc., a UTMB-based startup that has licensed the rights to optoacoustic monitoring, sensing, and imaging technology.

PA-1-4 (Invited)

Photoacoustic Wavelength-Modulated Differential Imaging: a novel high dynamic range modality for noninvasive diagnosis of cancer

A. Mandelis, B. Lashkari, S. Choi, and E. Dovlo

Center for Advanced Diffusion-Wave and Photoacoustic Technologies (CADIPT), Department of Mechanical and Industrial Engineering, University of Toronto, Toronto, Ontario, M5S 3G8, Canada.

This keynote talk will be divided into three topics the common theme of which is promising new developments in high-sensitivity, high-dynamic-range multi-wavelength frequency-domain photoacoustic detection with potential impact in biomedical imaging. First, I will discuss Wavelength Modulated Differential Photoacoustic Spectroscopy (WM-DPAS) for noninvasive early cancer detection and continuous hypoxia monitoring through ultrasensitive measurements of hemoglobin oxygenation levels (StO_2). WM-DPAS measures simultaneously two signals induced from square-wave modulated laser beams at two different wavelengths where the absorption difference between deoxy- and oxy-hemoglobin is maximum and minimum, respectively. The two-wavelength measurement efficiently suppresses background, greatly enhances the signal to noise ratio and thus enables WM-DPAS to detect very small changes in total hemoglobin concentration (CHb) and oxygenation levels, thereby identifying pre-malignant tumors before they are anatomically apparent.

PA-1-5

Multimodal imaging of skin

M.J. Leahy[1]
[1]NBIPI Tissue Optics and Microcirculation Imaging Facility, School of Physics, National University of Ireland, Galway, IRELAND
martin.leahy@nuigalway.ie

This paper will report several modalities developed for imaging of human skin. Imaging the skin helps to reveal it structure and function which are still not well understood. Better knowledge is required to understand the mechanism of diseases such as various forms dermatitis, eczema, psoriasis, progeria and cancers, especially melanoma. Simply imaging the skin with a well-designed and standardized camera can have significant advantages. There is significant evidence that the dermascope in the hands of an expert can improve sensitivity by 20% and specificity by 10%. Dermatologists now prefer to use polarized light sources and cameras to remove the specular reflection without the need for a liquid medium. Laser Doppler has been available commercially since the late 1980s and in imaging form since the 1990s. It is a versatile imaging instrument which has been applied to many research questions, but has struggled to find mainstream acceptance as a diagnostic imaging instrument, with the possible exception of burns [1]. We became interested in optical coherence tomography (OCT) [2] when it became possible to use 1300 nm light sources and image sufficiently fast to avoid motion artefact on living subjects. We developed the correlation mapping optical coherence tomography (cmOCT) algorithm to more elegantly render the microcirculation [3]. cmOCT operates by comparing two adjacent or better repeated B-Scans in the same location and rendering the areas with low correlation in a bright colour to indicate flow. Examples of skin imaging can be seen in Figure 1. While the images of structure and function with OCT are impressive, it is generally limited in depth penetration to about 1 mm in practice. Photoacoustics combines the advantages of power and light to get greater penetration depth along with spectral sensitivity to view chromophores and measure oxygen saturation. These measurements are currently limited due to the lack of knowledge of the local fluence, but several schemes have been proposed to solve this. Depths of many millimetres can be imaged using photoacoustics and the limit is the diffuse penetration depth of the light used [4]. This can be up to 5- 7 cm in theory. Imaging the skin has advanced significantly, but there is much more to do to obtain the resolution and sensitivity at clinically useful depths. Efforts in this direction will be discussed.

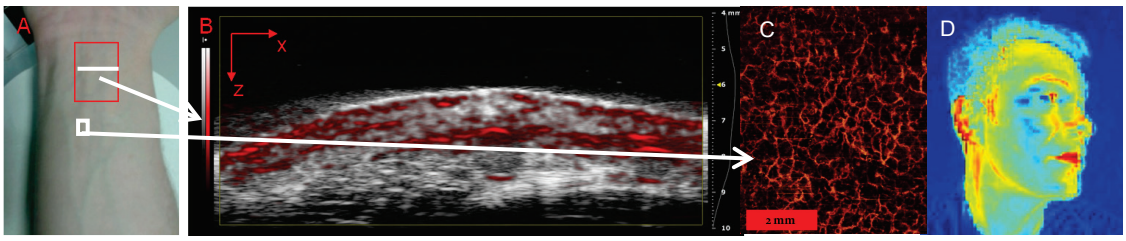

Figure 1. A) A photograph of a human wrist. B) A section, marked by the white line, imaged with high resolution ultrasound and photoacoustics. C) cmOCT of the area marked by the white box showing the blood vessels. D) Map of blood concentration in a human face taken using the GoPhoton Colours App.

ACKNOWLEDGMENTS

Science Foundation Ireland, The Irish Research Council, Galway University Foundation, UL Foundation, Compact Imaging, Inc., Fujifilm, The Higher Education Authority of Ireland.

REFERENCES

[1] *Microcirculation Imaging,* Martin J. Leahy (ed.), Wiley-VCH, Weinheim (2012).
[2] D. Huang*, et al.*, "Optical Coherence Tomography," *Science* **254**, 1178-1181 (1991).
[3] J. Enfield*, et al.*, "In vivo imaging of the microcirculation of the volar forearm using correlation mapping optical coherence tomography (cmOCT)," *Biomed. Opt. Express* **2**, 1184–1193. (2011).
[4] H. Zafar, A. Breathnach, H. M. Subhash, M. J. Leahy, "Linear-array based photoacoustic imaging of human microcirculation with a range of high frequency transducer probes," *Journal of Biomedical Optics* **20** (5), 051021 (2015).

PA-1-6 (Invited)

Novel compact photoacoustic imaging system with an Alexandrite pulsed laser for small vascular imaging

Toshiro Hayakawa, Kaku Irisawa

Medical Systems Research & Development Center, R&D Management Headquarters, FUJIFILM Corporation, 798, Miyanodai, Kaisei-machi, Ashigarakami-gun, Kanagawa 258-8538, Japan.

e-mail: toshiro.hayakawa@fujifilm.com.

One of the features of photoacoustic (PA) imaging is small-vessel visualization realized without a contrast agent or exposure to X-rays. For carrying out clinical researches in this field, a prototype PA imaging system has been developed. The compact PA system, shown in Fig.1, was prepared in order to fit the clinical environments, where current ultrasound (US) systems are used. The PA imaging system is easy to set-up and use due to the designs of components, as below.

(1) Compact and short-pulsed Alexandrite laser unit (Fig.1(a)):
For the light source, the system was equipped with a newly developed, compact light weight Alexandrite laser unit which can be placed on a cart for a portable US system. The laser unit emits pulsed light with energy of 80 mJ/pulse, short pulse width of 50±10ns and 10 Hz pulse repetition rate at a wavelength of 750 nm.

(2) US unit based on technologies of FUJIFILM's compact US system FC-1:
The US unit mounts many-core MPU for enhancing the image quality of B-mode and color Doppler mode. The PA imaging system provides combined images of these conventional US images with PA image [1], which displays smaller vascular detected by PA imaging than that by Doppler imaging.

(3) Hand-held type probes for PA/US imaging:
Intra-cavity (Fig.1(b)) and linear (Fig.1(c)) probes are prepared to realize the handheld PA/US imaging. Compact diffusive optics for pulsed-laser illumination is attached to the sides of the linear or convex US transducer array, respectively.

By utilizing this system, exploratory clinical researches for observing small-vascular are ongoing by our collaborative clinical partner, National Defence Medical College (Japan). As an application for intra-cavity PA probe is trans-rectal use, that is, periprostatic neurovascular bundle and prostate cancer [2] are intended to be imaged. Another application is trans-vaginal use that is a challenge to image uterine cervical lesions. For applications of linear-type PA probe, diabetic foot and connective tissue disease are ongoing. Images obtained in these clinical researches will be introduced.

[1] K. Irisawa, K. Hirota, et al., Photoacoustic imaging system for peripheral small-vessel imaging based on clinical ultrasound technology, Proc. SPIE, 9708, 970807, (2016).
[2] M. Ishihara, A. Horiguchi, et al., Comparison of photoacoustic, Doppler and magnetic resonance imaging for prostate cancer detection, Proc. SPIE, 9708, 970852, (2016).

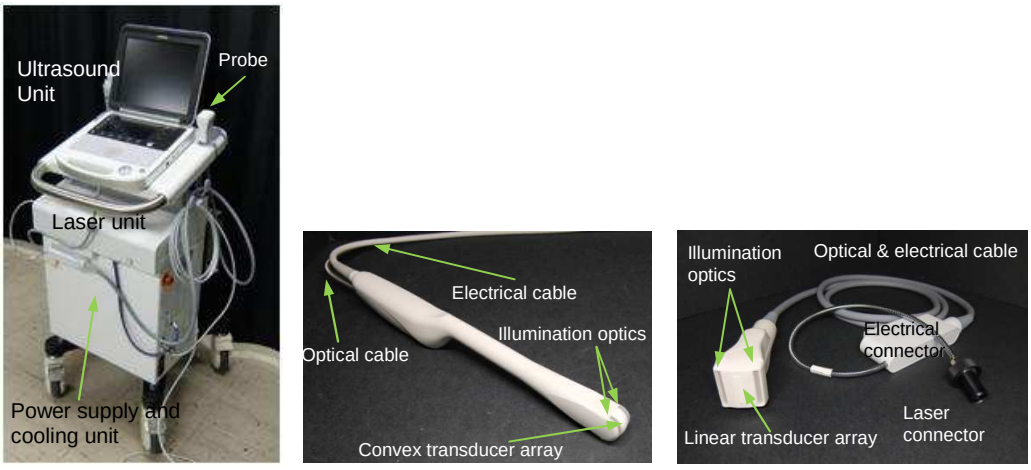

(a) Photoacoustic imaging system (b) Intra-cavity probe (c) Linear probe

Figure 1. Appearance of photoacoustic system

PA-P-1

Photoacoustic manipulation of heavy metal microparticles

V.I. Alekhnovich[1], A.N. Savkin[1], M.A. Yakimova[1]
[1]Moscow State Technical University n.a. Bauman, Moscow, Russia
e-mail: marya.korotaeva@yandex.ru

We have experimentally demonstrated the ability to control the position of metal micro-particles suspended in the liquid with pulses of nanosecond laser diameter from 2 to 8 microns. Particles were placed in a standard microscope slide between a slide and cover glass in the fuchsine solution in ethylene. Slide "shelled" laser pulses with a wavelength of 532 nm and a pulse width of 10 ns, following a frequency of 1 Hz. The diameter of the laser beam is 18 mm. When the laser had been switched on, randomly settling particles (Fig. 1a) moved towards the annular zone near the border of the laser beam (Fig. 1b). Once in this area, particles began to oscillate about the equilibrium position.

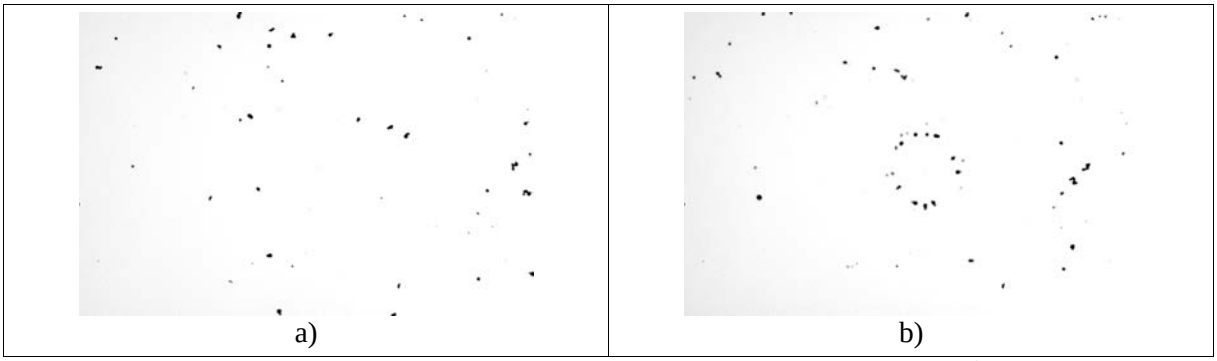

Fig. 1. The zinc microparticles movement under laser pulse action: a) initial position; b) position after 90 laser pulses.

We explain this behavior of microparticles by their interaction with the sound field arising due to opto-acoustic effect of the passage of laser radiation through the absorbing fluid. The field interacts with microparticles suspended in the liquid, which tend to take a position at a certain distance from the axis of the laser beam, as shown by theoretical calculations [1]. Such microparticles, namely the behavior of their position, can be controlled by moving the laser beam. This phenomenon can be used to control the position of the microparticles in biomedical research, including in Lab on chip systems.

The results may be used in bio-medicine for micro- and nanoparticles manipulation.

[1] V. Zharov, T. Malinsky, and V. Alekhnovich, ‘Photoacoustic manipulation of particles and cells’, *Rev Sci Instrum*, vol. 74, pp. 779–781, 2003.

Multi-scale structural and functional imaging of the human microvasculature using combined co-registered high frequency photoacoustic/ultrasound and correlation mapping optical coherence tomography

Haroon Zafar*[1,2], Faisal Sharif[2,3], Martin. J. Leahy[1,4,5]

[1]*Tissue Optics & Microcirculation Imaging Group, National University of Ireland, Galway, Ireland.*
[2]*School of Medicine, National University of Ireland, Galway.*
[3]*Department of Cardiology, University Hospital Galway.*
[4]*National Biophotonics & Imaging Platform, Dublin, Ireland.*
[5]*Royal College of Surgeons, Dublin, Ireland.*

**h.zafar1@nuigalway.ie*

Recently, there has been an enormous interest in biomedical imaging to combine multiple imaging modalities to provide comprehensive insights into physiology. In this work the combination of co-registered high frequency photoacoustic (PA)/ultrasound(US) and correlation mapping optical coherence tomography (cmOCT) was used for multi-scale structural and functional imaging of the human microvasculature. 3D OCT, PA and US scans of the human forearm skin were acquired. OCT imaging was performed using swept source OCT system and the resulting OCT volume was processed using the cmOCT technique. The cmOCT technique uses dense scanning OCT image acquisition and post processing protocol based on correlation statistics [1]. Combined PA/US imaging was performed using multi-element high frequency linear-array transducer combined with multichannel collecting system [2]. 3D multi-scale structural and functional maps of the forearm skin were obtained (Figure 1). The combination of cmOCT and PA imaging brings several advantages. Firstly both are noninvasive and provide completely complementary imaging contrasts. The absorption based contrast of PA imaging can be used to reveal the structure and oxygenation status of the microvasculature to depths of several millimetres whilst the scattering based contrast of cmOCT can reveal surrounding tissue microvasculature with high resolution.

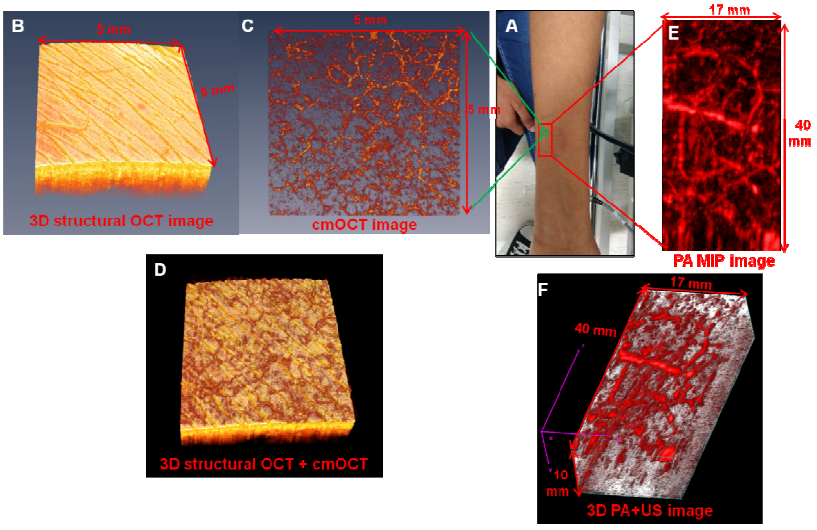

Fig. 1 Combined PA/US and cmOCT imaging. (A) The photograph taken from the subject, showing the forearm skin examined by PA/US (red rectangle) and OCT (green square). (B) 3D structural OCT data. (C) MIP image through the cmOCT volume. (D) Combined OCT structural and functional data. (E) MIP through the PA volume. (F) Co-registered PA and US data. [Haroon et al., unpublished image]

[1] Zafar H, Enfield J, O'Connell ML, Ramsay B, Lynch M, Leahy MJ. Assessment of psoriatic plaque *in vivo* with correlation mapping optical coherence tomography. *Skin Res Technol.* 2014; 20(2):141-6.
[2] Zafar H, Breathnach A, Subhash HM, Leahy MJ. Linear array-based photoacoustic imaging of human microcirculation with a range of high frequency transducer probes. *J Biomed Opt*; 2015:20(5).

PA-P-3

Impact evaluation of heavy metals at contaminated plants and fruits using IR spectroscopy

C. Achim (Popa)[1], M. Bercu (Petrus)[1], A.M. Bratu[1], C. Matei[1], M. Patachia[1], D.C. Dumitras[1,2]

1- Department of Laser, National Institute for Laser Plasma and Radiation Physics, 409 Atomistilor St., PO Box MG-36, 077125 Bucharest, Romania
2- University Politehnica of Bucharest, Faculty of Applied Sciences, 313 Splaiul Independentei St., Bucharest, Romania

Main author email address: cristina.achim@inflpr.ro

Plants lack glands that produce and secrete hormones, instead, each cell is capable of producing hormones. Under normal conditions, plants grow and reproduce; yet, plants are often faced with a changing – sometime extreme – external environment that can cause unfavourable conditions; in such an environment plants are considered to be stressed [1]. Some of these stress factors (like heavy metals) may fluctuate significantly in intensity and duration on time scales on hours, days, seasons, or years; other may change slowly and gradually affect plant growth conditions. Since plants are sessile organisms and have only limited mechanisms for stress avoidance, they need flexible means for acclimation to changing environmental conditions. In order to improve a plant's protection, it is important to understand the mechanisms contributing to stress tolerance [2].

The present study is focus on all those stress factors which can alter the food quality and intends to assess the ethylene gas from plants and fruits exposed to heavy metals (Cd, Zn, Cu, Pb, Hg) by the means of an analytical method: laser photoacoustic spectroscopy (LPAS).

The determination of the ethylene gas compound was investigated using a CO_2 LPAS, a well known method in the field of trace gas detection, used for quantitative determination of gases [3].

We obtained a strong association ethylene gas and heavy metals which can indicate that the species are potentially toxic because first: they are reactive and second, may lead to the unspecific oxidation and may contribute to the increased production of ethylene.

Based on a non-invasive method, stable in biological materials, and easy to measure, we conclude that CO_2 LPAS instrument distinguish plants and fruits with different heavy metals from data controls.

Acknowledgements

We acknowledge the financial support of the CNCS-UEFISCDI, project number PN-II-PT-PCCA-2013-4-0608 (72/2014).

References

[1] http://www.ebi.ac.uk/chebi/searchId.do?chebiId=37848
[2] A. Schutzendubel, A. Polle, Plant responses to abiotic stresses: heavy metal- induced oxidative stress and protection by mycorrhization, J. Exp. Bot., 53 (372): 1351-1365. doi: 10.1093/jexbot/53.372.1351, (2002).
[3] D. C. Dumitras, D. C. Dutu, C. Matei, A. M. Magureanu, M. Petrus and C. Popa, "Laser photoacoustic spectroscopy:principles,instrumentation,and characterization" Journal of Optoelectronics and Advanced Materials, Vol 9, No. 12, pp: 3655-3701 (2007).

Assessment of cutaneous melanoma and basal cell carcinoma with photoacoustic imaging

Aedán Breathnach[1*], Jemima Dorairaj[2], Liz Concannon[2], Shazrinizam Shaharan[2], Hrebesh M. Subhash[1], Jitin Jose[1], James McGrath[1], Jack Kelly[2], and Martin Leahy[1,3]

[1] Tissue Optics and Microcirculation Imaging Facility, National Biophotonics and Imaging Platform, National University of Ireland, Galway, Ireland

[2] Dept. of plastic and reconstructive surgery, Galway university hospital, Ireland

[3] Royal College of Surgeons (RCSI), Dublin, Ireland.

*e.breathnach1@nuigalway.ie

ABSTRACT

Photoacoustic (PA) imaging is a non-invasive imaging modality which combines high optical contrast with high-resolution ultrasonic imaging, and can directly map optical absorption within biological tissue. PA imaging can be used to image pigmented skin lesions due the high absorption of melanin in the visible and near-infrared wavelength rage, and hence can be used to determine lesion shape and depth of invasion. In this study we investigate the clinical usefulness of PA imaging in diagnosing and assessing pigmented skin cancers such as cutaneous melanoma and basal cell carcinoma. Pre-operative PA images of patients with suspected cases of either cutaneous melanoma or basal cell carcinoma were taken with the Vevo Lazr® 2100 PA imaging system at several wavelengths. The distribution and maximum thickness of suspect lesions was determined by imaging at 700nm, and the surrounding vasculature was imaged at 900 nm. Information obtained from the PA images was compared with histological examination of resected surgical specimens.

Keywords: photoacoustic imaging, cutaneous melanoma, basal cell carcinoma, histology.

Sensors

SN-1-1 (Invited)

Adaptive laser interferometry sensory systems for ultrasound inspection of materials

Heming Wei, Sridhar Krishnaswamy
Center for Smart Structures and Materials
Northwestern University
Evanston, IL 60208, USA.

s-krishnaswamy@northwestern.edu

Ultrasound has been widely used to nondestructively characterize material properties and to image defects in materials. Conventionally, ultrasound has been generated and detected using piezoelectric transducers, which require some coupling medium between the transducers and the test objects. In situations where non-contact inspection is needed, laser ultrasonics or photoacoustics methods have been developed. Photoacoustic techniques are a subset of ultrasonic methods wherein *laser generated* stress waves are used to obtain information about structural and material properties. Photoacoustic techniques have found application over length scales ranging from macro-structures to nanometer-sized thin films and coatings.

In photoacoustic techniques, the ultrasound is typically also detected using optical detection, thereby enabling truly non-contact nondestructive characterization of the material properties of structures. This talk will focus on adaptive laser interferometric sensor systems that can be robust enough to be used under non-ideal conditions such as non-polished surfaces that scatter light and in situations where ambient noise preclude the use of classical optical interferometry. A brief review of various adaptive interferometric methods that have been developed in both my lab and by other groups will be provided. Recent developments from my lab on dynamic strain sensing using interferometric methods for spectral demodulation of Fiber-Bragg Grating signals as well as using polymer optical waveguide sensors will be discussed. Applications to defect imaging, characterization of thin films and coatings as well as fiber-optic acoustic emission sensing systems will be discussed.

SN-1-2 (Invited)

Microfibre Structures for Sensing Applications

Y. Semenova

Photonics Research Centre, School of Electrical and Electronic Engineering, Dublin Institute of Technology, Kevin St., Dublin 8, Ireland

yuliya.semenova@dit.ie

There has been an increasing demand in recent years from a wide variety of industries for sensors which combine high sensitivity, fast response, compact size and low power consumption. Optical microfibre structures can generate easily accessible evanescent fields with a large intensity and short decay distance which make them very suitable candidates as the basis for ultrasensitive miniature devices for a variety of application areas.

This paper summarises the principles of several different physical, chemical and biosensors utilising optical microfibre structures and gives examples of their practical applications. A variety of sensing structures associated with tapered microfibers [1-3], microfibre couplers [4-5], microstructured fibres [6-7] and whispering gallery mode fibre resonators [8] have been considered. Finally, we discuss future prospects and challenges for devices and systems based on these principles.

[1] P. Wang, G. Brambilla, M. Ding, Y. Semenova, Q. Wu, G. Farrell, High-sensitivity, evanescent field refractometric sensor based on a tapered, multimode fiber interference, Optics Letters, vol. 36, pp. 2233-2235, (2011).

[2] P. Wang, L. Bo, C. Guan, Y. Semenova, Q. Wu, G. Brambilla and G. Farrell, Low temperature sensitivity periodically tapered photonic crystal fiber based refractometer, Optics Letters, vol. 38, pp. 3795-3798, (2013).

[3] P. Wang, M. Ding, L. Bo, C. Guan, Y. Semenova, W. Sun, L. Yuan, G. Brambilla and G. Farrell, A photonic crystal fiber half taper probe based refractometer, Optics Letters, vol. 39(7), pp. 2076-2079, (2014).

[4] L. Bo, P. Wang, Y. Semenova, G. Farrell, High sensitivity fiber refractometer based on an optical microfiber coupler, Photonic Technology Letters, vol. 25(3), pp. 228-230, (2013).

[5] L. Bo, C. C.-O'Mahony, Y. Semenova, N. Gilmartin, P. Wang, G. Farrell, Microfiber coupler based label-free immunosensor, Optics Express, vol. 22(7), pp. 8150-8155, (2014).

[6] D. Liu, A. K. Mallik, J. Yuan, C. Yu, G. Farrell, Y. Semenova, Q. Wu, High sensitivity refractive index sensor based on a tapered SCSMF structure, Optics Letters, Vol. 40(17), pp. 4166-4169, (2015).

[7] A. Mahmood, V. Kavungal, S. Ahmed, G. Farrell, Y. Semenova, Magnetic-field sensor based on whispering gallery modes in a photonic crystal fiber infiltrated with magnetic fluid, Optics Letters, vol. 40 (21), pp. 4983-4986, (2015).

[8] A. K. Mallik, D. Liu, V. Kavungal, Q. Wu, G. Farrell, Y. Semenova, "Agarose coated spherical micro resonator for humidity measurements", Optics Express, in press.

SN-1-3 (Invited)

Laser processed Molecularly Imprinted Polymers for sensing applications

Laura Chia Gomez[1], Yannick Fuchs[2], Xuan-Anh Ton[2], Ihab Dika[1], Arnaud Spangenberg[1], Karsten Haupt[2], Olivier Soppera[2]

[1] Mulhouse Institute for Material Sciences, CNRS LRC 7228, Mulhouse 68200, France
[2] Compiègne University of Technology, CNRS UMR 6022, Compiègne 60205, France

olivier.soppera@uha.fr

In the context of chemical microsensors or microbiosensors, Molecularly Imprinted Polymers (MIPs) are particularly well adapted as synthetic biomimetic recognition materials, because of their greater chemical and physical stability compared to their biological counterparts like enzymes or antibodies, and easier processing and engineering.

Recent examples of MIP have demonstrated their interest for chemical sensors associated to a wide range of chemicals for which these materials exhibit both specificity and sensitivity. However, their development in devices has been confronted to the difficulty to interface the functional material with the transducer or with a microchip. The photochemical route that we proposed significantly simplifies the integration of the functional material into the sensor device. Specific MIP precursors formulations were prepared to fulfill the requirements for micropatterning and molecular imprinting.

Molecularly Imprinted Polymers (MIP) were prepared by photochemical route. Photoinduced polymerization with laser irradiation was used to achieve the preparation of the MIP and at the same time spatially controlled irradiation allowed shaping the material to confer it an optical function useful for interrogation. Such route significantly simplifies the integration of MIP in sensors[1]. Advanced methods of photopatterning were used including interference (holography)[3,4], optical near-field[2], lithography on optical fibers[5] and two-photon stereolithography[6]. Laser photopatterning appears thereby as one of the most suitable methods for patterning MIP at the micro and nano scale, directly on the transducer surface. Demonstration of use of these strategies for sensor application is presented. Such route opens new opportunities for low cost, highly sensitive and highly specific sensors.

1. Fuchs, Y.; Soppera, O.; Haupt, K., **Analytica Chimica Acta** 2012, 717, 7-20.
2. Fuchs, Y.; Linares, A. V.; Mayes, A. G.; Haupt, K.; Soppera, O., **Chem. Mater**. 2011, 23 (16), 3645-3651.
3. Fuchs, Y.; Kunath, S.; Soppera, O.; Haupt, K.; Mayes, A. G. **Adv. Funct. Mater**. 2013.
4. Fuchs, Y.; Soppera, O.; Mayes, A. G.; Haupt, K., **Adv. Mater**. 2013, 25 (4), 566-570.
5. Ton, X. A.; Bui, B. T. S.; Resmini, M.; Bonomi, P.; Dika, I.; Soppera, O.; Haupt, K., **Angew. Chem.-Int. Ed.** 2013, 52 (32), 8317-8321.
6. Gomez, L. P. C., Spangenberg, A., Ton, X.-A., Fuchs, Y., Bokeloh, F., Malval, J.-P., Tse Sum Bui, B., Thuau, D., Ayela, C., Haupt, K. and Soppera, O. **Adv. Mater.** 2016. doi:10.1002/adma.201600218

Optical fiber sensors-based Smart Structures

Zhi ZHOU

Dalian University of Technology，Dalian，China
Email：zhouzhi@dlut.edu.cn

ABSTRACT

This invited presentation will introduce the advances of optical fiber sensors-based smart structures for civil infrastructures in our research center. It includes a series of OFS-based smart materials, smart components, smart structures and even smart prefabricated structures utilizing building materials with built-in OFS. Also, some latest deployment case studies will given.

SN-1-5

A Colour-Changing Holographic Pressure Sensor

D. Cody[1], T. Mikulchyk[1], Sabad-e-Gul[1], E. Mihaylova[2], I. Naydenova[1]

1-Centre for Industrial and Engineering Optics, School of Physics, College of Sciences and Health, Dublin Institute of Technology, Dublin 8, Ireland

2-Department of Mathematics, Informatics and Physics, Agricultural University, Plovdiv, Bulgaria

dervil.cody@dit.ie

Pressure sensors are widely used for control and monitoring of pressure in thousands of everyday applications. The sectors requiring pressure sensing devices vary greatly, including the petrochemicals, automotive, dental and medical device industries. The market size of pressure sensors in the year 2011 was $5.11 billion and is expected to reach $7.34 billion by 2017, and in particular, strong growth of optical sensing technologies for pressure sensing is predicted [1].

A holographic pressure sensor has been developed. Reflection holograms recorded in an elastic diacetone acrylamide photopolymer respond to applied pressure via a change in the hologram fringe spacing (Λ). The change in fringe spacing, which can be quantified using white light spectroscopy due to the resultant change in the hologram reconstruction wavelength, produces a colour map of pressure distribution. Optimisation of the photopolymer composition and holographic recording conditions has been carried out in order to maximize the diffraction efficiency i.e. hologram brightness, so as to ensure the colour change due to pressure is easily viewable [2]. This pressure-sensitive material is low toxicity, low cost and easy to produce. The pressure sensitivity and reversibility of the sensor are reported. A hologram which changes colour under pressure is an attractive technology for medical device, dental, security and anti-counterfeiting applications.

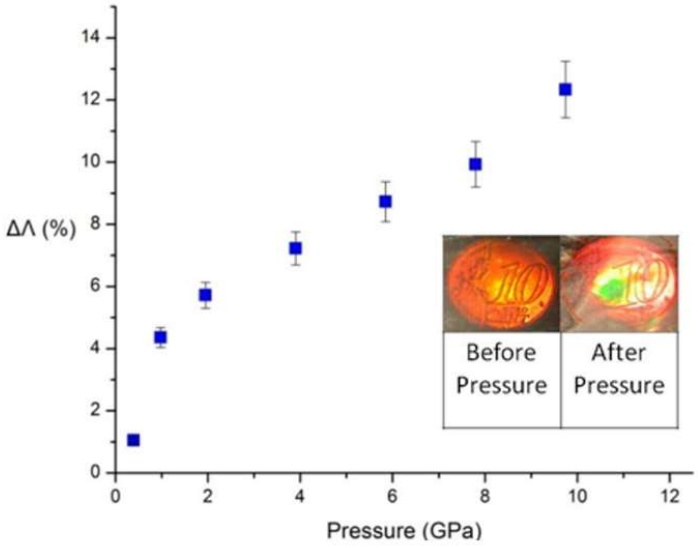

Figure: % change in reflection hologram fringe spacing (ΔΛ) as a function of applied pressure (GPa). Insert: photographs of a reflection hologram of a 10c coin before and after pressure application.

[1] MarketsandMarkets, "Pressure Sensor Market (2012 – 2017) - Global Forecast, Trend & Analysis – Segmentation by technology [Piezoresistive, Capacitive, Electromagnetic (Reluctance), Resonant Solid State, Optical], Applications [process and non process] and Geography", Market Research Report (2012).

[2] D. Cody, S. Gribbin, E. Mihaylova, I. Naydenova, Low-Toxicity Photopolymer for Reflection Holography, ACS Applied Materials and Interfaces, In Press, (2016).

SN-1-7 (Invited)

Russian experience of development and applications of fiber-optic sensors

I. Shelemba[1], V. Shishkin[1]

1- Inversion-Sensor Co. Ltd., 106 25 Oktyabrya St., Perm, Russia, 614990

shelemba@i-sensor.ru

Nowadays sensors based on fiber Bragg gratings (FBG) and Raman scattering are some of the most advanced from existing and successfully utilized measurement technologies. Fiber optic sensors have many advantages in comparison with their electrical analogs, what makes them attractive for application in major industries. Inversion Sensor Co. Ltd. is a leading company in production and implementation of fiber optic sensors in Russia.

Inversion Sensor was founded in 2004 as a spin-off from Institute of Automation and Electrometry, in Novosibirsk, and in 2013 was moved to the industrial site of Fiber-optic technologies cluster "Photonics" (Perm, Russia), which helped to significantly accelerate growth of the company. At present time production of company is utilized in major industries such as: civil engineering, energy, oil and gas, aerospace etc. As well foreign companies show growing interest in the products.

Every product is developed according to requirements of industry leaders and the technical solutions are reviewed by leading specialized institutes. Furthermore Inversion Sensor team is working on continuous improvement of current design of sensors.

Most of producing sensors are based on fiber Bragg grating technology and designed to measure strain, pressure, liquid level, temperature. Today total amount of produced FBG-based sensors exceeds 1000 units per month.

Besides FBG-sensors company produce distributed temperature sensors (DTS) based on Raman scattering for real-time temperature monitoring of complex structures. This technology has successfully proven itself in critical applications such as fire detection in tunnels, coalmines, multi-storey car parks, temperature monitoring of industrial conveyor belts, power cables and transmission lines, leakage detection at dams and pipelines, borehole temperature logging.

Both technologies were successfully implemented in a great number of projects, the biggest and most complex of which are structural health monitoring of soccer arena [1], monitoring of Zaramag hydroelectric power plant [2], temperature monitoring of turbo generator [3].

Inversion Sensor Co. Ltd. never stops creating innovations based on optical fiber sensing technologies. Future plans include development of new types of fiber optic sensors: current sensor, high frequency accelerometer, sensor for power transmission lines ice load monitoring, sensors for nuclear power industry application, high spatial resolution distributed sensor based on infinitely long Bragg grating, miniaturized interrogator based on integrated optics.

[1] V. Shishkin, A. Churin, D. Kharenko, M. Zheleznova, I. Shelemba, Structural health monitoring system of soccer arena based on optical sensors, Proc. SPIE 9157, 23rd International Conference on Optical Fibre Sensors, (2014).
[2] A. Kuznetsov, A. Agabyan, V. Dubok, A. Makushin, I. Shelemba, I. Sergeev, I. Granyov, Application of fiber optic sensors on Zaramag HPP-1 at the construction stage, Proceedings of All-Russian conference "Hydropower industry. Innovations and advanced technologies", (2013).
[3] E. Gurevich, A. Lyamin, I. Shelemba, Temperature measurements of stator winding by fiber optic sensors during testing of turbo generator, Electric power plants, pp. 42-47, (2010).

SN-1-8 (Invited)

Hollow Whispering Gallery Resonators for Sensing and Nonlinear Optics

J. M. Ward[1], Y. Yang[1], S. Kasumie[1] S. Nic Chormaic[1]

Light-Matter Interactions Unit, Okinawa Institute of Science and Technology Graduate University, Onna, Okinawa 904-0495, Japan.

Jonathan.ward@oist.jp

There are many whispering gallery mode (WGM) resonators reported in the literature; for example, microdisks, microspheres, microtoroids, micropillars, micocapillaries, microbottles and microrings [1]. An interesting type of microcavity is the microbubble WGM resonator [2][3], which is essentially a thin spherical glass shell supported on a hollow stem that allows fluids to be passed through the core of the bubble. The microbubble can support WGMs in the bubble wall. Light is evanescently coupled into the microbubble wall via a tapered optical fibre. The same tapered optical fibre is used to couple light out of the microcavity and the transmitted power contains the WGM spectrum. The WGM also creates an evanescent field along the inner and outer surfaces of the microbubble and this field allows the mode to interact simultaneously with the environment inside and outside the microbubble. These properties make hollow WGM resonators uniquely suited for sensing applications since minute changes to the environment or to the surface of the bubble result in a change in the WGM spectrum [2-4]. The microbubble core can be filled with a fluid in which nanoparticles, for example, are suspended. As the nanoparticles interact with the WGM of the bubble they cause a shift in the WGM resonance position due to either increased optical path length, change in refractive index, or due to the particles' excess polarisability.

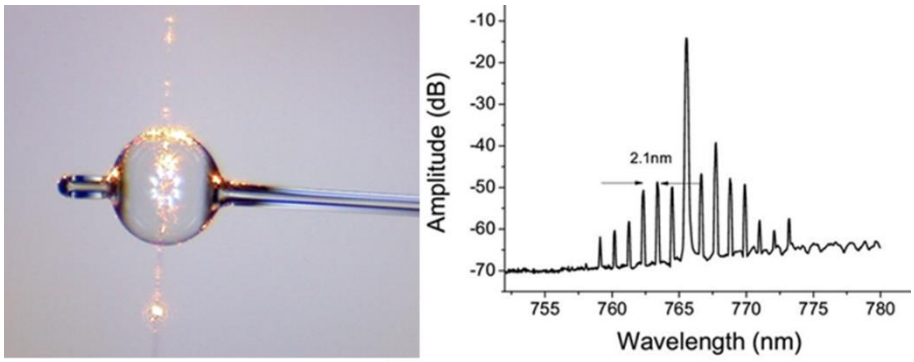

Figure: (left) Single input microbubble WGM resonator. (right) Visible frequency comb generated in a microbubble resonator [5].

The spherical shell geometry of these resonators also offers a unique opportunity to engineer the optical dispersion in the cavity by controlling the bubble wall thickness. The ability to control the geometric dispersion enables us to shift the zero dispersion wavelength towards visible wavelengths. This allows us to directly create optical frequency combs at visible wavelengths [4].
We will present some of our recent work on the detection, trapping and propulsion of nanoparticles in liquid filled quasi-droplet WGM microbubble resonators. For air filled microbubbles, the generation of visible frequency combs is also presented.

[1] J. Ward and O. Benson "WGM microresonators: sensing, lasing and fundamental optics with microspheres," Laser & Photonics Reviews 5, 553-570, (2011).
[2] Y. Yang, J. Ward, S. Nic Chormaic "Quasi-droplet microbubbles for high resolution sensing applications," Opt. Exp. 22, 6881-98 (2014).
[3] J. M. Ward, N. Dhasmana and S. Nic Chormaic, "Hollow-core, whispering gallery resonator sensors," Eur. Phys. J. Special Topics 223, 1917 (2014).
[4] J. M. Ward, Y. Yang, S. Nic Chormaic, "Highly Sensitive Temperature Measurements with Liquid-Core Microbubbles Resonators," IEEE Photon. Technol. Lett., 25, 2350 (2014).
[5] Y. Yang, X. Jiang, S. Kasumie, G. Zhao, L. Xu, J. Ward, L. Yang and S. Nic Chormaic, "Four-wave mixing parametric oscillation and frequency comb generation at visible wavelengths in a silica microbubble resonator," arxiv.org/abs/1606.03334 (2016).

SN-2-1 (Invited)

Plasmonic nanostructures for fluorescence-based biosensors

Colette McDonagh

Irish Photonic Integration Centre (IPIC), Optical Sensors Laboratory
School of Physical Sciences, Dublin City University, Glasnevin, Dublin 9, Ireland

Colette.mcdonagh@dcu.ie

Abstract

Nanoparticles (NPs) of different composition and size are widely used for biomedical applications. In particular, nanobiophotonic approaches using fluorescence offer the potential of high sensitivity and selectivity in applications such as fluorescence-based bioassays, intracellular sensing and imaging. In this presentation, the focus is on metal nanoparticles/nanostructures for plasmonically enhanced fluorescence using Cy5 dye. The enhanced fluorescence achieved using these approaches is illustrated for fluorescence-based immunoassays towards point-of-care applications.

Metal-enhanced fluorescence (MEF) occurs when a fluorescent dye e.g. Cy5, is adjacent to but not in contact with a metal nanoparticle/nanostructure and where the wavelength of the localised surface plasmon resonance (LSPR) associated with the metal particle is matched to the dye spectroscopy. Under these conditions, the large E-field at the metal surface couples to the absorption/emission band of the dye subsequently leading to an enhancement of the fluorescence emission. A number of MEF-LSPR approaches are described briefly including self-assembled spherical silver NPs and self-reducing silver patterned substrates for which enhanced fluorescence-based bioassays are demonstrated.

The use of noble metal gratings as a suitable platform for sensitive biological fluorescence applications is also explored. Gratings are particularly advantageous as they can be produced with a high degree of accuracy and their plasmonic properties can be tuned to a wide range of wavelengths. Rotations about the azimuth provides a convenient approach to maximise the coupling between the grating and excitation source while achieving enhancements comparable to traditional optical configurations where the grating and in plane light vectors are parallel. In this investigation, gold gratings are fabricated using a laser interference lithography technique. This approach yields a 30 fold enhancement in the fluorescence signal, while opening up the range of possible orientations and configurations suitable for fluorescence enhancement applications.

The presentation concludes with a summary of the main challenges and obstacles in relation to the potential widespread use of these structures for diagnostics and therapeutics.

SN-2-2 (Invited)

Plasmonic nanostructures for bio-and chemosensors: laser fabrication and application

Oleg Vitrik

Institute of Automation and Control Processes FEB RAS, Vladivostok, Russia

SN-2-3 (Invited)

The chemosensory structures based on complex analysis of the parameters of photo induced luminescence

S. Voznesenskiy[1], A. Sergeev[1,2], Yu. Kulchin[1,2], A. Mironenko[3], A. Mirochnik[3], A. Leonov[1,2]

1 - Institute of Automation and Control Processes, Far Eastern Branch of Russian Academy of Sciences, 5, Radio St., Vladivostok, Russia, 690041

2 - Far Eastern Federal University, 8, Sukhanova St., Vladivostok, Russia, 690950,

3- Institute of Chemistry, Far Eastern Branch of the Russian Academy of Sciences, 159, Prosp. 100-letiya Vladivostoka, Vladivostok, Russia, 690022

email address: vss@iacp.dvo.ru

The existing methods for measuring of analyte presence and concentration are based on registration of changes in intensity and/or profile of sensitive layer luminescence spectrum. This work proposed a method for implementing of chemosensory systems, which consists in the simultaneous registration of several fluorescent parameters, such as the integrated intensity, the spectral position of the maximum intensities, profile of the excitation spectrum and luminescence lifetime value, as informative parameters of sensory response.

It was shown that sensing element based on europium chelate complexes registries amines in a gas medium. The possibility of increasing the sensitivity and selectivity of this sensor system by simultaneous measuring of integrated luminescence intensity and lifetime value was shown. An important advantage of such approach is the compensating of water vapor influence, which, unlike the amines, quenched europium chelates luminescence.

Another example of using the complex analysis of luminescence parameters for increasing sensor characteristics is a sensor system for copper ions registration in aqueous medium. Here, the sensing element based on a well-known indicator lyumocupferon $(CH_3)_2NC_6H_4CH=C(COOH)NHCOC_6H_5$ [1] embedded in a hydrophilic chitosan matrix.

In a presence of copper ions occurs catalytic formation of lyumocupferon fluorescent dimers. Lyumocupferon considered as a highly sensitive reagent (sensitivity to presence of copper is 0.0002 μg/ml). However its use is limited to analysis of high-purity substances with dependence of its sensor features both of copper concentration and presence of other ions in analyzing medium. At concentration value of a number of metal and compounds ions in one milliliter of solution more than two micrograms lyumocupferon is impossible to use [2]. Lower concentrations of impurities leads to sensor response noising.

We have shown that the use of luminescence excitation spectrum profile as an additional parameter, allows twofold increasing sensitivity of the sensor system through compensation the noise level. Moreover, in the case of presence Fe^{2+}, $A1^{3+}$, Pb^{2+} ions which included in the list of "hindering lyumocupferon usage" in the analyzed solution it is shown that an additional analysis of the luminescence lifetime allows to reduce their influence and increase the selectivity of the sensor system.

It is shown that the registration of number of the luminescence parameters allows carrying out both qualitative and quantitative determination of the concentration of pollutants and provides increase of selectivity of the measuring system. The obtained results show potential ability to develop chemosensory systems, which combine the sensitivity of analytical methods and operative measurements in real conditions.

[1] E. Bozevol'nov, S. Kreyngold, R. Lastovsky, V. Sidorenko, Luminescentny analiz neorganicheskih veschestv, Doklady AS USSR, vol. 153, pp. 97-112 (1963).

[2] S. Kreyngold, E. Bozevol'nov, Katalimatria v analize reaktivov i veschestv osoboy chistoty, Zhurnal analiticeskoy himii, Vol. 18, pp. 942-949, (1963).

SN-2-4

Surface-enhanced infrared spectroscopy for cortisol analysis

O. Cherkasova[1, 2], A. Milekhin[1, 3], I. Milekhin[1], S. Kuznetsov[1], E. Rodyakina[1, 3], A. Latyshev[3]

1- Novosibirsk State University, Pirogova st., 2, Novosibirsk, 630090, Russia

2- Institute of Laser Physics of SB RAS, pr. Lavrentyeva, 13/3, Novosibirsk, 630090 Russia

3- A.V. Rzhanov Institute of Semiconductor Physics, pr. Lavrentyeva, 13, Novosibirsk, Russia

e-mail: o.p.cherkasova@gmail.com

Cortisol is the major corticosteroid hormone secreted by the adrenal gland. This compound is glucocorticoid with catabolic effects facilitating the conversion of protein into glucose and glycogen [1]. The determination of cortosol in biological samples and pharmaceutical drugs can be done by chromatography [1, 2], immunoassays and other methods of analysis [3]. However, these methods are time and cost consuming. In this regard, the development of new methods of analysis is highly relevant. In the studies of small amounts of molecules, conventional IR spectroscopy suffers from relative low molecular IR absorption signals compared to background noise. One way to increase sensitivity is to use field-enhanced spectroscopy techniques as surface-enhanced infrared spectroscopy (SEIRS). The basic principle of the method is resonant excitation in the infrared of specially designed metal nanoparticles known as resonant plasmonic nanoantennas to provide the local electromagnetic field of high intensities [4].

Spectral properties of steroids are well described in infrared (IR) spectral range [5], however, steroid hormones have not been investigated using this technique yet. This work discusses fabrication of special nanoantennas and their application for cortisol analysis.

The method of nanostructuring metal surfaces by means of nanolithography was optimized and Au nanoantenna arrays with the controllable structural and optical parameters on the Si and SiO_2 surfaces were formed. Based on the comparison of the data obtained by IR spectroscopy with those of modelling, the interrelation between the energy of the localized surface plasmon resonance (LSPR) and structural parameters of nanoantennas (length, width of linear and T-shaped antennas, distance between antennas) was established. We designed our nanoantenna with specific lengths L in order to obtain the energy of the fundamental plasmonic resonance close to that of the absorption bands of cortisol and therefore to exploit the maximum near field enhancement.

Cortisol was dissolved in ethanol with different concentrations and dropped onto the substrate surface from solutions. The drop volume was 2 μL. The ratio between IR spectra polarized along and perpendicular to nanoantennas was analyzed. IR spectrum of as-prepared nanoantenna arrays demonstrates a broad absorption band near 1600 cm^{-1} corresponding to the LSPR absorption. After dropping cortisol a blue shift of LSPR energy which is due to the change of the dielectric function of the media surrounding the nanoantennas is observed. Three additional features at 1470 cm^{-1} (deformation vibrations of C-H bonds), 1660 cm^{-1} (stretching vibrations $C^3{=}O^3$ bond), and 1735 cm^{-1} (stretching vibrations $C^{20}{=}O^{20}$ bond) which are characteristic vibrational modes of cortisol are also seen in IR spectrum for cortisol concentration down to 100 pmole. Thus, a possibility of application of nanoantenna arrays for cortisol analysis was shown.

This work was supported by Russian Science Foundation (project 14-12-01037).

[1] O. P. Cherkasova, V. G. Selyatitskaya. Adrenocortical and Renin-Angiotensin Systems in Dynamics of Experimental Diabetes, Biochemistry (Moscow) Supplement Series B,: Biomedical Chemistry, vol. 7 (1), pp. 90-94 (2013).

[2] S. Lee, H.-S. Lim, H.-J. Shin, S.A. Kim, J. Park, H.-C. Kim, H. Kim, H. J. Kim, Y.-T. Kim, K.-R. Lee, Y.-J. Kim, Simultaneous Determination of Cortisol and Cortisone from Human Serum by Liquid Chromatography-Tandem Mass Spectrometry, Journal of Analytical Methods in Chemistry, vol 2014, Article ID 787483, 6 pages (2014)

[3] A. G. Holder, Measurement of glucocorticoids in biological fluids, Methods in Molecular Biology, vol. 324, pp. 141–157 (2006).

[4] F. Neubrech, A. Pucci, T. W. Cornelius, S. Karim, A. García-Etxarri, and J. Aizpurua, Resonant plasmonic and vibrational coupling in a tailored nanoantenna for infrared detection, Phys. Rev. Lett, vol. 101(15), pp. 157403 (2008).

[5] A. Kasal, M. Budesinsky, W. J. Griffiths, "Spectroscopic Methods of Steroid Analysis" in Steroid Analysis, ch. 2, H.L.J. Makin and D.B. Gower, Eds. Springer Science+Business, 2010, pp. 27-161.

Measurement of the *E. coli* concentration in liquid media with an integrate optics sensor

C.M.S. Vicente[1,2,3], R. Oliveira-Silva[1,2], N. J. O. Silva[1,2], M. Tacão[4,5], J. P. da Costa[6], R.A.S. Ferreira[1,2], P.S. André[3,7]

1– Physics Department, University of Aveiro, Portugal
2– CICECO – Aveiro Institute of Materials, University of Aveiro, Portugal
3– Instituto de Telecomunicações, University of Aveiro, Portugal
4–CESAM & Department of Biology, University of Aveiro, Portugal
5– Institute for Research in Biomedicine, iBiMED, Health Sciences Program, University of Aveiro, Portugal
6– CESAM and Department of Chemistry, University of Aveiro, Portugal
7– Department of Electric and Computer Engineering and Instituto de Telecomunicações, Instituto Superior Técnico, University of Lisbon, Portugal

Paulo.andre@ist.utl.pt

Escherichia coli (*E. coli*) naturally occur in the intestinal tract of humans and warm-blooded animals consisting on a diverse group of bacteria most of them innocuous and one integral and important part of a healthy human intestinal tract. However, some *E. coli* strains are pathogenic and may cause disease, including severe diarrhea [1]. The detection and quantification of *E. co*li are commonly assessed by time consuming culture tests, requiring a minimum of 24 hours. These facts pose a challenge to the scientific community, as there is the need to develop low cost and dispensable devices, in order to detect and determine the presence of *E. coli* with simpler and less time-consuming methods. Optical biosensors are powerful alternatives to conventional analytical techniques due to their ease of manipulation, fast response times, high specificity, sensitivity, small size and cost effectiveness, particularly when integrated optics is combined with microfluidic systems, resulting in a low reagent consumption, short analysis time and opening prospects for point of care applications [2]. Among these optical biosensors, waveguide interferometer biosensors are advantageous combinations of evanescent field and optical phase difference measurement methods [3], which can be produced in several material fabrication platforms. Sol-gel derived siloxane-based organic-inorganic hybrid materials have been considered particularly suitable for the fabrication of integrated optics devices [4]. Within the variety of organic-inorganic hosts that have been developed, the so-called di-ureasils present a satisfactory transparency, mechanical and thermal stability which allow them to be processed both as thin films and as transparent and shape-controlled monoliths. Previously, we have reported the use of di-ureasils as cost effective substrates in integrated optics, namely in the production of Mach-Zehnder (MZI) interferometers with applications in temperature sensing [5]. Herein, we report the fabrication and optical characterization of an *E. coli* optical sensor based on a MZI with photopatternable di-ureasil hybrids. The sensor was tested for the real-time determination of *E. coli* grown in an aqueous medium, *E. coli* concentration was measured during an induced concentration process of the suspension from 3.9×10^{-9} to 5.4×10^{-10} cells.mL^{-1} within 5 minutes. The proposed sensor constitutes a compact, fast and cost effective solution for monitoring the concentration of cells, namely, of *E. coli*, in biological fluids.

References

[1] P. M. Griffin and R. V Tauxe, "The epidemiology of infections caused by Escherichia coli O157:H7, other enterohemorrhagic E. coli, and the associated hemolytic uremic syndrome.," *Epidemiol. Rev.*, vol. 13, pp. 60–98, 1991.

[2] D. D. and T. Goswami, "Optical Biosensors: A Revolution Towards Quantum Nanoscale Electronics Device Fabrication," *J. Biomed. Biotechnol.*, vol. 2011, p. 7, 2011.

[3] P. Kozma, F. Kehl, E. Ehrentreich-Förster, C. Stamm, and F. F. Bier, "Integrated planar optical waveguide interferometer biosensors: a comparative review.," *Biosens. Bioelectron.*, vol. 58, pp. 287–307, Aug. 2014.

[4] B. Lebeau and P. Innocenzi, "Hybrid materials for optics and photonics," *Chem. Soc. Rev.*, vol. 40, no. 2, pp. 886–906, Feb. 2011.

[5] R. A. S. Ferreira, C. D. S. Brites, C. M. S. Vicente, P. P. Lima, A. R. N. Bastos, P. G. Marques, M. Hiltunen, L. D. Carlos, and P. S. André, "Photonic-on-a-chip: a thermal actuated Mach-Zehnder interferometer and a molecular thermometer based on a single di-ureasil organic-inorganic hybrid," *Laser Photon. Rev.*, vol. 7, no. 6, pp. 1027–1035, Nov. 2013.

Acknowledgments: This work was funded by National Funds through FCT - Fundação para a Ciência e a Tecnologia under the project UID/EEA/50008/2013 and partially developed in the scope of the project CICECO - Aveiro Institute of Materials (Ref. FCT UID /CTM /50011/2013), financed by Portuguese funds through FCT/MEC and FEDER. Carlos M.S. Vicente also acknowledges FCT for the grant SFRH/BPD/87473/2012.

SN-3-1 (Invited)

Molecular-like Metal Clusters Stabilized in Zeolites: Synthesis, Preparation and Applications

S. Mintova,[1,*] J. Grand,[1] A. Khartchenko,[1] I. Naydenova,[2] V. de Waele[3]

[1]Laboratoire Catalyse et Spectrochimie, Normandie Université, ENSICAEN, CNRS, 6 boulevard Maréchal Juin, 14050 Caen, France

[2]Centre for Industrial and Engineering Optics/School of Physics, Dublin Institute of Technology, Ireland

[3]Laboratoire de Spectrochimie Infrarouge et Raman (LASIR), Université de Lille I, CNRS, 59655 Villeneuve d'Ascq Cedex, France

In the past decades, metal and semiconductor nanoparticles (NP) with the sizes in the range of 1–10 nm have attracted considerable interest due to their unique catalytic behavior and tunable optical, magnetic and electronic properties. The features of metal nanoparticles are strongly affected by their size, and therefore it is important to develop methods for the controlled preparation and stabilization of small metal particles.

Nanosized zeolites have been utilized as a host for metal NPs owing to their high ion exchange capacity, large surface area, regular pore system and topology giving defined locations for metal species. In addition, the metal NPs in zeolites are expected to have high accessibility and high chemical reactivity. The dispersion, structure and oxidation state of the metal species influence their performances, and hence, require detailed investigation.

In this work, we present the preparation of metal nanoparticles (Cu, Pt and Ag) in nanosized zeolite (LTL and EMT-type framework structures), followed by their comprehensive characterization including HRTEM, UV-vis and FTIR spectroscopy, NMR and EPR.

The introduction of metal species in the zeolite host by ion exchange or direct synthesis approaches follow by chemical reduction will be reported. The size and the shape of the metal nanoparticles are controlled by changing the conditions of preparation and amount of metals species introduced in the zeolites.

The applications of metal nanoparticles stabilized in zeolites as selective chemical sensors for exhaust gases and hydrocarbons and medical uses as gas delivering systems will be revealed.

Acknowledgements: We acknowledge the financial support provided by TAR-G-ED ANR project.

SN-3-2 (Invited)

Thermal conductivity evaluation of ultrathin silicon on insulator with Raman technique

Anastasia Salnikova[3], **Jacobo Munguía**[1], **Michel Mermoux**[2], **Vladimir Lysenko**[4], **Mykola Isaiev**[3,5], **Jean-Marie Bluet**[4]

[1] Instituto Politécnico Nacional (IPN), Av. Luis Enrique Erro S/N, Unidad Profesional Adolfo López Mateos, Zacatenco, Delegación Gustavo A. Madero, C.P. 07738, Ciudad de México, México
[2] LEPMI, Grenoble INP, rue de la Piscine—BP75 38402, Saint Martin d'Hères, France
[3] Taras Shevchenko National University of Kyiv, 64/13, Volodymyrska Str., Kiev 01601, Ukraine
[4] University of Lyon, Nanotechnology Institute of Lyon, UMR CNRS 5270, INSA de Lyon, F69621, France
[5] Laboratoire LEMTA, Faculté des Sciences et Technologies, CNRS UMR 7563, Université de Lorraine, BP 70239, 54506 Vandoeuvre les Nancy Cedex, France

mykola.isaiev@knu.ua

Silicon on insulator (SOI) is a basics system of the nowadays micro-, opto, and nanoelectronics. SOI system has sandwich-like multilayered structure with the top layer of thin silicon films located on the silica grown on the silicon substrate. The application of the SOI technology leads to miniaturization of microelectronic devices and allows increasing their operating frequencies. However, the issues connected with the self-heating and heat energy evacuation from the active zones of the devices becomes crucial. Therefore, one should further improve thermal conduction properties of the mentioned above materials and systems.

The improvement could be achieved with the systematical study of thermal conduction properties of SOI systems prepared with different methods and experimental data analysis. Particularly, the experimental data can be the basis of the numerical simulations for achieving the better conditions of SOI fabrication. Therefore, the development of the new express methods of the thermal conductivity evaluation is essential. Particularly, Raman technique successfully applied for the thermal conductivity evaluation of the ultrathin samples [1]. This method is based on the excitation of the thermal perturbation in the sample and simultaneous measurements of the Raman spectra from the heated region. Since the position of the Raman peaks [2] and Stocks/Antistocks ratio [3] strongly depend on the temperature, there is a possibility for precisely evaluation of the temperature in irradiated zone.

In this paper, we will present result of the thermal conductivity study of the ultrathin silicon film on insulator with the thickness 15 nm by Raman technique. For the thermal perturbation excitation, we used ultraviolet laser radiation to perform strong optical absorption and as a result heat source localization in the film. We proposed mathematical model for temperature field formation in the sample. This model takes into account features of light absorption and thermal resistance between layer. The fitting of the experimental results with theoretical ones allows us to evaluate in-plane thermal conductivity of the film. The founded value is in correlation with other theoretical results evaluated with molecular dynamics and Boltzman transport equation solution [4].

References

[1] Balandin A.A., Ghosh S., Bao W., Calizo I., Teweldebrhan D., Miao F., and Lau C.N. 2008 Superior thermal conductivity of single-layer graphene *Nano letters* **8** 902-7

[2] Stoib, B., Filser, S., Petermann, N., Wiggers, H., Stutzmann, M., and Brandt, M.S. 2014. Thermal conductivity of mesoporous films measured by Raman spectroscopy. *Applied Physics Letters*, 104(16), 161907(1–4)

[3] Rodichkina S.P., Osminkina L.A., Isaiev M., Pavlikov A.V., Zoteev A.V., Georgobiani V.A., … Timoshenko V.Y. 2015. Raman diagnostics of photoinduced heating of silicon nanowires prepared by metal-assisted chemical etching. *Applied Physics B*, *121*(3), 337–344.

[4] Chantrenne P., Barrat J.L., Blase X., and Gale J.D. 2005. An analytical model for the thermal conductivity of silicon nanostructures. *Journal of Applied Physics*, 97(10), 104318.

SN-3-3 (Invited)

THE SYSTEM OF THE EMERGENCY SHUTDOWN OF THE LASER RADIATION

A.B. Lyukhter[1], K.V. Skvortsov[2], D.A. Kochuev[2]

1- Vladimir State University named after Alexander and Nikolay Stoletovs, Gorky Street 87, Vladimir, Russia.
2- Engineering Centre at VlSU, Gorky Street 87, Vladimir, Russia.
E-mail: skv@laser33.ru

In this paper shows a concept of system ensuring of the active laser safety by the emergency shutdown of the laser radiation (LR) source; the results of its tests and example of introduction of system.
During operation of the robotic laser complexes (RLC) there is a probability of emergence dangerous and contingency situations: the formation of powerful reflected LR from the treated surface; leaving of LR out of borders of the processed detail/area of processing towards probable finding of personnel (burning the workpiece through, inaccuracy of positioning, failure of control program). A high probability of causing of severe injuries to operating personnel by laser radiation exists when appear an emergency.
The developed system of the emergency shutdown of a laser radiation (SESLR) provides for the implementation of the active laser safety requirements [1] for 4-class hazard of the laser radiation, which include in the laser technological complexes. The system of the active laser safety is equipped by a two-volume protective frameless cabinet. For exclusion false triggering because of different carrying out of laser processing, the sensing element is located in the internal volume of the protective panel. Thanks to an original structure of butt joint of panels, “blind zones” are absent. Shutdown of laser source happens at the time of destruction of any area of the panel surface by laser radiation. The construction of SESLR provides shutdown of laser source when any components of system are fail. For example: destruction of a photodetector, loss of contact with the sensor both in case of laser influence and mechanical failure components of RLC.
SESLR is equipped with autonomous system of self-diagnostics. It is necessary for check of operability of all modules, indication of a condition of protection system and simplification of a complex operation. Procedure of self-diagnostics have carried out at turning on of a laser complex, also it is possible to execute upon the demand of the operator. As an element of self-diagnostics of system the source of radiation corresponding to a wavelength of LR used in a laser technological complex is applied.
SESLR is integrated into the overall security system of the laser robotic complex. Probability of failure-free operation was calculated. Results meet the requirements of [2-4] to the elements of security systems.
The development takes into account the shortcomings of similar SESLR existing active laser security systems [5,6]. For example, the sensitivity range of the sensor is 850 ÷ 1200 nm; eliminated false alarms from spurious sources of heat and light; registration of laser radiation is carried out both in direct and in the case of multiple reflections.
Functional module of ESSLR has passed certification tests on the base of "IPG IRE-Polus" Ltd. Also, the paper presents the investigations of the impact of LR on the panel sections.
We can conclude that the feasibility of using development as a means of collective protection against exposure of LR.

[1] IEC 60825-1:2014 Standard. Safety of laser products.
[2] GOST 31581 -2012 - Laser safety. General safety requirements for development and operation of laser products.
[3] EN ISO 13 849-1:2006 - Safety-related Parts of Control Systems.
[4] EN 62061 Safety of machinery, functional safety of safety - related electrical, electronic and programmable electronic control systems.
[5] Patent US 8,013,998 B2, Pub. Date: 6.09.2011- METHOD AND ARRANGEMENT FOR RECOGNITION OF OPTICAL RADIATION, Inventor: Klaus R. Goebel, Darmstadt (DE), Assignee: Ingenieurburo Goebel GmbH, Darmstadt (DE).
[6] Patent US 2012/0312970 A1, Pub. Date: Dec. 13, 2012, ASSEMBLY AND METHOD FOR DETECTING RADIATION, Inventors: Klaus R. Goebel, Darmstadt (DE), Matthias Miessen’ Eschweiler (DE), Assignees: INGENIEURBURO GOEBEL GMBH’ Darmstadt (DE); REIS GROUP HOLDING GMBH & Co‘KG’ Obemburg (DE) Co‘KG’ Obemburg (DE).

Tilted fiber Bragg gratings acoustically modulated for sensing applications

Carlos A. F. Marques[1], Nélia J. Alberto[2], Fátima Domingues[1], Cátia Leitão[3], Paulo Antunes[1], Paulo André[4]

1- Instituto de Telecomunicações and Physics Department & I3N, Universidade de Aveiro, Campus Universitário de Santiago, 3810-193 Aveiro, Portugal
2- Instituto de Telecomunicações and Mechanical Engineering Department, Centre for Mechanical Technology and Automation, Universidade de Aveiro, Campus Universitário de Santiago, 3810-193 Aveiro, Portugal
3- Physics Department & I3N, Universidade de Aveiro, Campus Universitário de Santiago, 3810-193 Aveiro, Portugal
4 - Instituto de Telecomunicações and Department of Electrical and Computer Engineering, Instituto Superior Técnico, Technical University of Lisbon, 1049-001 Lisbon, Portugal
email: cmarques@av.it.pt

Abstract: Optical fiber sensors have become one of the most promising sensing technologies. Within all the optical fiber sensing technologies, the tilted fiber Bragg gratings (TFBGs) are one of the most attractive, due to their intrinsic properties. On the other hand, the acousto-optic effect is an important, fast and accurate mechanism that can be used to change and control several properties of fiber gratings in silica and polymer optical fiber [1, 2]. It has been successfully applied in the design and construction of various all-optical devices for optical communications and sensing [1-4]. In this work, we present the recent results regarding the production of optical sensors, through the acousto-optic effect in TFBGs. The cladding and core modes amplitude of a TFBG can be controlled by means of the power levels from acoustic wave (AW) source. Also, the cladding modes of a TFBG can be coupled back to the core mode by launching acoustic waves. Different physical parameters like temperature, and refractive index are analyzed in detail when acoustic waves are turned on.

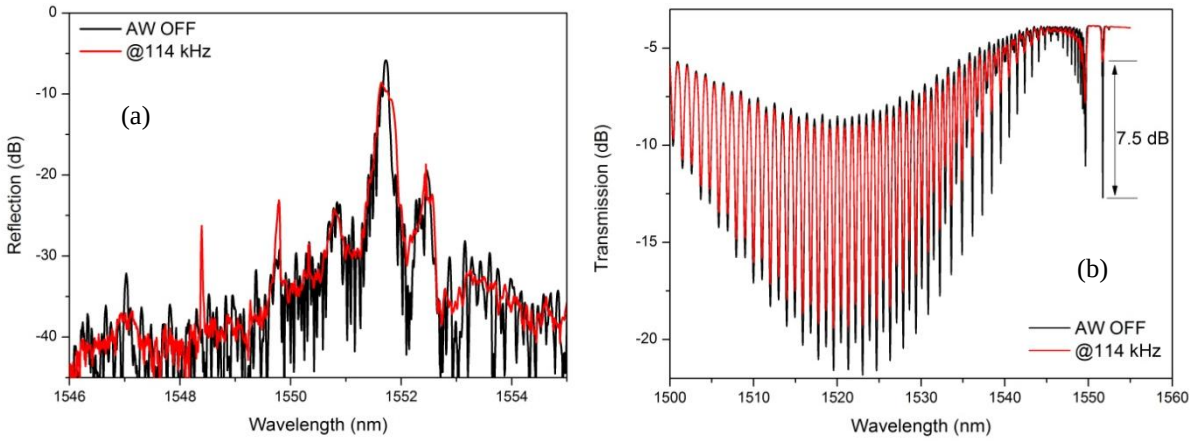

Figure 1- a) Reflection spectra of a TFBG when acoustic wave is OFF and ON. (b) Transmission spectra when an acoustic wave source excited the TFBG at 114 kHz resonance frequency.

Acknowledgments: This work is funded by Fundação para a Ciência e Tecnologia (FCT)/MEC through national funds and when applicable co-funded by FEDER – PT2020 partnership agreement under the projects UID/EEA/50008/2013, UID/CTM/50025/2013, UID/EMS/00481/2013. C. Marques, N. Alberto, F. Domingues, C. Leitão and P. Antunes also acknowledge the financial support from FCT through the fellowships SFRH/BPD/109458/2015, SFRH/BPD/78141/2011, SFRH/BPD/101372/2014, SFRH/BD/84076/2012 and SFRH/BPD/76735/2011, respectively.

[1] C. A. F. Marques, *et al.*, "Acousto-Optic effect in microstructured polymer fiber Bragg gratings: simulation and experimental overview", IEEE/OSA J. Lightw. Technol. 31, 1551 (2013).
[2] C. A. F. Marques, *et al.*, "Tunable acoustic bursts for customized tapered fiber Bragg structures," J. Opt. Soc. Amer. B 29, 3367 (2012).
[3] R .A. Oliveira, *et al.*, "Compact dip-style viscometer based on the acousto-optic effect in a long period fiber grating", Sensors and Actuators B: Chemical 157, 621 (2011).
[4] R. A. Oliveira, *et al.*, "Control of the long period grating spectrum through low frequency flexural acoustic waves," Measurement Science & Technology 22, 045205 (2011).

SN-P-2

Development of highly sensitive holographic sensors for metal ion detection

Sabad-e-Gul[1], Monika Zawadzka[1], Suzanne Martin[1],

John Cassidy[2], Izabela Naydenova[1]

[1]Centre for Industrial and Engineering Optics/School of Physics,

College of Sciences and Health, Dublin Institute of Technology, Kevin Street, Dublin 8

[2]School of Chemical and Pharmaceutical Sciences, College of Sciences and Health,

Dublin Institute of Technology, Kevin Street, Dublin 8

*corresponding author: izabela.naydenova@dit.ie

Abstract

There is an urgent requirement for inexpensive mass producible clinical diagnostic devices that allow measurements on site. Much effort has been devoted to decrease the expense and time that are associated with the study and optimisation of fermentative and cell culture bioprocesses in the pharmaceutical, fine chemicals, food and environmental industries. The development of selective alkali metal ions sensors is a subject of much interest. The research aims to increase sensitivity, reduce sample size, lower operating costs and make single-use disposable devices and improve portability. In this respect, the level of blood electrolytes, particularly H^+, Na^+, K^+ and Cl^- , is widely used to monitor aberrant physiologies associated with pulmonary emphysema, acute and chronic renal failure, heart failure, diabetes. Particularly K^+ ions analysis attracts great attention due to interference from high concentrations of Na^+ in blood.

The sensors reported in this paper are created by holographic recording of surface relief structures in a self-processing photopolymer material. The structures are functionalized by incorporation of chelating agent dibenzo-18-crown-6 in plasticised polyvinyl chloride. Interrogation of these structures by light allows indirect measurements of chemical analytes' concentration in real time. We present results on the optimisation and testing of the holographic sensor. Self-processing acrylamide-based photopolymer was used to fabricate the required photonic structures. Recording light conditions such as intensity and time of exposure were optimised in order to obtain optimised surface relief structures. The performance of the sensors for detection of K^+ and Na^+ was investigated. It was observed that the functionalisation with dibenzo-18-crown-6 provides a selective response of the devices to K^+ over Na^+. The sensor responds to K^+ within the physiological ranges.

SN-P-3

Nanoparticle counting efficiency with photon correlation LDA

Péter Jani, Lénárd Vámos, István Rigó, Péter Schlosser

Wigner Research Center for Physics, Institute of Solid State Physics and Optics,
29-33 Konkoly-Thegestr.H-1121.Budapest, Hungary

schlosser.peter@wigner.mta.hu

Photon correlation Laser Doppler Anemometer (LDA) was developed to monitor the presence of nanoparticles during manufacturing processes, in clean rooms and in the environment [1]. The system uses a Russian DPSS laser with 50 mW output power and 533 nm wavelength. The backscattering arrangement assures the online, in-situ, non-invasive measurements without further fine tuning. The system is suitable to measure simultaneous particle number, velocity and size measurements down to the 50nm particle size. Since the measurements are online and in situ the particle synthesis process can be monitored with high temporal and spatial resolution. In this way a nanoparticle generator, Differential Mobility Analyzer (DMA), can be analyzed and, for instance, the source of an unwanted broad size distribution may be identified, as well as the degree of agglomeration and related properties can be controlled. The accuracy limits of individual velocity and size estimations were investigated with monodisperse paraffin particles separated by DMA. Although the signal-to-noise ratio decreases for nanoparticles, the particle sizing remains correct due to the high power increasing of the scattered intensity with the size [2].

a)

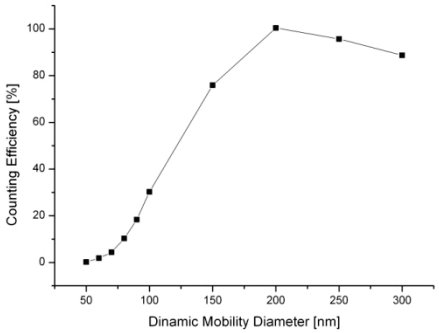

b)

Figure 1. a) “Nano” Laser Doppler Anemometer; b) Nano LDA counting efficiency [3]

The so called Nano LDA is a highly sensitive photon correlation system, which was developed for in-situ characterization of nanoparticles (particle number, particle size and flow velocity) in industrial processes or environment [4]. The light scattering technique makes the system able to measure the above mentioned parameters in extreme conditions (high temperature, acidic environment, high pressure etc.) too. The high counting efficiency combined with high quantum efficiency single photon counting makes it possible to reach the submicron/nanometer size range.

[1] Vámos, Lénárd, Péter Jani. "Optimization algorithm of LDA signal processing for nanoparticles." SPIE Optics+ Photonics. International Society for Optics and Photonics, 2006.
[2] Vámos, Lénárd, Péter Jani. "Lee filtered burst selecting in the photon correlation LDA signal processing." Photonics Europe. International Society for Optics and Photonics, 2008.
[3] Vámos, Lénárd, and Péter Jani. "Particle sizing by photon correlation laser Doppler anemometer in the submicron/nanometer size range." Optical Engineering 49.1 (2010).
[4] Vamos, Lenard, et al. "Calibration measurements down to 50nm with photon correlation nano LDA." Nanotechnology (IEEE-NANO), 2012 12th IEEE Conference on. IEEE, 2012.

SN-P-4

Implementation of an insole matrix of FBG sensors for plantar pressure monitor

M. Fátima Domingues[1,3], Anselmo F. Neto[2], Carlos Marques[1], Cátia Leitão[1], E. Rocon de Lima[3], Paulo André[4], Paulo Antunes[1]

[1]*Instituto de Telecomunicações and University of Aveiro, Physiscs Department & I3N, Campus de Santiago, 3810-193 Aveiro*
[2]*Federal University of Espírito Santo, Department of Electrical Engineering, Av. Fernando Ferrari, 514, Goiabeiras, Vitória 29075-910, Brazil*
[3]*CSIC-UPM, ctra. Campo Real, 28500 Arganda del Rey, Madrid, Spain*
[4]*Instituto de Telecomunicações and University of Lisbon, Department of Electrical and Computer Engineering, Superior Technical Institute , Av. Rovisco Pais, Lisbon 1049-001, Portugal*
email: fatima.domingues@ua.pt

Abstract: In the physical rehabilitation field, one of the critical parameters to monitor is the foot plantar pressure, once an uneven distribution may indicate abnormal posture shifts and other pathologies that may evolve to severe plantar deformities [1, 2]. Although a considerable number of solutions for plantar pressure have been reported, they are mainly based in electronic or imaging devices, presenting some drawbacks such as fragility, instability and inconsistent feedback [3]. In this work is presented a new solution for plantar pressure monitor, using optical fiber sensors technology and its advantages such as robustness, flexibility, immunity to electromagnetic interference, ability to multiplex (optimal for sensing networks), among others [4, 5]. The developed optical platform consists of a cork sole in which 5 Fiber Bragg Grating (FBG) sensors were incorporated in specific points of analysis [3, 6], as shown in Figure 1 a). To evaluate the insole FBGs response, a gait movement was repeated 5 times and the wavelength shift was recorded. We verify that the sensors response is similar in the 5 tests, confirming the repeatability of the insole sensors. In Figure 1.b) is presented the wavelength shift registered for one step, in which is evident the sequence in which the sensors are displayed and activated during the gait movement. The maximum amplitude obtained for each sensor is temporally registered according to what is expected in a gait movement, and from the sum of the 5 sensors response is possible to obtain a typical gait curve, Figure 1 b), [3]. Therefore, the sensors feedback was within the expected behavior, which indicates that the method implemented is an adequate solution for plantar pressure monitoring.

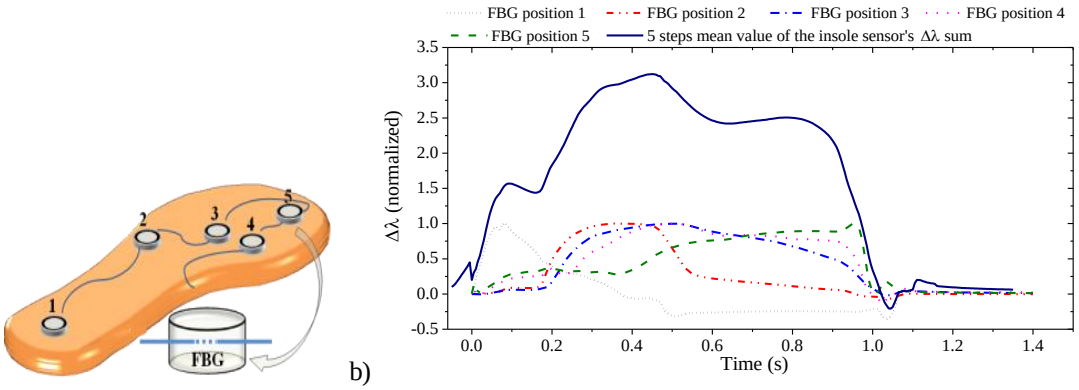

Figure 1- a) Schematics of the cork sole with the incorporated sensors; b) typical wavelength shift registered during a step for the 5 sensors in the sole and the sum of its values.

Acknowledgements: FEDER funds through COMPETE 2020 Program, National Funds through FCT—Portuguese Foundation for Science and Technology under the projects UID/EEA/50008/2013, UID/EMS/00481/2013 and UID/CTM/50025. M. F. Domingues, P. Antunes, C. Leitão and C. Marques acknowledge the following FCT fellowships: SFRH/BPD/101372/2014, SFRH/BPD/76735/2011, SFRH/BD/84076/2012 e SFRH/BPD/109458/2015, respectively. Anselmo F. Neto and E. Rocon de Lima acknowledges a CAPES (8887.095626/2015-01 and PVE nº A126/2013), and FAPES (67566480).

[1]. Abboud, R. J., "(i) Relevant foot biomechanics", Current Orthopaedics, 16(3): 165-179, 2002.
[2]. Monteiro, M., et al., "Influence of obesity and sarcopenic obesity on plantar pressure of postmenopausal women", Clinical Biomechanics, 25(5): 461-467, 2010.
[3]. Abdul Razak, et al. "Foot plantar pressure measurement system: A review", Sensors, 12(7):9884-9912, 2012.
[4]. Antunes, P., et al. "Optical Fiber Microcavity Strain Sensors Produced by the Catastrophic Fuse Effect", IEEE Photonics Technology Letters, 26 (1): 78 - 81, January, 2014.
[5]. Alberto, N., et al. "Optical fiber technology for eHealthcare."Chapter in Handbook of Research on ICTs and Management Systems for Improving Efficiency in Healthcare and Social Care, IGI Global: 180-200, 2013.
[6]. Tao, Weijun, et al. "Gait analysis using wearable sensors", Sensors, 12(2): 2255-2283, 2012.

Fluorescence Imaging of Multi-Mode Propagation in Waveguide Bends and Tapers

Brian D. Jennings, Nicolás Abadía, Chuan Zhong, Ertuğrul Karademir, David McCloskey, John F. Donegan

School of Physics, Trinity College Dublin, College Green, Dublin, Ireland

Centre for Research on Adaptive Nanostructures and Nanodevices, Trinity College Dublin, College Green, Dublin, Ireland

jenninbd@tcd.ie

Abstract: Propagation of light through planar waveguides is important for photonic integrated circuits. Experimentally imaging light intensity within multimode waveguides shows how different modes interfere. These images can be used to determine waveguide properties.

Planar waveguides are an important element for photonic integrated circuits, aiding technologies such as bio-sensing and optical communications. The waveguides used for these applications often support only a single-mode, however, multi-mode waveguides are used in developing areas such as spatial-division multiplexing [1, 2]. Mode-division multiplexing increases the number of signals carried on the separate modes of the waveguide. Dielectric waveguides, such as those fabricated from silicon nitride, are now widespread due partly to the low propagation losses that can be achieved at frequencies of visible light [3]. The method of leakage radiation microscopy has been used to characterise planar plasmonic elements [4]. Here we show how it can be used to determine some properties of multi-mode planar silicon nitride waveguides.

To determine different waveguide characteristics we use a method based on imaging the fluorescence caused by the fields of waveguide modes. The waveguides used consist of a 400 nm thick layer of LPCVD silicon nitride (Si_3N_4) on a 2 μm substrate of thermal silicon dioxide grown on a silicon base wafer. The relatively high refractive index (2.05) of the Si_3N_4 means it can be used as the guiding layer. A cladding layer of polyvinyl acetate (5% w/w in water), doped with Rhodamine B (RhB, 10^{-4} M), is spin coated to a thickness of 100 nm on the Si_3N_4 providing a uniform source of emission from the waveguide. A laser diode of wavelength 532 nm is used in experiments, overlapping quite well with the absorption spectrum of RhB. The fluorescence of the dye is centred around 580 nm and a dichroic mirror is used to remove the green input from experimental images.

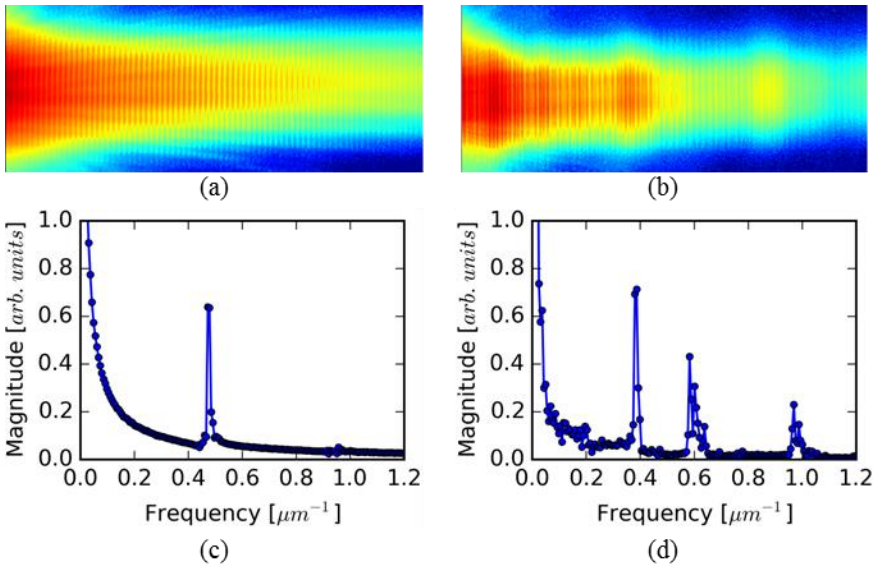

Fig. 1: Intensity colourmap and Fourier transform for slab waveguide. (a) The fluorescence when a slab waveguide is coupled to by end-fire with TM polarised input with the modes propagating from left-to-right, (b) same for TE polarization . (c), (d) Fourier transforms of the intensity profiles along the direction of propagation for the images (a), (b) respectively.

Images of the fluorescence for a slab waveguide under TE and TM input are shown in Fig. 1. Light is coupled at the left, just outside the image, and propagates to the right. Confinement is only in the direction out of the page, with the thickness of the core being 400 nm in this case. This supports two modes in the TM polarized case and three in TE. The oscillation of intensity is a result of the modes going in and out of phase due to their different effective refractive indexes. The period of these oscillations is found by taking a Fourier transform (FT) of the intensity along the direction of propagation. The frequency value of the peaks in the FT are proportional to the difference in effective index of the interfering modes, producing one peak for TM and three for TE. An experimental value of 0.253 was found for the effective index spacing of the TM polarised modes comparing well with the theoretical value of 0.250. In TE polarisation the values found experimentally were 0.198, 0.309 and 0.526 while theory gave 0.202, 0.320 and 0.522.

A similar procedure has been carried out for rectangular waveguides of varying widths (in the range 1-10 μm). Reducing the width of the rectangular waveguides reduces the number of modes propagating in the waveguide, reducing the number of peaks in the FT, and changes the effective index spacing, moving the position of the peaks along the frequency axis. The effect of tapering the waveguide as well as introducing bend regions was examined. In these elements propagation losses are often increased and can be different for different modes, and on top of this inter-mode crosstalk may occur.

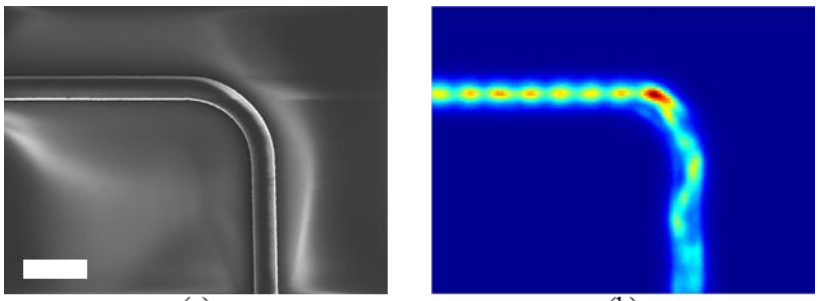

Fig. 2: A bend in a rectangular waveguide. SEM image (a) of a 90^{o} bend in a rectangular waveguide of width 2 μm. Fluorescence image (b) of the same waveguide. From the fluorescence image it is clear where most of the power is being lost in the bend (red spot) and also that the distribution of modes propagating after the bend is different to those before.

As in the case for the slab the FT can be used in regions before and after the taper or bend to determine the presence of particular modes. The image in Fig. 2(b) shows the how a introducing a curve into the waveguide effects the power distribution within the waveguide. How the modes develop in these regions can be seen directly in the images, while repeating the analysis mentioned for the slab waveguides provides a strong method of comparing the modes before and after the bend. The relative power in the modes before-and-after is then compared.

References

[1] Jeffrey B. Driscoll, Richard R. Grote, Brian Souhan, Jerry I. Dadap, Ming Lu, and Richard M. Osgood, "Asymmetric Y junctions in silicon waveguides for on-chip mode-division multiplexing", Opt. Lett. **38**, 1854-1856 (2013).

[2] Yue-De Yang, Yu Li, Yong-Zhen Huang, and Andrew W. Poon, "Silicon nitride three-mode division multiplexing and wavelength-division multiplexing using asymmetrical directional couplers and microring resonators", Opt. Express 22, 22172-22183 (2014).

[3] Subramanian, A.Z.; Neutens, P.; Dhakal, A.; Jansen, R.; Claes, T.; Rottenberg, X.; Peyskens, F.; Selvaraja, S.; Helin, P.; Dubois, B.; Leyssens, K.; Severi, S.; Deshpande, P.; Baets, R.; Van Dorpe, P., "Low-Loss Singlemode PECVD Silicon Nitride Photonic Wire Waveguides for 532–900 nm Wavelength Window Fabricated Within a CMOS Pilot Line", IEEE Photonics Journal, **5**, 6, 2202809 (2013).

[4] Q.Q. Cheng, T. Li, R.Y. Guo, L. Li, S.M. Wang, and S.N. Zhu, "Direct observation of guided-mode interference in polymer loaded plasmonic waveguide", Appl. Phys. Lett. **101**, 171116 (2012).

Laser Micromechanical Acoustic Wave Sensor Based on an Adaptive Interferometer

Roman V. Romashko[1,2], Timofey A. Efimov[1], Yuri N. Kulchin[1,2]

1- Laboratory of Precision Optical Measurement Techniques of Institute of Automation and Control Processes FEB RAS, 690041Radio Str. 5, Vladivostok 690041, Russia
2- School of Natural Sciences, Far-Eastern Federal University, Sukhanov Str. 8, Vladivostok 690091, Russia

romashko@iacp.dvo.ru

Micromechanical acoustic based on using of microcantilever wave sensors in its widest meaning can be used to indicate a number of significantly different devices. Their common characteristic is the fact that acoustic waves are involved in the operating principles. Microcantilevers can be used in the resonant mode or in a nonresonant regime. Due to the high quality factor Q of cantilevers, they show best sensitivity in a resonant mode [1]. In this work we present results of experimental study of applying adaptive interferometry technique based on dynamic holograms recorded in photorefractive crystal [2, 3] for detecting of acoustic wave by measuring of microcantilever`s vibration excited by acoustic wave.

The silicon microcantilever with dimensions 233×45×4 μm^3 was mounted on metal membrane with thickness of 20 μm and diameter of 50 mm (Figure 1.a). Acoustic wave produced by the electrodynamic transducer cause the out-of-plane vibrations of the metal membrane and microcantilever. The last were measured by the adaptive interferometer based on dynamic hologram continiousely recorded in CdTe crustal in orthogonal geometry of vectorial wave mixing [2]. The experimentally measured sensor frequency response is shown in Figure 1.b. The amplitude of the microcantilever vibration on frequency of 9.1 kHz was 115 nm at acoustic pressure of 1.2 Pa at the membrane plane that is corresponded to a sensitivity in 1.3 rad/Pa. As measured detection limit of microcantilever vibration is 1.7 nm, the pressure detection threshold is 17 mPa.

The research was financially supported by Russian Science Foundation (grant # 14-12-01122).

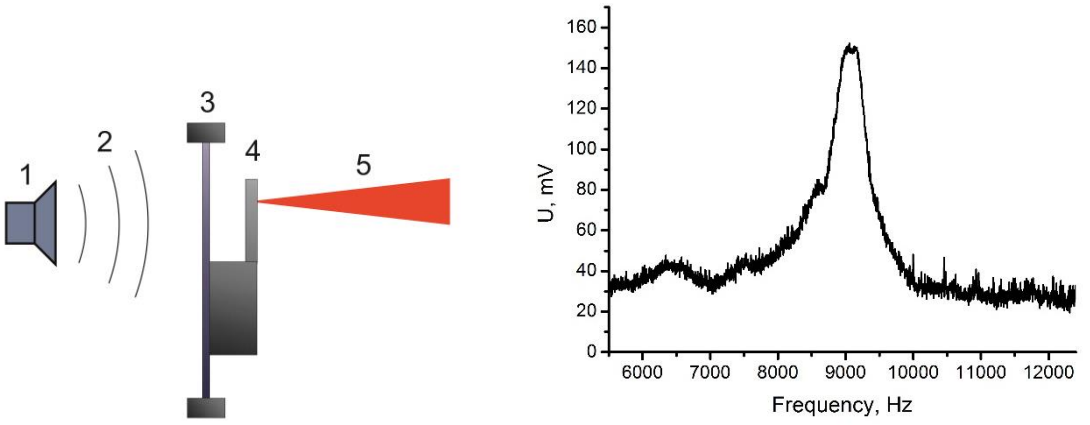

a) b)

Figure 1. a – The scheme of location of the test transmitter and the acoustic sensor. 1 – electrodynamic transducer; 2 – acoustic wave; 3 – metal membrane; 4 – microcantilever; 5 – probe beam of the adaptive interferometer. b – frequency response of the sensor on generated by electrodynamic transducer acoustic field with acoustic pressure of 1.2 Pa.

[1] F. Vittorio, and R. Lucklum. "Overview of acoustic-wave microsensors." Piezoelectric transducers and applications. Springer Berlin Heidelberg, pp. 39-62 (2009)
[2] S. Di Girolamo, R. V. Romashko, Y. N. Kulchin, A. A. Kamshilin, "Orthogonal geometry of wave interaction in a photorefractive crystal for linear phase demodulation," Opt. Commun., vol. 283, pp.128-131 (2010)
[3] A. A.Kamshilin, R. V. Romashko, Y. N. Kulchin. "Adaptive interferometry with photorefractive crystals," J.Appl. Phys., vol.105, No.3, pp.031101 (2009)

SN-P-7

Detection of Weak Seismic Waves in Sea-Ground Interface by Fiber-Optic Seismometer

O. Kamenev[1], Yu. Petrov[1], R. Romashko[1]

1- Institute of Automation & Control Processes, Far-Eastern Branch of Russian Academy of Sciences, Radio,5, Vladivostok, Russia

romashko@iacp.dvo.ru

Sensitivity of fiber-optic interferometric sensors can be increased if multiturn sensing elements are used [1, 2]. As a result a combination of high interferometric sensitivity with long optical path length can provide a measurement of displacements with resolution as low as 10^{-13} m. It opens opportunities for detection of weak seismic waves in sea-ground interface by fiber-optic interferometric seismometer. In our work the fiber-optic accelerometer on the basis of a Mach-Zehnder interferometer was used as the seismometer. Among existing interferometers the Mach-Zehnder interferometer (MZI) has one of the simplest schemes and can be easily used as a base for fiber-optic sensors. In order to maintain the interferometer output signal in the quadrature we applied an active phase control. When the interferometer is in quadrature, the output voltage amplitude is linearly proportional to acceleration amplitude with sensitivity 10^{-7} m/s^2. Such a high sensitivity is provided with multiturn sensing element at the interferometer signal arm.

In the experiment the described fiber-optic seismometer was tested for detection of weak acoustic waves passing through a sea-ground interface. The seismometer was placed ashore on the rock at 50 m above a sea level. Figure 1 shows the time evolution of Fourier spectrum of the signals detected by fiber-optic seismometer during time of the measurement (3 hours). There are noticeable signals which correspond to the heavy-tonnage vessel movement (1) and the small-size high-speed boat (2) passing apart several kilometers from the rock.

The research was financially supported by Russian Science Foundation (grant # 14-12-01122).

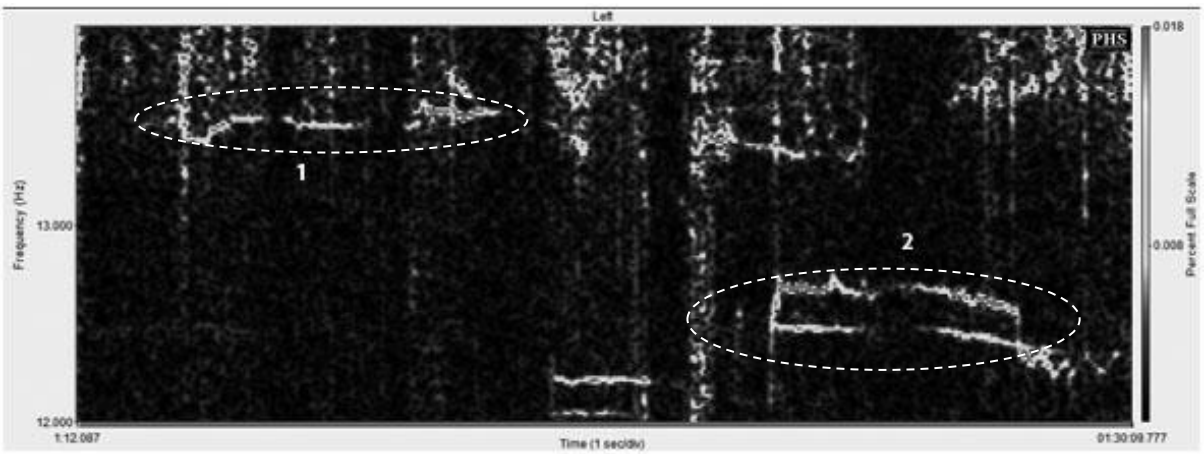

Figure 1. Time evolution of Fourier spectrum of the detected signals produced by a heavy-tonnage vessel (1) and small-size high-speed boat (2).

[1] O.T. Kamenev, Yu.N. Kulchin, Yu.S. Petrov, and R.V. Khizhnyak, Use of a fiber-optic Mach-Zehnder interferometer for creating a deformometer with extended gage length, Technical Physics Letters, vol.40, pp.119-122, (2014).

[2] O.T. Kamenev, Yu.N. Kulchin, Yu.S. Petrov, R.V. Khiznyak, and R.V. Romashko, Fiber-optic seismometer on the basis of Mach-Zehnder interferometer // Sensors and Actuators A, vol.244, pp.133-137, (2016).

SN-P-8

Fiber Optic NO_2 Gas Sensor

V.Krasovskii[1,2], D.Krichevsky[2], I.Likhachev[1], V.Pustovoy[1], A.Zasedatelev[2]

1-A.M.Prokhorov General Physics Institute of the RAS. 38, Vavilov st., Moscow, 119991, Russia
2-National Research Nuclear University MEPHI. 31, Kashirskoe sh., Moscow, 115409, Russia

pustovoy@nsc.gpi.ru

In this work, we have demonstrated the ability to measure small concentrations of the nitrogen dioxide interferometric fiber-optic sensor with a sensitive element on the basis of 2-((2'-hydroxymethyl)-benzyloxy)-9(10),16(17),23(24)-tri-tret-butyl -substituted low symmetrical zinc phthalocyanine complex bearing hydroxyl group on periphery (tZnPc-OH) (Fig.1).

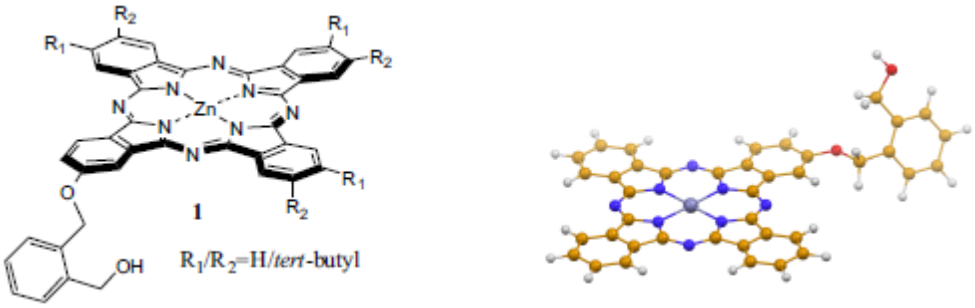

(a) (b)

Fig.1. (a) Phthalocyanine complex chemical structure and (b) calculated geometry

The sensing element was a plate of porous Al_2O_3, obtained with electrochemical etching, with average pore diameters of about 20 nm. The sensitivity to chemical substance was provided by introducing into the pores of the hybrid metal-organic nanoparticles consisting of a metal core and tZnPc-OH shell [1]. Phthalocyanine compounds have the ability to form complexes with the analyte; this changes the electronic structure of the compound, which entails a change in the absorption, refractive index and fluorescent properties. The presence of plasmonic nanoparticles increases these changes due to the local enhancement of the field and charge transfer [2].

The introduction of nanoparticles was carried out by impregnating the porous plate of Al_2O_3 colloidal solution of the hybrid nanoparticles in toluene and subsequent drying at room temperature. NO_2 was obtained by reaction of copper with concentrated nitric acid.

Registration of changes in the refractive index was carried out by spectrum analysis wide broadband radiation reflected from the sensor element using the device described in [3-5]. The measurement results showed the possibility of registering a NO_2 concentration of about 3 ppb.

This work was supported by The Russian Foundation for Basic Research (Grants 16-32-80032, 16-02-00694) and Program of fundamental researches of the Presidium of the Russian Academy of Sciences I.39P.

[1] D.M.Krichevsky, A.V.Zasedatelev, V.I. Krasovskii et al, NO_2 gas sensor based on Au-tZnPc-OH Langmuir-Blodgett thin film, 17-th International Conference «Laser Optics 2016», 27 June – 1 July, St. Petersburg, Russia. (2016).
[2] A.Zasedatelev, A. Karpo, I.Feofanov, V.Krasovskii, V.Pushkarev, Plasmon-Exciton Interaction in AuNP-Phtalocyanine Core/Shell Nanostructures Journal of Physics: Conference Series, vol. 541, 012064 (2014).
[3] S.A.Egorov, A.N.Mamaev, I.G.Likhachiev, High reliable, self calibrated signal processing method for interferometric fiber-optic sensors, SPIE, 1995, vol.2594, pp.193-197 (1995).
[4] K.B.Dedushenko, S.A.Egorov, Yu.Ershov, I.G.Likhachev, Interferometricheskaya volokonno-opticheskaya izmeritelnaya sistema “Dozor”, Pribory, vol.7, pp.23-27 (2002).
[5] I.G.Likhachev, V.I.Pustovoy, Volokonno-opticheskaya sistema izmereniya davleniya, Datchiki i Sistemy, vol.6, pp.56-60 (2011).

THz Sources and Applications

Terahertz imaging technology with direct terahertz detectors

P. Sahafi[1,2], R. Shaikhaidarov[1,3], M. Asada[4], and V.N. Antonov[1,3]
[1] Physics Department, Royal Holloway University of London, Egham, Surrey, TW20 0EX, UK
[2] National Physical Laboratory, Hampton Road, Teddington, TW11 0LW, UK
[3] Moscow Institute of Physics and Technology, 29 Institutskiy per., 141700 Dolgoprudny, Moscow Region, Russia
[4] Tokyo Institute of Technology, 2-12-1-S9-3 O-okayama, Meguro-Ku, Tokyo 152-8552, Japan
E-mail: v.antonov@rhul.ac.

Abstract – We perform terahertz imaging of the objects held at room temperature by using cryogenic direct detectors. Transmission and reflection images of an ivy leaf are taken and analysed. Within this content we study operation of the terahertz detectors themselves, including the graphene ones. The best detectors demonstrate sensitivity up to 10A/W at T~0.5K. Sensitivity degrades to 0.5 A/W at T~ 50K with a noticeable drop at T~ 2K. We model operation of the detectors with a phenomenological theory, and conclude that with a choice of material one can expect spectral sensitive operation at temperatures up to ~70K, where the compact cryo-coolers are readily available. This would allow a remote spectral terahertz imaging for the market applications.

Index Terms – terahertz, heterostructure, graphene

A spectroscopic terahertz remote imaging is enabled with the cryogenic direct detectors. The best performance of such a system has been demonstrated when using Josephson square-law detectors and superconducting bolometers [1, 2]. The application of the technology with these detectors is however unpractical as the bulky power consuming cryogenics with T < 40K are needed for operation. Less sensitive but more practical semiconductor and graphene plasmonic detectors may be an alternative for the terahertz imager. The plasmonic devices demonstrate spectral sensitive operation up to temperatures of ~150K, where compact Sterling and Peltier coolers are readily available [3]. In such a detectors the plasma waves can be resonantly excited in the two dimensional electron gas upon absorption of the terahertz photons. The plasma waves are further rectified at the non-uniform potential profile close to the point contact (PC) resulting in a *dc* voltage offset, and correspondingly the photocurrent, see Fig. 1. The detectors of this type are robust, scalable, spectral selective. They can be utilised in a terahertz imager [4, 5].

As a demonstration we take transmission and reflection image of the ivy leaf. Detector is fixed at the cold plate of cryo-cooler, while the terahertz source (Gunn diode with 2mW at 177GHz) and the leaf are at room temperature. The optical system delivering radiation to the detector has a total attenuation of 35dB. Reflection image of the leaf is shown in Fig. 1. The left

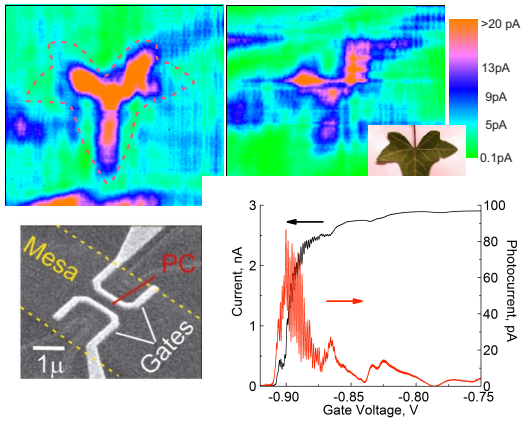

Fig. 1 Reflected images of the ivy leaf exposed to the air (left) and in the paper envelope (right). A 177GHz Gunn diode of nominal power of 2mW is used as a torch. SEM image of the plasmonic detector. Pinch-off curve of the PC current (black) and photocurrent induced by THz radiation (red). The detector is made of GaAs/AlGaAs heterostructure. It is kept at 0.7K.

image is a reflection of the leaf exposed to the air, while the right image is a reflection of the same leaf in a paper envelope. The photo signal drops by more than 40% when the leaf is placed in envelope. The signal also drops when temperature of the detector increases; the amplitude is only 15% at 6.5K of that at 0.7K.

We have modelled operation of the plasmonic detectors, and argue that one can lift operation to temperatures, where the compact cryo-coolers are available, with a proper choice of material, like new 2D graphene.

REFERENCES

[1] Divin, Y., Poppe, U., Gubankov, V. N. & Urban, K.. IEEE Sensors J. 8, 750–757 (2008)
[2] Ilin, K. S. et al, Appl. Phys.Lett. 73, 3938–3940 (1998)
[3] Muravev, V. M. & Kukushkin, I. V. Appl. Phys.Lett. 100, 082102 (2012)
[4] Pelling, S. et al. J Appl Phys 112, 014322 (2012)
[5] Shaikhaidarov, R. et al, Phys. Rev. App., **5**, 024010 (2016)

Terahertz homodyne self-mixing and its application to two-dimensional tomographic terahertz imaging

Wolfgang Elsäßer

Institute of Applied Physics, Technische Universität Darmstadt, Schlossgartenstrasse 7, 64289 Darmstadt, Germany
email address: elsaesser@physik.tu-darmstadt.de

Terahertz research is actually a booming field, with respect to both, a multitude of applications for terahertz radiation and also accompanied by new developments [1], as e.g. for spectroscopy and imaging. Terahertz imaging benefits from the opacity of many materials and the specific spectral finger-prints of a multitude of molecules located in the terahertz region. In this contribution, we experimentally demonstrate a novel and compact terahertz spectroscopy concept by combining both continuous-wave (CW) terahertz radiation generation and phase-sensitive detection in one single photoconductive antenna (PCA). This concept offers a significantly reduced complexity and consequently lower cost of the terahertz spectroscopy setup. Finally, we perform 2D terahertz tomography imaging and reconstruct the two-dimensional image of a hollow-core Teflon cylinder filled with α–lactose as a proof-of-concept application.

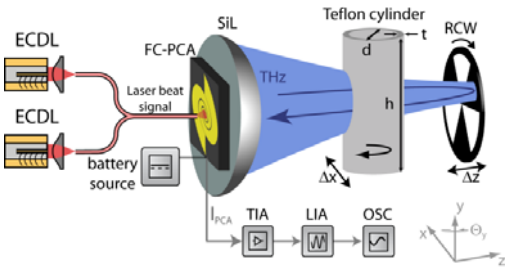

Fig. 1 Schematic of the experimental set-up:ECDL external cavity diode laser; FC-PCA fibercoupled photoconductive antenna; SiL silicon lens; RCW revolving chopper wheel; TIA transimpedance amplifier; LIA lock-in amplifier OSC - digital oscilloscope.

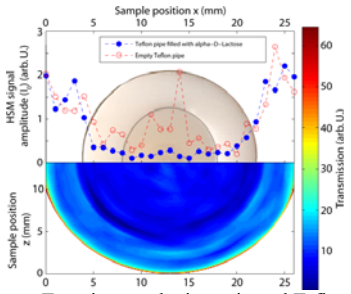

Fig. 2 Upper part: Top view on the investigated Teflon cylinder and experimentally HSM signal amplitudes I_0 for a sample scan in x-direction and for a rotation angle Θ of 0° without (empty circles) and with (filled circles) α-Lactose filling. Lower part: Two-dimensional image of the Teflon cylinder filled with α -Lactose reconstructed by the inverse Radon transformation at 0.19 THz.

The output of two single-mode lasers are superimposed by a fibre based 50:50 beam combiner to generate the optical beat signal, which impinges on a fibre-coupled PCA (FC-PCA). The PCA is electrically connected to a 9 V battery that provides a constant bias voltage. Within the Rayleigh length of the terahertz radiation a revolving chopper wheel (RCW) is placed on a linear translation stage. The terahertz radiation is back-reflected by the surface of this chopper wheel onto the FC-PCA, which gives rise to an AC photocurrent in the FC-PCA. The total photocurrent is electrically amplified and separated in its AC and DC contributions by a transimpedance amplifier. A homodyne self-mixing (HSM) signal, which is proportional to the electric field of the back-reflected terahertz wave [2], is obtained by multiplication of amplitude and the cosine of the phase both measured by a lock-in amplifier. By measuring the HSM signals for the Teflon cylinder at different x-positions and for different rotation angles, the cylinder and its filling will be reconstructed tomographically for two different terahertz frequencies of 0.19 and 0.539 THz [3]. Details of the tomography considering refractive index and diffraction effects will be discussed and perspectives for future research will be given

References

[1] J. P. Guillet, B. Recur, L. Frederique, B. Bousquet, L. Canioni, I. Manek-Hönninger, P. Desbarats, P. Mounaix, "Review of Terahertz Tomography Techniques"', Journal of Infrared, Millimeter, and Terahertz Waves 35(4), 382-411 (2014).
[2] T. Mohr, S. Breuer, D. Blömer, M. Simonetta, S. Patel, M. Schlosser, A. Deninger, G. Birkl, G. Giuliani, W. Elsäßer, "Terahertz homodyne self-mixing transmission spectroscopy", Applied Physics Letters 106, 061111 (2015),
[3] T. Mohr, S. Breuer, W. Elsäßer, "Two-dimensional tomographic terahertz imaging by homodyne self-mixing", Optics Express 23, 27221 (2015)

THz-1-3 (Invited)

Nonthermal impact terahertz radiation on the different level organization of living systems

S.E. Peltek[1], I.A. Mescheryakova[1], E.V. Demidova[1], T.N. Goryachkovskaya[1], E.A. Demidov[1], A.V. Bryanskaya[1], S.V. Sergeeva[1], S.L. Kiselev[3], M.A. Lagarkova[3], G.N. Kulipanov[2], A.I. Semenov[2], N.A. Vinokurov[2], N.A. Kolchanov[1], V.M. Popik[2]

1 The Institute of Cytology and Genetics The Siberian Branch of the Russian Academy of Sciences;
2 Budker Institute of Nuclear Physics the Siberian Branch of the Russian Academy of Sciences;
3 Vavilov Institute of General Genetics, RAS, Moscow,

We studied the impact of terahertz radiation on E. coli biosensor cells containing plasmids with promoters of stress-sensitive genes controlling the expression of GFP. GFP level was measured by fluorometry. The impact of terahertz radiation was nonthermal, i.e. special care was taken to keep specimen temperature at the 35±2°C range during irradiation so that heat shock genes are not induced. We have found that terahertz radiation activates genes associated with oxidative stress response. Results of the Ames test and SOS-chromotest indicate that terahertz radiation produces neither mutagenic nor genotoxic effects.

The exposure of E. coli cells under terahertz radiation causes increased expression of 7 genes of rapid response. Among these genes was glutamine synthetase gene (glnA). By using the glnA gene promoter we have designed biosensor sensitive to the effects of the terahertz radiation.

Since human embryonic stem cells (hESCs) are extremely sensitive to environmental stimuli, we have therefore utilized this cell model to investigate the non-thermal effects of THz irradiation. We have studied DNA damage and transcriptome responses in hESCs exposed to the narrow-band THz radiation (2.3 THz) under strict temperature control.

This work was supported by a grant from the Ministry of Education and Science of the Russian Federation (agreement № 14.616.21.0053 (RFMEFI61615X0053).

THz-1-4 (Invited)

Powerful THz sources - the path to new technologies

M.Glyavin, S. V. Golubev, G. G. Denisov, M. Yu. Tretyakov and A. V. Vodopyanov

Institute of Applied Physics RAS, 46 Ulyanov Str., Nizhny Novgorod, Russia

glyavin@appl.sci-nnov.ru

Development of compact, simple and reliable sources of high-power coherent sub-THz and THz radiation is important for numerous applications [1]. The last decade has contributed to the rapid progress in the development of THz sources, in particular gyrotrons [2]. The unique capability of gyrotrons to generate high–power coherent sub-THz and THz CW beams with high stability of both the output power and frequency makes them appropriate radiation sources for several novel spectroscopic techniques in this frequency range. Among them are: Electron Spin Resonance (ESR) spectroscopy; Nuclear Magnetic Resonance (NMR) spectroscopy with a signal enhancement through Dynamic Nuclear Polarization (NMR–DNP); X-ray detected magnetic resonance (XDMR); and a novel high–precision spectroscopy for studying the energy levels and hyper–fine splitting (HFS) of positronium (Ps). The most advanced, namely NMR–DNP is in fact the first techniques where a gyrotron has been used in spectroscopy. At present, NMR–DNP spectroscopy is considered as a key analytical tool that opens new frontiers in such strategic investigations as: protein structure and genome research; biosynthesis of bio-molecules, materials engineering, etc.

The series of CW gyrotrons for NMR–DNP developed at MIT (USA) and FIR UF (Japan) with frequencies 0.25-0.52 THz and power about 100 W. The CW gyrotron developed at IAP RAS provides radiation with a power up to 100 W and a frequency of 0.26 THz. The advanced concepts that are under consideration is based on planar gyrotrons with ribbon–shaped electron beam and transverse diffractive extraction of the wave as well as multi–beam tubes. Pulsed tube developed at IAP RAS based on a pulsed 28 T magnet (cooled by liquid nitrogen) demonstrate an operating frequency of 0.67 THz, output power of 200 kW and pulse duration of 30 μs has been developed at IAP RAS.

One of the latest applications of sub–THz gyrotrons is the remote detection of concealed radioactive materials. The idea of the method is to initiate a gas breakdown focusing a gyrotron beam on a small spot (having a size comparable to the wavelength of the radiation) where the gamma rays emitted by the shielded material and passing through the walls of the container had created a seed ionization of the ambient air molecules in a breakdown–prone volume. Provided the wavelength is short enough and the wave power is sufficiently high it is possible to realize conditions such that the breakdown rate is small when the radioactive material is absent and high when it is present. Localased gas discharge is promising for development of both a point source of multi–charged ions and a source of high–energy ultraviolet (a.k.a. extreme ultraviolet EUV or XUV). In the experiments, carried out to measure the power of the generated UV light by PIN diode levels about 10 kW have been registered with a pulsed 0.67 THz tube. The gas discharge has been successfully obtained also with CW IAP RAS gyrotron mentioned above. The same CW gyrotron has been used also for the, high-resolution molecular spectroscopy in a gas mixture. The sensitivity of the radio-acoustic detector increase about three orders. The last interesting feature is high speed production of pure nanopowders by material evaporation and condensation. In the case of evaporation by 1kW/CW/0.26THz radiation, the evaporation rate was increased approximately in order in comparison with traditional heating methods. Observing the rapid evolution of the THz gyrotrons and their successful applications in a growing number of scientific and technological fields we believe that they have bright future prospects and will be used on an ever larger scale worldwide [3].

References

[1] Handbook of Terahertz Technologies: Devices and Applications Editors: H.-J.Song, T.Nagatsuma. Taylor & Francis Group, 2015
[2] M. Glyavin, T. Idehara, S. Sabchevski Development of THz gyrotrons at IAP RAS and FIR UF and their applications in physical research and high–power THz technologies. , IEEE Trans. on TST, 5 (5), 788-797 (2015)
[3] C. Armstrong. The truth about terahertz. IEEE Spectrum, 49(9), 36–41 (2012)

THz-1-5 (Invited)

Classical optics experiments with CW terahertz radiation of different mode structures

B. A. Knyazev[1,2], V. V. Cherkassky[2], Yu. Yu. Choporova[1,2], B. G. Goldenberg[1], O. E. Kameshkov[1,2], N. D. Osintseva[1,5], V. S. Pavelyev[3,4], B. O. Volodkin[3]

1 Budker Institute of Nuclear Physics SB RAS, Novosibirsk, 630090, Russia
2 Novosibirsk State University, Novosibirsk, 630090, Russia
3 Samara University, Samara, 443086, Russia
4 Image Processing Systems Institute of the RAS, Samara, 443001, Russia
5 Novosibirsk State Technical University, 630073, Russia

b.a.knyazev@inp.nsk.su

For many years, wideband sources and time-domain experimental techniques dominated in the terahertz science and technology. Gradual progress in the development of CW terahertz radiation sources, such as quantum cascade lasers and free electron lasers (FELs), has triggered interest in creating a novel instrumental base and enabled revisiting classical optics experiments in the THz range. The terahertz line of the Novosibirsk free electron laser [1] emits a plane-polarized monochromatic tunable radiation in the region from 90 to 280 μm. We have developed a set of binary phase diffractive optical elements for the transformation of a high-power Gaussian beam into Laguerre-Gaussian, Hermite-Gaussian, and Bessel-Gaussian ones, including beams with orbital angular momentum ("vortex beams"), and for shaping it into determined volumes and areas. The beams obtained had practically ideal mode structures, which agreed well with the numerical modelling.

The large wavelengths of terahertz beams facilitates conduction of experiments in physical optics using amplitude, phase or phase-amplitude optical transparencies. In particular, we have studied the transmission of Gaussian beam through 1D and 2D periodic structures made of conductors or dielectrics; the latter were transparent or non-transparent to THz radiation. The phenomenon of self-imaging of periodic gratings, referred to as the Talbot effect, is well known and widely used, but this effect has not been practically investigated yet for gratings with near-wavelength apertures. We have demonstrated experimentally that the Talbot self-imaging existed for gratings with opening sizes d / λ, where λ is the wavelength and d is the characteristic size of slit or hole, varied from 7 to 0.75. Surprisingly, numerical modeling using Matlab in the Fresnel-Kirchhoff approximation agreed with the images recorded with a microbolometer matrix, albeit formally the scalar theory is not applicable to such opening sizes. We first studied the transmission of vortex beams through the gratings. In this case, there was no self-imaging, but there were observed some complex periodical patterns ("quasi-Talbot effect"). Further investigation of this phenomenon is a subject of high interest in the vortex photon studies.

Another set of experiments dealt with the diffraction of vortex beams of different topological charges on obstacles: half-plane and double-slit (Young's experiment) ones, as well as with generation of surface plasmon polaritons (SPPs) on an edge ("end-fire coupling") of metal-ZnS-air interface. The diffraction patterns observed are specific to each type of vortex beam and can find practical application to detection of swirled beam characteristics. We have observed a dramatic difference in the efficiency of the SPP generation on the interface left and right sides relative to the optical axis depending on the beam rotation direction. This effect can be employed as a novel one-bit plasmonic switch for optoelectronic devices.

This work was supported in parts by the Ministry of Education and Science of the Russian Federation (project 1879), RFBR grant 15-02-06444 and RSF grant 14-50-00080. The authors are grateful to G. N. Kulipanov and N. A. Vinokurov for stimulated discussions and to the NovoFEL team for the support of the experiments.

[1] G. N. Kulipanov, E.G. Bagryanskaya, E.N. Chesnokov, et al., Novosibirsk free electron laser: Facility description and recent experiments, IEEE Trans. THz Sci. Technol., vol. 5, pp. 798-809, (2011).
[2] Yu Yu. Choporova, B. A. Knyazev, M. S. Mitkov, V. S. Pavelyev and B. O. Volodkin, Generation of terahertz surface plasmon polaritons using non-diffractive Bessel beams with orbital angular momentum, Phys. Rev. Letters, vol. 115, 163901, 2015, 5p.

THz-1-6 (Invited)

THz spectroscopy of atmospheric compounds using electronic, optoelectronic or synchrotron sources

A. Cuisset, R. Bocquet, C. Bray, F. Hindle, G. Mouret, A. Roucou

Laboratoire de Physico-Chimie de l'Atmosphère, 189A Avenue M. Schumann 59140 Dunkerque, France

These 10 last years, the LPCA in Dunkirk have performed new developments of electronic and opto-electronic TeraHertz (THz) spectrometers in order to obtain a powerful tool for high-resolution spectroscopy. Amongst the spectroscopic applications of those spectrometers, precise recording of pure rotational high J line profiles of OCS, HCN, CH_3Cl have been performed, allowing the determination of new broadening parameters include in the HITRAN spectroscopic database [1]. With an improved sensitivity by means of a THz propagation in a multipass cell [2] and a unique frequency metrology technique based on femtosecond laser frequency comb [3], the THz rotational spectra of major atmospheric compounds such as H_2S, SO_2, H_2CO, CH_4, CH_3D, CH_3OH, CH_3Cl, CH_3CN, C_2H_5OH, ... have been measured and analyzed. More recently, the THz optoelectronic source based on photomixing demonstrated its unique capability to study the spectroscopy of small radicals with both environmental and astrophysical interest such as OH, SH or SO. [4] The THz spectra of stable and heaviest volatil organic compounds involving a large density rotational states are now studied using a versatil subTHz spectrometer dedicated for trace gas analysis. The THz radiation is generated via an electronic process of frequency multiplication. Gas phase spectroscopy of industrial organosulfur compounds such as $SOCl_2$ or $SO(CH_3)_2$ may be easily studied using those electronic source. The sensitivity obtained by this prototype instrument permits the analysis of various samples extracted during the industrial sintering of iron ore as part of the manufacturing of steel. [5]

In 2009, the french military agency asked us to test the ability of the THz spectroscopy to study in gas phase the low-frequency vibrational fingerprints of weakly volatil organic molecules. This study concerned the gas phase rovibrational spectroscopy of organosulfide and organophosphorous which are considered as non toxic model compounds in the analysis of chemical weapon materials, high pathogenic and mutagenic agents, and other environmentally interesting air-borne species. Due to the weak intensity of Far-IR bands and the huge density of states in the THz region, a very sensitive and broadband THz technique was required. In this context, we undertook a study using the exceptional properties of the THz source produced by the AILES beamline located of the SOLEIL synchrotron. The coupling of the synchrotron radiation with multipass cells and the FTIR spectrometer allowed to obtain very conclusive results in term of sensitivity and resolution and improved the previous results obtained with classical sources[6]. Finally in 2014, benefiting from our experiences developed these last years both with synchrotron and laboratory THz sources, we have resolved the discrete nature of the coherent THz synchrotron radiation. Indeed we demonstrated that dense powerful THz frequency comb is generated over one decade of frequency by coherent synchrotron radiation. The THz frequency comb has been fully characterized and is demonstrated to be offset free. This discovery opens new perspectives for broadband high resolution spectroscopy [7].

[1] M. Guinet, F. Rohart, J. Buldyreva, V. Gupta, S. Eliet, R. A. Motyenko, L. Margulès, A. Cuisset, F. Hindle, G. Mouret, *Experimental studies by complementary terahertz techniques and semi-classical calculations of N*2*-broadening coe*fficients *of* CH_3Cl, J. Quant. Spectrosc. Radiat. Transfer, 113: 1113, (2012).

[2] F. Hindle, C. Yang, G. Mouret, A. Cuisset et al., *Recent Developments of an Opto-Electronic THz Spectrometer for High-Resolution Spectroscopy*, Sensors, 9: 90.39, (2009).

[3] F. Hindle, G. Mouret, S. Eliet, M. Guinet, A. Cuisset, R. Bocquet, T. Yasui, D. Rovera, *Widely tunable THz synthesizer,* Appl. Phys. B, 104: 763, (2011). `

[4] M. A. Martin-Drumel, F. Hindle, G. Mouret, A. Cuisset, J. Cernicharo; *A complete spectroscopic characterization of SO and its isotopologues up to the THz domain,* AstroPhys. J, 799, 115–126, (2015).

[5] G. Mouret, M. Guinet, A. Cuisset, L. Croize, S. Eliet, R. Bocquet, F. Hindle,*Versatile sub-THz spectrometer for trace gas analysis*, I.E.E.E. Sensors, 13: 6353492, (2013).

[6] I. Smirnova, A. Cuisset, R. Bocquet, F. Hindle, G. Mouret, O. Pirali, P. Roy, *Gas phase synchrotron FTIR spectroscopy of weakly volatile alkyl phosphonate and alkyl phosphate com- pounds : vibrational and conformational studies in the THz/Far-IR spectral domains,* J. Phys. Chem. B, 114: 16936-16947, (2010).

[7] S. Tammaro, O. Pirali, P. Roy, J. F. Lampin, G. Ducournau, A. Cuisset, F. Hindle, G. Mouret, High density THz frequency comb produced by coherent synchrotron radiation, Nature Communications, 6, 20, 7733, (2015)

Laser Terahertz Emission Microscope for the Evaluation of Solar Cells and GaN Wafers

Masayoshi Tonouchi

Institute of Laser Engineering, Osaka University
Osaka JAPAN

One can observe terahertz (THz) radiation from various kinds of materials and devices, when excited with a femtosecond laser, owing to ultrafast current modulation, which reflects ultrafast transient phenomena in optically excited ones. By scanning the laser beam on them, THz emission images are obtained with a resolution of around laser beam diameter rather than THz wavelength. Thus construction of a laser-THz emission microscope (LTEM) would provide a new tool for material/device science and applications. We proposed and have been developing LTEM since 1997. Here we reports the recent progress on LTEM development, dynamic LTEM, near field LTEM, and some examples such as noncontact localization of LSI failure, evaluation of solar cells, imaging of surface potential of GaN wafers.

THz-2-1 (Invited)

Manipulating the Quantum State of Dilute Silicon Donors with Infrared and THz Light

Stephen A. Lynch[1]

1- School of Physics and Astronomy, Cardiff University, Queen's Buildings, The Parade, Cardiff CF24 3AA, Wales.

Main author email address: LynchSA@cardiff.ac.uk

Crystalline silicon can be conveniently doped by substituting a small number of silicon atoms at lattice sites with atoms from the adjacent group-V (pnictogen) column of the periodic table. At low temperatures the extra electron left over after bonding remains loosely bound to the positive core. This object looks and behaves like an isolated hydrogen atom. There is an analogous Rydberg series of narrow lines in the absorption spectrum but they are shifted towards much lower (THz) energies.

Silicon doped with phosphorus is a particularly interesting material from the point of view of quantum control, and this has lead to a dramatic resurgence of activity in the research field. Much of this renewed interest stemmed from a proposal by Kane that silicon doped with group-V donors might be exploited to realise a quantum computer [1]. A related scheme involving group-V donors in silicon was also proposed by Stoneham [2].

A number of experiments designed to investigate the feasibility of Stoneham's quantum computing scheme have now been performed using THz laser light, and are described in this paper. THz pump-probe measurements reveal the lifetimes of the excited states, while THz photon echo experiments show how these states can be manipulated coherently at a quantum level. This was also the first demonstration of a THz photon echo. All of the experiments were performed using the FELIX free electron laser at the FOM institute in the Netherlands. The silicon phosphorus lifetime results are discussed in detail in [3], while a full description of the THz pump-probe technique be found in [4]. A full discussion describing the discovery of a THz photon echo and how it was exploited to demonstrate quantum control can be found in a recent paper [5]. The main cogent points, however, will be summarised in this invited talk.

[1] B. E. Kane, "A silicon-based nuclear spin quantum computer," Nature, vol. 393, pp. 133–137, May 1998.
[2] A. M. Stoneham, A. J. Fisher, and P. T. Greenland, "Optically driven silicon-based quantum gates with potential for high-temperature operation," J. Phys. Condens. Matter, vol. 15, no. 27, p. L447, July 2003.
[3] N. Q. Vinh, P. T. Greenland, K. Litvinenko, B. Redlich, A. F. G. van der Meer, S. A. Lynch, M. Warner, A. M. Stoneham, G. Aeppli, D. J. Paul, C. R. Pidgeon, and B. N. Murdin, "Silicon as a model ion trap: time domain measurements of donor Rydberg states," Proc. Natl. Acad. Sci. USA, vol. 105, no. 31, pp. 10 649–10 653, August 2008.
[4] S. A. Lynch, G. Matmon, S. G. Pavlov, K. L. Litvinenko, B. Redlich, A. F. G. van der Meer, N. V. Abrosimov, and H.-W. H¨ubers, "Inhomogeneous broadening of phosphorus donor lines in the far-infrared spectra of single-crystalline SiGe," Phys. Rev. B, vol. 82, no. 24, p. 245206, December 2010.
[5] P. T. Greenland, S. A. Lynch, A. F. G. van der Meer, B. N. Murdin, C. R. Pidgeon, B. Redlich, N. Q. Vinh, and G. Aeppli, "Coherent control of Rydberg states in silicon," Nature, vol. 465, no. 7301, pp. 1057–1061, June 2010.

THz-2-2 (Invited)

Prospects of Superconducting Single-Photon Detectors SNSPD for THz single-photon detection

A. Korneev[1,2]

1- Moscow Institute of Physics and Technology (State University), 9 Institutskiy per., Dolgoprudny, Moscow Region, 141700, Russian Federation
2- Moscow State Pedagogical University, 1 Malaya Pirogovskaya str., Moscow, 119991, Russian Federation

korneev.aa@mipt.ru

Superconducting nanowire single-photon detectors (SNSPD or SSPD) were first introduced in 2001 [1] and have evolved into a mature novel technology offering high detection efficiency, very low dark counts rate, picosecond timing resolution of photon detection (timing jitter) [2]. SNSPDs successfully compete with Si and InGaAs single-photon avalanche diodes in a range of quantum optics applications in visible light and near infrared such as single-photon source characterization, LIDARs, quantum cryptography and long-range space-to-Earth communication. Although many applications are confined to standard telecom band around 1550 nm, SNSPDs are feasible for single-photon detection at much longer wavelengths. Unlike bolometers and transition edge sensors, SNSPD is cooled down well below its critical temperature and biased with the subcritical current. Absorbed photon breaks Cooper pairs and suppresses superconductivity in a local region which is called “hot-spot”. If the hot-spot is sufficiently large the detector cannot carry subcritical current and switches to the resistive state producing a voltage pulse. Operation under such non-equilibrium conditions enables fast recovery time of the detector and low timing jitter. One of the key parameters ultimately limiting the minimum detectable photon energy is the superconducting gap of the material used for SNSPD fabrication. In niobium nitride (NbN), a material frequently used for SNSPD, the gap is about 1eV which is an order of magnitude smaller compared to infrared photon energy. The use of materials with lower critical temperature and thus lower gap, such as recently introduced WSi [3], is even more feasible for achieving of improved sensitivity in middle infrared. Here we present our research into SNSPD operation beyond 1550 nm wavelengths and the prospects of further SNSPD technology promotion to middle infrared and ultimately to THz range.

[1] G. Gol’tsman, O. Okunev, G. Chulkova, A. Lipatov, A. Semenov, K. Smirnov, B. Voronov, A. Dzardanov, C. Williams, R. Sobolewski, Picosecond superconducting single-photon optical detector, Applied Physics Letters 79, 705-707 (2001)
[2] Chandra M. Natarajan, Michael G. Tanner, Robert H. Hadfield, Superconducting nanowire single-photon detectors: physics and applications, Supercond. Sci. Technol., 25, 063001, (2012)
[3] F. Marsili, V. B. Verma, J. A. Stern, S. Harrington, A. E. Lita, T. Gerrits, I. Vayshenker, B. Baek, M. D. Shaw, R. P. Mirin and S. W. Nam, Detecting single infrared photons with 93% system efficiency, Nature Photonics, 7, 210 (2013)

THz-2-3 (Invited)

Down-conversion in doped GaSe for spectroscopic applications

Z. Huang[1], J. Huang[1], Y. Gao[1], Q. Yang[1], Yu. Andreev[2,3,4], K. Kokh[5], G. Lanskii[2,3,4], V. Svetlichnyi[3,4], J. Molloy[2,6]

1 – National Laboratory for Infrared Physics, Shanghai Institute of Technical Physics CAS, 500 Yutian Road, Shanghai, 200083, China
2 - Laboratory of Advanced Materials and Technologies, Siberian Physical–Technical Institute of Tomsk State University, 1 Novosobornaya Sq., Tomsk, 634050, Russia
3 - Institute of Monitoring of Climatic and Ecological Systems SB RAS, 10/3 Akademicheskii Ave., Tomsk, 634055, Russia
4 - High Current Electronics Institute SB RAS, 2/3, Akademicheskii Ave., 634055, Tomsk, Russia
5 - Laboratory of Crystal Growth, Institute of Geology and Mineralogy SB RAS, 3 Koptyug Ave., Novosibirsk 90, 630090, Russia
6 - National Physical Laboratory, Hampton Rd., Teddington TW11 0LW, UK,

zmhuang@mail.sitp.ac.cn, john.molloy@npl.co.uk

Physical properties of nonlinear p-type ε-GaSe crystal have paid great attention due to its outstanding ability to generate broadband emission from the near IR through the mid- and far-IR (THz) and further into the mm-range. This lecture introduces the current state of the art of the solid solution synthesis and growth technology of pure, light and heavy doped GaSe single crystals, the physical properties and the results achieved for the applications in laser frequency conversion into the mid-IR and THz range, and standoff detection of generated emission of 0.5-1 mm wavelength at distances over 110 m. To improve the optical quality of the synthesized GaSe material, the synthesis was conducted in heavily charged, up to 65% by volume, quartz ampoules to decrease the quantity of rest gases. The quartz ampoules were covered by pyrolytic carbon to decrease interaction of melts with the ampoules impurities. Modified vertical Bridgman growth technology includes application of a rotating heat field to achieve high melt uniformity and thin crystallization front resulting in high optical quality of crystals. To further improve optical quality and strengthen the lattice structure, GaSe was doped with different impurities. Significant improvement of optical quality was achieved for the first time by identified optimal doping with isovalent elements that form isostructural binary compounds. The best result was achieved by doping with small atomic size S atoms that allowed formation of solid solution $GaSe_{1-x}S_x$ single crystals with mixing ratio x up to 0.44. Accumulative effect was found in the improvement of optical quality after double element doping independent on the type of doping element. Doping with Al demonstrated the possibility to control plasma frequency and absorption, which finally allowed control dispersion properties in THz regime. It also resulted in the efficient lattice strengthening possibly through formation of strong chain-type guest atoms bounding. As a result, S & Al doping in layered and extremely soft GaSe result in the crystals to avoid of cracking under strong mechanical or optical impact. Optical properties were also studied over the entire transparency range and criterion for selection adequate measurement data recorded in the THz region. It was also shown that visual criterion cannot be used in the determination of the optical damage threshold.

The most important results achieved in frequency conversion include multistage frequency conversion of non selective CO laser in single GaSe sample with fixed position into wide range (2.3–8.5 μm), demonstrating the equality of GaSe and $ZnGeP_2$ nonlinear susceptibility coefficients and standoff detection of narrow bandwidth (<0.1 cm^{-1}) THz emission generated by DFG of Nd:YAG and near IR KTP OPO systems within 0.5-1 mm region at distances over 110 m. Two model of room temperature Schottky diodes were used, as well as LHe cooled Si bolometer. Other results will be presented in details.

Acknowledgment. This work was supported in part by NFS of China under Grant Nos. 61274138 and 61290302 and the Russian Science Foundation under project No. 15-19-10021.

[1] J. Guo, J. Xie, D. Li, G. Yang, F. Chen, C. Wang, L. Zhang, Yu. Andreev, K. Kokh, G. Lanskii, V. Svetlichnyi, Doped GaSe crystals for laser frequency conversion (Review), Light: Science & Applications, Vol. 4. e362, (2015); K. Kokh, J. Molloy, M. Naftaly, Yu. Andreev, V. Svetlichnyi, G. Lanskii, I. Lapin, T. Izaak, A. Kokh, Growth and optical properties of solid solution crystals $GaSe_{1-x}S_x$, Materials Chemistry and Physics, Vol. 154, pp. 152-157 (2015); M. Naftaly, J. Molloy, Yu. Andreev, K Kokh., G Lanskii., V. Svetlichnyi, Dispersion properties of sulfur doped gallium selenide crystals studied by THz TDS, Optics Express, Vol. 23, No. 25, pp. 32820–32834, (2015).

THz-2-4 (Invited)

THz time-domain characterization of absorbing materials, including comparison of reflection/transmission studies and a combined Kramers-Kronig analysis

Maxime Bernier, Frédéric Garet, and Jean-Louis Coutaz

IMEP-LAHC, UMR CNRS 5130, University Savoie Mont-Blanc, 73376 Le Bourget du Lac Cedex, France

coutaz@univ-savoie.fr

Terahertz time-domain spectroscopy (THz-TDS) is a powerful technique to determine the refractive index and the coefficient of absorption of materials over a large band in the far infrared domain. It is based on the measurement of both the THz waveform transmitted or reflected by the sample, and a reference one recorded without sample in transmission, or reflected by a quasi-perfect metallic mirror in reflection. Then, the ratio of the Fourier transforms of the transmitted/reflected waveform and the reference one gives the complex transmission/reflection coefficient of the sample from which the material parameters can be obtained by solving an inverse electromagnetic problem.

Generally, transmission THz-TDS is employed when dealing with rather transparent samples, while reflection THz-TDS is used with highly absorbing or even opaque samples. Here we first address the intermediate case. From our theoretical study validated by experimental results, we deduce rules to select the most precise technique (transmission or reflection THz-TDS) depending on the sample properties and on the set-up noise and dynamics [1]. If the material exhibits absorption peaks at which transmission vanishes, we show that the loss of phase can be retrieved by combining reflection and transmission data, and thus the material parameters can be determined with a great precision over the whole THz range. When only transmission THz-TDS can be performed, absorption is fairly well extracted at any frequency except nearby the peaks. A Kramers-Kronig (KK) transformation of this so-obtained absorption spectrum gives a good estimation of the refractive index over the whole spectrum, because the error due to missing data is spread over the entire spectrum. Moreover, improvements of the technique based on a careful analysis of the phase and on the single-subtractive KK transformation leads to a very precise estimation of the material parameters [3].

Finally, we use the combined THz-TDS/KK analysis to simply discriminate, from only a single transmission THz-TDS record, scattering losses from absorption ones in an inhomogeneous material. Indeed, the absorption spectrum can be derived with a KK transformation from the refractive index obtained by THz-TDS (scattering does not change noticeably the refractive index), while KK does not involve scattering. Thus the difference between the measured and so-calculated values corresponds to the signal that has been lost due to scattering [4].

[1] M. Bernier, F. Garet, J.-L. Coutaz, and E. Kato, Comparative study of transmission and reflection THz time-domain spectroscopy, in preparation (2016).

[2] M. Bernier, F. Garet, and J.-L. Coutaz, Precise determination of the complex refractive index of samples showing low transmission bands by THz time-domain spectroscopy, IEEE THz Sci. and Technol., 3, 295 (2013).

[3] M. Bernier, F. Garet, J.-L. Coutaz, H. Minamide, and A. Sato, Accurate characterization of resonant samples in the terahertz regime through a technique combining time-domain spectroscopy and Kramers-Kronig analysis, IEEE THz Sci. and Technol. 6, 442-450 (2016).

[4] M. Bernier, F. Garet, and J.-L. Coutaz, Fast and simple method for estimating the scattering loss in an inhomogeneous material at THz frequencies, in preparation (2016).

THz-2-5

Terahertz time-domain spectroscopy for study of the dielectric function of aqueous solutions

O. P. Cherkasova[1], M. M.Nazarov[2], A. P. Shkurinov[2, 3]

1-Institute of Laser Physics of SB RAS, pr. Lavrentyeva, 13/3, Novosibirsk, 630090 Russia

2-Institute on Laser and Information Technologies of RAS, 1 Svyatooserskaya St., Shatura, 142092

3-Lomonosov Moscow State University, Leninskie Gory, GSP-1, Moscow, 119991, Russia

e-mail: o.p.cherkasova@gmail.com

THz spectroscopy is a unique tool that can be used for analysis of solutions because changes in relative proportions of free and bound water and in relaxation times for either of these states can all be observed in THz range. The THz time-domain spectroscopy (THz-TDS) has been used for measuring of glucose and bovine serum albumin (BSA) solutions. To detect small-scale changes in solutions and to increase the significance of observations, we have performed measurements using both transmission in 0.5 mm cell and attenuated total internal reflection (ATR). By combining the results obtained in both configurations, the reliable range of the obtained complex dielectric function spectrum can be considerably broadened (0.07-2.7 THz).

The THz time-domain spectrometer used in the study was described previously [1]. It is known that the biological solutions spectral shape is mainly determined by Debye gamma-relaxation (or "slow" relaxation) of water molecules [2], thus we should move to as low frequencies as possible. We analyzed the reasons for the THz transmission changes of studied solutions comparing experimental spectra to the model dielectric function of water. The insertion of glucose into water leads only to an increase of relaxation time τ_1 of the slow Debye process of this solution. This simple approach describes observed spectral changes in a broad frequency range and for a number of concentrations from 25 mM to saturated solution.

We have found that increasing of BSA concentration in the solution results in a decrease of the amplitude $\Delta\varepsilon_1$ of the slow Debye relaxation process. The dependence of $\Delta\varepsilon_1$ from concentration of BSA in solution is not linear and has a bend at 30 mg/ml. We have not confirmed anomalous changes observed in papers [3, 4] at low concentrations and at low frequencies.

In conclusion, dielectric properties of BSA and glucose solutions were details measured at 0.07-2.7 THz. It was found that the most significant is the reduction $\Delta\varepsilon_1$ (or increase τ_1) of the slow Debye relaxation process with increasing concentrations of solute.

This work has been supported by RFBR (grant № 14-02-00846).

[1] A.A. Angeluts, A.V. Balakin, M.G. Evdokimov et al., "Characteristic responses of biological and nanoscale systems in the terahertz frequency range", *Quantum Electronics*, vol. 44, N 7, pp. 614 – 632, 2014.

[2] O.P. Cherkasova, M.M. Nazarov, A.A. Angeluts, A.P. Shkurinov, "The Investigation of blood plasma in the terahertz frequency range", *Optics and Spectroscopy*, vol. 120, N 1, pp. 50-57, 2016.

[3] J.W. Bye, S. Meliga., D. Ferachou et al., "Analysis of the Hydration Water around Bovine Serum Albumin Using Terahertz Coherent Synchrotron Radiation", *J. Phys. Chem. A*, vol. 118, N 1, pp. 883-888, January, 2014.

[4] O. Sushko, R. Dubrovka, R.S. Donnan, "Sub-terahertz spectroscopy reveals that proteins influence the properties of water at greater distances than previously detected", *The Journal of Chemical Physics*, vol. 142, pp. 055101-1 – 055101-9, January, 2015.

Apply virtual adaptive optics to Shack-Hartmann sensor based coherent imaging

Hai Gong[1], Oleg Soloviev[1,2], Dean Wilding[1], Paolo Pozzi[1], Gleb Vdovin[1,2], Michel Verhaegen[1]

1- DCSC, TU Delft, Mekelweg 2, 2628 CD, Delft, The Netherlands
2- Flexible Optical BV, Polakweg 10-11, 2288 GG Rijswijk, The Netherlands

h.gong@tudelft.nl

Holographic coherent imaging by Shack-Hartmann (SH) sensor, as shown in Figure 1, has been proved its feasibility by our group recently. The SH sensor is an array of micro-lenses which can detect the local wavefront tilts. The complex amplitude in the pupil of an optical system can be directly registered through a high resolution SH sensor. Different from the conventional holography, this single-shot registration progress does not require any reference beam which leads to a simple and robust setup. In most cases, imaging systems suffer from wavefront distortions which caused by static systematic aberrations and dynamic medium aberrations. Adaptive optics (AO) is a technique to cancel wavefront distortions by actively introducing opposite phase with wavefront correction device, like deformable mirror or lens. A standard AO system consists the wavefront sensor, wavefront corrector and its controller [1-3]. The idea here is with the optical field known, we can correct the aberrations computationally to achieve a virtual AO system without the using of real wavefront corrector. In Figure 2, we have experimentally demonstrated the effect of virtual wavefront correction. As the arrangement in Figure 1, a resolution test chart was put in 0.5 m away from the SH sensor. Figure 2 (a) shown the reconstructed phase of the complex field in the sensor plane. Figure 2 (b) was the intensity obtained by propagating this field to 0.5 m. From these results, it was easy to find a defocus aberration with a focal length of 1.65 m existed which caused by the imperfect collimation. After subtracting this defocus, we reconstructed a sharp image of the resolution test chart at the right plane, in Figure 2 (c). A wavefront was also registered without any sample as a reference. Then the image, in Figure 2 (d), was reconstructed by subtracting this reference. This demonstration shows the virtual AO method is a promising way to increase the performance of the SH sensor based imaging technique.

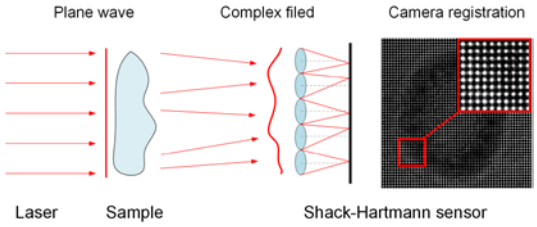

Figure 1 Scheme of complex field registration with SH sensor.

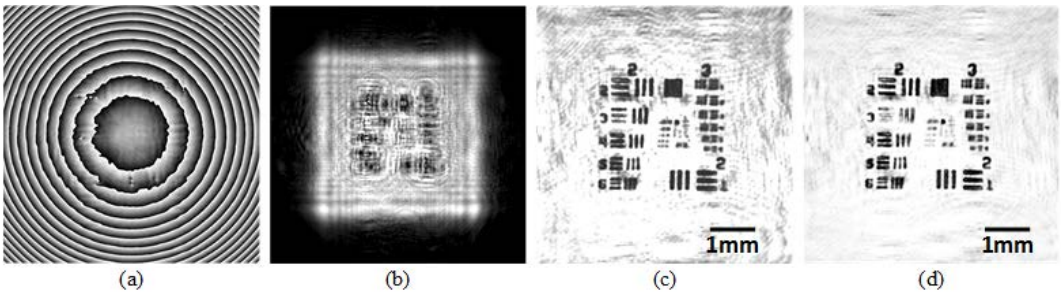

Figure 2 (a) is the uncorrected phase, (b) is the propagation with the uncorrected wavefront, (c) is the propagation with the corrected wavefront, (d) is the propagation with the wavefront subtract the reference.

[1] M. Verhaegen, G.Vdovin, and O.Soloviev, Control for High Resolution Imaging, TU Delft, 2016.
[2] P. Ferraro, S. De Nicola, A. Finizio, G. Coppola, S. Grilli, C. Magro, and G. Pierattini, Compensation of the inherent wave front curvature in digital holographic coherent microscopy for quantitative phase-contrast imaging, Applied optics 42, 1938–1946 (2003).
[3] G. Vdovin, H. Gong, O. Soloviev, P. Pozzi, and M. Verhaegen, Lensless coherent imaging by sampling of the optical field with digital micromirror device, Journal of Optics 17, 122001 (2015).

THz-3-1 (Invited)

Multifrequency IR-THz spectroscopy for Analytical Research

V.Vaks[1,2,3], V.A.Anfertev[1,2], E.G.Domracheva[1,2,3], S.I.Pripolzin[1], L.S.Revin[1,2], M.B.Chernyaeva[1,2]

1- IPM RAS, 7, Akademicheskaya str., Afonino village, Nizhny Novgorod region, 603087 Russia
2- Lobachevsky State University, 23, Gagarina av., Nizhny Novgorod, 603950 Russia
3- ITMO University, St.-Petersburg, 197101 Russia

vax@ipmras.ru, masha@ipmras.ru

Now the actual problems in the gas analysis field have been associated with development of novel methods of analytical research of multicomponent gas mixtures and its application in medical diagnostics (for example, exhaled breath analysis), safety (detection of explosives and poisonous substances) etc. Most of these applications call for precision quantifying of substance in a multicomponent gas mixture, which requires high sensitivity at a 30-100 ppt level. Today, there are a lot of papers which report detection of these gases (CO, NO, ammonia, methane) in the infrared (IR) range (near-infrared range (NIR) and mid-infrared range (MIR)) with detection limit of about 1 ppm - 500ppb. Although, most of these results are obtained for two gas mixtures (usually gas-marker in mixture with N_2), thus avoiding vibrational bands overlapping, which worsens selectivity and hinders gas identification in multicomponent mixtures. Among the spectroscopic methods, the only approach to date that ensures a near-theoretical-limit sensitivity along with a good spectral resolution limited just by the Doppler effect is the nonstationary spectroscopy based on free dumping polarization effect. Other advantages of the spectrometers include easy-to-use configuration and measurement time of several microseconds that provide registration of unstable gases. Application of this method will also benefits in registration of gas-markers absorption lines at one shot without overlapping effect and performing minimal measuring time of few microseconds.

Development of a combined MIR-THz gas analyzer increases the number of gases that can be identified and the reliability of the detection by confirming the signature in both THz and MIR ranges.

The THz and MIR radiation sources of the spectrometer based on solid state harmonics generator and QCL are developed. The THz radiation source can be realized on the solid state generator or backward-wave oscillator with frequency multiplying. The multipliers on the base of Schottky diode or quantum semiconductor superlattice (SL) were used. It has a number of advantages comparing with other well-known microwave generators. Also for THz and MIR ranges the QCLs can be used. They have a high output power and can generate radiation in pulse and continuous modes together with fast tuning of frequency. The cornerstone of the QCL-based radiation source design is a phase-lock loop (PLL) and modulation system. The PLL systems for THz DFB QCL were elaborated. Detection of the radiation in all two frequency ranges (THz and MIR) are realized by the unique receiver block based on SL.

The preliminary investigations of gas-markers in two frequency ranges have demonstrated the advantages of the combined MIR-THz spectrometer for noninvasive medical diagnostics based on exhaled breath research (diabetes, lung or gastrointestinal tract cancer) and remote detection of explosives (e.g. RDX, PETN) for security systems.

The authors acknowledge for partial support from of the Russian Foundation for Basic Research (grant N 15-42-02330 r_povoljie), The Ministry of Education and Science of the Russian Federation (Grants No 2014/134, No 074-U01), Russian Science Foundation (project N 15-12-10035)

High power terahertz sources based on the gas and nono-cluster medium

A.V. Balakin[1], M.S. Dzhidzhoev[1], V.M. Gorgienko[1], M.N. Esaulkov[2], I.A. Zhvaniya[1], I.A. Kotelnikov[3,4], N.A. Kuzechkin[2], I.A. Ozheredov[1], A.B. Savel'ev[1], A.Yu. Sidorov[1], P.M. Solyankin[1], M.B. Smirnov[5], A.P. Shkurinov[1,2,*], and V.Ya. Panchenko[2]

[1]*Faculty of Physics and International Laser Center, Lomonosov Moscow State University, Leninskie Gory, Moscow, 119991, Russia*

[2] *Institute on Laser and Information Technologies of the Russian Academy of Sciences, Shatura, Moscow region, 140700, Russia*

[3]*Budker Institute of Nuclear Physics, Novosibirsk, 630090, Russia*

[4]*Novosibirsk State University, Novosibirsk, 630090, Russia*

[5]*RSC "Kurchatov Institute", IMP, Kurchatov Sq. 1, 123182 Moscow, Russia*

[*] *ashkurinov@physics.msu.ru*

Interactions of laser radiation with gas cluster targets have been investigated in the past two decades. Cluster jet, obtained by the adiabatic condensation of gas flow, has pronounced nonlinear optical properties and combines the advantages of solid-state and gas target. Cluster inherits high local density and this implies high value of nonlinear response. At the same time cluster beams are not exposed to ablation and renew their properties before each act of interaction with the laser pulse. There were observed and predicted various nonlinear effects during interaction of intense laser pulses with cluster jets: generation of X-ray radiation, generation of optical harmonics, self-focusing, Stimulated Raman Scattering. It was shown theoretically and experimentally that absorption of laser radiation in cluster beam can reach high value (up to 95%) which is related to linear (Mie) and nonlinear resonance interactions. Resonance absorption of pulse energy results in efficient production of X-Ray and fast charged particles. In this way, further studies of interaction of intense laser pulses with clusters seems reasonable due to the possibility of usage in various practical applications and solving fundamental problems of behavior of matter under intense laser fields.

In some recent publications, intense THz generation in cluster beam excited by ultrashort laser pulses was reported. It was observed more than two orders of magnitude enhancement of THz pulse intensity in Ar cluster jet compared to that in gaseous Ar with equal average atomic density. With increasing of excitant pulse energy up to its maximum value of 70 mJ (corresponding to the vacuum intensity ~10^{17} W/cm^2) THz pulse energy increased by the square law without saturation. There was reported in that the directivity pattern of terahertz radiation from clustered plasma has four-lobed structure.

At the present moment there is no clear theoretical interpretation of the experimental results and complete understanding of the mechanism of low-frequency emission in cluster plasma. It seems reasonable to carry out further study of terahertz generation in a clustered plasma, and examine this process in both ways: as a fundamental issue of laser-matter interaction on the way to solving a problem of the dynamics of laser-cluster interaction, and as a practical goal of obtaining an effective source of pulsed THz radiation. In addition, there is possible to apply two-color excitation scheme, which has been successfully used in the past to increase the efficiency of the optical to terahertz conversion in laser-induced plasma of gas media. In this scheme, the fundamental laser frequency at ω is mixed with its second harmonic at 2ω. Two-color scheme allows to increase THz yield by 2–3 orders of magnitude and nowadays this scheme is widely used for THz generation in gaseous media. Nevertheless, optical to terahertz conversion efficiency in laser-plasma generation method is still low [16]. In addition, there was observed a saturation of THz yield in a two-color scheme at high excitant pulse energy that originates from THz absorption in dense plasma. Cluster target seems to be attractive to solve these problems.

In this paper we present the results of experimental and theoretical studies of generation of terahertz emission in the laser-induced clustered plasma. We have performed experiments using both single-color and two-color excitation schemes. Simultaneously with the control of terahertz emission of clustered plasma we measured the power of accompanying X-ray radiation, which is an important source of information about the processes that occur in a cluster plasma. In the theoretical section we made an attempt to explain the experimental results.

Plasmonic terahertz sources based on two-dimensional structures

D. Svintsov[1,2], M. Rudenko[1,2], V. Vyurkov[1,2], V. Ryzhii[3]

1- Moscow Institute of Physics and Technology, Dolgoprudny, Russia
2- Institute of Physics and Technology RAS, Moscow, Russia
3- Research Institute of Electrical Communication, Tohoku University, Sendai, Japan
svintcov.da@mipt.ru

The plasmonic terahertz emitters based on the field-effect transistors (FETs) with two-dimensional (2d) electron gas are recognized among most promising due to their compactness, scalability and possibility of frequency tuning [1,2]. In such devices, the passage of dc current leads to the excitation of plasma waves, and their radiative decay results in the THz emission. The excitation of plasma waves is typically attributed to the Dyakonov-Shur instability [3] which relies on the amplified reflection of small charge density perturbations from the drain contact of the FET. This instability is possible provided the FET is connected to a current source, which does not correspond to the experimental situation. The origin of the plasma wave excitation in the FETs with 2d channels thus remains unclear, which hinders further optimization of the THz emitters.

In this paper, we propose a mechanism of plasma wave instability and self-excitation in the 2d FETs, which is consistent with recent observations of the THz emission. The instability occurs in the FETs with partly gated channel, as shown in Fig. 1. Our effect is based on the amplified reflection of small electron density perturbations from the boundary of the gated and ungated sections of the channel. In the absence of direct current, the plasma wave reflection coefficient from such boundary is close to unity due to large ratio of plasma wave velocities in the two regions, similar to the Fresnel reflection from the boundary of materials with large ratio of refractive indices. In the presence of current, the reflection of plasma waves from the boundary becomes amplified, which leads to the growth of plasma oscillations. The frequency of plasma oscillations weakly depends on the length of the ungated section L_2, but depends on the gate length L_1, carrier density n and gate-to-channel separation d. At realistic values $n = 10^{12}$ cm^{-2} and L_1=0.5 μm it is order of 1 THz.

Our estimates show that the self excitation is possible with accessible values of electron mobilities order of 10^4 cm^2/(V s), which corresponds to the gallium arsenide at room temperature (Fig. 2). Further numerical simulations based on the time-dependent nonlinear equations of electron hydrodynamics show that the instability develops into periodic plasma oscillations. The amplitude of voltage oscillations is roughly half of the FET drain voltage; hence, the efficiency of the THz emission is limited only by the radiative decay of plasmons. Last but not least, the predicted instability does not rely on the current saturation, contrary to that of Ref. [4]. Hence, it can occur in the FETs where the saturation is hardly achievable, particularly those based on graphene [5].

The work was supported by the grant # 16-19-10557 of the Russian Scientific Foundation.

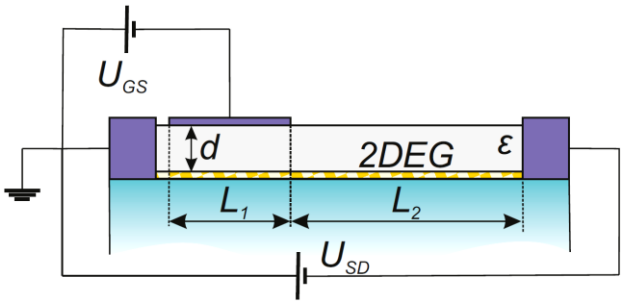

Fig. 1. Schematic view of the FET with partly gated channel, in which the proposed mechanism of plasma wave excitation is realized. L_1 and L_2 are the lengths of gated and ungated sections, d and ε are the thickness and permittivity of the gate insulator.

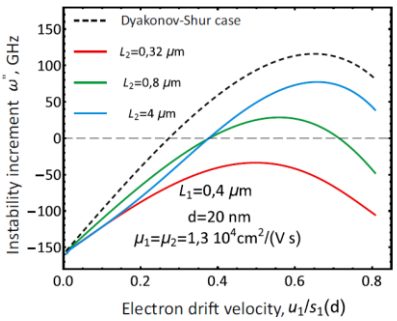

Fig. 2. Calculated plasma instability increment in the FET of Fig. 1 vs. electron drift velocity (in units of plasma velocity) at various ungated section lengths L_2. Dashed line shows the theoretical increment of the Dyakonov-Shur instability

[1] N. Dyakonova *et.al*. Room-temperature terahertz emission from nanomter field-effect transistors, Appl. Phys. Lett. **88**, 141906 (2006)
[2] A. El Fatimy et.al. AlGaN/GaN high electron mobility transistors as a voltage-tunable room temperature terahertz sources, J. Appl. Phys. **107**, 024504 (2010).
[3] M. Dyakonov and M. Shur Shallow water analogy for a ballistic field effect transistor: new mechanism of plasma wave generation by dc current, Phys. Rev. Lett. **71**, 2465-2468 (1993).
[4] V. Ryzhi, A. Satou, M. Shur Transit-time mechanism of plasma instability in high electron mobility transistors, Phys. Stat. Solidi (a) **202**, R113-R115 (2005).
[5] I. Meric et.al. Current saturation in zero-bandgap, top-gated graphene field-effect transistors, Nature Nanotechnology **3**, 654-659 (2008).

THz-3-4 (Invited)

Photonics-Based Approach for THz Industrial Applications

IL-Min Lee, Eui Su Lee, Kiwon Moon, Sang-Pil Han, Hyun-Soo Kim, Jeong-Woo Park, Dong-Woo Park, and Kyung Hyun Park*

Terahertz Basic Research Section, ETRI Daejeon, 305-700, KOREA

**khp@etri.re.kr*

Terahertz (THz) technologies have gathered attentions on its potential in many industrial applications such as non-destructive imaging, spectroscopy, medical imaging, sensing, and communications. Along with the recent achievements in this field, the expectations on the practically applicable THz systems in various industrial field gets higher. However, to bring the THz applications to our everyday life, continuous efforts to make the technology to be easy-to-use, cost-effective, and highly reliable one are still highly demanded. For the compact and low-cost THz devices and systems, we have focused on the photonics-based approaches which includes the developments of the monolithic integrated one-chip beating sources such as dual-mode laser (DML) and dual-wavelength laser (DWL), photomixers such as low-temperature grown (LTG) semiconductor photomixers, evanescently coupled photodiodes (ECPDs), and uni-traveling-carrier photo-diodes (UTC-PDs), detectors including photomixers and Schottky barrier diode (SBD) detectors, and the application systems for the imaging, spectroscopy, thickness measurements, and telecommunications which utilizes our own-developed devices. According to our research roadmap for the easily-accessible industrial applications, we are currently persuiting various approaches to enhance the performances of each device, including developements of arrayed devices and nano technology based devices. In this talk, our progresses over last 5 years along with our recent achievements in the field of CW THz systems based on photonics technologies [1-3] will be presented.

[1] K. Moon, et al., “Bias field tailored plasmonic nano-electrode for high-power terahertz photonic devices,” Scientific Reports, vol. 5 13817 (2015).
[2] E. S. Lee et al., “SOA-integrated dual-mode laser and a PIN-photodiode for compact CW terahertz systems,” ETRI Journal, to be published (For early access view, doi: http://dx.doi.org/10.4218/etrij.16.0115.0882).
[3] S.-P. Han et al., “Real-time imaging of moving living objects using a compact terahertz scanner,” Applied Physics Express, vol. 9 022501 (2016).

Dual-Functional Terahertz Metamaterial based on VO_2 Thin Film

Han-Cheol Ryu[1], Jun-Hwan Shin[2], Kyung Hyun Park[3]

1- Department of Car Mechatronics, Sahmyook University, Seoul 139-742, Korea

2- KU-KIST Graduate School of Converging Science and Technology, Korea University, Seoul 02841, Korea

3- Terahertz Basic Research Section, Broadcasting-Media Basic Technology Research Group, Broadcasting-Media Research Laboratory, ETRI, Daejeon 305-700, Korea

hcryu@syu.ac.kr

We propose an dual-functional terahertz metamaterial based on insulator-metal transition in vanadium dioxide (VO_2) thin film. For the dual functionality, a square-loop shape metamaterial was adopted. The square-loop shape can play roles as a resonating metamaterial and a micro-heater to electrically control a conductivity of VO_2 at the same time. The electric control of the metamaterial can remove the external devices, such as a heater, laser, for the active control of the metamaterial [1, 2]. Thus, the electrical control for the phase transition of VO_2 is preferred for the practical applications. A dual-resonant square-loop structure was designed for the stable transmission characteristics in the desired frequency band as shown in Fig. 1. The measured electromagnetic properties of the metamaterials agreed relatively well with the simulated results. The measured Q-factors of the basic and scaled-down metamaterials fabricated on VO_2 thin films were 2.22 and 1.61 at the center frequencies of 0.44 and 1.14 THz, respectively. The transmittances of the active metamaterials based on VO_2 thin film were successfully controlled by directly applying a bias voltage instead of using an external heater. The amplitude modulation depths of the dual-resonant metamaterials were over 0.82 in the passbands. Our results clearly show the possibility of electrically controllable THz active devices based on VO_2 metamaterial [3].

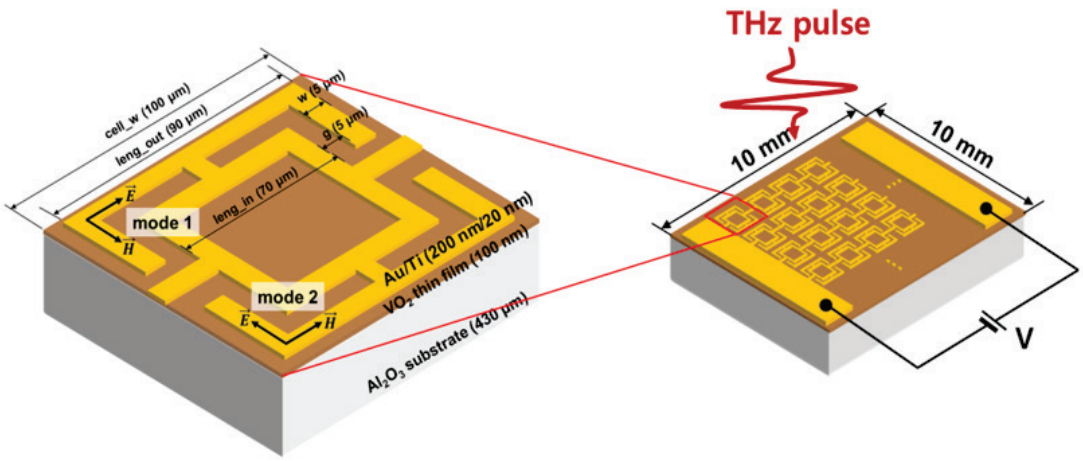

Figure 1. Dual-resonant Square-loop Metamaterial

[1] M. Liu, H. Y. Hwang, H. Tao, A. C. Strikwerda, K. Fan, G. R. Keiser, A. J. Sternbach, K. G. West, S. Kittiwatanakul, J. Lu, S. A. Wolf, F. G. Omenetto, X. Zhang, K. A. Nelson, and R. D. Averitt, Terahertz-field-induced insulator-to-metal transition in vanadium dioxide metamaterial, Nature vol. 487, pp. 345-348, (2012).

[2] L. Ju, B. Geng, J. Horng, C. Girit, M. Martin, Z. Hao, H. A. Bechtel, X. Liang, A. Zettl, Y. R. Shen, and F. Wang, Graphene plasmonics for tunable terahertz metamaterials, Nat. Nanotech., vol. 4, pp. 630-634, (2011).

[3] J. H. Shin, K. H. Park, and H. C. Ryu, Electrically controllable terahertz square-loop metamaterial based on VO2 thin film, Nanotechnology, vol. 27, pp. 195202, (2016).

Time-resolved ultrafast phase transition dynamics in VO_2 films in a wide temperature range

P. Solyankin[2], M. Esaulkov[1], V. Zaitsev[2], L. Parshina[1], V. Mikhalevskii[1], O. Novodvorskii[1], I. Chernykh[3], M. Zanaveskin[3], A. Shkurinov[2]

1- ILIT RAS - Branch of FSRC "Crystallography and Photonics" RAS, 140700, 1 Svyatoozerskaya St., Shatura, Russia
2 - Faculty of Physics, M.V. Lomonosov Moscow State University, 119992, 1 Leninskie Gory St., Moscow, Russia
3- Russian Research Centre Kurchatov Institute, 123182, Moscow, Russia

Soluankp@yandex.ru

Vanadium dioxide is one of the most prospective materials for terahertz beam controlling applications due to its insulator to metal phase transition which occurs at 68°C in bulk VO_2 material. During this phase transition, even for 100 nm thick VO_2 films, THz transmission decreases by up to 85% enabling various THz beam modulation possibilities. As shown in numerous studies, this decrease occurs at picosecond time scales. More important, the phase transition can be initiated optically. Time-resolved studies of the VO_2 film conductivity show that while the transition to the metallic state occurs at ultrashort time scale, the reverse phase transition takes much longer time [1] therefore limiting the maximum attainable modulation frequency for the possible beam-controlling devices. Thus a way to enable a fast phase transition in both directions needs to be elaborated. As was found in [2], the phase transition induced by 800 nm femtosecond optical pulses shows two distinct mechanisms of triggering: injection of 6 THz phonons which leads to breaking of the Peierls distortion and enables the structural transition, and direct injection of electrons into the conductivity zone which can break the Mott condition. Both mechanisms showed to have a threshold character.

The dynamics of optically-induced phase transition at room and elevated temperatures was thoroughly investigated by many groups. In our work, we study the optically-induced phase transition in a wide range of temperatures including cryogenic studies to define a region of experimental conditions at which only the Mott transition occurs without the structural phase transition. Ultrafast dynamics of VO2 conductivity in this regime is poorly investigated. For this we use an optical pump-terahertz probe spectrometer with a cryostat which allows measurements down to temperature of 200K.

We also propose a means to decrease the threshold value of the electron injection mechanism and Mott-type phase transition by means of photosensibilization of VO_2 film with a thin layer of organic dye. When pumped with radiation at the maximum absorption wavelength of the dye, the dye provides electrons into the conduction band of the VO_2 layer without significant heating of the sample [3]. Therefore, the critical number of electrons needed for breaking the Mott condition decreases, and the energy requirements for the ultrafast (on the timescale of 1-2 ps) femtosecond pulse-assisted phase transition are softened.

This work was supported by RFBR Grant № 16-29-11800

[1]. A. Pashkin, C. Kubler, H. Ehrke *et al*, "Ultrafast insulator-metal phase transition in VO2 studied by multiterahertz spectroscopy," Phys. Rev. B., vol. 83, pp. 195120, Apr., 2011
[2]. T.L. Cocker, L.V. Titova, S. Fourmaux *et al*, "Phase diagram of the ultrafast photoinduced insulator-metal transition in vanadium dioxide," Phys. Rev. B., vol. 85, pp. 155120, Apr., 2012
[3] L. V. Levshin, D. Sc. Thesis, M.V. Lomonosov Moscow State University, 2000.

Efficiency of terahertz generation in femtosecond laser breakdown microplasma

M. Esaulkov[1], P. Solyankin[2], A. Borodin[2], A. Sinko[2], A. Frolov[3], A. Shkurinov[2]

1- ILIT RAS - Branch of FSRC "Crystallography and Photonics" RAS, 140700, 1 Svyatoozerskaya St., Shatura, Russia
2 - Faculty of Physics, M.V. Lomonosov Moscow State University, 119992, 1 Leninskie Gory St., Moscow, Russia
3- Joint Institute for High Temperatures of the Russian Academy of Sciences, 125412, 13 Izhorskaya St, Moscow, Russia

Esaulkov_mich@mail.ru

Plasma of femtosecond optical breakdown of gases attracts much interest as a source of pulsed terahertz (THz) radiation due to its broad bandwidth, high field amplitude and simplicity. As it was shown in many studies, the THz radiation efficiency increases rapidly after the optical radiation intensity reaches the ionization threshold value. To reach this threshold, amplified Ti:Sapphire laser systems are usually used and the minimum energy required is on the order of 0.1 mJ per pulse with duration of approximately 100 fs.
In order to make this technique available for a wide range of lower-energy femtosecond laser systems it is needed to solve the problem of reducing the minimum energy threshold of THz generation.
One of the promising ways to decrease the energy requirements for THz generation in gases is tight focusing of the optical radiation. In this case, optical breakdown occurs only in a limited space with dimensions of tens of microns in each direction, and this regime is called “microplasma” [1]. The use of microplasma regime softens the energy threshold for terahertz generation, but properties of this kind of source of THz radiation differ from that of an elongated plasma spark.
In our work, we study the energy, polarization and spatial properties of optical breakdown-based source of THz radiation as we move stepwise from the regime of elongated filament (when laser radiation is focused with a lens having f=10-20 cm) to the microplasma regime (when we use focal distances down to 4.6mm). We use a helium-cooled Silicon bolometer to measure the spatial distribution of energy of THz radiation from laser sparks and microplasmas. Our measurements allow to compare the efficiency of energy conversion into THz radiation for these two regimes and with the regime when first and second harmonic radiation is used for the optical breakdown. Example of angular distribution of THz energy for the case of long and short focal distances can be seen in the Figure 1.

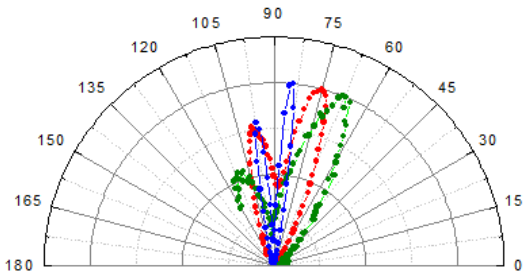

Figure 1. Angular distribution of THz intensity for focusing of ω and 2ω radiation with f=10 cm lens (blue); only ω radiation with f=10 cm lens (red); only ω radiation with f=0.7 cm lens (green)

This work was supported by RFBR Grant № 15-32-20961

[1]. F. Buccheri, X.-C. Zhang, “Terahertz emission from laser-induced microplasma in ambient air,” Optica., vol. 2, № 4, p. 366, Apr., 2015

Numerical simulation of mobility and noise in n-type semi-metallic $Hg_{1-x}Cd_xTe$ quantum well for THz detection applications

E.O. Melezhik, J. V. Gumenjuk-Sichevska, F. F. Sizov

V.E.Lashkaryov Institute of semiconductor physics of NAS of Ukraine,
03028, pr. Nauki 41, Kyiv, Ukraine

emelezhik@gmail.com

$Hg_{1-x}Cd_xTe$ quantum wells (QWs) are interesting in terms of demonstrating high electron mobility and high intrinsic concentration in semi-metallic phase even at T = 77 K, also strongly non-parabolic energy dispersion law characterizes them. That's why these structures could be chosen for creation of THz hot-electron bolometer (HEB) channel with improved sensitivity, low resistance and noise.

Construction of real devises has to be forwarded by numerical simulation of properties of lateral transport in such QWs. Thus our work is dedicated to numerical modeling of dependencies of energy spectra, electron mobility, lateral resistance and noise in such wells on QW growth parameters. Also the goal of our work is to develop optimal sets of QW parameters needed for the production of high-mobility and low-noise quantum wells of considered type for the liquid nitrogen temperature. Our simulation of energy spectra and carrier wave-functions was provided using 8-band k.p method, which accounts bands mixing and allows describing onsets of semi-metallic and semi-conducting states in the well [1].

Charged impurities, holes, and longitudinal polar optical phonon scattering are main electron scattering mechanisms in such system. As last type of scattering is sufficiently inelastic, simple relaxation time approximation becomes inapplicable for mobility calculations. Thus we provided direct numerical solution of Boltzmann transport equation which accounted both non-parabolicity of the dispersion law and inelasticity of electron scattering.

All three main scattering mechanisms are based on Coulomb interaction, thus they are influenced by the screening of 2DEG in the well. In semi-metallic QWs with intrinsic or n-type conductivity, Fermi level is located high in the conduction band; consequently, the energy dispersion law near it is close to the linear type. Recent experiments [2] confirmed that screening in such QWs could be described by graphene-like screening function. In our work this type of screening function was introduced to the mobility calculations in considered systems [3].

We have obtained that the electron mobility for intrinsic conductivity in the semi-metallic $Hg_{1-x}Cd_xTe$ quantum wells is sufficiently low. This is explained by a high concentration of holes. The electron concentration increasing at stable charged impurities concentration leads to the growth of electron mobility by several orders of magnitude. This effect is explained by simultaneous decrease of holes concentration and screening function magnification with the electron concentration growth. Also we have found that increase of molar composition x in the semi-metallic compositions region leads to the growth of the electron mobility. Charged centers (impurities and holes) scattering was found to be the main scattering mechanism, while optical phonon scattering was found to be sufficiently dumped.

It was found that for n-type samples, the temperature noise is dominant, while the generation-recombination noise is an order of magnitude smaller [4]. In addition, we have found that low noise and resistance, and high mobility can be achieved in semi-metallic $Hg_{1-x}Cd_xTe$ QWs, which have non-zero composition, high electron concentration (and, consequently, low holes concentration), and concentration of residual charged impurities that does not exceed 10^{15} cm^{-3}. Electron concentration can be adjusted by barrier delta-doping or by application of top-gate voltage.

[1] E.O. Melezhik, J.V. Gumenjuk-Sichevska, S.A. Dvoretskii, Intrinsic concentration dependences in the HgCdTe quantum well in the range of the insulator-semimetal topological transition, Semiconductor physics, quantum electronics and optoelectronics, vol. 17(2), pp. 179-183, (2014).

[2] C. Brüne, C. Thienel, M. Stuiber, J. Böttcher, H. Buhmann, E. G. Novik, Ch.-X. Liu, E. M. Hankiewicz, L. W. Molenkamp , Dirac-Screening Stabilized Surface-State Transport in a Topological Insulator, Phys. Rev. X, vol. 4, p. 041045, (2014).

[3] E. O. Melezhik, J. V. Gumenjuk-Sichevska and F. F. Sizov, Modeling of electron energy spectra and mobilities in semi-metallic $Hg_{1-x}Cd_xTe$ quantum wells, Journal of Applied Physics, vol. 118, p. 194305, (2015).

[4] E. O. Melezhik, J. V. Gumenjuk-Sichevska and F. F. Sizov, Modeling of Noise and Resistance of Semimetal $Hg_{1-x}Cd_xTe$ Quantum Well used as a Channel for THz Hot-Electron Bolometer, Nanoscale Research Letters, vol. 11(181), pp. 1-6, (2016).

Broad Gain 1.55-μm Dual-Mode DFB Laser for Tunable Continuous-Wave Terahertz Generation

Hyun-Soo Kim, Namje Kim, Donghun Lee, Kiwon Moon, Sang-Pil Han, Eui Su Lee, Il-Min Lee, Won-Hui Lee, and Kyung Hyun Park*

THz Photonics Creative Research Center, ETRI, Daejeon 305-700, Republic of Korea

*khp@etri.re.kr

Terahertz (THz) technology has received enormous interest for application in spectroscopy, imaging, security, and wireless communication [1]. The optical beat source is a key component to achieve compact and low cost for CW THz system. In this work, we fabricated broad gain 1.55-μm DML using asymmetric multiple quantum well (AMQW) for wide tunability.

The wavelength tunable DML was fabricated as shown in Fig. 1. The DML consisted of two $\lambda/4$ phase-shifted DFB sections, one phase section and spot-size converter. The lengths of DFB sections and phase section are 400 μm and 50 μm, respectively. The initial wavelength spacing was set to 4 nm. A buried heterostructure with a p/n/p current blocking layer was used. The active layer consisted of asymmetric multiple quantum well (AMQW). The AMQW was composed of four 7 nm-thick InGaAsP wells (λ=1.61 μm, ε=+0.8%,) and four 5 nm-thick InGaAsP wells (λ=1.61 μm, ε=+0.8%) alternately, which were separated by 10 nm-thick InGaAsP barriers (λ=1.3 μm, ε=-0.6%). The conventional MQW (CMQW) consisted of seven 7 nm-thick InGaAsP wells (λ=1.61 μm, ε=+0.8%) and the same barriers of AMQW. The total well thickness of AMQW is almost equal to that of CMQW. The MQW was sandwiched between 1.24 μm InGaAsP(t=50nm)/1.1 μm InGaAsP (t=50nm) two-step separated confinement heterostructure (SCH) layer. In photoluminescence (PL) at room temperature, full width at half maximum (FWHM) of AMQW and CMQW are 26.6 meV and 49 meV, respectively. The active layer was butt-jointed to 0.33 μm-thick InGaAsP (λ=1.3 μm). In order to tune the operating wavelength independently, μ-heaters were integrated on top of each DFB sections Figure 2 shows the superimposed tuning spectra of AMQW DML and CMQW DML. The front DFB (DFB1) was only biased at 50mA. The maximum heat power was injected up to 0.62 W. The side mode suppression ratio (SMSR) of both DMLs is maintained over above 35 dB through the whole tuning range. As μ-heater power increases, the degradation of output power appears due to the increased difference between gain peak and Bragg wavelength. The degradation of output power in case of DFB LD with AMQW was 3 dB at a 4nm wavelength tuning, which is a 6 dB improvement to the case of CMQW. In order to measure the CW THz radiation, a typical homodyne configuration was set up using low temperature grown (LTG) a log-spiral antenna integrated InGaAs photmixers as THz emitter and detector. The measured CW THz spectrum is shown in Fig.3. We successfully measured CW THz radiation from 191 GHz to 926 GHz. The inset shows the CW THz waveform at a frequency of 191 GHz and 926 GHz.

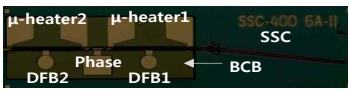

Fig. 1. 1.55 μm DML

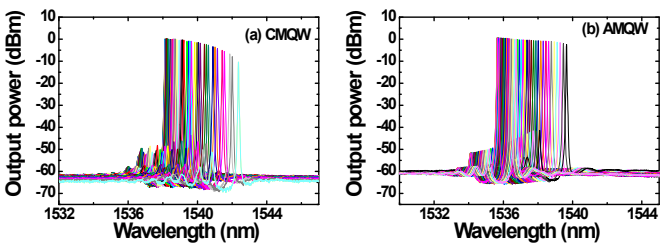

Fig.2 wavelength tuning spectra of 1.55 μm DML; DFB1=50mA, DFB2=0mA

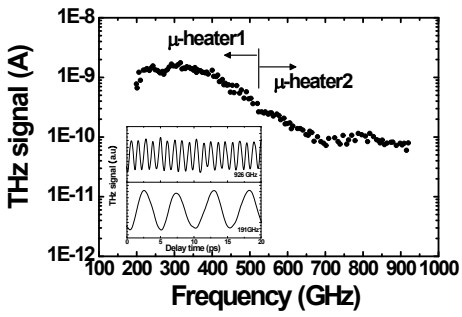

Fig. 3. CW THz spectrum measured with DML and photomixers. Inset shows the THz waveforms of 191 GHz and 926 GHz.

[1] M. Tonouchi., "Cutting-edge terahertz technology," Nat. Photonics **1,** 97-105 (2007).

THz-P-2

Optical generation and detection of THz signal by 1.55 μm devices

P. Landais[1]

1- School of Electronic Engineering, Dublin City University, Glasnevin, Dublin 9, Ireland

Main author email address: landaisp@eeng.dcu.ie

In this communication we present the generation of continuous wave (cw) THz signal based on a semiconductor laser emitting at 1.55 μm and working at room temperature. There is no direct or external modulation applied on this laser, and neither there is a saturable absorber required. The THz generation results from intra-cavity four-wave mixing. The beating between the different longitudinal modes of the laser generates a self-modulation of both carrier density and effective index into its cavity. Therefore it requires having a longitudinal spectrum characterised by a free-spectral range, Δf within the THz region. Commonly semiconductor lasers are between 300 μm to 1mm long, which is too long to achieve 300 GHz emission or above. We have demonstrated that using grooves at key locations along the active layer, the longitudinal spectrum can be controlled and cw THz can be achieved [1,2].

To complete this communication we propose an experimental set-up to accurately measure, in the electrical domain, the frequency of the THz signal generated by this multimode laser. This set-up requires a semiconductor optical amplifier (SOA) under injection of two optical signals. The SOA undergoes a modulation of its complex gain due to the beating occurring at the frequency $\Delta f_{ECL}=c|1/\lambda_1 - 1/\lambda_2|$, where λ_1 and λ_2 are the wavelengths of the two optical signals. When the optical output of the multimode semiconductor laser is also injected into the SOA, there are two beatings one at the THz frequency Δf and the second one at Δf_{ECL}. These beatings produce a modulation at an intermediate frequency, Δf_{RF} given by the difference between Δf and Δf_{ECL}. Therefore, providing that both ECL wavelengths can be known and tuned with a good precision, and assuming they are far enough from the semiconductor laser wavelengths in such a way they do not beat with each other, the cw THz can be spectrally resolved through the measurement in the electrical domain of the intermediate frequency Δf_{RF}. The measurements are in good agreement with previous experiments achieved with the multimode laser. This process can be extended to a large range of detuning frequencies associated with the THz signals. The accuracy of the measurement is determined by the ESA resolution [3].

[1] P. Landais, "A self-pulsating laser," Patent filed on 26/04/2005.

[2] S. Latkowski, F. Surre, P. Landais "Terahertz wave generation from a dc-biased multimode laser," Appl. Phys. Lett. vol. 92, pp. 081-109 (2008).

[3] S. Latkowski, R. Maldonado-Basilio, J. Parra-Cetina, Kevin Carney, S. Philippe, P. Landais, "Semiconductor optical amplifier-based heterodyning detection for resolving optical THz beat-tone signals from passively mode-locked semiconductor lasers," Applied Physics Letters, vol. 97, 081113, (2010).

KEY FOR AUTHORS

Name	*Number*
Abadia N.	SN-P-5
Abbott W.M.	LM-P-11
Abdurashitov A.	BP-P-11
Abreu H.	LSM-2-4
Achim (Popa) C.	LDS-1-4, LDS-P-7, PA-P-3
Agrba P.D.	BP-1-3 (Invited)
Aguiló M.	LSM-3-1 (Invited)
Akila S.	LM-3-8, LM-P-12
Alberto N.J.	SN-P-1
Aldaleeli N.	LDS-P-2
Alekhnovich V.I.	PA-P-1
Alexandrov S.A.	BP-4-4, BP-P-14, BP-P-16
Allahverdiyev K.R.	LDS-P-1
Alyshev S.V.	LM-5-6 (Invited)
Amorim A.	LSM-2-4
Anandarajah P.M.	LM-1-3 (Invited), LDS-2-4
Ananskaya A.A.	BP-P-19, LM-P-2
Anchal A.	LM-1-3 (Invited)
Andersson-Engels S.	PA-1-2 (Invited)
André P.S.	SN-2-5, SN-P-1, SN-P-4
Andreev Yu.	THz-2-3 (Invited)
Anfertev V.A.	THz-3-1 (Invited)
Annou K.	LM-4-8
Anokhin K.V.	BP-2-3, BP-P-18
Antipov A.A.	LM-5-2 (Invited)
Antonov V.N.	THz-1-1 (Invited)
Antunes P.	SN-P-1, SN-P-4
Apresyan L.A.	LSM-P-14
Arakelian S.M.	LM-2-2 (Invited), LM-5-2 (Invited)
Armstrong J.	LDS-P-8
Aronov A.N.	LSM-P-1
Aryshev A.	LM-P-5
Asada M.	THz-1-1 (Invited)
Asadova A.A.	BP-P-3
Atta Khedr M.	LM-3-8, LM-P-12
Auyeung R.	LM-1-5 (Invited)
Avsievich T.I.	BP-P-2, BP-P-7
Azamoum Y.	LM-2-4 (Invited)
Bagratashvili V.	BP-6-5 (Invited)
Balakin A.V.	THz-3-2 (Invited)
Baldycheva A.	LSM-1-2 (Invited)
Ballantine K.E.	LM-1-2 (Invited)
Banchelli M.	BP-6-1 (Invited)
Banita S.	LDS-1-4, LDS-P-7
Bari F.	BP-2-2 (Invited)
Barry L.P.	LDS-2-4, LSM-P-13

Name	*Number*
Beke D.	LDS-1-6
Belousov V.V.	BP-3-4 (Invited), BP-P-17
Bennaceur-Doumaz D.	LM-4-8
Bercu (Petrus) M.	LDS-P-7, PA-P-3
Bernier M.	THz-2-4 (Invited)
Berzin T.M.	BP-5-7 (Invited)
Bildé A.	LM-2-1 (Invited)
Bluet J.-M.	SN-3-2 (Invited)
Boccafoschi F.	BP-4-4
Bocquet R.	THz-1-6 (Invited)
Borodin A.	THz-4-3
Boulmer-Leborgne C.	LM-3-5, LM-P-4
Boyko A.A.	LSM-3-2 (Invited)
Brasse G.	LSM-2-2 (Invited)
Bratu A.M.	LDS-P-7, PA-P-3
Braud A.	LSM-2-2 (Invited)
Bray C.	THz-1-6 (Invited)
Brazier J.A.	BP-6-6 (Invited)
Breathnach A.	PA-P-4
Bruns S.	BP-4-3 (Invited)
Bruns T.	BP-4-3 (Invited)
Bryanskaya A.V.	THz-1-3 (invited)
Bryant J.	LDS-P-8
Buckley K.	BP-5-3 (Invited)
Buckley M.	BP-P-9
Burke Ch.	BP-5-2 (Invited)
Bustamante-Lopez S.	BP-6-4 (Invited)
Buzanov O.	LSM-P-3
Byrne A.	BP-5-2 (Invited)
Byrne H.J.	LDS-1-1 (Invited)
Byrne R.	BP-P-10
Cadier B.	LSM-P-10
Caminati G.	BP-6-1 (Invited)
Camy P.	LSM-2-2 (Invited)
Canalias C.	LSM-3-4 (Invited)
Cardin C.J.	BP-6-6 (Invited)
Cardin D.J.	BP-6-6 (Invited)
Carvalho S.	BP-5-4 (Invited)
Cassidy J.	SN-P-2
Čerkauskaitė A.	LM-1-1 (Invited)
Chaika M.	LSM-P-6
Chan H.	LM-4-6
Chang-You Song	BP-3-5 (Invited)
Charipar N.A.	LM-1-5 (Invited)
Charmasson L.	LM-2-4 (Invited)
Chen W.-D.	LSM-2-1 (Invited)
Chen Y.-F.	LSM-2-1 (Invited)

Name	*Number*
Fedotov I.V.	BP-2-3, BP-3-4 (Invited), BP-P-17, BP-P-18
Fedyanin A.A.	LDS-2-1 (Invited)
Ferré A.	LM-2-4 (Invited)
Ferreira R.A.S.	SN-2-5
Filatova S.A.	BP-P-8
Filipescu M.	LM-4-4 (Invited)
Firstov S.V.	LM-5-6 (Invited)
Firstova E.G.	LM-5-6 (Invited)
Froehly L.	LM-3-7
Frolov A.	THz-4-3
Frolov O.O.	BP-P-5
Frolov S.V.	BP-P-2, BP-P-7
Fuchs Ya.	SN-1-3 (Invited)
Furfaro L.	LM-3-7
Fűrjes P.	LDS-1-6
Furukawa Y.	LM-2-5
Galagan B.I.	LSM-P-2, LSM-P-15
Gao Y.	THz-2-3 (Invited)
Garet F.	THz-2-4 (Invited)
Gérard B.	LSM-P-10
Giannini C.	BP-4-4
Gikas P.D.	BP-5-3 (Invited)
Gil-Villalba A.	LM-3-7
Giust R.	LM-3-7
Gladkova N.D.	BP-1-3 (Invited)
Glass T.E.	BP-6-4 (Invited)
Glyavin M.	THz-1-4 (Invited)
Godin T.	LSM-2-2 (Invited)
Goldenberg B.G.	THz-1-5 (Invited)
Goldsmith J.D.	BP-5-7 (Invited)
Golovan L.A.	LDS-2-5, LM-3-4, LM-P-9
Golubev S.V.	THz-1-4 (Invited)
Gomez L.C.	SN-1-3 (Invited)
Gong H.	THz-2-6
Goodship A.E.	BP-5-3 (Invited)
Gordo P.	LSM-2-4
Gorgienko V.M.	THz-3-2 (Invited)
Goryachkovskaya T.N.	THz-1-3 (invited)
Grand J.	SN-3-1 (Invited)
Gribble A.	BP-3-1 (Invited)
Griebner U.	LSM-3-1 (Invited)
Grigoriev K.S.	LM-4-7
Grisard A.	LSM-P-10
Gubarkova E.V.	BP-1-3 (Invited)
Gueiral N.	BP-5-4 (Invited)
Guillaume Huyet	LSM-1-3 (Invited)
Guizard S.	LM-2-1 (Invited)
Gumenjuk-Sichevska J.V.	THz-4-4

Name	*Number*
Gunnlaugsson T.	BP-6-6 (Invited)
Gurfinkel Yu.I.	BP-6-3 (Invited)
Gurung S.P.	BP-6-6 (Invited)
Guryanov A.N.	LM-5-6 (Invited)
Hafez M.A.	LM-3-8, LM-P-12
Hall J.P.	BP-6-6 (Invited)
Hammad O.	BP-P-10
Han S.-P.	THz-3-4 (Invited), THz-P-1
Hashida M.	LM-1-4 (Invited), LM-2-5
Hata S.	LM-4-2 (Invited)
Haupt K.	SN-1-3 (Invited)
Hayakawa T.	PA-1-6 (Invited)
He B.	LSM-1-5, LSM-1-6, LSM-P-9
Henrique R.	BP-5-4 (Invited)
Hideur A.	LSM-2-2 (Invited)
Himics L.	LDS-1-5, LDS-1-6, LDS-P-3
Hindle F.	THz-1-6 (Invited)
Hobro A.J.	BP-3-3 (Invited)
Hogan J.	BP-P-15, BP-P-16, BP-P-20
Holomb R.	LDS-P-9
Howard J.	BP-P-10
Hristu R.	BP-4-6
Hu M.	LSM-1-6
Huang J.	THz-2-3 (Invited)
Huang Z.	THz-2-3 (Invited)
Huber G.	LSM-3-3 (Invited)
Huseyinoglu M.F.	LDS-P-1
Iakimova M.	LDS-P-5
Inoue S.	LM-1-4 (Invited), LM-2-5
Ionin A.A.	LM-5-4 (Invited), LM-P-6, LSM-P-4
Irisawa K.	PA-1-6 (Invited)
Isaiev M.	SN-3-2 (Invited)
Iskhakova L.D.	LSM-P-15
Itzkan I.	BP-5-7 (Invited)
Ivashkina O.I.	BP-2-3, BP-P-18
Ivleva L.I.	LSM-3-7 (Invited)
Jain G.	LSM-P-8
Jani P.	SN-P-3
Jennings B.D.	LM-3-3, SN-P-5
Jose J.	PA-P-4
Kabashin A.V.	BP-6-2 (Invited)
Kachkovsky O.	LDS-2-3 (Invited)
Kainerstorfer J.M.	BP-2-4 (Invited)
Kakkar A.	BP-4-7 (Invited)
Kalachev Yu.L.	LDS-P-10, LSM-P-11

Name	*Number*
Lee E.S.	THz-3-4 (Invited), THz-P-1
Lee I.-M.	THz-3-4 (Invited), THz-P-1
Lee K.	BP-5-5, BP-5-6, BP-6-3 (Invited), BP-P-13
Lee S.	LDS-P-11
Lee W.-H.	THz-P-1
Leitao C.	SN-P-1, SN-P-4
Leonov A.	SN-2-3 (Invited)
Lesage F.	BP-4-7 (Invited)
Likhachev I.	SN-P-8
Lipatiev A.S.	LM-2-7
Lippert Th.	LM-4-4 (Invited)
Liu N.	BP-5-1 (Invited)
Lohmüller T.	LM-3-2 (Invited)
Loiko P.	LSM-3-1 (Invited)
Lotin A.A.	LM-P-1, LSM-P-1, LSM-P-5
Lu J.-L.	LSM-2-1 (Invited)
Lugovtsov A.E.	BP-5-5, BP-5-6, BP-6-3 (Invited), BP-P-13
Lutsyk P.	LDS-2-3 (Invited)
Lynch G.	BP-P-14
Lynch S.A.	THz-2-1 (Invited)
Lyng F.	LDS-1-3 (Invited), LDS-P-8
Lysenko V.	SN-3-2 (Invited)
Lyukhter A.B.	SN-3-3 (Invited)
Maestroni V.	LSM-3-4 (Invited)
Mahon A.	BP-P-10
Makarov V.A.	LM-4-7
Mandelis A.	PA-1-4 (Invited)
Mani A.A.	BP-5-1 (Invited)
Marangos J.P.	LDS-2-6
Marchev G.M.	LSM-3-2 (Invited)
Marenkin S.F.	LSM-P-1
Markova M.D.	BP-P-6
Marques C.A.F.	SN-P-1, SN-P-4
Martin S.	SN-P-2
Masuno S.	LM-1-4 (Invited)
Matei C.E.	LDS-1-4, LDS-P-7, PA-P-3
Mateos X.	LSM-3-1 (Invited)
Matolín V.	LDS-P-9
Matousek P.	BP-5-3 (Invited)
Matsuoka S.	LM-2-5
Matteini P.	BP-6-1 (Invited)
Maydykovskiy A.	BP-P-12
McCloskey D.	LM-3-3, LM-P-7, LM-P-11, LSM-2-6, LSM-P-8, SN-P-5
McDaniel C.	LM-3-6
McDonagh C.	SN-2-1 (Invited)
McEnroe T.	BP-P-10
McGrath J.	BP-4-4, PA-P-4

Name	*Number*
McNamara P.M.	BP-P-15, BP-P-16, BP-P-20
Meade A.D.	LDS-P-8
Medipally D.K.	LDS-P-8
Meehan R.	LSM-P-8
Meglinski I.	BP-1-4 (Invited)
Meissner K.E.	BP-6-4 (Invited)
Melezhik E.O.	THz-4-4
Melkumov M.A.	LM-5-6 (Invited)
Meller A.E.	BP-1-3 (Invited)
Melnikov D.	LDS-P-6
Melninkaitis A.	LM-2-1 (Invited)
Menyhárt Á.	BP-2-2 (Invited)
Mercer I.P.	LDS-2-6
Mermoux M.	SN-3-2 (Invited)
Mescheryakova I.A.	THz-1-3 (invited)
Meyer R.	LM-3-7
Mezentsev V.K.	LM-2-7
Michalevsky V.A.	LSM-P-5
Midorikawa K.	LM-4-1 (Invited)
Mihaylova E.	SN-1-5
Mikhailov V.A.	LDS-P-10, LSM-P-11
Mikhalevsky V.A.	LM-P-1, LSM-P-1,THz-4-2
Mikheev N.G.	LSM-2-3
Mikulchyk T.	SN-1-5
Milanick M.A.	BP-6-4 (Invited)
Milekhin A.	SN-2-4
Milekhin I.	SN-2-4
Millon E.	LM-3-5
Milne D.	LM-4-6
Milyaev K.	LM-5-1 (Invited)
Minassian A.	LSM-1-1 (Invited)
Mintova S.	SN-3-1 (Invited)
Mirochnik A.	SN-2-3 (Invited)
Mironenko A.	SN-2-3 (Invited)
Mirzade F.Kh.	LM-2-6, LM-P-8, LM-P-10
Mitsa V.	LDS-P-9
Mizoshiri M.	LM-4-2 (Invited)
Moeini M.	BP-4-7 (Invited)
Mokrousova D.V.	LM-5-4 (Invited), LSM-P-4
Molchanov V.Ya.	LSM-2-5
Molloy J.F.	THz-2-3 (Invited)
Momgaudis B.	LM-2-1 (Invited)
Moncorgé R.	LSM-2-2 (Invited)
Moon K.	THz-3-4 (Invited), THz-P-1
Morozov V.B.	LSM-2-3
Morozov Yu.A.	LSM-P-7
Mouret G.	THz-1-6 (Invited)
Mousavi M.	PA-1-2 (Invited)
Munguía J.	SN-3-2 (Invited)
Muzhikyan P.	LDS-P-4

Name	*Number*
Smith N.	BP-3-3 (Invited)
Soifer V.A.	LM-4-5
Soloviev O.	THz-2-6
Solyankin P.M.	THz-3-2 (Invited), THz-4-2, THz-4-3
Soppera O.	SN-1-3 (Invited)
Sottile A.	LSM-1-4 (Invited)
Soulard R.	LSM-2-2 (Invited)
Sowoidnich K.	BP-5-3 (Invited)
Spangenberg A.	SN-1-3 (Invited)
Spassky D.	LSM-P-3
Spigulis J.	BP-2-5 (Invited)
Stanciu G.A.	BP-4-6
Stanciu S.G.	BP-4-6
Stoian R.	LM-2-3 (Invited)
Stolz A.	LM-3-5, LM-P-4
Subhash H.	BP-4-4, BP-P-16, PA-P-4
Subochev P.	PA-1-1 (Invited)
Sugioka K.	LM-4-1 (Invited)
Sunchugasheva E.S.	LM-5-4 (Invited), LSM-P-4
Sverchkov S.E.	LSM-P-2, LSM-P-15
Svetikov V.	LM-P-13
Svetlichnyi V.	THz-2-3 (Invited)
Svintsov D.	THz-3-3 (Invited)
Tacão M.	SN-2-5
Takács P.R.	LDS-1-6
Talbi A.	LM-3-5, LM-P-4
Tcheremiskine V.	LM-2-4 (Invited)
Tchiffo-Tameko C.	LM-3-5
Thomann A.L.	LM-3-5
Thomas G.M.	LSM-1-1 (Invited)
Tikhonova T.N.	BP-6-3 (Invited)
Timashev S.	BP-6-5 (Invited)
Timchenko E.V.	BP-P-1, BP-P-3, BP-P-4, BP-P-5, BP-P-6
Timchenko P.E.	BP-P-1, BP-P-3, BP-P-4, BP-P-5, BP-P-6
Timoshenko V.Yu.	LDS-2-5
Tiribilli B.	BP-6-1 (Invited)
Tisch J.W.G.	LDS-2-6
Tjörnhammar S.	LSM-3-4 (Invited)
Tofail S.A.M.	BP-5-1 (Invited)
Tolmachov O.	LSM-P-6
Ton X.-A.	SN-1-3 (Invited)
Tonelli M.	LSM-1-4 (Invited)
Tonouchi M.	THz-1-7 (Invited)
Tóth S.	LDS-1-5, LDS-1-6, LDS-P-3
Towrie M.	BP-6-6 (Invited)
Tranca D.E.	BP-4-6
Tregyb N.V.	BP-P-4

Name	*Number*
Tretyakov M.Yu.	THz-1-4 (Invited)
Tsvetkov V.B.	BP-P-8, LSM-P-2
Tsud N.	LDS-P-9
Tuchin V.V.	BP-2-1 (Invited), BP-5-4 (Invited), BP-P-11
Tukmakov K.N.	LM-4-5
Tulin I.V.	LSM-2-3
Turchin I.	PA-1-1 (Invited)
Turzhitsky V.	BP-5-7 (Invited)
Tyazhev A.	LSM-2-2 (Invited)
Ustinov D.I.	LSM-2-3
Ustinov V.D.	BP-6-3 (Invited)
Utéza O.	LM-2-4 (Invited)
Vaicenavicius J.	LM-2-1 (Invited)
Vaks V.L.	THz-3-1 (Invited)
Vamos L.	SN-P-3
Vartanyan T.	LM-5-2 (Invited)
Vdovin G.	THz-2-6
Veiko V.	LM-5-1 (Invited), LM-P-3, LM-P-5
Velmiskin V.V.	LSM-P-15
Verbitsky A.	LDS-2-3 (Invited)
Veres M.	LDS-1-5, LDS-1-6, LDS-1-7, LDS-1-8, LDS-P-3, LDS-P-9
Verhaegen M.	THz-2-6
Veronesi S.	LSM-1-4 (Invited)
Vicente C.M.S.	SN-2-5
Vinokurov N.A.	THz-1-3 (invited)
Vinton V.	BP-5-3 (Invited)
Vitkin A.	BP-3-1 (Invited)
Vitkin E.	BP-5-7 (Invited)
Vitkin I.A.	BP-1-3 (Invited)
Vitrik O.	LM-3-1 (Invited), SN-2-2 (Invited)
Vlasov M.Yu.	BP-P-5
Vlasova T.V.	LSM-P-14
Vodopyanov A.V.	THz-1-4 (Invited)
Volodkin B.O.	LM-4-5, THz-1-5 (Invited)
Volova L.T.	BP-P-1, BP-P-5, BP-P-6
Vondráček M.	LDS-P-9
Vovk O.	LSM-P-6
Voznesenskiy S.	SN-2-3 (Invited)
Vyurkov V.	THz-3-3 (Invited)
Wallace M.	LSM-P-8
Walther A.	PA-1-2 (Invited)
Ward J.M.	SN-1-8 (Invited)
Watanabe K.	LM-2-5
Weber P.	BP-4-3 (Invited)